Low-power sensor interfaces for detection of sporadic events

Gazivoda, Marko

Doctoral thesis / Disertacija

2022

Degree Grantor / Ustanova koja je dodijelila akademski / stručni stupanj: **University of Zagreb, Faculty of Electrical Engineering and Computing / Sveučilište u Zagrebu, Fakultet elektrotehnike i računarstva**

Permanent link / Trajna poveznica:

Rights / Prava:

Download date / Datum preuzimanja: **2025-01-11**

University of Zagreb

FACULTY OF ELECTRICAL ENGINEERING AND COMPUTING

Marko Gazivoda

LOW-POWER SENSOR INTERFACES FOR DETECTION OF SPORADIC EVENTS

DOCTORAL THESIS

Zagreb, 2022

University of Zagreb

FACULTY OF ELECTRICAL ENGINEERING AND COMPUTING

Marko Gazivoda

LOW-POWER SENSOR INTERFACES FOR DETECTION OF SPORADIC EVENTS

DOCTORAL THESIS

Supervisor: Professor Vedran Bilas, Ph.D.

Zagreb, 2022

Sveučilište u Zagrebu

FAKULTET ELEKTROTEHNIKE I RAČUNARSTVA

Marko Gazivoda

SENZORSKA SUČELJA NISKE POTROŠNJE ZA DETEKCIJU SPORADIČNIH DOGAĐAJA

DOKTORSKI RAD

Mentor: prof. dr. sc. Vedran Bilas

Zagreb, 2022.

Supervisor: Professor Vedran Bilas, Ph.D.

The thesis has 164 pages.

Thesis No.: _____

About the Supervisor

Vedran Bilas was born in Makarska in 1968. He received Dipl.Eng., M.Sc. and Ph.D. degrees in electrical engineering from the University of Zagreb, Faculty of Electrical Engineering and Computing (FER), Zagreb, Croatia, in 1991, 1995 and 1999, respectively. From January 1992 he has been working at the Department of Electronic Systems and Information Processing at FER. In June 2016 he was promoted to Full Professor.

He participated in several scientific projects financed by the Ministry of Science and Education of the Republic of Croatia, a PoC BICRO project, a COST project and 2 EU FP7 projects. He was principal investigator of the research projects supported by SBCF (UK), SNF (Swiss) and ONRG (USA). He is a member of the Research centre of excellence in data science and cooperative systems.

He published more than 150 papers in journals and conference proceedings in electromagnetic inductive methods, electronic systems for harsh environment and smart sensors and sensor networks.

Prof. Bilas is a member of IEEE and a member of the Croatian Society for Biomedical Engineering and medical Physics. He participated in international programs committees of the IEEE SAS and IEEE I2MTC and he was a general co-chair for the IEEE I2MTC 2020. He is a Senior Area Editor of the IEEE Transactions on Instrumentation and Measurement, and he serves as a technical reviewer for various international journals. He received silver medal "Josip Lončar" from FER for outstanding Ph.D. theses in 2000 and IEEE Croatia Section Outstanding Educator Award in 2011.

Since March 2022 he is the Dean-Elect of the Faculty of Electrical Engineering and Computing (FER), University of Zagreb, for the term of 2022/2023 and 2023/2024.

O mentor

Vedran Bilas rođen je u Makarskoj 1968. godine. Diplomirao je, magistrirao i doktorirao u polju elektrotehnike na Sveučilištu u Zagrebu Fakultetu elektrotehnike i računarstva (FER), 1991., 1995. odnosno 1999. godine. Od siječnja 1992. godine radi na Zavodu za elektroničke sustave i obradbu informacija FER-a. U lipnju 2016. godine izabran je u redovitog profesora u trajnom zvanju.

Sudjelovao je na više znanstvenih projekata Ministarstva znanosti i obrazovanja Republike Hrvatske, PoC projektu BICRO, COST projektu te dva EU FP7 projekta. Vodio je istraživački projekt HRZZ, te projekte financirane od zaklada SBCF (Velika Britanija), SNF (Švicarska) i agencije ONRG (SAD). Član je Znanstvenog centra izvrsnosti za znanost o podatcima i kooperativne sustave.

Objavio je oko 150 radova u časopisima i zbornicima konferencija u području elektromagnetskih induktivnih mjerenja, elektroničkih sustava za rad u teškim uvjetima te inteligentnih senzora i senzorskih mreža.

Prof. Bilas član je stručne udruge IEEE i Hrvatskog društva za biomedicinsko inženjerstvo i medicinsku fiziku. Sudjeluje u međunarodnim programskim odborima konferencija IEEE SAS i IEEE I2MTC kojom je predsjedao u 2020. godini. Član je uredničkog odbora časopisa IEEE Transactions on Instrumentation and Measurement, te sudjeluje kao recenzent u većem broju inozemnih časopisa. Godine 2000. primio je srebrnu plaketu "Josip Lončar" FER-a za posebno istaknutu doktorsku disertaciju, a 2011. godišnju nagradu Nagrada Hrvatske sekcije IEEE za izniman doprinos u inženjerskom obrazovanju.

U ožujku 2022. godine izabran je za Dekana Fakulteta elektrotehnike i računarstva (FER), Sveučilišta u Zagrebu, za mandatno razdoblje 2022./2023. i 2023./2024.

Preface

I would like to express my gratitude to my thesis supervisor Professor Vedran Bilas, Ph.D., for his continuous guidance and support in all aspects of my work, as well as for his help and contribution to the scientific papers included in this thesis and the productive, healthy, and enjoyable work environment. It was truly great working with such a wonderful mentor.

I also wish to express thanks to my parents, brother, family, friends, and colleagues for their support and encouragement during my doctoral study and years of education. Finally, thank you Lucija, for helping with the aesthetic appeal of many of my illustrations throughout my work, but even more so for always being supportive and encouraging through every step of this journey.

Marko Gazivoda

Abstract

The focus of this thesis was on exploring and developing wake-up sensor interfaces, used in two-stage sensor nodes for lowering power consumptions to levels allowing years of energy autonomy. The developed interfaces were designed to detect sporadic transient events, generating weak signals (around 10 mV on a passive transducer) in the lower acoustic spectrum (up to 2.5 kHz), lasting from around half a second up to a few seconds. The passing motor vehicle (speedboat) event was chosen as a representative case of this event group.

An analysis of acoustic signal features was performed, and a set of criteria was developed and used to determine the feature's applicability in low-power interfaces for passing speedboat detection. Based on the criteria, the spectro-temporal decomposition and level-crossing rate interface architectures were selected and further explored. Two prototype interfaces were developed and functionally tested. The results showed both architectures were applicable for detection of sporadic transient acoustic events, with true positive event detection rates exceeding 90%. They also showed that the level-crossing rate architecture was functional with two times lower input voltages, required around 40% less area and components to implement and had over three times lower power consumption. This emphasized the impact of feature choice on interface architecture and demonstrated the potential advantages of the level-crossing rate interface.

Further examination of the spectro-temporal decomposition architecture pointed to its envelope detector limiting the interface's detection accuracy. To solve this problem, utilization of a switched inductor was proposed to increase the energy efficiency of conventional envelope detectors. Several envelope detectors were developed and tested, including one using a switched inductor. Following this, two feature extractors were developed, one utilizing an electrically and the other a mechanically switched inductor. The feature extractors utilizing the electrically and mechanically switched inductors achieved 43% and 72% lower power consumptions and had four- and two-times lower minimal input voltage, respectively, compared to the conventional spectro-temporal decomposition interface, demonstrating the applicability and advantages of the switched inductor in low-power sensor interfaces for detection of sporadic acoustic events.

Keywords: always-on wake-up interfaces, interface architectures, acoustic event detection, acoustic signal features, switched inductor feature extractor, passive electromechanical feature extractor

Prošireni sažetak

Sve učestalija upotreba bežičnih senzorskih mreža u detekciji i praćenju pojava i događaja od interesa definira nove zahtjeve u dizajnu senzora. Kako bi senzorske mreže bile primjenjive u praksi i kako bi mogle svoju funkciju obavljati autonomno, senzori moraju biti jeftini, malih težina i dimenzija i imati niske potrošnje. Razine potrošnje koje bi senzorima omogućile energetsku autonomiju nisu ostvarive uz kontinuirani rad cijelih senzorskih čvorova. Zato se u današnjim senzorima koristi koncept aktivacije, u kojem je većina komponenata senzorskog čvora isključena ili u stanju niske potrošnje većinu vremena, a potpuno se aktivira za obavljanje zadataka samo u kratkim vremenskim intervalima.

Takva aktivacija može se izvoditi sinkrono, u unaprijed određenim fiksnim vremenskim trenutcima. U konceptu sinkrone aktivacije pojavljuju se problemi propuštenih događaja koji se dogode kada je senzor po rasporedu isključen te nepotrebnih aktivacija kada nema događaja od interesa, koje dovode do nepotrebne potrošnje energije. Kako bi se riješilo navedene probleme aktivacija se može izvoditi asinkrono, kada se pojavi događaj od interesa, koristeći koncept "buđenja" (engl. wake-up).

Istraživanje u sklopu ove doktorske disertacije prvenstveno je bilo usmjereno na uvijek uključena senzorska sučelja niske potrošnje namijenjena smanjenju potrošnje senzorskog čvora kroz upotrebu koncepta buđenja. U konceptu buđenja senzorski čvor sadrži senzorsko sučelje za buđenje, koje je uvijek aktivno, obrađuje senzorske signale, izvlači značajke iz njih i detektira događaje od interesa te po potrebi aktivira ostatak senzorskog čvora, koji u pravilu sadrži kompleksnije sklopovlje za digitalnu obradu signala i komunikaciju te provodi kompleksniju i detaljniju analizu događaja od interesa. Iz željene primjene senzorskih sučelja za buđenje proizlazi da su navedenim senzorskim sučeljima najznačajniji parametri točnost detekcije, jednostavnost implementacije i potrošnja energije. Točnost detekcije u kontekstu ovih sučelja podrazumijeva i razinu točno detektiranih događaja od interesa i razinu lažno pozitivnih detekcija.

U sklopu istraživanja analizirano je stanje tehnologije senzorskih sučelja za buđenje, njihovih implementacija i signali koje koriste. Rezultati analize pokazali su da suvremena senzorska sučelja za buđenje postižu visoke razine točne detekcije događaja (oko ili preko 90%) te da se većina istraživanja bavila mješovitim i analognim senzorskim sučeljima za buđenje.

Također, iz rezultata analize vidljivo je da potrošnja senzorskih sučelja za buđenje značajno varira (od nekoliko nanovata do nekoliko stotina mikrovata) i ovisna je o vrsti signala koje sučelje koristi, primjeni i implementaciji sučelja, kao i odabranoj metodi klasifikacije događaja. Za daljnji rad odabrana su akustička senzorska sučelja zbog bogatstva lako dobavljivim informacijama koje karakterizira akustičke signale, a omogućava izradu jednostavnih sučelja niske potrošnje i visoke točnosti detekcije. Analiza suvremenih sučelja za buđenje također je pokazala širok raspon primjenjivosti akustičkih sučelja, što je jasno vidljivo i iz činjenice da akustička sučelja predstavljaju preko 55% svih suvremenih sučelja za buđenje prikazanih u literaturi.

Namjena razvijanih sučelja bila je detekcija sporadičnih prolaznih akustičkih događaja koji generiraju signale niskih naponskih razina (oko 10 mV na pasivnom mjernom pretvorniku) u donjem dijelu akustičkog spektra (do 2.5 kHz), trajanja između pola i nekoliko sekundi. Kao reprezentativni primjerak ove skupine događaja odabran je prolazaka motornih vozila, konkretnije glisera.

Senzorska sučelja za buđenje detektiraju događaj od interesa prema značajkama (karakteristikama) signala koje događaji od interesa stvaraju. Zbog toga značajke signala, koje ovise o signalima koje stvaraju događaji od interesa, predstavljaju osnovu za detekciju događaja.

Sukladno tome, u ovom istraživanju je provedena općenita analiza akustičkih značajki, s posebnim naglaskom na značajke iz vremensko-frekvencijske i vremenske skupine, koje su se pokazale primjenjivim u senzorskim sučeljima niske potrošnje namijenjenim detekciji sporadičnih prolaznih akustičkih događaja. Navedene značajke korištene su u preko 90% svih senzorskih sučelja niske potrošnje za detekciju akustičkih događaja. S posebnim interesom analiziran je utjecaj odabira značajki na arhitekture senzorskih sučelja. Provedena je i analiza arhitektura i njihovih implementacijskih specifičnosti s obzirom na značajke koju koriste za detekciju događaja. Razvijen je set kriterija namijenjen raspoznavanju značajki koje omogućavaju realizaciju arhitektura senzorskih sučelja za buđenje zadovoljavajućih funkcionalnosti i karakteristika. Upotrebom razvijenih kriterija izbor značajki je sužen na one koje omogućavaju implementaciju ugradbenih sučelja visokih razina točnosti detekcije, koja su u stanju raditi s ulaznim signalima niskih naponskih razina (oko 10 mV), a značajke ekstrahiraju i obrađuju u analognoj domeni, bez potrebe za kompleksnim sklopovljem za analogno-digitalnu pretvorbu. Primjenom navedenih kriterija izbor značajki sužen je na vremensko-frekvencijsku

dekompoziciju (anvelopu, snagu, ili energiju signala u vremenu i frekvenciji) i stopu prolazaka kroz zadanu razinu (ili nulu).

Za navedene dvije značajke razvijeni su simulacijski modeli i prototipna sučelja te su procijenjene njihove performanse u detekciji prolazećih glisera, s posebnim naglaskom na potrošnjama sučelja, kompleksnostima njihove implementacije, minimalnim potrebnim ulaznim naponima i radu sa signalima s visokim razinama šuma. Rezultati navedenog istraživanja pokazali su da su obje arhitekture upotrebljive za detekciju sporadičnih prolaznih akustičkih događaja (prolazaka glisera) te da obje ispravno prepoznaju događaje od interesa s preko 90% točnosti. Također su pokazali da arhitektura bazirana na stopi prolazaka kroz zadanu razinu može raditi s dvostruko nižim ulaznim naponima (10 mV od vrha do vrha u odnosu na 20 mV od vrha do vrha), uz preko tri puta nižu potrošnju (9.1 µW u odnosu na 34.6 µW) te da je za njenu implementaciju potrebna 40% manja površina i otprilike 40% manje komponenata. Arhitektura bazirana na vremensko-frekvencijskoj dekompoziciji pokazala se uspješnija u radu sa signalima s visokom razinom šuma. Ovi rezultati naglasili su prethodno slabo istražen, ali presudan utjecaj koji odabir značajki ima na funkcioniranje senzorskog sučelja za detekciju događaja te prikazali prednosti arhitekture bazirane na stopi prolaska kroz zadanu razinu.

Detaljna analiza arhitekture bazirane na vremensko-frekvencijskoj dekompoziciji ukazala je na nisku energetsku efikasnost njenog ispravljača, koja ograničava osjetljivost i, posljedično, točnost detekcije koju sučelje može ostvariti. Nelinearna prijenosna karakteristika dioda koje se koriste u ispravljačima dodatno potiskuje signale niskih naponskih razina s kakvima uobičajeno moraju raditi ovakva senzorska sučelja. Kao rješenje navedenog problema predložena je upotreba ispravljača s preklapanom zavojnicom.

Razvijeno je nekoliko aktivnih i pasivnih ispravljača, uključujući i ispravljač s preklapanom zavojnicom te su njihove karakteristike uspoređene u detekciji sintetičkih signala u donjem akustičkom spektru. Ispravljač s preklapanom zavojnicom pokazao se upotrebljivim u detekciji akustičkih signala u donjem dijelu spektra, što je usmjerilo daljnje istraživanje u smjeru implementacije i karakterizacije ekstraktora značajki s preklapanom zavojnicom.

Osmišljen je sklop za ekstrakciju značajki koji upotrebljava preklapanu zavojnicu, a sastoji se od sklopke koja zatvara i otvara put struje između zavojnice i izvora, čime se prekida struja kroz zavojnicu zbog čega se na zavojnici inducira napon viših razina od ulaznog napona (postiže se efekt podizanja ulaznog napona). Osim što podiže napon, sklop s preklapanom zavojnicom se

također pokazao frekvencijski selektivan. Zbog navedenih svojstava, sklop s preklapanom zavojnicom u konvencionalnoj arhitekturi sučelja baziranog na vremensko-frekvencijskoj dekompoziciji može zamijeniti ne samo ispravljač, već i filtar.

Razvijeni su simulacijski modeli i prototipi dva takva sklopa, od kojih je jedan koristio električki, a drugi mehanički preklapanu zavojnicu. Koristeći razvijene modele i prototipe provedeno je niz simulacija i eksperimenata sa sintetičkim i snimljenim akustičkim signalima u donjem dijelu akustičkog spektra (do 2.5 kHz). Rezultati rada dva ekstraktora značajki uspoređeni su međusobno, a arhitekture sučelja koje ih koriste uspoređene su s ranije razvijenom konvencionalnom arhitekturom baziranom na vremensko-frekvencijskoj dekompoziciji.

Rezultati međusobne usporedbe rada ekstraktora pokazali su da ekstraktor s mehanički preklapanom zavojnicom ima prednosti niže potrošnje (pasivan je), inherentne pojasnopropusne frekvencijske karakteristike i elektronički jednostavnije implementacije, dok je preciznija kontrola postupka preklapanja i više raspoloživih parametara dizajna omogućilo ekstraktoru s električki preklapanom zavojnicom ostvarivanje veće maksimalne osjetljivosti.

Rezultati usporedbe arhitektura s novim ekstraktorima značajki s našom ranije razvijenom konvencionalnom arhitekturom baziranom na vremensko-frekvencijskoj dekompoziciji pokazali su da upotreba ekstraktora značajki baziranog na električki, odnosno mehanički preklapanoj zavojnici omogućava smanjenje potrošnje od 43%, odnosno 72% i rad s četverostruko, odnosno dvostruko nižim minimalnim ulaznim naponom. Time je ne samo demonstrirana primjenjivost preklapanih zavojnica u senzorskim sučeljima niske potrošnje za detekciju sporadičnih događaja, nego i značajna unaprjeđenja funkcionalnosti koja njena primjena donosi u odnosu na konvencionalna vremensko-frekvencijska senzorska sučelja.

U konačnici, upotrebom pasivnog ekstraktora značajki s mehanički preklapanom zavojnicom predloženog u sklopu ove disertacije učinjen je prvi korak prema implementaciji potpuno pasivnih senzorskih sučelja za buđenje baziranih na mikroelektromehaničkim komponentama, koji predstavljaju budućnost senzorskih sučelja za detekciju događaja od interesa.

Ovaj rad sastoji se od osam radova koji su diseminirani u uglednim međunarodnim znanstvenim časopisima i konferencijama. Opisima i rezultatima eksperimenata prikazanih u radovima prethodi predstavljanje motivacije i teorijske pozadine istraživanja, bazirano na postojećoj literaturi relevantnoj za područje rada. Objedinjeni radovi predstavljaju izvorni

znanstveni doprinos ove doktorske disertacije koji se sastoji od detaljne analize značajki akustičkih signala i njihovog utjecaja na arhitekture sučelja za buđenje, dizajna dviju novih arhitektura za detekciju sporadičnih prolaznih akustičkih događaja te novom rješenju za problem ograničene funkcionalnosti ispravljača u konvencionalnoj arhitekturi sučelja za buđenje baziranoj na vremensko-frekvencijskoj dekompoziciji upotrebom preklapane zavojnice.

Ključne riječi: uvijek aktivna senzorska sučelja za buđenje, arhitekture sučelja, detekcija akustičkih događaja, značajke akustičkog signala, ekstraktor značajki s preklapanom zavojnicom, pasivni elektromehanički ekstraktor značajki

Contents

Chapter 1

Introduction

1.1 Overview

The ever-growing desire to understand, evaluate and manage our surroundings leads to an increased interest in continuous monitoring of events and processes, utilizing sensor networks that consist of large numbers of sensor nodes [1]–[4]. To meet the demands of these applications the sensor nodes must be disposable, small and light-weight and the networks they form must be operational for long periods of time (on the order of decades) with minimal or ideally no maintenance and interventions. The final goal is a wireless sensor network of fully autonomous sensor nodes, in terms of their functionality, energy and ways they interact with the world around them [2].

However, monitoring and detecting events by continuous operation of complex power-hungry systems leads to a sensor nodes with high power consumption and short lifetime (on the order of days or weeks) that requires frequent interventions [5], [6]. Reducing a sensor node's power consumption to levels that allow sensor node energy autonomy can only be achieved if the sensor node (or most of its components) are kept in a low-power ("sleep") mode for most of the time and only fully activate to perform their tasks during limited time windows [2], [5], [6].

This activation can be done synchronously, at predefined time intervals (duty cycling). Alternatively, in detection of sporadic events, a better solution is to utilize the wake-up concept, that implies asynchronous event-driven activation [3], [7]. In this concept the sensor node consists of an always-on wake-up sensor interface which is used to wake up the main subsystem only when an event of interest is detected. These wake-up interfaces determine the presence of potential events of interest by performing low-power extraction and analysis of the sensor signal's features [8]–[11]. Therefore, the key emphasis in their design is on low power consumption, cheap and simple design, and accurate detection [7], [11]–[14] to ensure low false

detection rates even in the most adverse conditions, as false event detections increase the overall system's power consumption by causing unnecessary activations of the main stage.

An especially interesting application for such sensor interfaces is power-constrained acoustic-based event detection because acoustic signals contain a lot of easily extracted information [15]–[17], enabling design of simple and reliable detectors.

1.2 Thesis scope and scientific contributions

This thesis was focused on exploration of low-power sensor interfaces applied in acoustic wake-up event detectors. The first step was to analyze the literature on wake-up systems in general (Pub2), followed by research specifically focused on acoustic wake-up sensor interfaces (Pub1) to obtain insight on the wake-up sensor interface state-of-the-art.

Next it was important to define the events of interest. The primary research interest was developing interfaces for detecting sporadic transient events in the lower acoustic range (up to 2.5 kHz), lasting from around half a second up to a few seconds and generating weak signals (around 10 mV) on a passive acoustic transducer. The passing motor vehicle was chosen as a representative of this group of events and multiple simulation and experimental studies were performed, with synthetic signals modeled after those generated by these events, and with real-world prerecorded signals of passing speedboats. The simulation studies were performed utilizing Texas Instruments' simulation programs TINA TI and PSPICE for TI. For all the input signal synthesis and both input and output signal preprocessing and conditioning, as well as signal acquisition control and result representation the program MATLAB was used.

After defining the event of interest and its signals, an analysis of the features that could be used in detection of the chosen event was performed. The acoustic signal features used in event detection were explored and, through literature analysis, the selection of features was narrowed down to only those utilized in low-power wake-up event detectors.

Then the interface architectures stemming from the chosen detection schemes and features were analyzed. A set of criteria was defined to further narrow down the list of considered features to only those that could be utilized to design architectures appropriate for detection of passing motor vehicles. These criteria defined the goal of developing architectures which could be designed in embedded implementation, were reliably operational with weak input signals (on the order of 10 mV), and extracted and processed features in the analog domain.

This led to further analysis of two wake-up interface architectures, the level-crossing rate and the spectro-temporal decomposition architecture. Prototypes architectures were developed and their applicability in detection of passing motor vehicles was researched by analyzing their performances in terms of power consumptions, implementation complexities, input operational voltages and signal-to-noise ratios (SNRs).

Finally, an in-depth analysis of the spectro-temporal decomposition wake-up sensor interface was made which pinpointed to its envelope detector as a chokepoint. Inspired by an approach utilized in weak vibration energy harvesting, the switched inductor was explored as a potential solution for this design chokepoint. Synthetic signals were first utilized to characterize and compare the performances of several envelope detectors, including the switched inductor envelope detector. This led to developing a switched inductor element which could be used as both a filter and an envelope detector, therefore replacing the interface's entire feature extractor. Two feature extractors were developed, one utilizing an electrically and the other a mechanically switched inductor and their performances compared to those of the feature extractor of our previously developed spectro-temporal decomposition interface, in terms of their measurement resolutions, sensitivities, detection accuracies and power consumptions. In these experiments both synthetic and prerecorded speedboat passing signals were employed with varied amplitudes and SNRs.

Within this scope two major contributions are presented. First, an analysis of the architectures for selected applicable features in sporadic acoustic event detection is performed, two embedded prototypes are developed, their functionalities tested, and the importance of feature and architecture choice in design and performance of low-power sensor interfaces is emphasized. Second, a design problem in the spectro-temporal sensor interface architecture is identified, and the switched inductor is presented as an element to improve the envelope detector's efficiency.

1.3 Thesis organization

This thesis is a compilation of eight publications addressing the research objectives. Chapter 2 shows the motivation for low-power acoustic sensor interface research, presents the theoretical background and advantages of utilizing wake-up interfaces, emphasizes the importance of signal feature choice and subsequentially the interface's architectures in its performance and presents

generalized considerations on two researched low-power wake-up sensor interface architectures. Chapter 3 presents an in-depth analysis of the spectro-temporal decomposition-based low-power wake-up sensor interface architecture, with emphasis on a novel solution for the architecture's chokepoint, the envelope detectors, which proposes to increase their efficiency through utilization of switched inductors. Chapter 4 presents the scientific contributions of the doctoral thesis, validated and evaluated through the results of the included publications. In Chapter 5 a list of included publications is given and in Chapter 6 the authors contribution to each publication is discussed. Finally, the thesis conclusion is presented in Chapter 7.

Chapter 2

Acoustic low-power sensor interfaces

2.1 Sensor nodes and networks

Sensors are defined as devices that react to physical stimuli by generating electric signals, forming the point of interaction between the real, physical world and electronic systems. They are an essential part of an electronic system, enabling it to perceive its surroundings. Therefore, sensors represent the basic element and the foundation of event detection, and to a great extent, define key event detection parameters, such as accuracy and efficiency.

Sensors are deployed into the environment in the form of sensor nodes which typically consist of a transducer to convert the physical value into an electric signal, a sensor interface to condition the raw sensor signal and partially transform it into data usable by the following stages, an A/D converter, a digital processing and control unit and communication hardware (Fig. 2.1).
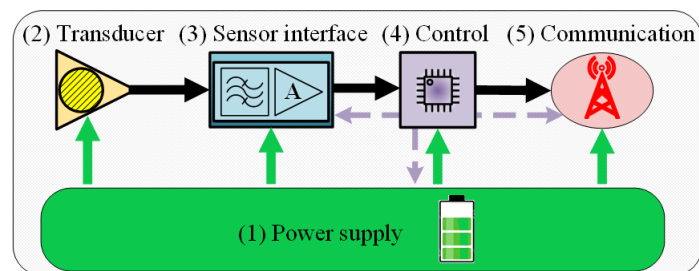

Figure 2.1: A block schematic of a typical sensor node.

Events of interest can be detected utilizing different sensor modalities, meaning that a sensor node can have different transducers, from acoustic, to temperature, pressure, humidity, light, vibration and many more. The choice of the transducer can greatly impact the utilized event detection scheme and therefore the required signal processing and the sensor interface's architecture. In our research acoustic sensors were chosen because acoustic signals contain a lot of easily extracted information [15]–[17].

In most event detection schemes multiple sensor nodes operate together, joined into a wireless sensor network, to allow for a more practical implementation and deployment. This leads to an ever-increasing need for wireless intelligent low-power sensor nodes and networks [2], [3] spanning multiple applications from surveillance and security [5], [18]–[25], speech and voice detection [26]–[32], environment [12], [33], biomedical [31], [34]–[40] and structural health monitoring, non-destructive testing and machinery diagnosis [31], [41], communication channel monitoring [42]–[46] and many others [8], [13], [17], [47]–[52].

These applications require inexpensive, easily deployable sensor nodes and networks functional for long periods of time with minimal maintenance and intervention, with the final goal of developing a wireless sensor network of completely autonomous sensor nodes, in terms of their functionality, energy and ways they interact with their environment [2].

A necessary prerequisite to achieve this is energy autonomy [53], also called energy autarky [22], [54], or neutrality by some authors [12]. This concept proposes a sensor that can stay active forever without the need for intervention, from the energy point of view.

Working towards sensor node energy autonomy, there have been several research fields established, focused on improving sensor node power sources, lowering sensor node power consumptions and increasing their energy efficiency.

In terms of sensor node power sources, there is a lot of research focused on improving batteries [1], [55], reducing their size, increasing capacity, reducing self-discharge and other unwanted effects. Another prominent concept for powering sensor nodes, that could potentially replace battery-powered systems altogether [1], is energy harvesting, which entails generating electrical energy on the sensor node using the energy of the phenomena in its surroundings, such as ambient vibration [41], [56], light [41], [57] and thermal gradients [41], or even microbes [58].

To reduce a sensor node's power consumption and increase its energy efficiency to levels that allow sensor node energy autonomy, the sensor node (or most of its components) must be kept in a low-power ("sleep") mode for most of the time and only fully activate to perform their tasks during limited time windows [2], [5], [6].

To achieve sensor node energy autonomy, sufficient lowering of the sensor node's power consumption and increasing of its energy efficiency can only be achieved if the sensor node (or

most of its components) are kept in a low-power ("sleep") mode for most of the time and only fully activate to perform their tasks during limited time windows [2], [5], [6].

This activation can be done synchronously, at predefined time intervals, utilizing a concept called duty cycling. However, considering the sporadic nature of most events, which entails them appearing rarely and with no predefined schedule, utilizing duty cycling will sometimes lead to wasting energy for unnecessary activations when no event of interest is present and occasionally cause the sensor node to miss events, if they occur during a period in which the system is scheduled to be in stand-by mode [17].

A better solution for this activation, especially when the events of interest are sporadic, is to utilize asynchronous event-driven activation [3], [7] and the wake-up concept, in which the sensor node consists of an always-on wake-up sensor interface which is used to wake up the main subsystem only when an event of interest is detected. These interfaces determine the presence of potential events of interest by performing low-power extraction and analysis of the sensor signal's features [8]–[11].

This motivates further research of low-power acoustic wake-up sensor interfaces used as basis of sporadic event detection, with a focus on their architectures and the signal features they use.

2.2 Wake-up sensor interfaces

2.2.1 Principle of operation

As explained previously, sensor nodes are used to detect events, which for many applications occur rarely and with no predefined schedule. The event activity, *EA*, is defined as the percentage of time during which events of interest are present. While the whole sensor node is in active mode it has a mean power consumption of P_m, that can be reduced by powering down most parts of the sensor node and only activating them when necessary.

This activation can be done synchronously, with a fixed schedule, utilizing duty cycling, with a duty cycle of *D*, which is set to an appropriate value depending on the approximate expected event activity. The duty cycled sensor node's power consumption can be expressed as:

$$P_D = D \cdot P_m \qquad\qquad (1)$$

However, due to the contrast between the scheduled (fixed) activation of a duty cycled sensor node and the sporadic nature of the events of interest, there will be instances when the sensor node activates only to conclude there is no need for activation (no event of interest) and then goes back to stand-by mode, only wasting energy for activation. Additionally, such a sensor node can miss all events of interest that occur during a period in which the sensor node is scheduled to be in stand-by mode [17].

To mitigate these problems, a more energy-efficient solution is to asynchronously power-up the sensor node utilizing the wake-up concept [3], [7], that proposes a two-stage sensor node consisting of two subsystems (Fig. 2.2 a)).
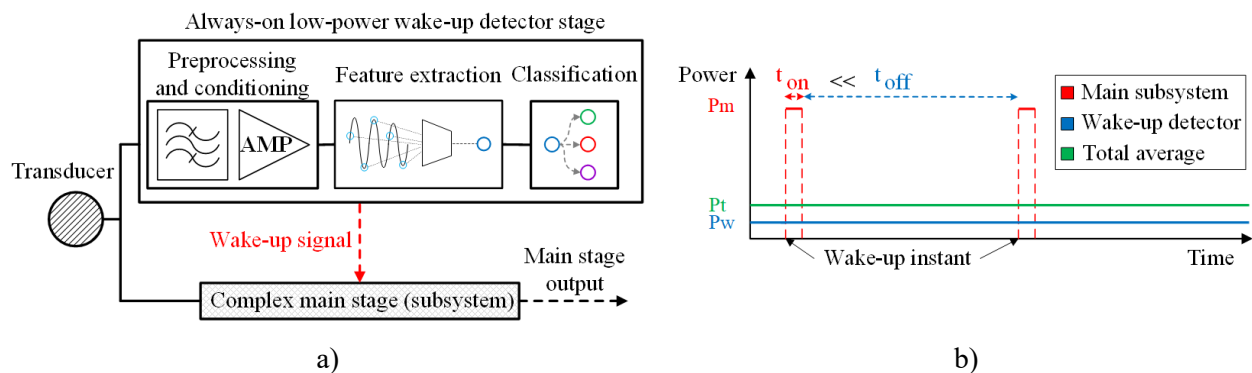

Figure 2.2: a) A block schematic of a two-stage sensor node utilizing the wake-up concept. b) Power consumption reduction principle of the wake-up concept.

The first subsystem, called the wake-up sensor interface, or the wake-up detector, is always on, has low power consumption of $P_w \ll P_m$, acquires the signals, conditions them, extracts features from them, and detects feature patterns. Then, if the wake-up interface determines that an event of interest occurred, it sends an activation (wake-up) signal to activate the second subsystem (or the rest of the sensor node) with a higher power consumption (P_m) that performs a more detailed analysis of the event. While the function of the wake-up sensor interface finishes with accurate detection and discrimination of events of interest, the detailed analysis performed by the second stage is usually the main function of the entire sensor node. This functionality provides more data on the event of interest, by utilizing more resources and more complex processing techniques or even a different transducer modality, leading to this stage often being referred to as the main stage. As an example, a sensor node operating as a vehicle detector can utilize an acoustic wake-up sensor interface, which, upon detection of a passing vehicle, powers

up a more complex main stage that allows for a higher quality acoustic analysis, or even activation of magnetic or seismic sensors to provide a more detailed characterization of the detected vehicle (vehicle type, propulsion type, size and so on).

The wake-up sensor interface correctly recognizes events of interest with a true positive rate of *TP* ([59]) and mistakes other signals for events of interest with a false positive rate of *FP* [59]. The power consumption of a two-stage sensor node with a wake-up sensor interface can be expressed as:

$$P_{2S} = P_w + EA \cdot TP \cdot P_m + (1 - EA) \cdot FP \cdot P_m \tag{2}$$

The overall power consumption of a two-stage sensor node with a wake-up sensor interface is primarily defined by the wake-up interface's power consumption, its true and false positive rates and the event activity and it should be considerably lower than that of the sensor node's main stage ($P_{2S} << P_m$).

A graphical representation of the wake-up concept's principle of lowering a sensor node's power consumption is shown in Fig 2.2 b).

2.2.2 Prolonging the sensor node's lifetime

After explaining the wake-up concept's principle of operation, the sensor node lifetime extension that utilizing wake-up sensor interfaces can provide is further analyed, by calculations, as well as real-world examples.

A battery-powered sensor node's lifetime, *T*, depends on the energy stored within its battery, *E*, and the sensor node's power consumption, *P*, and can be approximated as:

$$T = \frac{E}{P} \cdot 0.7 \tag{3}$$

The 0.7 multiplication factor accounts for external factors affecting the battery lifetime estimation [60].

2.2.2.1 Example 1

A sensor node's lifetime analysis was illustrated through an example battery-powered sensor node with a battery energy of $E = 100$ mWh, the mean power consumption of the sensor node's main stage of $P_m = 1$ mW. The sensor node can be synchronously activated with a duty cycle of $D = 5\%$, or asynchronously activated by a wake-up interface with power consumption ranging from $P_w = 0.001 \cdot P_m = 1$ µW to $P_w = 0.1 \cdot P_m = 100$ µW. The wake-up interface detects all event of interest ($TP = 100\%$) and has false positive detection rates of $FP = 0\%$ or $FP = 5$ %.

Figure 2.3 illustrates the lifetimes of a battery-powered sensor node without wake-up (sensor node's main stage always active), with synchronous duty cycle activation and with asynchronous wake-up sensor interface activation. In these calculations the impact of the power consumption caused by the switching action of the main stage is disregarded, as it should be negligible compared to other consumptions if the activation system is designed correctly.
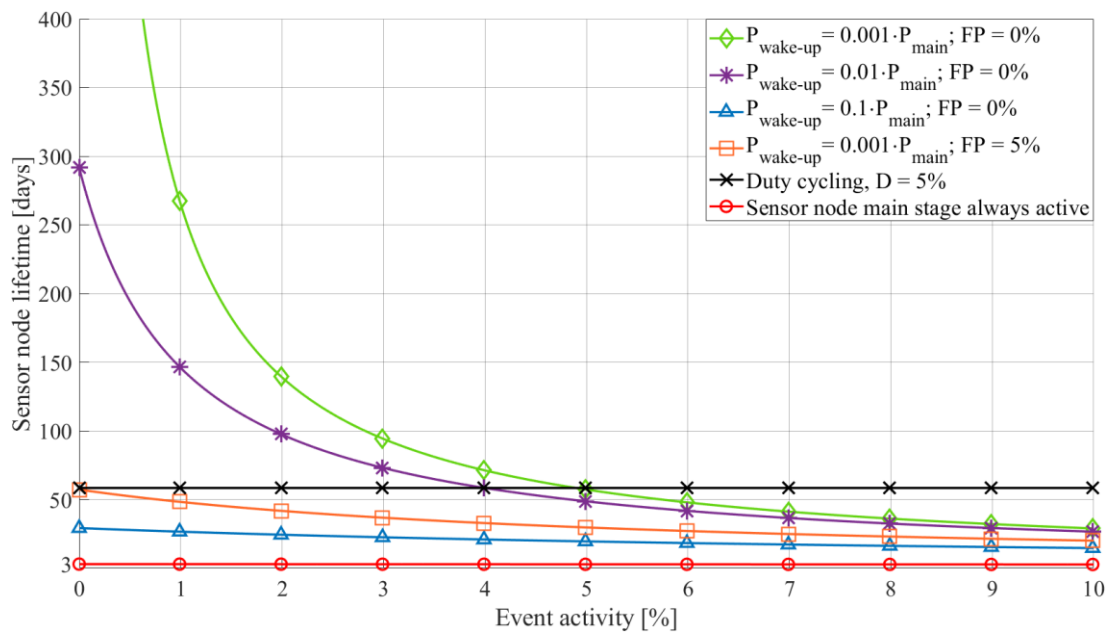

Figure 2.3: Lifetimes of a sensor node utilizing duty cycling or a wake-up detector. The red line represents the sensor node's lifetime if its main stage is always active (no wake-up) and the black line represents the sensor node's lifetime utilizing duty cycling with a duty cycle $D = 5\%$. The other lines represent the sensor node's lifetime utilizing a wake-up interface with no missed events ($TP = 100\%$), a power consumption and false positive rate of: $P_w = 0.001 \cdot P_m$ and $FP = 0\%$ (green), $P_w = 0.01 \cdot P_m$ and $FP = 0\%$ (purple), $P_w = 0.1 \cdot P_m$ and $FP = 0\%$ (blue), $P_w = 0.001 \cdot P_m$ and $FP = 5\%$ (orange).

From Fig. 2.3 it can be seen that the sensor node utilizing a wake-up sensor interface achieves a longer lifetime compared to the duty cycled one if event activity drops below the duty cycle (around 1% under the set duty cycle) and the wake-up interface has a low power consumption (100 or more times lower than the main stage power consumption, $P_w \leq 0.01 \cdot P_m$).

Additionally, it can be observed that a higher false positive rate ($FP = 5\%$) can significantly degrade a wake-up interface's functionality, drastically reducing or even completely annulling the lifetime extension, due to unnecessary activations of the whole sensor node.

Clearly, decreasing the wake-up interface's true positive rate increases the sensor node's lifetime, but also leads to a less functional event detector, less able to detect events of interest, so in most application scenarios this is not a valid method for extending a sensor node's lifetime.

2.2.2.2 Example 2

The sensor node's lifetime extension provided by a wake-up interface was also illustrated through an example in which the low-power always-on wake-up sensor interfaces presented in [12] and [15] are used to wake up an FPGA sound classifier used for acoustic surveillance [19], as shown in Fig. 2.2 a) (the interfaces from [12] and [15] function as the wake-up stage and the sound classifier from [19] represents the main stage).

The energy of the sensor node's battery was set to $E_{ps} = 10000$ mWh. The sound classifier from [19] has a power consumption of $P_m = 47$ mW. The wake-up sensor interface from [12] has a power consumption of $P_w = 26.89$ µW, a true positive rate of $TP = 98.67\%$ and a false positive rate of $FP = 10\%$ and the wake-up sensor interface from [15] has a power consumption of $P_w = 26.89$ µW, a true positive rate of $TP = 100\%$ and a false positive rate of $FP = 0\%$. Event activities, EA, considered are 1%, 3% and 5%. The lifetime comparison results are presented in Table I.

TABLE I – Sensor node lifetime extension by utilizing a wake-up detector

Event activity [%]	Sensor node lifetime [days]			Extension [times]	
	Only [19]	[19] using [12]	[19] using [15]	by [12]	by [15]
1	8.87	81.00	838.55	9.13	94.54
3	8.87	69.71	289.98	7.86	32.69
5	8.87	61.17	175.3	6.90	19.76

With the results of this example, the sensor node lifetime extension that utilizing a wake-up sensor interface can provide was demonstrated, and the importance of wake-up interface design was emphasized, as it is clear that parameters like false positive rate can drastically impact the wake-up interface efficiency.

The main topic of this thesis is the design of these low-power wake-up sensor interfaces for sporadic event detection. Our first step in this extensive research was performing a detailed state-of-the-art (SOTA) wake-up sensor interface analysis, whose results can be seen in [Pub1], followed by focused research of acoustic low-power wake-up sensor interfaces, with special emphasis on the features they utilize and the consequential architectures they employ.

2.3 Features

As our research is focused on the acoustic low-power wake-up sensor interfaces, the first step is to examine the acoustic signal features utilized in acoustic event detection. Following an analysis of literature on acoustic signal features [61]–[63], an acoustic signal feature categorization was devised, grouping features into five major groups, as shown in Table II.

Table II Acoustic signal feature categorization

Temporal	Spectral	Spectro-temporal	Cepstral	Other
Level-crossing rate-based	Spectral shape-based	Spectro-temporal decomposition-based	Mel-frequency cepstral coefficient-based	Eigenspace-based
Temporal amplitude-based	Brightness-based	Hurst parameter-based	Other cepstral coefficient-based	Acoustic environment-based
Temporal power-based	Tonality-based	MP-based Gabor features		
Rhythm-based	Chroma-based	Sparse coding tensor-based		
Correlation-based				

Next, the features' applicability in power-constrained acoustic event detection was examined. To this end, an analysis of SOTA acoustic wake-up sensor interfaces was perform, exploring their implementations, feature extraction domains (analog, digital, or mixed), power consumptions and detection accuracies (true and false positive rates). The detector implementation is divided into embedded made with commercial-off-the-shelf (COTS) components and custom-made integrated, both further divided into analog, digital and mixed-signal.

Table III shows the results of the SOTA acoustic wake-up detector analysis.

Table III Acoustic wake-up sensor interfaces

Feature group	Feature subgroup	Feature	Ref.	Interface implementation	Feature extraction domain	Power (µW)	Detection accuracy	
							TP (%)	FP (%)
Spectro-temporal	Spectro-temporal decomposition	Spectro-temporal envelope	[24, 64]	Embedded mixed	Analog	7.33; 34.92	90.91	Not stated
			[8, 15]	Embedded mixed	Analog	26.89	98.67; 100	14; 0
			[16]	Integrated mixed	Analog	43	100	0
		Spectro-temporal energy	[65]	Integrated mixed	Analog	1.01	Not stated	Not stated
			[30]	Integrated digital	Digital	~ 100	96.63	2.33
		Spectro-temporal power	[66]	Integrated mixed	Mixed	0.142	90 – 91.5	Not stated
		Spectro-temporal RMS	[67]	Integrated mixed	Analog	6	89	Not stated
		Spectro-temporal (absolute) voltage	[17]	Integrated mixed	Digital	0.012	96 – 98	0
			[28]	Integrated analog	Analog	2.5	Not stated	Not stated
			[26], [68]	Integrated mixed	Analog	1; 27.77	~ 85; ~ 80	Not stated; 0
		Spectro-temporal instant rate of change	[52]	Integrated digital	Digital	0.148	85 – 99	1 – 18
Temporal	Level crossing rate	Zero crossing rate	[13]	Embedded analog	Analog	34	Not stated	Not stated
			[8]	Embedded digital	Digital	~ 600	Not stated	Not stated
		Zero-crossing rate with peak amplitude (ZCPA)	[69]	Integrated digital	Digital	Not stated	98	Not stated
		Zero crossing with Short-Time Magnitude Difference	[34]	Embedded digital	Digital	30.71	91	Not stated
	Correlation	Autocorrelation	[29]	Integrated digital	Digital	24.4	55 – 95	5 – 20
			[70]	Integrated mixed	Digital	0.835	97	0
		Crosscorrelation	[71]	Integrated mixed	Mixed	1.5	92	7
	Short time energy	Short time energy difference	[29]	Integrated digital	Digital	8.5	55 – 95	5 – 20
	Multiple	Rise time, min/max, energy	[72]	Embedded mixed	Digital	8.7	100	Not stated
Spectral	Spectral shape	Power spectrum density	[73]	Integrated mixed	Digital	4.7	Not stated	Not stated
Cepstral	Cepstral coefficients	Mel-frequency CC	[32], [74]	Integrated digital; Integrated mixed	Digital; Mixed	0.51; 28.8	97.3; 98.2	2 – 2.3; Not stated

From Table III we see that most acoustic wake-up sensor interfaces utilize spectro-temporal (54% of analyzed interfaces) or temporal features (35% of all interfaces). Within those feature groups, interfaces mostly utilize spectro-temporal decomposition (61%), level-crossing rate (17%) and correlation (13%).

With this insight into feature utilization in low-power wake-up sensor interfaces the next step is the analysis of their architectures.

More details regarding feature and architecture utilization in power-constrained event detection can be seen in the results of [Pub1] and [Pub2].

2.4 Architectures

As stated previously, the feature an interface uses for event detection defines the interface's architecture details. The SOTA analysis showed several prominent feature subgroups, which were further analyzed to determine how they were extracted, processed, and utilized in event detection by the interfaces employing them and how the feature choice impacted the interface architecture and implementation options.

The spectro-temporal decomposition interface architectures (Fig. 2.4) filter the input signal into sub-bands and continuously extract each sub-band's feature of interest, be it the envelope, energy, power, or root mean square (RMS). After extraction they quantify the feature and convert it into a binarized spectro-temporal sequence. A classifier determines this sequence's resemblance to a preset template, defined by the event of interest. These interfaces are usually implemented as mixed-signal, extracting and processing the features in the analog domain and performing classification in the digital domain.
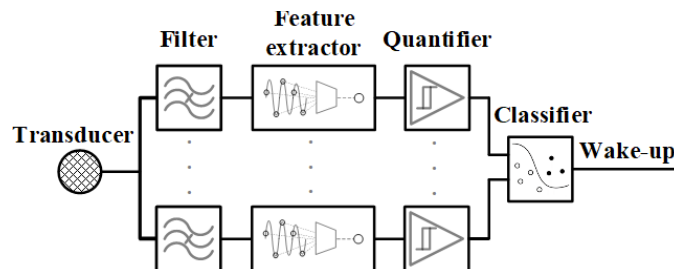

Figure 2.4: Spectro-temporal decomposition wake-up sensor interface generalized architecture.

The level-crossing rate interface architectures (Fig 2.5) convert the input signal's crossings of a preset level into pulses of fixed length and amplitude, counting those pulses in a defined time interval, quantifying the pulse and therefore the level-crossing rate and determining whether it is within the bounds of level-crossing rates specific for the events of interest. These interfaces are usually implemented as fully digital, but they can also be implemented completely in the analog domain.
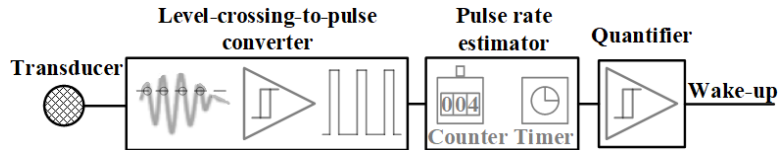
Figure 2.5: Level-crossing rate wake-up sensor interface generalized architecture.

The correlation-based interface architectures (Fig. 2.6) compare the input signal to a delayed version of itself (autocorrelation) or a preset template representing the event of interest (crosscorrelation). Autocorrelation interfaces can estimate the input signal's spectral content by detecting the local maxima of the autocorrelation function, which appear with delay times equal to periods of the input signal's dominant spectral components. While the crosscorrelation architecture requires only a single channel compared to the autocorrelation architecture's multiple, the requirement of synchronization significantly complicates its design. These interfaces are usually implemented as digital because it is impractical to implement some required elements, such as delay lines or memories for storing templates, in the analog domain.
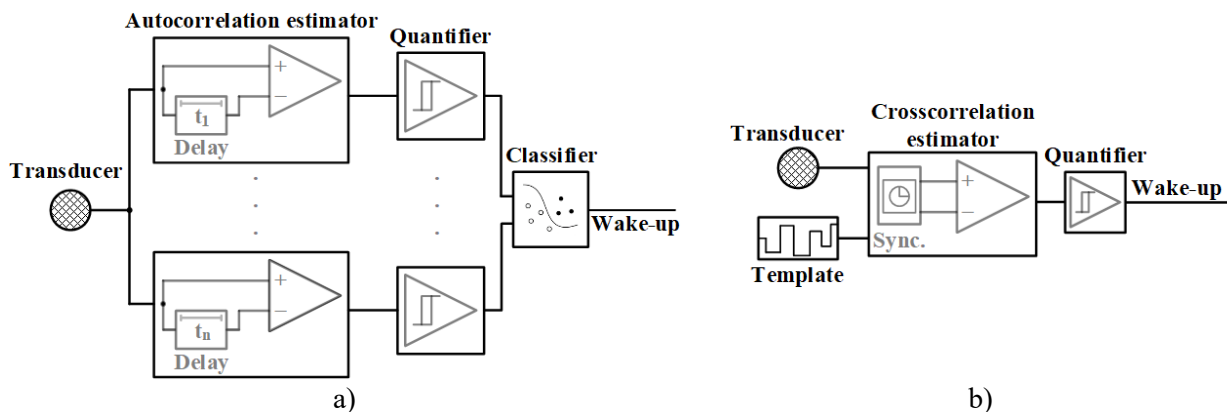

Figure 2.6: a) Autocorrelation and b) crosscorrelation wake-up sensor interface generalized architecture block schematic.

Interface architectures utilizing short-time energy measure the input signal's energy in short time windows and compare it to a preset template. While the SOTA interface utilizing this feature subgroup [29] is implemented as digital, a mixed-signal implementation similar to the architecture utilizing the spectro-temporal decomposition could also be considered (Fig. 2.7). However, it is also clear that this feature provides only a portion of the information compared to, for instance, spectro-temporal energy.
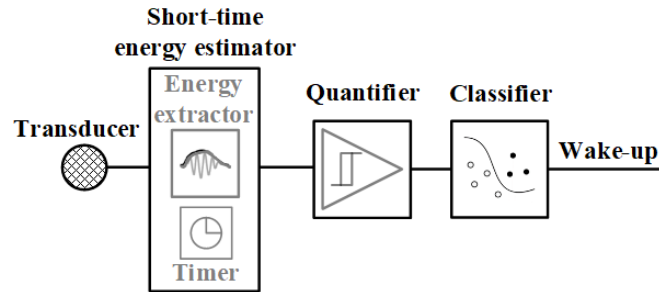
Figure 2.7: Short-time energy wake-up sensor interface generalized architecture block schematic.

Interface architectures using spectral shape (Fig. 2.8) extract the input signal's spectrum and then examine and quantify certain parameters of its shape. These interfaces are implemented as digital in order to get a detailed enough spectrum representation required for its shape analysis.
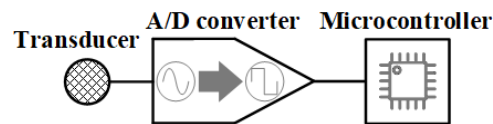

Figure 2.8: Spectral shape-based wake-up sensor interface generalized architecture block schematic.

Interface architectures utilizing cepstral coefficients entail estimating the signal's spectrum, dividing it into sub-bands, calculating the logarithm of the sub-band amplitudes or powers, and then performing discrete cosine transformation on them, generating a cepstrum. The amplitudes of the cepstrum peaks represent cepstral coefficients. While interfaces utilizing these features are most often implemented as fully digital, mixed-signal implementations are also possible, employing analog domain filtering and squaring followed by analog-to-digital (AD) conversion and digital domain logarithm calculation and discrete cosine transformation (Fig. 2.9).
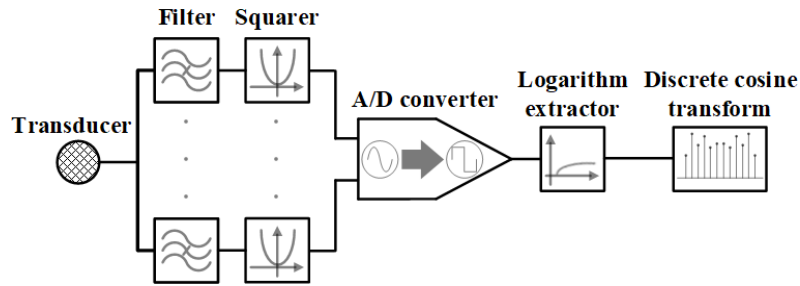
Figure 2.9: Cepstral coefficient-based mixed-signal wake-up sensor interface generalized architecture block schematic.

Looking further at the results of the SOTA analysis (Table III) it can be seen that acoustic wake-up sensor interfaces generally have high detection accuracies (over 90% true positives and under 15% false positive, where stated) regardless of their architecture. However, their power consumptions vary significantly, from around 10 nW to around 600 µW, greatly depending on the interface implementation and the utilized feature, with integrated mixed-signal and digital spectro-temporal decomposition interfaces reaching sub-µW power consumptions, contrasted by embedded level-crossing rate interfaces reaching tens or even hundreds of µW.

It is also clear that integrated custom implementations dominate the wake-up sensor interface design, accounting for 69% of all analyzed acoustic wake-up sensor interfaces, while embedded implementations utilizing COTS components constitute around 31%.

The number of architectures that extract the features in purely analog or digital domain is approximately the same, with only a few detectors extracting features in both domains simultaneously (around 10%).

2.4.1 Architecture selection

A set of criteria is developed to further narrow down the list of features utilized in acoustic wake-up interfaces to just those applicable for the passing motor vehicle detection use-case, with the aim of developing a wake-up sensor interface for detection of sporadic, transient acoustic events, lasting for several seconds, with the bandwidths spanning up to 2.5 kHz.

The desired wake-up interface architectures should allow for embedded implementation, utilize COTS components, extract and process features in the analog domain, thus avoiding power-hungry analog-to-digital (AD) conversion [16]. These interfaces should be directly

connected to acoustic sensors, preferably with no need for amplification, and should therefore reliably operate with weak electric input signals (on the order of 10 mV).

Finally, a wake-up sensor interface must have high detection accuracy, which entails both high true positive rates, as a detector should not miss events of interest, and low false positive rates, because false detections lead to wasting power through unnecessary activations of the power-hungry main stage of the sensor node.

The visual representation of these criteria and the interface selection based on is presented in Table IV.

Table IV Sensor interface selection

Interfaces utilizing	Criteria			
	Applicable for signals of interest	Embedded implementation	No AD conversion	Detection accuracy
Correlation	✓	✗	✗	✓
Level-crossing rate	✓	✓	✓	✓
Spectro-temporal decomposition	✓	✓	✓	✓
Other features	✓	✗	✗	✓

As can be seen from Table IV, wake-up sensor interfaces utilizing level-crossing rate and spectro-temporal decomposition met all our selection criteria and therefore became the focus point of our further research.

2.5 Spectro-temporal decomposition and level-crossing rate wake-up sensor interfaces

Seeing how the level-crossing rate and spectro-temporal decomposition interfaces met our criteria, an embedded implementation of each was developed, utilizing COTS components, and

tested their functionality in detecting passing speedboats. The goal of this study was to determine and evaluate the importance of the sparsely explored impact of feature choice on the interface's architecture and its functionality, by determining the interface's power consumption, implementation complexity, minimal input voltages and operation with signals of varying SNR.

2.5.1 Spectro-temporal decomposition detector implementation

An embedded spectro-temporal decomposition wake-up interface using spectro-temporal envelope was developed and characterized in [Pub5] (schematic and photograph shown in Fig. 2.10).
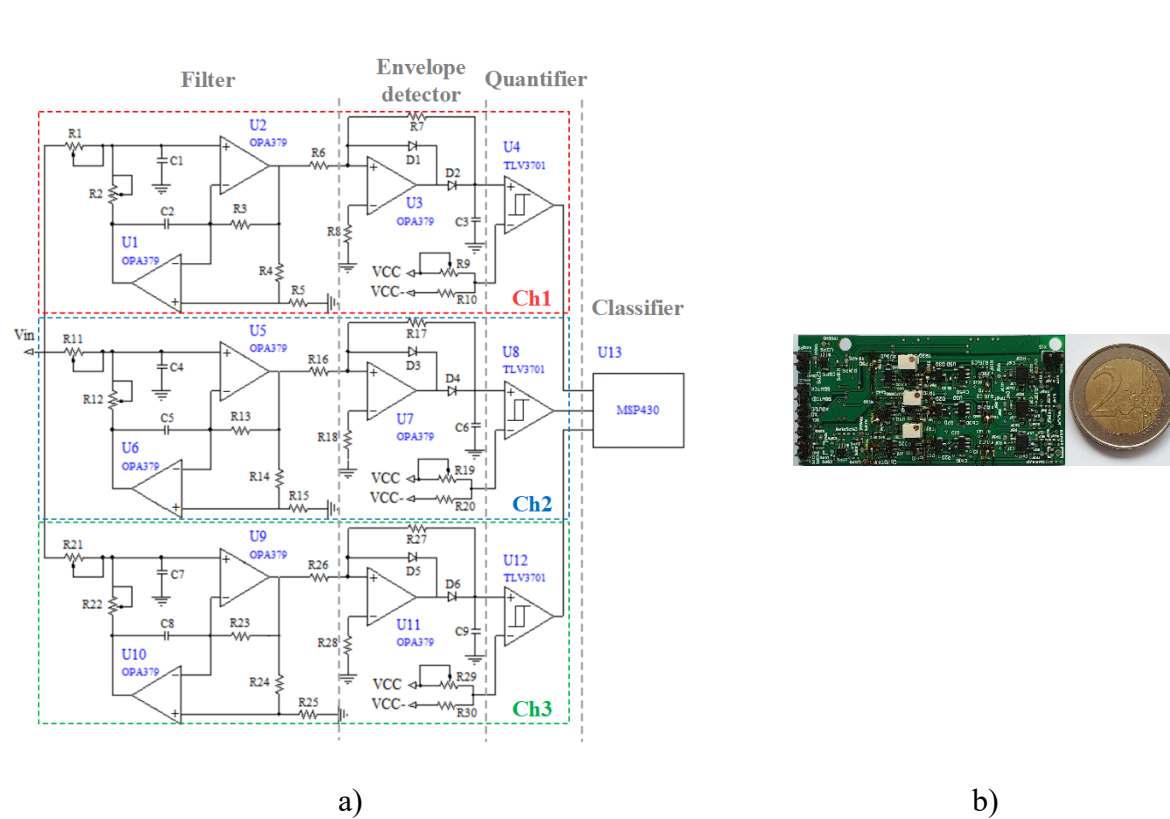

a)   b)

Figure 2.10: An embedded spectro-temporal decomposition wake-up sensor interface implemented using COTS components: a) schematic and b) photograph.

The developed sensor interface consists of three channels, that decompose the input signal into frequency bands using a digitally programmable active bandpass filter in the general impedance converter (GIC) topology, implemented with two MCP6142 operational amplifiers. The first channel covers the frequency band from 200 Hz to 500 Hz, the second spans the

frequency band from 500 Hz to 1 kHz and the third covers the band from 1 kHz to 2.5 kHz. Both the central frequency and the pass band width of each filter are digitally programmable (within each channel's limits) in 256 steps using AD5144 digital potentiometers.

After filtering, an active voltage doubler, consisting of a MCP6141 operational amplifier and two diodes, is used to extract the envelope, which is then quantified by a TLV3701 comparator, with a digitally adjustable threshold, adjusted by an AD5144 potentiometer.

Quantified envelopes form spectro-temporal binary sequences which are sent to a 3-channel digital binary template-matching state-machine classifier implemented on an MSP430F2013 low-power microcontroller, which also stores a preprogrammed template representing the signal of interest. If the spectro-temporal sequences generated by the quantified envelopes match the preprogrammed template, a wake-up signal is generated to trigger a more power-hungry digital audio signal processing stage. The state-machine compares the comparator outputs in each state S_0, …, S_k, to the prestored 3-channel template. A more detailed explanation on the basics of the state-machine implementation can be found in [9].

2.5.2 Level-crossing rate detector implementation

As part of [Pub2] a novel embedded level-crossing rate detector is developed and presented, as an improved adaptation of a detector presented in [13] (schematic and photograph shown in Fig. 2.11).

The level-crossing wake-up sensor interface consists of three main parts. In the first part, each time the input signal crosses a preset level, a TLV3701 comparator with an adjustable threshold changes its output. Every comparator output change to high state triggers a monostable (consisting of two SN74AUP1G02 NOR gates) to generate a pulse of fixed duration and amplitude. These pulses are then summed up by a passive RC-circuit, whose output is therefore a representation of the number of times the input signal crossed the preset level.

The second part is a timer consisting of a capacitor connected to a TLV3701 comparator with an adjustable threshold. The capacitor is charged by a fixed voltage source over a trimmer resistor and its charge time is determined by the trimmer resistor value and comparator threshold. Once the capacitor voltage reaches the comparator threshold, the comparator output changes, which closes the S1 switch (TMUX1101) propagating the RC-circuit voltage to the quantifier as the final interface part. Following this, after an interval determined by the delay line parameters,

the reset switches S2 and S3 (TMUX1101) connected to the RC-circuit and timer close, connecting their capacitors to the ground and allowing them to fully discharge. During this reset the S1 switch opens and disconnects the RC-circuit from the quantifier. After the RC-circuit and timer resets are complete, the reset switches S2 and S3 open and a new timer interval starts.

The final part, the quantifier consists of two TLV3701 comparators with adjustable thresholds and an AND logic gate. If the propagated RC-circuit voltage is both higher than the lower threshold and lower than the higher one, the level-crossing rate is within the set bounds, an event of interest is detected and a wake-up pulse is generated, at the AND gate output.
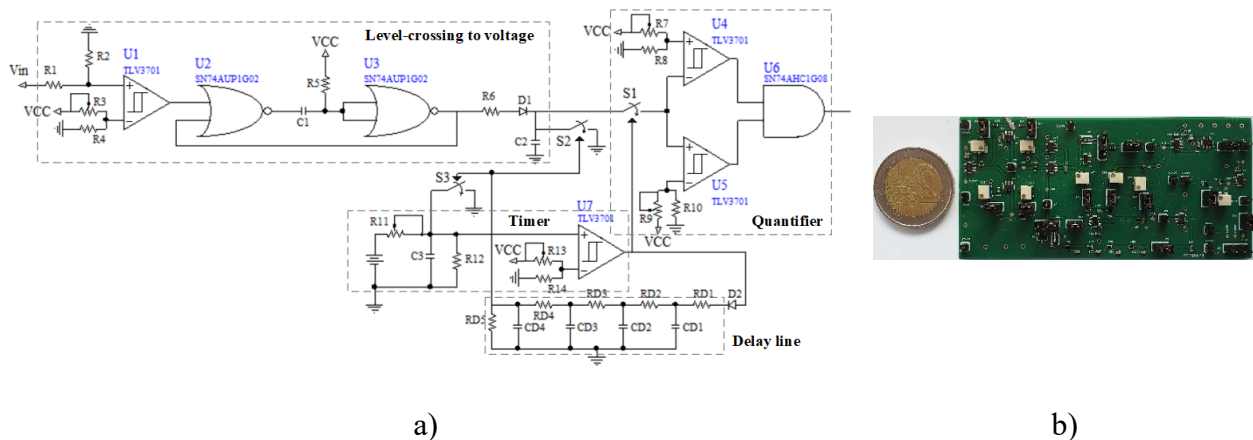

a)   b)

Figure 2.11: Novel level-crossing rate wake-up detector: a) schematic and b) photograph.

2.5.3 Architecture comparison results

In the results of [Pub2] both analyzed wake-up sensor interface architectures were shown to be applicable in detecting passing motor vehicles. These results also showed that the level-crossing rate interface has a significantly lower component count (around 40%) and power consumption (over three times), requires a smaller area to implement (around 40%), and is operational with two times lower input voltages, while the spectro-temporal interface performs slightly better with low-SNR signals. These results proved the importance of feature choice on low-power interface architectures and functionalities and presented the level-crossing rate as a novel interface architecture solution which shows potential for outperforming the more conventionally utilized spectro-temporal decomposition interface in detecting sporadic transient acoustic events.

The spectro-temporal decomposition interface's higher architecture complexity and power consumption were in no small part due to the fact it required multiple channels to perform the same task the level-crossing rate interface did with a single. Considering this disadvantage, the spectral signatures of the signals of interest were reconsidered, with the idea of exploring the possibility of reducing the number of channels of the spectro-temporal decomposition interface. This exploration showed that reducing the number of channels past an application-specific minimal number would either lead to reduced detection accuracy due to reduced spectral coverage, or increased power consumption from the frequent tuning of the channels' frequency characteristics during the interface operation.

Chapter 3

Spectro-temporal decomposition interface

The spectro-temporal decomposition interface is the most frequently utilized and most researched of acoustic wake-up sensor interfaces, due to its high detection accuracy, low-power consumption, relatively simple architecture, multiple implementation options and a broad application range.

Following the basic architecture description presented in subchapter 2.5.1, a spectro-temporal decomposition sensor interface was developed and characterized in detail (Fig. 3.1 a) – d)).
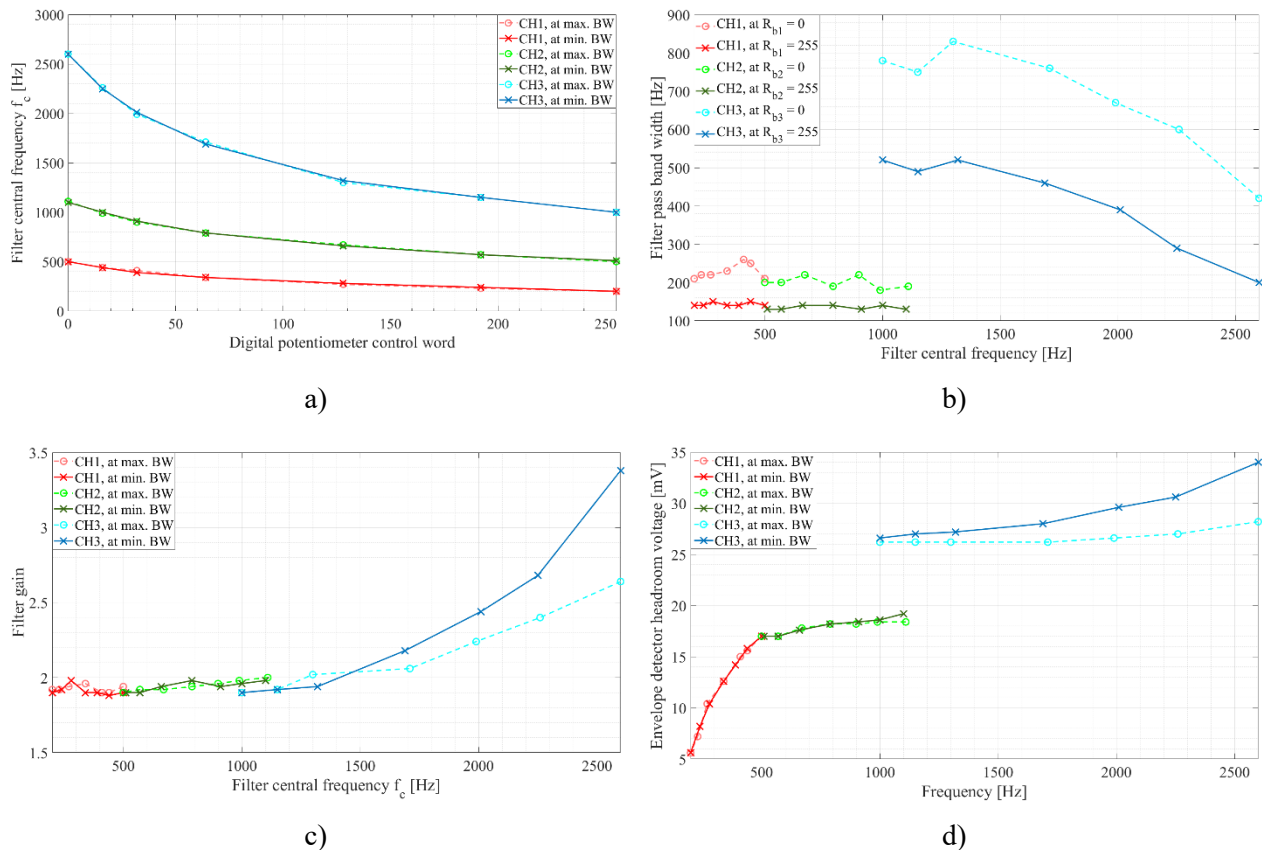
Figure 3.1: Spectro-temporal decomposition wake-up sensor interface prototype characterization: a) filter central frequency with potentiometer control word b) filter pass band width with digital potentiometer control word, c) filter passband gain with its central frequency, d) envelope detector output headroom voltage with frequency.

Results of the characterization were divided into two groups, the first showing the adjustable ranges of each channel's programmable parameters, its filter central frequency (Fig. 3.1 a)) and bandwidth (Fig. 3.1 b)) and the second showing the effects of nonidealities (Fig. 3.1 c) and d)). The programmable parameters and their programming accuracies are of crucial importance because they allow the interface to be tuned to different frequency ranges which allows it to detect different events of interest.

Figure 3.1 a) shows the range of filtering channels' central frequencies f_c with values of digital potentiometers R_2, R_{12}, and R_{22} (Fig. 2.5 a)). As can be seen, all the channels were successfully implemented to have the desired range of adjustable central frequencies as described in subchapter 2.5.1, with the central frequency of CH1 being adjustable from 200 to 500 Hz, of CH2 from 500 to 1100 Hz, and of CH3 from 1.0 to 2.6 kHz.

As can be seen from Fig. 3.1 b) the first two channels, CH1 and CH2, are tuned to operate with narrow pass band widths of $B = 150 - 200$ Hz by R_1 and R_{11} respectively (Fig. 2.5), while the third channel, CH3, is enabled to operate with broader bands of $B_l = 500 - 800$ Hz at its lower central frequencies and $B_h = 200 - 500$ Hz at higher ones, set by R_{21}.

Ideally, the gain of each channel's filter should be around 2, but seeing how higher-frequency signals typically exhibit lower power-spectrum density, the frequency-dependent gain of the third channel's filter was used to increase its outputs at higher frequencies, as seen in Fig. 3.1 c).

Finally, the output headroom voltage of each channel was measured (Fig. 3.1 d)) as the ripple-free voltage difference between the envelope detector's output voltage with no input and its lowest steady-state output voltage with a given input, floating around $V_{ref} = 0.9$ V. The overall channel sensitivity was defined as the ratio of the output headroom voltage and the input voltage.

The envelope detectors play a crucial role in determining the channel's overall sensitivity, limiting an architecture using an active envelope detector to operation with input signals with amplitudes of at least 5 mV, while other architectures, that utilize passive envelope detectors require even higher input voltages, with amplitudes of at least around 20 mV. Our research was therefore focused on improving the envelope detectors to alleviate the chokepoint in this spectro-temporal decomposition interface architecture.

3.1 Envelope detector

State-of-the-art spectro-temporal decomposition wake-up sensor interfaces usually incorporate envelope detectors or trackers, used to extract the features of interest from the input signals. The envelope detector output is usually quantified by the following interface stage to evaluate the feature of interest. This quantization depends on the envelope detector output signal, which can be defined by its characteristic values of rise time, fall time and headroom voltage (Fig. 3.2).
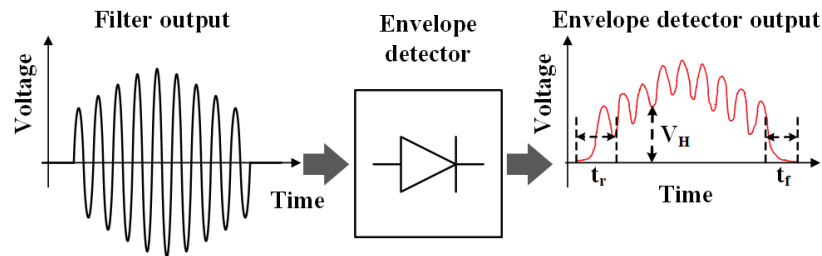

Figure 3.2: An envelope detector's output signal waveform and characterizing values. Envelope detector output signal characterizing values: t_r – rise time, t_f – fall time, V_H – headroom voltage.

As can be seen from Fig. 3.2, the envelope detector's output headroom voltage (V_H) is the ripple-free voltage difference between the envelope detector's output voltage with no input and its lowest steady-state output voltage with a given input. It plays a crucial role in determining the whole interface's detection accuracy, because low headroom voltage values make it impossible to set an appropriate threshold that would allow reliable feature quantization in the following interface stage.

Additionally, the timing parameters were also considered through the rise time (t_r), defined as the time required for the output signal to stably rise from the baseline to half the headroom voltage and the fall time (t_f), defined as the time it took the output signal to settle back to baseline from half the headroom voltage. These parameters define which events the interface can detect, because the interface can not detect events shorter than its rise time and can not distinguish between two event closer in time than its fall time.

However, despite their frequent use in spectro-temporal decomposition wake-up sensor interfaces, the envelope detectors exhibit low energy efficiency, which drives the sensitivity of the entire interface down, lowering one of its crucial parameters, the detection accuracy.

A lot of research has therefore been focused on developing efficient envelope detectors. In [75] the authors present a passive envelope detector operational with input voltages as low as 100 mV at frequency ranges from DC to 100 MHz. In [76] a 10 nW low-power envelope detector is presented, operational with input voltages of 50 mV at 50 Hz frequency. The authors in [77] present a low-power envelope detector with a power consumption of around 100 nW, that can operate with input voltages over 100 mV at a frequency of 4 Hz. It should also be noted that all these envelope detectors ([75]–[77]) were implemented as custom-made integrated detectors.

The functionalities of several passive and active envelope detectors utilizing COTS components were compared. The examined detectors included three conventional detectors, the single-diode passive half-wave detector, the two-diode passive half-wave voltage doubler (Greinacher circuit), and the amplifier-based active two-diode half-wave detector (Fig. 3.3 a) – c)). Additionally, a novel concept adopted from weak-signal vibration energy harvesting [78]– [80] was considered, the active full-wave envelope detector with a switched inductor (Fig. 3.3 d)), not previously utilized in weak-signal estimation or detection.
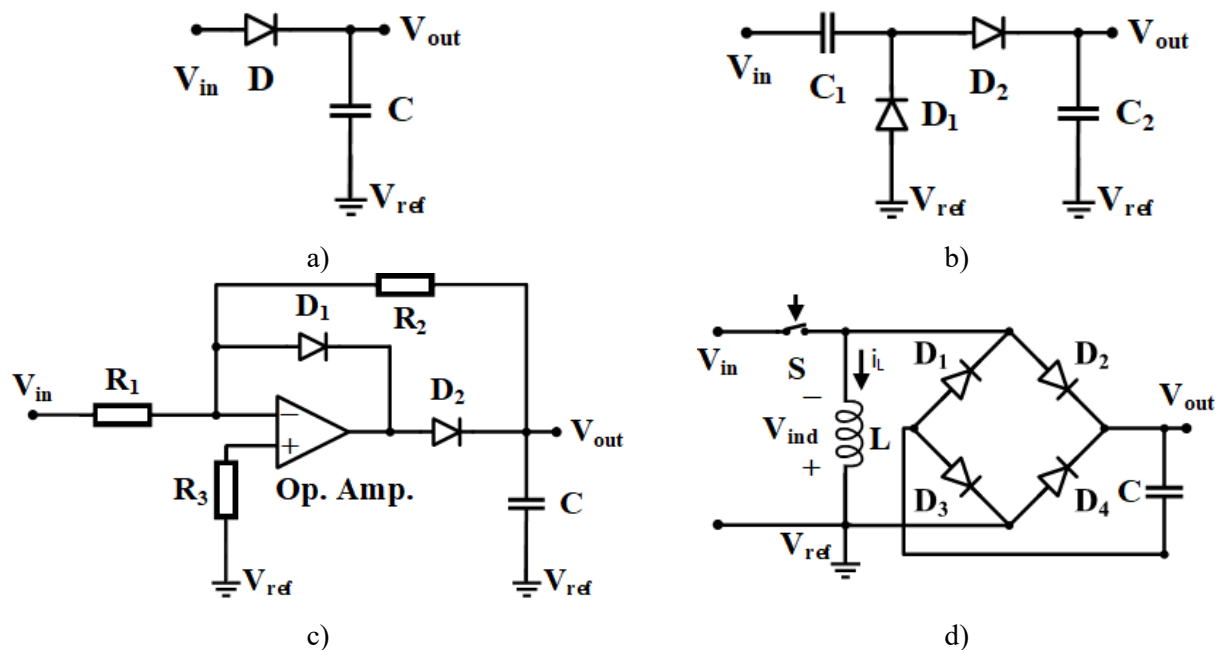

Figure 3.3: Envelope detector topologies a) passive single-diode half-wave envelope detector, b) passive two-diode half-wave voltage doubler (Greinacher circuit), c) active two-diode half-wave voltage doubler utilizing an operational amplifier and d) active full-wave envelope detector utilizing a switched inductor.

Even though the comparison results (presented in greater detail in [Pub8]) showed the conventional active amplifier-based envelope detector topology performed best, it also pointed to the great potential of the novel switched inductor envelope detector, motivating its further examination and design improvements.

3.2 Envelope detector with a switched inductor

The study of envelope detectors pointed to employing switched inductors as a potential solution for the conventional envelope detector's limited energy efficiency. As can be seen from Fig. 3.3 d) the switched inductor consists of a switch connecting and disconnecting an inductor to a voltage source, using the inductor's voltage induction principle to create a voltage boosting effect.

In this way the switched inductor increases the efficiency of the envelope detector, by boosting its input voltage, $V_{in}(t)$, prior to rectification, which allows the input signal to bypass the envelope detector's diodes' nonlinearity that causes low-voltage signals to be suppressed more.

While the switch S is closed, the input signal energy is stored in the magnetic field of the inductor, L, which changes the inductor's current by Δi_L:

$$\Delta i_L = \frac{1}{L} \int_{t_1}^{t_2} V_{in}(t) dt \tag{4}$$

where $V_{in}(t)$ is the input signal voltage and t_1 and t_2 are the beginning and ending moment of storing energy in the inductor's magnetic field, respectively.

At the time instant t_o, when the switch opens, the energy stored in the inductor's magnetic field generates an induced voltage, V_{ind}:

$$V_{ind} = L \frac{di_L(t)}{dt} \bigg|_{t=t_o} \tag{5}$$

The inductor current time derivation at t_o can be approximated as:

$$\frac{di_L(t)}{dt} \bigg|_{t=t_o} = \frac{i_L(t_O)}{\Delta t} = \frac{\frac{1}{L} \int_{t_C}^{t_O} V_{in}(t) dt}{\Delta t} \tag{6}$$

where $i_L(t_o)$ is the inductor current at the switch opening instant, t_c is the switch closing time instant, and Δt is the time required for the inductor current to fall to zero.

If the induced voltages on the inductor are high enough to pass over the diodes' thresholds, they charge the output capacitor, reaching a steady state output voltage:

$$V_{out\_ss} = \frac{\int_{tc}^{to} V_{in}(t)dt}{\Delta t} - 2 \cdot V_D \tag{7}$$

where V_D is the diode threshold voltage.

Neglecting energy losses, the maximal obtainable envelope detector output voltage V_{out_max} depends on the inductance L, capacitance C, and the current through the inductor at the instant the switch opens, $i_L(t_o)$ (8) [81].

$$V_{out\_max} = i_L(t_O) \cdot \sqrt{\frac{L}{C}} \tag{8}$$

While the output capacitor C is not being charged, it gradually discharges (as seen in Fig. 3.4) due to the leakage currents of the reversely polarized diodes and the input impedance of the next interface stage.

In addition to the increased energy efficiency and sensitivity that a switched inductor provides the envelope detector, through our research the possibility of using it as filter for the input signal was also explored, which would allow it to replace two components of the conventional spectro-temporal decomposition detector and further lower its power consumption.

Authors in [82], [83] presented the switched inductor filter, which was used to electrically tune the inverter outputs' frequency characteristics, by suppressing unwanted harmonics. A simulation model of a switched inductor filter was developed and its electrically tunable frequency characteristic were explored, with its dependency on the switch control function's duty cycle as its tuning parameter.

Through several steps, presented in greater detail in [Pub3] and [82], it can be shown that the effective value of the filter inductance L_{feff} is proportional to:

$$L_{feff} \propto \frac{L_f}{A_0{}^2} \qquad (9)$$

where A_0 represents the switching function average value (dependent on the switching function's duty cycle) and L_f represents the filter's inductor actual value. This led to the conclusion that the switching function's duty cycle can be used to tune the filter's frequency characteristic.

By studying this filter and its frequency characteristics, it was concluded that, with proper adjustments, the switched inductor can also be employed as an electrically tunable filter.

More results concerning both the voltage boosting and filtering characteristics of a switched inductor can be found as part of [Pub3].

3.2.1 Electrically switched inductor

Following our exploration of potential advantages of applying a switched inductor to an envelope detector, further improvements to our design of the envelope detector with an electrically switched inductor used in the experiments in [Pub8] were implemented.

Using this approach, inspired by the switched inductor bandpass filter [82], [83], and the switched inductor energy harvester [80], [84], [85], a novel, low-power, frequency selective, voltage boosting feature extractor (Fig. 3.4 a)) is devised, operational with signals under 5 mV peak-to-peak in the low acoustic frequency range, from 100 Hz to 1 kHz. In this interface the switched inductor acts as both part of the filter and the envelope detector.

In examining this feature extractor, several of its characteristics were considered, with the first being its sensitivity (Fig. 3.4 c)), i.e., the ratio of output headroom voltage and input voltage. Next, the stopband sensitivity was considered, because the maximal expected stopband voltage defined the lowest passband voltage levels with which the interface could reliably detect events (spurious-free range, Fig. 3.4 b). This led to the next considered characteristic, the frequency selectivity, i.e., the difference between the interface's passband and stopband sensitivities (Fig. 3.4 b) and c)). The final considered characteristic was the extractor's power consumption.
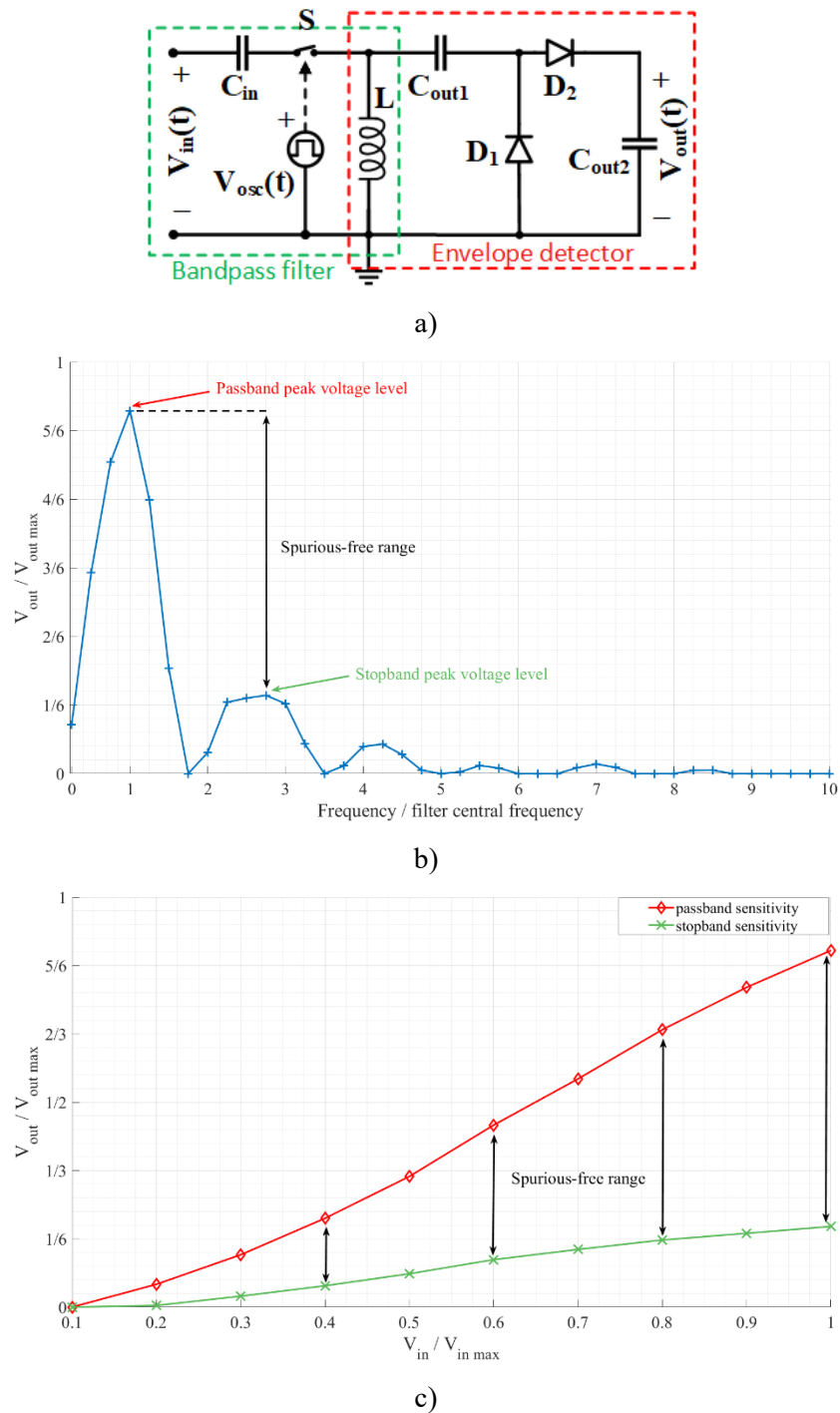
a)

b)

c)

Figure 3.4: a) Proposed feature extractor (with marked bandpass filter and envelope detector blocks), b) normalized frequency characteristic and c) normalized output headroom voltage with input voltage.

From the feature extractor's principles of operation and its desired characteristics, its key design parameters were determined and divided in two groups: switch control signal parameters and passive component values.

The considered switch control signal parameters were the switch control signal frequency, duty cycle, and delay between the switch control and input signal (the switch is controlled by an independent voltage signal $V_{osc}(t)$, as shown in Figure 3a).

The considered passive components were the input capacitor C_{in}, the inductor L, Q factor of the input switched inductor filter, and output capacitors, C_{out1} and C_{out2}, which were analyzed in detail in our previous work [86], [87]. The diodes were also chosen based on previous work analyzing their influence on weak-signal rectifier performance [88], [89].

Both a simulation model and a hardware prototype were developed and all the afore mentioned parameters and their interactions were examined, with all the simulation and experimental results presented in [Pub3].

In addition to the presented results, several other simulations were performed, exploring the optimal switching frequency for a given signal of interest (and consequential filter central frequency setting) and examining the influence of the inductor's inductance on the peak attainable sensitivity.

In simulations concerning the switching frequency, it was concluded that the optimal number of switch openings per input signal period, from the perspective of sensitivity, is two (Fig. 3.6). Seeing how the induced voltage on the inductor is dependent on the integral of the input sinusoidal signal, opening the switch less than two times per period would lead to lowering of the induced and consequentially the output voltage, as sinusoidal signals have highest integral values when integrated over half of their period. Opening the switch more than two times would lead to more occurrences of induced voltage, but of proportionally lower induced voltages. Seeing how the diodes in the envelope detector are nonlinear, these multiple lower voltages would lead to an overall lower output voltage. Additionally, it should be stated that while more than two switch openings per input signal period reduces the interface sensitivity, it also lowers the interface's susceptibility to the time delay between the input and switch control signal, as more openings mean each contributes less to the overall output voltage, which means that optimal positioning of each opening instant is less crucial.
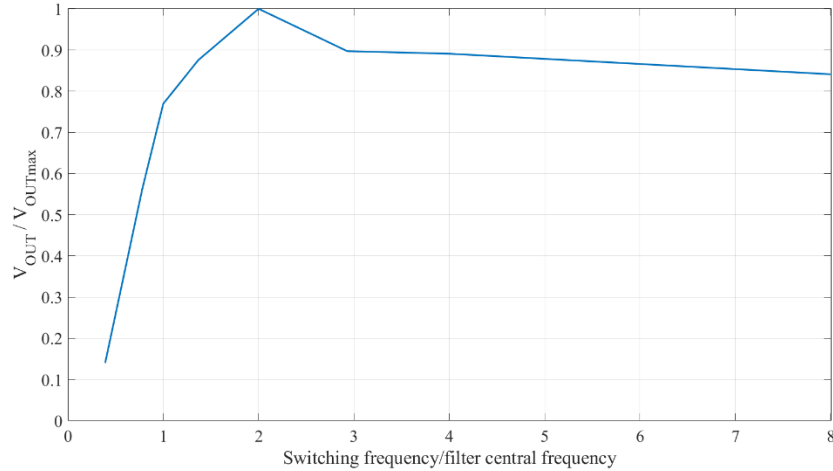
Figure 3.5: Output voltage with switch control signal frequency. Switch control signal duty cycle set to 50%. Input signal frequency set to filter central frequency. Output voltage normalized with regards to maximal output voltage (which occurs with switching signal frequency set to twice the filter central frequency) and switching signal frequency normalized with regards to filter central frequency.

In the simulations concerning the switched inductor circuit's maximal obtainable sensitivity an analytical expression of the circuit's sensitivity in dependance on the input signal frequency ω and the values of the output capacitance C, the inductor's inductance L and parasitic resistance R_L was established.

$$\frac{V_{out}}{V_{in}} = \frac{1}{\sqrt{C_{out}}} \cdot \frac{1}{\sqrt{L \cdot \left(\omega - \frac{\omega_R^2}{\omega}\right)^2 + \frac{R_L^2}{L}}} \tag{10}$$

As can be seen from Fig. 3.6, these simulations showed that if the input signal frequency is set precisely to the resonant frequency of the switched inductor circuit, the switched inductor circuit sensitivity constantly increased with inductance. However, if the input signal is not precisely tuned to match the switched inductor circuit's resonant frequency, then there is a finite inductance value for which maximal sensitivity is obtained.
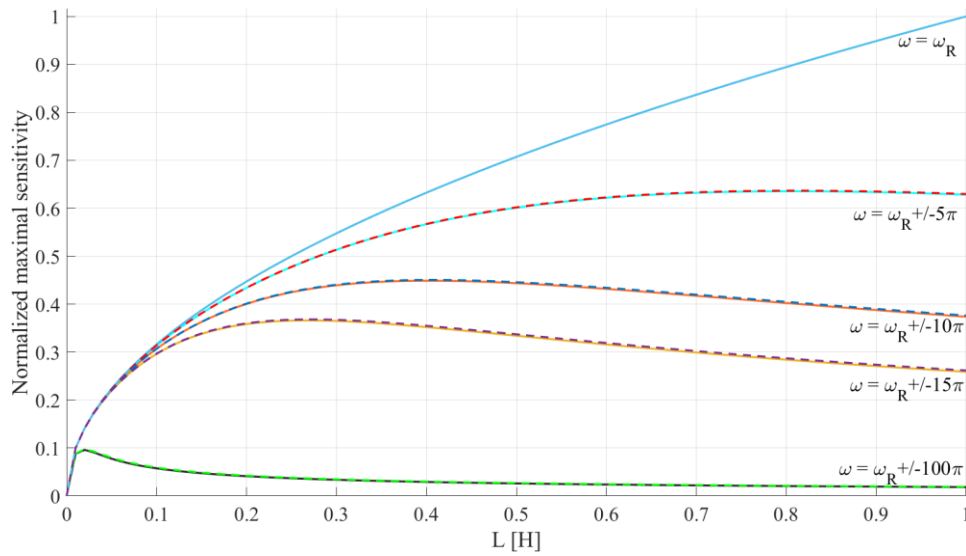
Figure 3.6: Switched inductor circuit's maximal obtainable sensitivity with inductance L. Resonant frequency set to $\omega_R = 655 \cdot 2\pi$ Hz, capacitance value $C_{out} = 1$ µF and inductor's resistance $R_L = 7.1$ Ω.

This study led to the conclusion that the novel interface utilizing the electrically switched inductor was not only applicable for detection of passing motor vehicles (speedboats), but also outperformed a modified version of our conventional spectro-temporal decomposition wake-up sensor interface from [Pub5] being operational with four times lower input voltages, while having around 43% lower power consumption, thus enabling life-time extension or improved detection accuracy.

3.2.2 Mechanically switched inductor

Finally, after the switched inductor was proven applicable in low-power sensor interfaces for sporadic acoustic event detection with improvement to their functionality and reduction of their power consumption, a novel passive electromechanical acoustic signal feature extractor in low acoustic frequency range (200–1000 Hz) was devised, consisting of a piezoelectric vibration transducer and an envelope detector utilizing a mechanically switched inductor.

A simulation model of the novel feature extractor was developed, and with it a simulation study was performed, and a proof-of-concept device was developed and experimentally characterized. Its applicability in sporadic acoustic event detection was demonstrated through a case-study of detecting passing speedboats and its advantages compared to the active electrical

feature extractor utilized as part of the interface presented in [Pub5] were shown. At the time, this presented one of the first attempts in literature of using passive electromechanical elements to further lower the power consumption of low-power analog wake-up event detector interface.
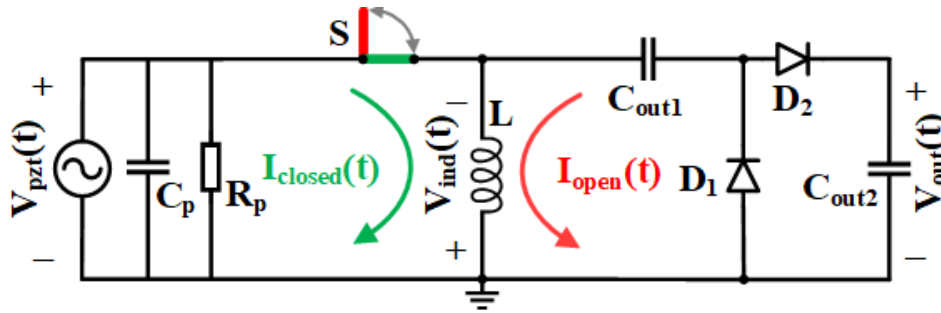

Figure 3.7: Schematic of the proposed passive electromechanical feature extractor (PEM FE). Green— current $I_{closed}(t)$—passing through the PEM FE while the switch S is closed. Red—current $I_{open}(t)$ passing through the PEM FE when the switch S opens. L—inductor and C_{out1}, C_{out2}—rectifier capacitors, D_1, D_2— rectifier diodes. R_P and C_P—parasitic resistance and capacitance of piezoelectric transducer, respectively. $V_{pzt}(t)$—voltage generated at piezoelectric transducer, $V_{ind}(t)$—voltage induced at the inductor, $V_{out}(t)$— extractor output voltage.

The mechanical structure of the proposed passive electromechanical feature extractor (PEM FE) (Fig. 3.7) is based on the Random Mechanical Switching Harvester on Inductor (RMSHI) [80], [90], developed for vibration energy harvesting utilizing a piezoelectric transducer. The motivation of using elements of this energy harvester came from its key advantage of high energy conversion efficiency [91], stemming from its non-resonant frequency response and utilization of a mechanically switched inductor.

The mechanical part of the feature extractor consisted of a metal cantilever beam with a permanent magnet at its free end, a metal stopper that formed a mechanical switch with the cantilever, and a fixed permanent magnet used to modify the elasticity of the vibration driven cantilever movement. A piezoelectric transducer was mounted at the base of the cantilever beam to transforms input vibrations into an electrical signal. The cantilever movement switches the mechanically switched inductor which is connected to an envelope detector that conditions the resulting electric signal.

When no external force was applied to the feature extractor, the repulsive force between its pair of magnets placed the beam in contact with the stopper (as shown in Fig. 3.7). While the

beam was in contact with the stopper, only its part in front of the stopper moved, while the whole beam moved only when the external force overcame the magnetic bias force. This two-part movement caused the beam to have a non-resonant, broader frequency characteristic, which was further explained in [90], [91].

When the beam and the stopper are in contact, the switch S is closed, and the piezoelectric transducer signal energy is stored in the inductor's (L) magnetic field (Fig. 3.7, green details). When the switch opens, the energy stored in the inductor's magnetic field, E_L, is transferred over the rectifier to the energy of the output capacitor's (C_{out2}) electric field, E_C, charging the capacitor to V_{out} (Fig. 3.7, red details). The switching of the inductor induces voltage, $V_{ind}(t)$, higher than the voltage generated by the piezoelectric transducer, $V_{pzt}(t)$, and the diode threshold, making the switched inductor a voltage booster. A more detailed description of the process can be found in [80], [90], [91].

With the presented passive electromechanical feature extractor several sets of simulations and measurements were performed. In the first group of measurements the extractor's transfer characteristic were determined, relating its output voltage to input vibration energy. In the second group the extractor's frequency selectivity was evaluated, comparing outputs for in-band and out-of-band vibration inputs. In the third group of measurements, the output capacitor choice and its influence on the output voltage ripple and rise and fall times was examined. Finally, a comparison of this novel feature extractor to a previously developed conventional active feature extractor from [Pub5] was performed, using various synthetic sinusoidal signals, as well as prerecorded passing speedboat signals. Additional details on the exact physical implementation of the extractor used in the study, as well as the experimental setup, procedure and results can be found in [Pub4].

The experiments in this research showed that the interface with the passive feature extractor was operational with two times lower input signals than our conventional spectro-temporal decomposition wake-up interface from [Pub5], was more robust in low SNR conditions (around 10 times less output headroom voltage loss for SNR range from −10 dB to 40 dB) and would decrease power consumption of a detector's channel by over 72%, enabling life-time extension and/or increased quality of detection with larger number of channels.

3.2.3 Comparing the electrically and mechanically switched inductor

Comparing the interfaces featuring the electrically and mechanically switched inductor led to several conclusions. The most obvious advantage of the mechanically switched inductor is that it extracts the envelope or energy of a given frequency band completely passively, using the energy of the event of interest, while the electrically switched inductor requires power for the switch control oscillator and the electrical switch itself (though this is almost negligible compared to the oscillator power consumption). The mechanical switch inherently has a bandpass frequency characteristic if designed properly, which makes filter implementation, as well as the overall electric circuit design rather straightforward. The permanent magnets can also be used to finely tune the frequency around the one determined by the mechanical properties of the switch. Additionally, seeing how the switching is driven by the occurrence of the event of interest, there is no need for additional synchronization between the input signal and the switching action.

At the added expense of a slightly higher power budget, the electrically switched inductor also showed certain advantages. While the circuit was more complex, to attain the bandpass characteristic inherent to the mechanically switched inductor, the electrically switched inductor had a lot finer control over the switching process, with switch control frequency, state duration (duty cycle) and switching instant completely under the control of the system designer. While this added complexity it also opened many additional options and design parameters not available with the mechanical switch. Additionally, this should allow the electrically switched inductor to achieve higher sensitivities than the mechanically switched one, if the optimal switching control is implemented.

It should also be stated that the developed feature extractor with the mechanically switched inductor was non-resonant, while the one with the electrically switched inductor was resonant.

Finally, the mechanically switched inductor interface would also allow easy implementation of energy harvesting, potentially enabling the design of zero-power or transient sensor interfaces, active only when an event of interest is present, generating enough power for their operation, while spending no power when there is no potentially interesting activity [7], [12], [54]. This is envisioned as the future of ubiquitous sensing, allowing the development and maintenance-free deployment of sensor networks consisting of thousands of small, light-weight and fully

autonomous sensor nodes. In [7] the authors postulate that near-zero-power consumptions in sensor interfaces will be achieved through utilization of electromechanical components.

Chapter 4

Main scientific contributions of the thesis

This thesis has two main scientific contributions:

1) Architectures of low-power sensor interfaces for selected features of low-frequency signals from sporadic events, with results disseminated in [Pub1, Pub2 and Pub5]; and

2) Analysis of applicability of a switched inductor rectifier for detection of low-level signal, with results disseminated in [Pub3, Pub4, Pub6, Pub7 and Pub8].

4.1 Architectures of low-power sensor interfaces for selected features of low-frequency signals from sporadic events

For this contribution the implications of feature choice on the interface architecture and functionality were examined. An analysis of the SOTA wake-up sensor interfaces was performed in [Pub1] and research focus was set towards acoustic signals and their features.

Through research presented in [Pub2] the optimal feature choice for detecting sporadic transient acoustic events was explored and spectro-temporal and temporal feature subsets were recognized as the most promising candidates for this application. A set of criteria was developed and used to evaluate the features' applicability in low-power interfaces for detection of sporadic transient acoustic events. The set criteria determined that the chosen features must allow development of embedded architectures, which were reliably operational with weak input signals (on the order of 10 mV), and extracted and processed features in the analog domain, thus avoiding power-hungry and complex AD conversion.

The spectro-temporal decomposition and level-crossing rate features met all the set criteria. Through research presented in [Pub5] a novel, tunable 3-channel spectro-temporal decomposition-based low-power wake-up sensor interface was developed and characterized, providing an improved energy-efficiency with no loss of accuracy compared to similar designs of the same architecture. In [Pub2] a novel level-crossing rate architecture was developed and the applicability of the two developed architectures in detection of passing speedboats was

examined, with emphasis on the interface power consumption, implementation complexity, minimal input voltages and operation in conditions of low SNR.

The results of this research showed that both architectures were applicable for detection of sporadic transient acoustic events, with true positive event detection rates exceeding 90%. The comparison of architecture performances showed that the level-crossing rate architecture was operational with two times lower input voltages, required around 40% less area and components for its implementation and had over three times lower power consumption, while the spectro-temporal decomposition architecture operated slightly better in conditions of low SNR.

This thesis contribution emphasized the previously sparsely explored but crucial impact of feature choice on interface architecture and its functionality and presented the potential of the novel level-crossing rate interface architecture for outperforming the more conventionally utilized spectro-temporal decomposition interface in detecting sporadic transient acoustic events.

Additionally, the results of the detailed analysis of the spectro-temporal decomposition wake-up sensor interface architecture pointed to its envelope detector as a design chokepoint and led to research for a solution constituting the second contribution of this thesis.

4.2 Analysis of applicability of a switched inductor rectifier for detection of low-level signal

The research of low-power wake-up sensor interface architectures led to a recognition that the low energy-efficiency of the spectro-temporal decomposition interface envelope detector presents the architecture's chokepoint, significantly limiting its sensitivity with a given power consumption. Therefore, a solution to increase the envelope detector's energy-efficiency by employing a switched inductor element was proposed, inspired by its previous use for the same purpose in weak vibration energy harvesting.

The switched inductor consists of a switch connecting and disconnecting an inductor to a voltage source, using the inductor's induced voltage to create a voltage boosting effect. While the switch is closed, the energy of the voltage source is transferred to the inductor's magnetic field, causing the inductor's current to raise. Once the switch opens, the change of inductor current causes the induction of voltage of significantly higher levels than those of the original

source. Additional to its voltage boosting effects, this element also displayed frequency selectivity.

As the first step in analyzing the applicability of the switched inductor in low-power interfaces for weak signal detection, in [Pub8], several passive and active envelope detectors, including the switched inductor envelope detector were developed, characterized, and compared, using synthetic signals in lower acoustic spectrum. Through the results of this study, the switched inductor envelope detector was shown to be a viable option in the application of interest.

Following this, a switched inductor feature extractor was devised to replace both the filter and the envelope detector of the conventional spectro-temporal decomposition interface. In [Pub3] a redesigned envelope detector from [Pub8] was used as basis for developing a feature extractor utilizing an electrically switched inductor. Through research presented in [Pub6], [Pub7] and [Pub4] a novel, fully passive feature extractor utilizing a mechanically switched inductor was developed.

The two novel feature extractors, utilizing the electrically and mechanically switched inductor, allowed for 43% and 72% power consumption reduction, and for a four- and two-times reduction of minimal input voltage, respectively, compared to the conventional spectro-temporal decomposition detector.

This thesis contribution and its related research not only proved the applicability of the switched inductor in low-power sensor interfaces for continuous detection of sporadic transient acoustic events, but also showed the considerable advantages and benefits of its application. This research paves the way for completely passive wake-up sensor interface architectures, featuring microelectromechanical system (MEMS) components driven by the energy contained within the events of interest. Additionally, it emphasizes the importance of the emerging concept of utilizing electromechanical solutions in developing near-zero-power wake-up sensor interfaces.

Chapter 5
List of publications

Pub 1 **Gazivoda, M.**, Bilas, V., "Always-on sparse event wake-up detectors: A Review", *IEEE Sensors Journal*, Early Access, pp 14, 2022, doi:10.1109/JSEN.2022.3162319

Pub 2 **Gazivoda, M.**, Oletić, D., Bilas, V., "Features and always-on wake-up detectors for sparse acoustic event detection", *Electronics*, Vol. 11, Issue 3, pp 14, 2022, doi:10.3390/electronics11030478

Pub 3 **Gazivoda, M.**, Bilas, V., "Low-Power Sensor Interface with a Switched Inductor Frequency Selective Envelope Detector", *Sensors*, Vol. 21, Issue 6, pp 21, 2021, doi:10.3390/s21062124

Pub 4 **Gazivoda, M.**, Oletić, D., Trigona, C., Bilas, V., "Passive Extraction of Signal Feature Using a Rectifier with a Mechanically Switched Inductor for Low Power Acoustic Event Detection", *Sensors*, Vol. 20, Issue 18, pp 19, 2020, doi:10.3390/s20185445

Pub 5 Oletić, D., **Gazivoda, M.**, Bilas, V., "A Programmable 3-Channel Acoustic Wake-Up Interface Enabling Always-On Detection of Underwater Events Within 20 μA", *Proceedings of the 32nd Eurosensors Conference*, Graz, Austria, pp. 1-7, 2018, doi:10.3390/proceedings2130768

Pub 6 **Gazivoda, M.**, Oletić, D., Trigona, C., Bilas, V., "Measurement of Weak Signal Energy at Acoustic Frequencies by using RMSHI as a Passive Conditioning Circuit", *Proceedings of the 2019 IEEE International Instrumentation and Measurement Technology Conference (I2MTC)*, Auckland, New Zealand, pp. 1735–1739, 2019, doi:10.1109/I2MTC.2019.8827042

Pub 7 **Gazivoda, M.**, Trigona, C., Bilas, V., "Weak Signal Detection Utilizing a Mechanically Switched Inductor", *Proceedings of the 8th International Workshop on Advances in Sensors and Interfaces*, Otranto, Italy, 1-6, 2019, doi:10.1109/IWASI.2019.8791307

Pub 8 **Gazivoda, M.**, Oletić, D., Bilas, V., "Characterization and Comparison of Envelope Detectors for Wake-up Sensor Interfaces at Audio Frequencies", *Proceedings of the 2020 IEEE International Instrumentation and Measurement Technology Conference (I2MTC)*, Dubrovnik, Croatia, pp. 1–6., 2020, doi:10.1109/I2MTC43012.2020.9128810

Chapter 6

Author's contributions to the publications

The results presented in this thesis are based on the research carried out during the period of 2017-2022 at the University of Zagreb Faculty of Electrical Engineering and Computing, Unska 3, Zagreb, Croatia, as part of the research project "Young Researchers' Career Development Project – Training of New Doctoral Students – SENSIRRIKA – advanced sensor systems for precision irrigation in karst landscape", IP-2016-06-8379, which was financially supported by the Croatian Science Foundation and a part of the research project "AWAKE – ultra low power wake-up interfaces for autonomous robotic sensor networks in sea/subsea environments", ONRG-NICOP-N62909-17-1-2160, which was financially supported by the U.S. Office of Naval Research Global. The thesis includes eight publications written in collaboration with three coauthors. The author's contribution to each paper consists of conceptualization and performance of the experiments and measurements, as well as methodology development, analysis and presentation of the research results and manuscript conceptualization and writing.

[Pub1] In the paper **"Always-on sparse event wake-up detectors: A Review"** the author presented the first all-encompassing review of wake-up sensor interfaces, to serve as both a starting point for this thesis' research, as well as potential guidelines to other researchers in this field. The paper explains the principle of operation of low-power wake-up sensor interfaces and the advantages of their utilization, presents a taxonomy for wake-up sensor interfaces and shows their sensor modalities, implementations and applications, key parameters and design space limits (in terms of achievable detection accuracies and power consumptions). The author compiled the review material through four years of research, wrote the entire text of the paper and made all the illustrations and data representation, guided by the coauthor. The author also wrote all the code for simulations used in explaining the advantages of the wake-up concept, in MATLAB programming language.

[Pub2] In the paper **"Features and always-on wake-up detectors for sparse acoustic event detection"** the author expanded on the review presented in [Pub1] with a focus on the most frequently utilized wake-up sensor interfaces, the acoustic ones. In this paper an in-depth

analysis of acoustic signal features applicable for low-power event detection is presented and wake-up sensor interface architectures stemming from feature choices are analyzed. Two features, spectro-temporal envelope and level-crossing rate, and wake-up sensor interface architectures applicable for motor vehicle passing detection are identified and developed and general conclusions on their application are presented. The author designed a novel hardware prototype and an improved version of a previously developed prototype (developed by the first coauthor) for testing and created the experimental methodology, performed all the tests and experiments, wrote all the text and developed all figures and supporting material for the paper, guided by the second coauthor and with inputs from the first coauthor.

[Pub3] In the paper **"Low-Power Sensor Interface with a Switched Inductor Frequency Selective Envelope Detector"** the author presented the electrically switched inductor as a novel solution for improving the efficiency of the envelope detector, as a recognized chokepoint of wake-up interface design. The proposed switched inductor envelope detector was shown to be more energy efficient than amplifier-based active envelope detectors and allowed for greater sensitivity than passive envelope detectors. The author made the simulation models and performed the simulations in PSpice for TI SPICE program and developed all the MATLAB coding for measurement acquisition and processing. The author also designed the test hardware, created the measurement setup and methodology, performed the measurements, characterized the circuit, wrote all the text of the paper and made all the figures and other data representation, guided by the coauthor.

[Pub4] In the paper **"Passive Extraction of Signal Feature Using a Rectifier with a Mechanically Switched Inductor for Low Power Acoustic Event Detection"** the author presented the mechanically switched inductor as a novel solution for improving the efficiency of both the filter and the envelope detector (a recognized chokepoint of wake-up interface design) of low-power wake-up sensor interfaces. The proposed envelope detector featuring the mechanically switched inductor represents a major achievement in low-power wake-up sensor interface design as it allows for completely passive feature extraction, while achieving sensitivity levels comparable to active envelope detectors. The author helped the second coauthor in determining parameters for the simulation model, developed all the MATLAB coding for processing the simulation results and prepared the simulation results visualizations. The author

also created the measurement setup and methodology, performed the measurements, wrote all the text of the paper and made all the figures and other data representation, guided by the first and the third coauthor.

[Pub5] In the paper **"A Programmable 3-Channel Acoustic Wake-Up Interface Enabling Always-On Detection of Underwater Events Within 20 µA"** the authors developed and characterized the novel 3-channel spectro-temporal decomposition-based low-power wake-up sensor interface architecture. The developed interface architecture achieved over 90% true positive event detection with a power consumption of around 35 µW, surpassing most other state-of-the-art embedded wake-up sensor interfaces. The author performed the state-of-the-art wake-up sensor interface literature analysis, performed a portion of measurements related to event detection and designed the prototype hardware (following a design previously developed by the first author). The author also gave council on a few final details in the writing of the original paper draft.

[Pub6] In the paper **"Measurement of Weak Signal Energy at Acoustic Frequencies by using RMSHI as a Passive Conditioning Circuit"** the author presented the first attempts of replacing a conventional diode-based envelope detector by an envelope detector featuring the Random Mechanical Switching Harvester on Inductor (RMSHI). This work, together with [Pub7] was the basis for later more extensive work presented in [Pub3] and [Pub4] and presented the initial proof-of-concept research. The author devised the measurement setup and procedure, performed and processed all the measurements, presented all the data and wrote all the text of the paper, in consultation with the coauthors.

[Pub7] In the paper **"Weak Signal Detection Utilizing a Mechanically Switched Inductor"** the author presented the first attempts of utilizing a mechanically switched inductor in weak signal detection. This work, together with [Pub6] was the basis for later more extensive work presented in [Pub3] and [Pub4] and presented the initial proof-of-concept research. The author devised the measurement setup and procedure, performed and processed all the measurements, presented all the data and wrote all the text of the paper, in consultation with the coauthors.

[Pub8] In the paper **"Characterization and Comparison of Envelope Detectors for Wake-up Sensor Interfaces at Audio Frequencies"** the author addressed the envelope detectors as a commonly examined chokepoint of wake-up sensor interfaces. In this work several different

envelope detector designs were examined (both active and passive) and this work presents the first research into characteristics of an envelope detector featuring an electrically switched inductor. The envelope detector featuring the electrically switched inductor achieved higher sensitivity than passive envelope detectors, but had both a higher power consumption and lower sensitivity than a conventional amplifier-based active envelope detector. This work served as proof-of-concept research for the envelope detector with an electrically switched inductor and as a starting point for the later improved envelope detector design and a more detailed study presented in [Pub3]. The author developed the simulation model of the novel envelope detector with an electrically switched inductor in TINA-TI (a SPICE program developed by Texas Instruments) and performed the simulation study and processing of the simulation results. The author also designed and developed the novel envelope detector with the electrically switched inductor and devised the measurement procedure and setup. The author performed and processed the measurements, presented all the data and wrote the text of the paper, in consultation with the coauthors.

Chapter 7

Conclusions and future research

7.1 Conclusions

The research presented in this thesis was focused on always-on low-power wake-up interfaces, utilized in two-stage sensor nodes for lowering power consumption via asynchronous event-driven activation of the sensor node's main stage. Stemming from the intended applications of these interfaces, detection accuracy, implementation complexity and power consumption were recognized as their key design parameters, playing a crucial role in determining a sensor node's overall power consumption and applicability.

An analysis of the SOTA wake-up sensor interfaces was performed, with emphasis on their implementations and utilized sensor modalities and further focus was set towards research of acoustic sensor interfaces, because their signals allowed the design of energy efficient interfaces capable of highly accurate event detection, with minimal power consumptions. This SOTA analysis also pointed to the wide application area of acoustic wake-up sensor interfaces, which constituted over 55% of all SOTA wake-up sensor interfaces presented in literature.

The developed interfaces intended application was detection of sporadic transient acoustic events, generating weak signals (around 10 mV on a passive transducer) in the lower acoustic spectrum (up to 2.5 kHz), lasting from around half a second up to a few seconds. The passing motor vehicle (speedboat) event was chosen as a representative case of this event group.

The acoustic signal features were analyzed, with emphasis on spectro-temporal and temporal features as subgroups applicable in low-power sensor interfaces for sporadic acoustic event detection. The previously sparsely analyzed influence of feature choice on the interface architecture and performance was analyzed in more detail. A set of criteria were developed for selecting features applicable in low-power interfaces for detection of passing speedboats. The set criteria were used to ensure the selected features allowed the development of embedded interface architectures, which were reliably operational with weak input signals (on the order of 10 mV), and extracted and processed features in the analog domain, thus avoiding complex and

power-hungry AD conversion components. Based on these criteria, the spectro-temporal decomposition and level-crossing rate interface architectures were selected and further explored.

Two prototype interfaces were developed and their functionality in detection of passing speedboats was examined, with emphasis on their power consumptions, implementation complexities, minimal input voltages and operation with varying signal-to-noise ratios. The experiments were performed with prerecorded speedboat passing signals with varied levels of added white noise for obtaining varied SNRs. The results of this research showed both architectures were applicable for detection of sporadic transient acoustic events, with true positive event detection rates exceeding 90%. The architecture comparison showed that the level-crossing rate architecture was operational with two times lower input voltages, required around 40% less area and components to implement and had over three times lower power consumption. This emphasized the previously sparsely explored but crucial impact of feature choice on interface architecture and its functionality and presented the potential of the novel level-crossing rate interface architecture for outperforming the more conventionally utilized spectro-temporal decomposition interface in detecting sporadic transient acoustic events.

Considering the operational disadvantage of the increased architecture complexity and power consumption of the spectro-temporal decomposition interface, the spectral signatures of the signals of interest was reconsidered, with the idea of exploring the possibility of reducing the interface's number of channels. This exploration showed that reducing the number of channels past an application-specific minimal number would either lead to reduced detection accuracy due to reduced spectral coverage, or increased power consumption from the frequent tuning of the channels' frequency characteristics during the interface operation.

Further exploration of the spectro-temporal decomposition wake-up interface architecture pointed to its envelope detector as the architecture's chokepoint, limiting the interface's detection accuracy with a given power budget. The nonlinear characteristics of the envelope detector's diodes further attenuated the weak signals characteristic for operation of these interfaces. To alleviate this problem, a solution utilizing a switched inductor was proposed to increase the energy efficiency of conventional envelope detectors. The switched inductor consisted of a switch connecting and disconnecting an inductor to a voltage source, using the inductor's induced voltage to create a voltage boosting effect. While the switch is closed, the energy of the voltage source is transferred to the inductor's magnetic field, causing the inductor's

current to raise. Once the switch opens, the change of inductor current causes the induction of voltage of significantly higher levels than those of the original source. Additional to its voltage boosting effects, this element also displayed frequency selectivity.

Several active and passive envelope detectors were developed, including one utilizing an electrically switched inductor and their performances in detection of synthetic signals in lower acoustic spectrum were compared. Their key operational parameters of headroom voltage and rise and fall times were evaluated. While the switched inductor envelope detector outperformed the two passive envelope detectors, the active operational-amplifier-based one generated higher headroom voltages (better sensitivity) with a lower power consumption.

Following this, a switched inductor feature extractor was devised to replace both the filter and the envelope detector of the conventional spectro-temporal decomposition interface. Simulation models and prototypes of the two feature extractors were developed, one utilizing an electrically and the other a mechanically switched inductor. Using these, multiple simulation and experimental studies were carried out, with both synthetic and real-world signals in the lower acoustic spectrum (up to 2.5 kHz) lasting around a few seconds. The feature extractors utilizing the electrically and mechanically switched inductor allowed for 43% and 72% power consumption reduction, and for a four- and two-times reduction of minimal input voltage, respectively, compared to the conventional spectro-temporal decomposition detector. This not only proved the applicability of the switched inductor in low-power sensor interfaces for continuous detection of sporadic acoustic events, but also showed the considerable advantages and benefits of its application.

7.2 Future research

Three tracks were considered for future research. The first considered research track envisions expanding the applicability studies of developed wake-up interface architectures to other signals of the same sporadic transient acoustic group, such as, for example, diver detection.

The other two tracks focus on further lowering the power consumptions of the developed interface architectures. One way of further reducing power consumption is using the developed embedded prototypes as the basis for developing integrated interfaces with the same architecture. The other track for further reducing power consumption entails development of MEMS solutions for the mechanically switched inductors enabling the design of fully passive electromechanical

wake-up sensor interfaces driven by the energy of the events of interest. This research track shows great promise as it follows the emerging concept of utilizing electromechanical solutions for development of near-zero-power wake-up sensor interfaces.

Bibliography

[1]   M. Alioto, "From Less Batteries to Battery-Less Alert Systems with Wide Power Adaptation down to nWs—Toward a Smarter, Greener World," *IEEE Des. Test*, vol. 38, no. 5, pp. 90–133, Oct. 2021.

[2]   M. Alioto, "IoT: Bird's Eye View, Megatrends and Perspectives," in *Enabling the Internet of Things*, M. Alioto, Ed. Cham: Springer International Publishing, 2017, pp. 1–45.

[3]   N. Goux and F. Badets, "Review on event-driven wake-up sensors for ultra-low power time-domain design," *Midwest Symp. Circuits Syst.*, vol. 2018-Augus, pp. 554–557, 2018.

[4]   Y. Bin Zikria, R. Ali, M. K. Afzal, and S. W. Kim, "Next-Generation Internet of Things (IoT): Opportunities, Challenges, and Solutions," *Sensors*, vol. 21, no. 4, pp. 1–7, Feb. 2021.

[5]   B. Thoen *et al.*, "Saving energy in WSNs for acoustic surveillance applications while maintaining QoS," *SAS 2017 - 2017 IEEE Sensors Appl. Symp. Proc.*, pp. 1–6, 2017.

[6]   G. Rovere, S. Fateh, and L. Benini, "A 2.2-µW Cognitive Always-On Wake-Up Circuit for Event-Driven Duty-Cycling of IoT Sensor Nodes," *IEEE J. Emerg. Sel. Top. Circuits Syst.*, vol. 8, no. 3, pp. 543–554, 2018.

[7]   R. H. Olsson, R. B. Bogoslovov, and C. Gordon, "Event driven persistent sensing: Overcoming the energy and lifetime limitations in unattended wireless sensors," *Proc. IEEE Sensors*, pp. 1–3, 2016.

[8]   M. Fourniol, V. Gies, V. Barchasz, and E. Kussener, "Low-Power Wake-Up System based on Frequency Analysis for Environmental Internet of Things," *Proc. 14th IEEE/ASME Int. Conf. Mechatron. Embed. Syst. Appl.*, pp. 1–6, 2018.

[9]   D. Oletic, L. Korman, M. Magno, and V. Bilas, "Time-frequency pattern wake-up detector for low-power always-on sensing of acoustic events," *I2MTC 2018 - 2018 IEEE Int. Instrum. Meas. Technol. Conf. Discov. New Horizons Instrum. Meas. Proc.*, pp. 1–6,

2018.

[10]   A. A. Anastasopoulos, "Signal Processing and Pattern Recognition of Ae Signatures," in *Experimental Analysis of Nano and Engineering Materials and Structures*, Dordrecht: Springer Netherlands, 2007, pp. 929–930.

[11]   U. Jensen, P. Kugler, M. Ring, and B. M. Eskofier, "Approaching the accuracy–cost conflict in embedded classification system design," *Pattern Anal. Appl.*, vol. 19, no. 3, pp. 839–855, 2016.

[12]   P. Mayer, M. Magno, and L. Benini, "Self-Sustaining Acoustic Sensor with Programmable Pattern Recognition for Underwater Monitoring," *IEEE Trans. Instrum. Meas.*, vol. 68, no. 7, pp. 2346–2355, 2019.

[13]   M. Fourniol *et al.*, "Analog Ultra Low-Power Acoustic Wake-Up System Based on Frequency Detection," in *2018 IEEE International Conference on Internet of Things and Intelligence System (IOTAIS)*, 2018, pp. 109–115.

[14]   S. Astapov, J. S. Preden, J. Ehala, and A. Riid, "Object detection for military surveillance using distributed multimodal smart sensors," *Int. Conf. Digit. Signal Process. DSP*, vol. 2014-Janua, no. August, pp. 366–371, 2014.

[15]   P. Mayer, M. Magno, and L. Benini, "A2Event: A Micro-Watt Programmable Frequency-Time Detector for Always-On Energy-Neutral Sensing," *Sustain. Comput. Informatics Syst.*, vol. 25, p. 100368, Mar. 2019.

[16]   S. Bhattacharyya, S. Andryzcik, and D. W. Graham, "An Acoustic Vehicle Detector and Classifier Using a Reconfigurable Analog/Mixed-Signal Platform," *J. Low Power Electron. Appl.*, vol. 10, no. 1, p. 6, Feb. 2020.

[17]   S. Jeong *et al.*, "Always-On 12-nW Acoustic Sensing and Object Recognition Microsystem for Unattended Ground Sensor Nodes," *IEEE J. Solid-State Circuits*, vol. 53, no. 1, pp. 261–274, 2018.

[18]   Y. Wang, R. Zhou, Z. Liu, and B. Yan, "A Low-Power CMOS Wireless Acoustic Sensing

Platform for Remote Surveillance Applications," *Sensors*, vol. 20, no. 1, pp. 1–15, 2020.

[19]   C. Salazar-García, R. Castro-González, and A. Chacón-Rodríguez, "RISC-V based sound classifier intended for acoustic surveillance in protected natural environments," *LASCAS 2017 - 8th IEEE Lat. Am. Symp. Circuits Syst. R9 IEEE CASS Flagsh. Conf. Proc.*, pp. 1–4, 2017.

[20]   U. Antao, J. Choma, A. Dibazar, and T. Berger, "Low power, long life design for smart Intelligence, Surveillance, and Reconnaissance (ISR) sensors," *2012 IEEE Int. Conf. Technol. Homel. Secur. HST 2012*, pp. 631–636, 2012.

[21]   S. J. Desai, M. Shoaib, and A. Raychowdhury, "An Ultra-Low Power, 'Always-On' Camera Front-End for Posture Detection in Body Worn Cameras Using Restricted Boltzman Machines," *IEEE Trans. Multi-Scale Comput. Syst.*, vol. 1, no. 4, pp. 187–194, 2015.

[22]   J. Vincke, S. Kempf, N. Schnelle, C. Horch, and F. Schäfer, "Ultra-Low Power Sensor System for Disaster Event Detection in Metro Tunnel Systems," *Sensors & Transducers*, vol. 212, no. 5, p. 7, 2017.

[23]   P. Dutta, M. Grimmer, A. Arora, S. Bibykt, and D. Culler, "Design of a wireless sensor network platform for detecting rare, random, and ephemeral events," *2005 4th Int. Symp. Inf. Process. Sens. Networks, IPSN 2005*, vol. 2005, pp. 497–502, 2005.

[24]   D. Oletic, M. Gazivoda, and V. Bilas, "A Programmable 3-Channel Acoustic Wake-Up Interface Enabling Always-On Detection of Underwater Events within 20 µA," in *Proceedings Eurosensors2018*, 2018, vol. 2, no. 13, p. 7.

[25]   V. Pinrod *et al.*, "Zero Power, Tunable Resonant Microphone with Nanowatt Classifier for Wake-Up Sensing," *Proc. IEEE Sensors*, vol. 2018-Octob, 2018.

[26]   M. Yang, C. H. Yeh, Y. Zhou, J. P. Cerqueira, A. A. Lazar, and M. Seok, "Design of an Always-On Deep Neural Network-Based 1-µ W Voice Activity Detector Aided with a Customized Software Model for Analog Feature Extraction," *IEEE J. Solid-State Circuits*, vol. 54, no. 6, pp. 1764–1777, 2019.

[27]   S. Lauwereins, W. Meert, J. Gemmeke, and M. Verhelst, "Ultra-low-power voice-activity-detector through context- and resource-cost-aware feature selection in decision trees," in *2014 IEEE International Workshop on Machine Learning for Signal Processing (MLSP)*, 2014, pp. 1–6.

[28]   J. E. G. Medeiros, L. A. P. Chrisostomó, G. Meira, Y. C. R. Toledo, M. Pimenta, and S. A. P. Haddad, "A fully analog low-power wavelet-based Hearing Aid Front-end," *2013 IEEE Biomed. Circuits Syst. Conf. BioCAS 2013*, pp. 242–245, 2013.

[29]   M. Price, J. Glass, and A. P. Chandrakasan, "A Low-Power Speech Recognizer and Voice Activity Detector Using Deep Neural Networks," *IEEE J. Solid-State Circuits*, vol. 53, no. 1, pp. 66–75, Jan. 2018.

[30]   A. Raychowdhury, C. Tokunaga, W. Beltman, M. Deisher, J. W. Tschanz, and V. De, "A 2.3 nJ/Frame Voice Activity Detector-Based Audio Front-End for Context-Aware System-On-Chip Applications in 32-nm CMOS," *IEEE J. Solid-State Circuits*, vol. 48, no. 8, pp. 1963–1969, Aug. 2013.

[31]   C. Tschope, F. Duckhorn, C. Richter, P. Bl, and M. Wolff, "An Embedded System for Acoustic Pattern Recognition," in *2017 IEEE SENSORS*, 2017, pp. 1–3.

[32]   W. Shan *et al.*, "A 510-nW Wake-Up Keyword-Spotting Chip Using Serial-FFT-Based MFCC and Binarized Depthwise Separable CNN in 28-nm CMOS," *IEEE J. Solid-State Circuits*, vol. 56, no. 1, pp. 151–164, Jan. 2021.

[33]   G. Mois, S. Folea, and T. Sanislav, "Analysis of Three IoT-Based Wireless Sensors for Environmental Monitoring," *IEEE Trans. Instrum. Meas.*, vol. 66, no. 8, pp. 2056–2064, 2017.

[34]   F. He, "A Portable Low-power Electronic Adherence Monitoring System for Cystic Fibrosis," University of Sheffield, Sheffield, United Kingdom, 2019.

[35]   D. Oletic and V. Bilas, "Energy-efficient respiratory sounds sensing for personal mobile asthma monitoring," *IEEE Sens. J.*, vol. 16, no. 23, pp. 8295–8303, 2016.

[36]   D. Oletic, B. Arsenali, and V. Bilas, "Low-power wearable respiratory sound sensing," *Sensors (Switzerland)*, vol. 14, no. 4. pp. 6535–6566, 2014.

[37]   D. Oletic and V. Bilas, "Piezoelectric sensor front-end for energy-efficient acquisition of ultrasonic emissions related to water-stress in plants," in *Proceedings of IEEE Sensors*, 2019, vol. 2019-Octob, pp. 1–4.

[38]   G. Cohn *et al.*, "An ultra-low-power human body motion sensor using static electric field sensing," *Proc. 2012 ACM Conf. Ubiquitous Comput. - UbiComp '12*, p. 99, 2012.

[39]   A. Page, C. Sagedy, E. Smith, N. Attaran, T. Oates, and T. Mohsenin, "A flexible multichannel EEG feature extractor and classifier for seizure detection," *IEEE Trans. Circuits Syst. II Express Briefs*, vol. 62, no. 2, pp. 109–113, 2015.

[40]   H. Ghasemzadeh and R. Jafari, "Ultra low-power signal processing in wearable monitoring systems," *ACM Trans. Embed. Comput. Syst.*, vol. 13, no. 1, pp. 1–23, 2013.

[41]   M. Delgado Prieto, D. Zurita Millan, W. Wang, A. Machado Ortiz, J. A. Ortega Redondo, and L. Romeral Martinez, "Self-powered wireless sensor applied to gear diagnosis based on acoustic emission," *IEEE Trans. Instrum. Meas.*, vol. 65, no. 1, pp. 15–24, 2016.

[42]   S. Moazzeni, M. Sawan, and G. E. R. Cowan, "An ultra-low-power energy-efficient dual-mode wake-up receiver," *IEEE Trans. Circuits Syst. I Regul. Pap.*, vol. 62, no. 2, pp. 517–526, 2015.

[43]   S. Oh, N. E. Roberts, and D. D. Wentzloff, "A 116nW multi-band wake-up receiver with 31-bit correlator and interference rejection," *Proc. Cust. Integr. Circuits Conf.*, pp. 13–16, 2013.

[44]   M. Magno and L. Benini, "An Ultra Low Power High Sensitivity Wake-Up Radio Receiver with Addressing Capability," *Wirel. Mob. Comput. Netw. Commun. (WiMob), 2014 IEEE 10th Int. Conf.*, pp. 92–99, 2014.

[45]   H. Fuketa, S. O'Uchi, and T. Matsukawa, "A 0.3-V 1- μw Super-Regenerative Ultrasound Wake-Up Receiver with Power Scalability," *IEEE Trans. Circuits Syst. II Express Briefs*,

vol. 64, no. 9, pp. 1027–1031, 2017.

[46]   G. Kim *et al.*, "A 695 pW standby power optical wake-up receiver for wireless sensor nodes," *Proc. Cust. Integr. Circuits Conf.*, pp. 1–4, 2012.

[47]   H. Khodr, N. Kouzayha, M. Abdallah, J. Costantine, and Z. Dawy, "Energy Efficient IoT Sensor With RF Wake-Up and Addressing Capability," *IEEE Sensors Lett.*, vol. 1, no. 6, pp. 1–4, 2017.

[48]   S. Kodali, P. Hansen, N. Mulholland, P. Whatmough, D. Brooks, and G.-Y. Wei, "Applications of Deep Neural Networks for Ultra Low Power IoT," *2017 IEEE Int. Conf. Comput. Des.*, pp. 589–592, 2017.

[49]   P. N. Whatmough, S. K. Lee, H. Lee, S. Rama, D. Brooks, and G.-Y. Wei, "A 28nm SoC with a 1.2GHz 568nJ/prediction sparse deep-neural-network engine with 0.1 timing error rate tolerance for IoT applications," in *2017 IEEE International Solid-State Circuits Conference (ISSCC)*, 2017, pp. 242–243.

[50]   V. Pinrod *et al.*, "Zero-power sensors with near-zero-power wakeup switches for reliable sensor platforms," *Proc. IEEE Int. Conf. Micro Electro Mech. Syst.*, pp. 1236–1239, 2017.

[51]   S. Kang, V. Rajaram, S. D. Calisgan, A. Risso, Z. Qian, and M. Rinaldi, "Near-Zero Power Integrated Microsystems for the IOT," in *2021 IEEE 34th International Conference on Micro Electro Mechanical Systems (MEMS)*, 2021, vol. 2021-Janua, no. January, pp. 143–148.

[52]   Z. Wang *et al.*, "A 148-nW Reconfigurable Event-Driven Intelligent Wake-Up System for AIoT Nodes Using an Asynchronous Pulse-Based Feature Extractor and a Convolutional Neural Network," *IEEE J. Solid-State Circuits*, pp. 1–1, 2021.

[53]   DARPA Microsystems Technology Office, "Near Zero Power RF and Sensor Operations," *Broad Agency Announc.*, 2015.

[54]   T. Frank, G. Gerlach, and A. Steinke, "Binary Zero-Power Sensors: An alternative solution for power-free energy-autonomous sensor systems," *Microsyst. Technol.*, vol. 18,

no. 7–8, pp. 1225–1231, 2012.

[55] K. Mikhaylov and J. Tervonen, "Experimental Evaluation of Alkaline Batteries's Capacity for Low Power Consuming Applications," in *2012 IEEE 26th International Conference on Advanced Information Networking and Applications*, 2012, pp. 331–337.

[56] Q. He, Z. Ni, F. Chen, J. Wang, and X. Li, "Sub-g Vibration-threshold Triggered Dual Functions of Energy-harvesting and Vibration-sensing," pp. 5–7, 2016.

[57] S.-Y. Park, K. Lee, H. Song, and E. Yoon, "Simultaneous Imaging and Energy Harvesting in CMOS Image Sensor Pixels," *IEEE Electron Device Lett.*, vol. 39, no. 4, pp. 1–1, 2018.

[58] I. Lee *et al.*, "System-On-Mud: Ultra-Low Power Oceanic Sensing Platform Powered by Small-Scale Benthic Microbial Fuel Cells," *IEEE Trans. Circuits Syst. I Regul. Pap.*, vol. 62, no. 4, pp. 1126–1135, 2015.

[59] T. D. Wickens, *Elementary Signal Detection Theory*. Oxford University Press, 2001.

[60] T. Koch, "Design of Micropower Microphone and Speech Detection Circuits, Master's Thesis at the Institute of Neuroinformatics (INI) UZH-ETH Zurich," 2008.

[61] F. Alías, J. C. Socoró, and X. Sevillano, "A review of physical and perceptual feature extraction techniques for speech, music and environmental sounds," *Appl. Sci.*, vol. 6, no. 5, 2016.

[62] R. Serizel, V. Bisot, S. Essid, and G. Richard, "Acoustic Features for Environmental Sound Analysis," in *Computational Analysis of Sound Scenes and Events*, Cham: Springer International Publishing, 2018, pp. 71–101.

[63] S. Chu, S. Narayanan, and C. J. Kuo, "Environmental Sound Recognition With Time–Frequency Audio Features," *IEEE Trans. Audio. Speech. Lang. Processing*, vol. 17, no. 6, pp. 1142–1158, 2009.

[64] M. Gazivoda and V. Bilas, "Low-power sensor interface with a switched inductor frequency selective envelope detector," *Sensors*, vol. 21, no. 6, pp. 1–21, Mar. 2021.

[65] E. Gutierrez, C. Perez, F. Hernandez, and L. Hernandez, "VCO-based Feature Extraction Architecture for Low Power Speech Recognition Applications," in *2019 IEEE 62nd International Midwest Symposium on Circuits and Systems (MWSCAS)*, 2019, pp. 1175–1178.

[66] S. Oh *et al.*, "An Acoustic Signal Processing Chip With 142-nW Voice Activity Detection Using Mixer-Based Sequential Frequency Scanning and Neural Network Classification," *IEEE J. Solid-State Circuits*, vol. 54, no. 11, pp. 3005–3016, Nov. 2019.

[67] K. M. H. Badami, S. Lauwereins, W. Meert, and M. Verhelst, "A 90 nm CMOS, 6 µW power-proportional acoustic sensing frontend for voice activity detection," *IEEE J. Solid-State Circuits*, vol. 51, no. 1, pp. 291–302, 2016.

[68] B. Rumberg, D. W. Graham, and V. Kulathumani, "A low-power, programmable analog event detector for resource-constrained sensing systems," in *2012 IEEE 55th International Midwest Symposium on Circuits and Systems (MWSCAS)*, 2012, pp. 338–341.

[69] Chang-Min Kim and Soo Young Lee, "A digital chip for robust speech recognition in noisy environment," in *2001 IEEE International Conference on Acoustics, Speech, and Signal Processing. Proceedings (Cat. No.01CH37221)*, vol. 2, pp. 1089–1092.

[70] D. H. Goldberg, A. G. Andreou, P. Julián, P. O. Pouliquen, L. Riddle, and R. Rosasco, "VLSI implementation of an energy-aware wake-up detector for an acoustic surveillance sensor network," *ACM Trans. Sens. Networks*, vol. 2, no. 4, pp. 594–611, 2006.

[71] M. Habibi, M. Shakarami, and A. A. Khoddami, "A low power mixed signal correlator for power efficient sound signature detection and template matching," *Sens. Rev.*, vol. 37, no. 3, pp. 213–222, Jun. 2017.

[72] F. Sutton *et al.*, "The Design of a Responsive and Energy-efficient Event-triggered Wireless Sensing System," in *Proceedings of the 14th International Conference on Embedded Wireless Systems and Networks (EWSN 2017)*, 2017, pp. 144–155.

[73] M. Cho *et al.*, "A 6×5×4mm 3 general purpose audio sensor node with a 4.7µW audio processing IC," in *2017 Symposium on VLSI Circuits*, 2017, pp. C312–C313.

[74]   Q. Li *et al.*, "MSP-MFCC: Energy-Efficient MFCC Feature Extraction Method With Mixed-Signal Processing Architecture for Wearable Speech Recognition Applications," *IEEE Access*, vol. 8, pp. 48720–48730, 2020.

[75]   R. S. Suri, N. T. Tasneem, and I. Mahbub, "Low-power highly efficient voltage-boosting rectifier for wide-band inductively-coupled power telemetry," *2019 United States Natl. Comm. URSI Natl. Radio Sci. Meet. Usn. NRSM 2019*, no. 1, pp. 1–2, 2019.

[76]   J. Gak, M. Miguez, E. Alvarez, and A. Arnaud, "Integrated ultra-low power precision rectifiers for implantable medical devices," *2019 Argentine Conf. Electron. CAE 2019*, pp. 27–30, 2019.

[77]   K. G. Sun, K. Choi, and T. N. Jackson, "Low-power double-gate ZnO TFT active rectifier," *IEEE Electron Device Lett.*, vol. 37, no. 4, pp. 426–428, 2016.

[78]   S. Du, G. A. J. Amaratunga, and A. A. Seshia, "A Cold-Startup SSHI Rectifier for Piezoelectric Energy Harvesters with Increased Open-Circuit Voltage," *IEEE Trans. Power Electron.*, vol. 34, no. 1, pp. 263–274, 2019.

[79]   X. Li and Y. Sun, "An SSHI Rectifier for Triboelectric Energy Harvesting," *IEEE Trans. Power Electron.*, vol. 8993, no. c, pp. 1–15, 2019.

[80]   C. Trigona, S. Giuffrida, B. Andò, S. Baglio, I. Elettrica, and V. A. Doria, "Micromachined 'Random Mechanical Harvester on Inductor ' to recovery energy from very low-amplitude vibrations with zero-voltage threshold," *Proc. - 2016 IEEE SENSORS*, pp. 2–4, 2016.

[81]   H. W. Ott, *Noise Reduction Techniques in Electronic Systems*. Livingston, New Jersey, USA: Wiley-Interscience, 1988.

[82]   C. C. Marouchos, *The switching Function: Analysis of Power Electronic Circuits*. London: The Institution of Engineering and Technology, 2006.

[83]   M. C. Argyrou, C. C. Marouchos, M. Darwish, E. Iosif, and F. Paterakis, "Investigation of the switched inductor circuit for harmonics compensation," in *2017 52nd International*

Universities Power Engineering Conference, UPEC 2017, 2017, vol. 2017-Janua, pp. 1–5.

[84]   S. Lu and F. Boussaid, "A Highly Efficient P-SSHI Rectifier for Piezoelectric Energy Harvesting," *IEEE Trans. Power Electron.*, vol. 30, no. 10, pp. 5364–5369, Oct. 2015.

[85]   L. Wu, P. Zhu, and M. Xie, "A Self-Powered Hybrid SSHI Circuit with a Wide Operation Range for Piezoelectric Energy Harvesting," *Sensors*, vol. 21, no. 2, p. 17, Jan. 2021.

[86]   M. Gazivoda, D. Oletić, C. Trigona, and V. Bilas, "Passive extraction of signal feature using a rectifier with a mechanically switched inductor for low power acoustic event detection," *Sensors (Switzerland)*, vol. 20, no. 18, pp. 1–19, 2020.

[87]   M. Gazivoda, D. Oletic, and V. Bilas, "Characterization and comparison of envelope detectors for wake-up sensor interfaces at audio frequencies," *I2MTC 2020 - 2020 IEEE Int. Instrum. Meas. Technol. Conf. Proc.*, pp. 1–6, 2020.

[88]   A. Alex-Amor, J. Moreno-Núñez, J. M. Fernández-González, P. Padilla, and J. Esteban, "Parasitics impact on the performance of rectifier circuits in sensing RF energy harvesting," *Sensors*, vol. 19, no. 22, 2019.

[89]   Y. Ming, C. Ziping, and L. Jun, "Characterization the influences of diodes to piezoelectric energy harvester.pdf," *Int. J. SMART NANO Mater.*, vol. 9, no. 3, pp. 151–166, 2018.

[90]   F. Giusa, A. Giuffrida, C. Trigona, B. Andò, A. R. Bulsara, and S. Baglio, "'Random mechanical switching harvesting on inductor': A novel approach to collect and store energy from weak random vibrations with zero voltage threshold," *Sensors Actuators, A Phys.*, vol. 198, pp. 35–45, 2013.

[91]   C. Trigona, B. Andò, and S. Baglio, "Performance Measurement Methodologies and Metrics for Vibration Energy Scavengers," *IEEE Trans. Instrum. Meas.*, vol. 66, no. 12, pp. 3327–3339, 2017.

Publications

Publication 1

Gazivoda, M., Bilas, V., "Always-on sparse event wake-up detectors: A Review", *IEEE Sensors Journal*, Early Access, pp 14, 2022, doi:10.1109/JSEN.2022.3162319

Always-on sparse event wake-up detectors: A Review

Marko Gazivoda, *Student Member, IEEE*, Vedran Bilas, *Senior Member, IEEE*

Abstract— **Recently there has been a significant increase in demand for wireless sensor networks, as their field of application is rapidly expanding, driven mostly by the growing importance and prevalence of the Internet of Things concept. To enable practical application of wireless sensor networks, sensor nodes must be inexpensive, small, light-weight, intelligent and autonomous. This paper presents a review of low-power always-on wake-up detectors used to reduce a sensor node's power consumption and enable continuous detection of sparse events. We describe the wake-up concept, discuss its advantages and present the wake-up detector's power consumption, detection accuracy and false positive rate as parameters of interest. We present a state-of-the-art analysis of wake-up detectors, grouping them based on their power consumption into zero-power and near-zero-power detectors and active detectors, which we further separate based on their implementation into digital detectors and mixed-signal and analog detectors. This analysis shows state-of-the-art wake-up detectors operate with detection accuracy over 90% and a wide range of power consumptions, spanning from a few nW to few tens of µW, because of their diverse applications and sensor modalities. Additionally, it shows that active mixed-signal wake-up detectors are currently the most utilized implementation, with emphasis on acoustic transducer modality. It also shows potential trends for future detector design utilizing more MEMS and NEMS to further lower detector power consumption. We also show techniques and ideas not yet integrated in the wake-up concept, to potentially improve the wake-up detector concept and present the wake-up detectors' common applications and their specifics.**
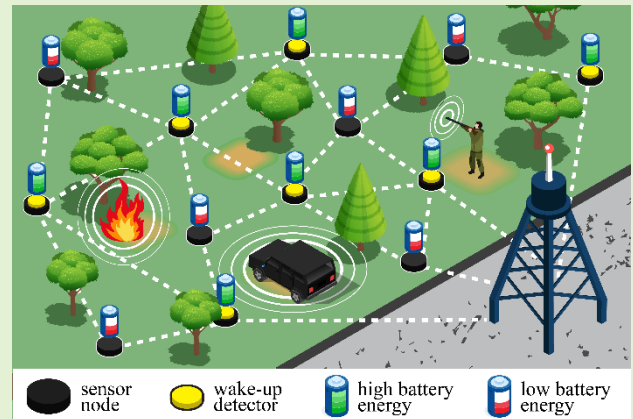
Index Terms— *detection and classification based on sensor data, energy consumption, sensor applications, sensor electronic circuits, sensor readout circuits, smart sensor systems, sensor testing and evaluation*

I. Introduction

Driven by the ever-growing interest in the Internet of Things (IoT), in recent times there has been a rapid increase in demand for intelligent low-power sensor nodes and networks [1], [2] for multiple applications from continuous surveillance and security [3]–[5], environmental monitoring [6], [7], speech or voice detection [8]–[10], biomedical and health monitoring [11]–[13], structural health monitoring, non-destructive testing and machinery diagnosis [14], [15], communication channel monitoring [16], [17] and many others [18]–[20].

These applications require the sensor nodes to be inexpensive, small and light-weight and the networks formed by these nodes to be functional for long periods of time with minimal maintenance and intervention. The final goal is a wireless sensor network of fully autonomous sensor nodes, in terms of their functionality, energy and ways they interact with the world around them [1]. A necessary prerequisite for this is energy autonomy [21], also called energy autarky [22], [23], or energy neutrality by some authors [6]. This concept envisions a circuit, or in this case a sensor that can, from an energy point of view, stay active forever without the need for intervention. Working towards the goal of achieving sensor node energy autonomy, research fields have been established focused on improving sensor node power sources, lowering sensor node power consumption, and increasing their energy efficiency.

Considering the sensor node power sources, there is a lot of research focused on improving batteries [24], [25], reducing their size, increasing energy capacity, reducing self-discharge and other unwanted effects. Another prominent concept for powering sensor nodes, that could potentially replace battery-powered systems [25], is energy harvesting, which implies generating electrical energy on the sensor node using the energy from its surroundings, such as ambient vibration

[15], [26], light [15], [27] and thermal gradients [15], or even microbes [28]. By utilizing energy harvesting, the sensor node generates electrical energy required for its operation, which potentially allows the sensor node to achieve full energy autonomy, if there is sufficient ambient energy to convert.

To achieve sensor node energy autonomy, sufficient reduction of the sensor node's power consumption and increase of its energy efficiency can only be achieved if the sensor node (or most of its components) is kept in a low-power ("sleep") mode for most of the time and only fully activated to perform its tasks during limited time windows [1], [4], [29]. This activation can be done synchronously, at fixed time intervals, utilizing a concept called duty cycling. However, due to the sporadic nature of most events of interest, it is potentially more advantageous to perform this activation asynchronously, using event-driven activation [2], [30] and the wake-up concept, in which the sensor node consists of an always-on wake-up detector which is used to wake up the main subsystem.

The wake-up concept originated in communication hardware because of its high contribution to the sensor node's overall power consumption. Wake-up receivers were developed to allow asynchronous activation of communication hardware, only when communication is requested [31]–[33].

Additional modifications and restrictions can be imposed to wake-up detectors by their application, from size and weight restrictions, detection accuracy, safety standards, design complexity, production and deployment price, and so on.

In this paper we present a review of low-power always-on wake-up detectors for continuous detection of sparse events (occurring rarely and with no predefined schedule) and present several contributions. To the best of the authors' knowledge, we present the first analysis of state-of-the-art (SOTA) wake-up detectors (for sensor activation) from the perspective of power consumption and implementation. We derive conclusions on detector parameters, implementations, transducer modalities, features and detector schemes. In addition to showing the state of wake-up detector technology, this work also shows potential guidelines for advancing the wake-up concept itself by showing new techniques and ideas not yet integrated in the wake-up concept. We also show an analysis of common applications of wake-up detectors and point to specifics stemming from those applications.

The rest of this paper is organized as follows: Section II demonstrates the wake-up concept, parameters of a wake-up detector and its advantages. Section III presents the analysis of SOTA wake-up detectors. In Section IV wake-up detector application fields are presented, and Section V concludes the paper.

II. WAKE-UP CONCEPT AND ITS ADVANTAGES

A. *Wake-up Concept*

A typical battery-powered sensor node (Fig. 1) consists of a power source (1), a transducer (2), a sensor interface (3) that conditions the transducer signal and converts the raw signal into data, a microcontroller (4) (or another form of node control) to regulate the node behavior, and communication hardware (5) to connect the sensor node to other elements of its network.
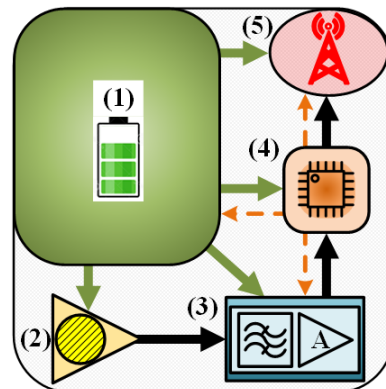
Fig. 1. A typical sensor node's block diagram, with marked key components: (1) power supply, (2) transducer, (3) sensor interface, (4) node control, (5) communication

This sensor node is used to detect sparse events, occurring rarely and with no predefined schedule, during the percentage of time defined as the event activity, *EA*. While the whole sensor node is active it has a mean power consumption of P_m. To reduce this power consumption, most parts of the sensor node can be powered down and only activated when necessary.

This can be done synchronously, with a fixed schedule, utilizing duty cycling, with a duty cycle of D. An appropriate duty cycle can be set once an approximate event activity is known. The power consumption of a sensor node utilizing duty cycling can be approximated as:

$$P_D = D \cdot P_m \qquad (1)$$

This approximation, as well as those in the following equations, does not account for the influence of the sensor node's inactive state power consumption and the additional power expended during the on and off switching of the sensor node's main stage.

Seeing how duty cycling is done with a fixed schedule, there will be times when the sensor node activates only to conclude there is no need for activation (no event of interest) and goes back to stand-by mode, only wasting energy for activation. Additionally, events of interest can be missed if they occur during periods when the sensor node is in stand-by mode [34].

To mitigate these problems, especially if the events of interest occur sparsely, a more energy-efficient alternative to duty cycling is to activate the sensor node asynchronously utilizing the wake-up concept [2], [30], which envisions a two-stage sensor node consisting of two subsystems (Fig. 2 a)). The first subsystem, the wake-up detector, is always on, has a low average power consumption of $P_w << P_m$, detects the signals of interest, conditions them, extracts features, and detects patterns. Then, if an event of interest is detected, it sends an activation (wake-up) signal to activate the second subsystem (or the rest of the sensor node), which has higher power consumption (P_m) but performs a more detailed analysis of the event. The reason for considering a wake-up detector's average power consumption is that, while power consumption profiles vary with each detector implementation, in general, most detectors experience a slight increase in their power consumption when processing a potential event of interest.

While the wake-up detector must be able to accurately detect and recognize events of interest, the detailed analysis

performed by the second stage usually constitutes the sensor node's main function, providing further data on the event of interest, by utilizing more resources, more complex processing techniques or even a different transducer modality. As an example of this, an artificial cochlea can have a voice activity wake-up detector, which, upon voice detection, activates a more complex main stage which allows high quality sound analysis when required.

The wake-up detector has a detection accuracy of DA (the percentage of correctly recognized events of interest, also referred to as true positive [35]) and a false positive rate of FP (the percentage of detections when no event of interest are present [35]). The average power consumption of such a two-stage sensor node utilizing a wake-up detector can be expressed as:

$$P_{2S} = P_w + EA \cdot DA \cdot P_m + (1 - EA) \cdot FP \cdot P_m \qquad (2)$$

where P_w and P_m represent the average power consumption of the wake-up detector and the main stage respectively and EA represents the event activity.

The power consumption of a two-stage sensor node utilizing a wake-up detector is defined by the wake-up detector's average power consumption, its detection accuracy, and its false positive rate, but also by the event activity. It is expected to be considerably lower than that of the sensor node's main stage ($P_{2S} << P_m$).
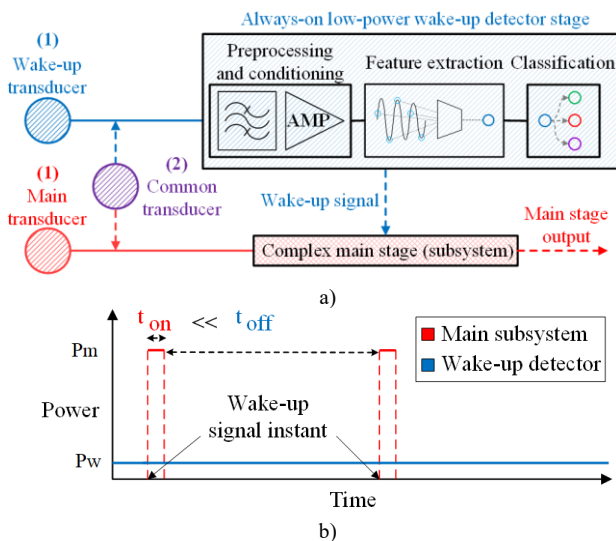
Fig. 2. a) Two-stage sensor node block schematic. The sensor node can be implemented with each stage utilizing their own transducer (1), or with both stages utilizing the same transducer (2). b) Power consumption of a two-stage sensor node utilizing the wake-up concept. t_{on} and t_{off} denote the time intervals in which the main stage is active and in sleep mode, respectively.

B. Sensor Node Lifetime Estimation

A battery-powered sensor node's lifetime, T, will depend on the energy stored within its power supply, E, and its average power consumption, P, and can be approximated as:

$$T = \frac{E}{P} \cdot 0.7 \qquad (3)$$

The factor of 0.7 accounts for factors such as temperature, ageing, charge and discharge current, depth of discharge, that affect the battery cycle life and effective capacity [36], [37].

To illustrate the analysis of a sensor node's lifetime we consider a sensor node with a battery energy of $E = 100$ mWh, the mean power consumption of the sensor node's main stage of $P_m = 1$ mW, the duty cycle of $D = 5\%$, and the wake-up detector's average power consumption ranging from $P_w = P_m / 1000 = 1$ µW to $P_w = P_m / 10 = 100$ µW. The detector misses no event of interest ($DA = 100\%$) and has false positive detection rates spanning from $FP = 0\%$ to $FP = 10\%$.

In Fig. 3 we illustrate the lifetimes of a battery-powered sensor node without wake-up (sensor node's main stage is always active), with synchronous duty cycle activation, and with asynchronous wake-up detector activation.
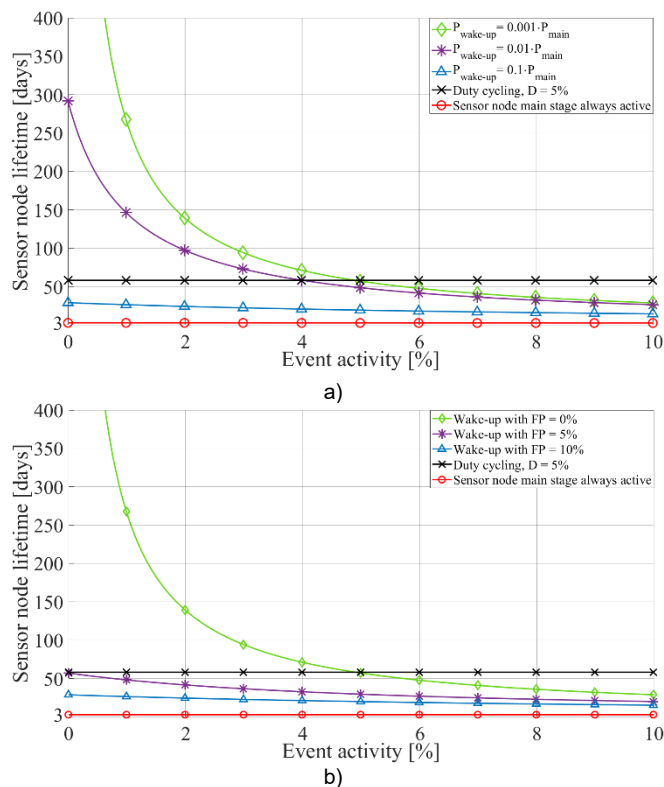
Fig. 3. Lifetimes of a sensor node utilizing duty cycling or a wake-up detector. The red lines in a) and b) represent the sensor node's lifetime if the main stage of the sensor node is active all the time (no wake-up) and the black line represents the sensor node's lifetime utilizing duty cycling with a duty cycle $D = 5\%$. a) Wake-up detector with a power consumption of $P_w = 0.001 \cdot P_m$ (green), $P_w = 0.01 \cdot P_m$ (purple), $P_w = 0.1 \cdot P_m$ (blue), with no missed events ($DA = 100\%$) and no false positive detection ($FP = 0\%$). b) Wake-up detector with a power consumption of $P_w = 0.001 \cdot P_m$, and false positive rates of 0% (green), 5% (purple) and 10% (blue) and no missed events ($DA = 100\%$).

In addition to mitigating the problem of missed events, as we can see from Fig. 3 a), the system utilizing the wake-up detector can also achieve a longer lifetime compared to the duty cycled one, if event activity drops below the duty cycle (to around 4%) and the wake-up detector's power consumption is low enough (100 or more times lower than the main stage power consumption, $P_w \leq 0.01 \cdot P_m$).

From Fig. 3 b) we can see that higher false positive rates ($FP \geq 5\%$) can considerably degrade a wake-up detector's functionality, severely reducing or even completely negating the provided lifetime extension, due to unnecessary activations of the whole sensor node. Decreasing detection accuracy would increase the sensor node's lifetime but would also lead to a detector with a lower ability to detect events of interest, so this would not present a valid method for extending a sensor node's lifetime.

Additionally, we present another example showing the sensor node's lifetime extension provided by utilizing a wake-up detector, in which the low-power always-on wake-up detector presented in [38] is used to wake up an FPGA sound classifier used for acoustic surveillance [39], as shown in Fig. 4.
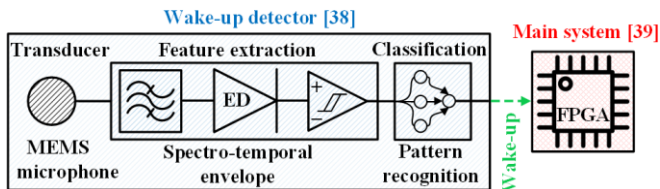
Fig. 4. The example two-stage sensor node consisting of a wake-up detector presented in [38] and a main stage sound classifier presented in [39].

We will consider the energy of the sensor node's battery to be E_{ps} = 10000 mWh. The sound classifier presented in [39] has a power consumption of P_m = 47 mW. The wake-up detector presented in [38] has a power consumption of P_w = 26.89 μW, a detection accuracy of DA = 100% and a false positive rate of FP = 0%. Considered event activities, EA, are 1%, 3% and 5%. The lifetime comparison results are presented in Table I.

TABLE I – Sensor node lifetime extension by utilizing a wake-up detector

Event activity	Sensor node lifetime [days]		
	Only [39]	[39] **utilizing** [38]	**Extension**
1%	8.87	838.55	94.54 times
3%	8.87	289.98	32.69 times
5%	8.87	175.3	19.76 times

Following the steps presented in these examples, any sensor node's lifetime can be analyzed and evaluated, with necessary data on the power consumption of its main stage and wake-up detector, its detector's detection accuracy and approximate event activity.

It should be noted that the sensor node's power source lifetime is just a part of its overall reliability. A sensor node's reliability also includes hardware and software faults, data reliability, communication reliability and so on [40]–[42]. Seeing how a sensor node malfunctions when any of its subsystems fail [42], adding a subsystem such as a wake-up detector increases the overall sensor node failure probability. However, since power source lifetime represents the basic requirement of reliability, and a wake-up subsystem greatly extends power source lifetime, adding a wake-up subsystem generally increases the sensor node's reliability. While a detailed sensor node's reliability study is beyond the scope of this paper, readers can find more information on sensor node reliability in literature [40]–[42].

III. STATE-OF-THE-ART WAKE-UP DETECTOR ANALYSIS

In this SOTA analysis we grouped the wake-up detectors with regards to their power consumption and implementation. Considering their power consumption, we grouped them into: A) Zero-power and near-zero-power detectors (with power consumption under 10 nW) and B) Active wake-up detectors (with a power consumption over 10 nW). Considering implementation, zero-power and near-zero-power detectors were implemented as custom-made MEMS or NEMS circuits, while active detectors were grouped into: 1) digital and 2) analog and mixed-signal detectors, all implemented utilizing either commercially available components or application-specific custom-made ones. Detectors that perform all (or a great majority) of their feature extraction and classification in the digital domain and/or utilize only simple analog preprocessing (amplification or prefiltering) are considered digital wake-up detectors and the rest are considered analog or mixed-signal detectors. Additionally, we examine the detectors from the perspective of their application and the energy domain which they use for event detection, grouping the detectors into mechanical (acoustic, vibrational), chemical, thermal, optical, and magnetic. For each wake-up detector we show its sensor (energy) modality, power consumption, detection accuracy, and, where available, false positive rate and reliability details.

A. Zero-power and Near-zero-power Wake-up Detectors

Zero-power and near-zero-power wake-up detectors are fully passive or ultra-low-power (under 10 nW) detectors that employ MEMS and NEMS circuits powered by the energy of the events of interest to generate and process the electrical signal and activate more complex systems upon event detection.

The amount of research of these detectors is still modest, but they are interesting from the perspective of power consumption, as they represent the peak of wake-up concept development.

It should also be noted here that, when considering zero-power and near-zero-power wake-up detector design, the electric circuit design is replaced by micro-electromechanical design, entailing manipulations with element dimensions, materials, and their interactions.

In [22] a zero-power binary sensor design is proposed to gate the power supply for the rest of the system, only when a potential event of interest is detected. The wake-up sensor is completely passive and utilizes a hydrogel transducer whose volume changes depending on the humidity or pH value of its surrounding. This volume change closes a switch, used for power-gating the more complex part of the system (Fig. 5). The utilized mechanical element is pre-stressed to allow nearly instantaneous switching action upon reaching a threshold value.
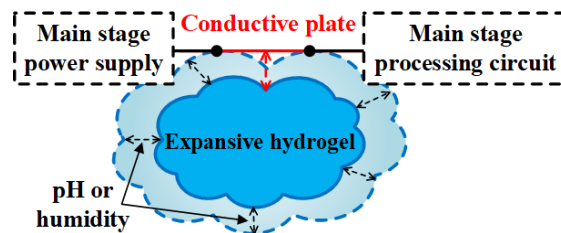

Fig. 5. Concept of the wake-up detector from [22]. Ambient humidity or pH levels change the hydrogel's volume, opening and closing the switch and power-gating the main sensor node stage.

Another zero-power wake-up sensor is reported in [43]. The system utilizes spectrally selective plasmonically enhanced MEMS photoswitches to mechanically create conducting channels upon detection of a specific infra-red spectral signature associated with the target of interest, thus triggering a wake-up. The utilized switches also have a dynamically tunable detection threshold, enabling the system to be utilized in multiple different applications (plant water content monitoring, human presence sensing, and flame detection). Utilizing this wake-up a near-zero-power sensor node with a power consumption of around 2.6 nW was developed. The zero-power wake-up is used to trigger a microcontroller which transmits data to alert a remote gateway.

In [44] a zero-power MEMS wake-up sensor is reported for vibration detection. The system utilizes a charged electret MEMS capacitor consisting of a fixed and a movable electrode. The capacitor's movable electrode is attached to a spring-loaded proof mass which vibrates with external stimulation. While the ambient vibrations are below a set threshold (determined by the sensor's mechanical design) the changing of the capacitor's inter-electrode gap causes induced charge, generating an alternating voltage ($Q = UC$) which is then rectified and stored. If vibrations exceed the preset threshold, a direct contact between the movable and fixed electrode is established and a wake-up pulse is generated. This makes this system both a wake-up sensor and an energy harvester when no event of interest is present.

A near-zero-power wake-up detector is presented in [45]. The system utilizes a custom-made zero-power piezoelectric transducer combined with near-zero-power NEMS switches (Fig. 6), to detect predefined patterns in the acceleration, rotation, and magnetic field signals and produce a wake-up signal if a template match is detected. To detect the magnetic field, permanent magnets are added to the piezoelectric beam to cause strain on it when exposed to a magnetic field. The piezoelectric transducer also acts as a filter because its geometry, mass and material define the signal frequencies to which it is sensitive. The reported power consumption of the system is under 5 nW, mainly due to biasing of the NEMS switches.

In [5] a near-zero-power tunable wake-up detector featuring a zero-power microphone and a 6 nW sub-threshold CMOS classifier for detection of sparse acoustic events (electric generator, passing truck) is reported. The system has a tunable resonant frequency, set by a tuning weight on the microphone and an adjustable sensitivity, set by the tunable load. The classifier is an ultra-low-power CMOS comparator. The achieved detection accuracy is 100% with a false positive rate of 1 per hour.

A very similar near-zero-power wake-up detector is reported in [46], where a piezoelectric MEMS accelerometer is coupled with a sub-threshold CMOS comparator to achieve a wake-up acceleration sensor with a power consumption of 5.4 nW. The comparator consists of a differential pair with a current mirror feeding into a common source amplifier and its output connects to a latch. The bias cell employs a bootstrap configuration with a startup circuit that only consumes power during the initial power-up. The threshold voltage is generated by mirroring a 1 nA current through a resistor, with a capacitor in parallel for reducing noise.

Another near-zero-power acceleration detector and a similar acoustic wake-up detector are reported in [47] and [48], respectively. In both detectors, MEMS design through manipulation of physical dimensions and materials is used to achieve the desired characteristics, such as frequency selectivity, DC input annulation, self-calibration and so on.
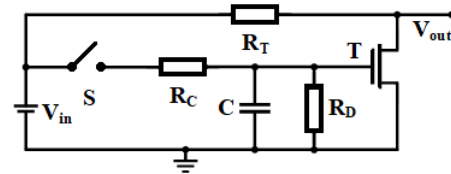
Fig. 6. Generalized schematic of wake-up detectors from [47] and [48]. The onset of vibration or an acoustic wave of interest closes a MEMS switch S, beginning a charging cycle of a capacitor. When the capacitor voltage reaches a preset level (1 V) a transistor pulls the output voltage low, generating a wake-up signal.

Both detectors report a power consumption under 1 nW without the signal of interest and below 10 nW when the signal of interest is present. Also, both detectors report no false alarms and the detector in [48] reports a detection accuracy of 100% (while true positive detection rate is not separately considered in [47]).

While this analysis shows the extremely low power consumption of zero-power and near-zero-power detectors, it should be noted that many of these detectors achieve their passive or ultra-low-power operation at the expense of lower sensitivity and detection accuracy, which can considerably increase the sensor node's power consumption due to unnecessary activations caused by false detections.

B. Active Wake-up Detectors

This subsection presents the active wake-up detectors (those with a power consumption exceeding 10 nW), their power consumption and detection accuracy, but also explores different techniques and ideas authors employed to further reduce the wake-up detector's power consumption.

1) Digital active wake-up detectors

The system reported in [49] utilizes a digital application-specific integrated circuit (ASIC) voice activity detector (VAD) to wake up a more complex speech recognizer (Fig. 7). The VAD can detect voice by comparing the short-time energy of input signal sections (voice and noise carry different energy levels), by evaluating periodicity using autocorrelation (voice is periodic to an extent, unlike noise), or by decomposing the input signal into its spectral components (voice and noise differ in spectrum).
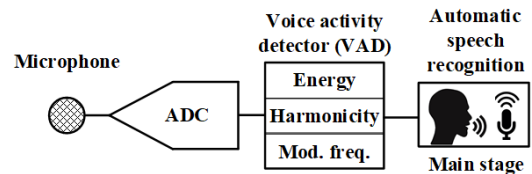

Fig. 7. Block schematic of the wake-up detector presented in [49].

The VAD's power consumption and voice detection accuracy vary depending on the used algorithm, the target voice and background noise (power varying from around 8.5 µW to around 24.4 µW and detection accuracy from 55% to 95%).

This article has been accepted for publication in IEEE Sensors Journal. This is the author's version which has not been fully edited and content may change prior to final publication. Citation information: DOI 10.1109/JSEN.2022.3162319

Marko Gazivoda *et al*.: Always-on sparse event wake-up detectors: A Review   5

Similarly, another CMOS ASIC VAD utilized for waking up a more complex speech processing unit is presented in [50]. The VAD performs a fast Fourier transform (FFT) and estimates noise energy comparing it to the input signal energy. If the input signal energy exceeds noise energy, there is an additional signal besides noise, pointing to voice activity. The VAD's overall power consumption consists of the power consumptions of the core, memory, and peripheral parts, and is, at its lowest setting, around 100 µW. The VAD's detection accuracy is over 90%.

In [51] an FPGA wake-up detector is developed which allows asynchronous sensors, modeled after the human brain, using the AER (address-event representation) spike to interface to the synchronous microcontrollers. Using this detector, a time stamp is added to the AER spike, turning it into an address-event-time representation (AETR) spike. This way the information on the time difference between two spikes is preserved and the spikes can be stored in a buffer, which means that the microcontroller can be powered down into standby mode, significantly reducing power consumption, only to be woken up when the buffer fills up with AETR spikes. The detector has a power consumption between 50 µW, when there are no events, and 4.5 mW for a data rate of 550 kiloevents/s.

In [52] a CMOS ASIC wake-up detector is reported, implementing an improved autocorrelation algorithm, consuming 835 nW. The detector determines the presence of certain predefined harmonics, characteristic for the event of interest and has a detection accuracy exceeding 90%.

An ultra-low-power acoustic event detector was developed in [34] (Fig. 8). The detector acquires the signal via a MEMS microphone and amplifies it using an audio amplifier consisting of a low-noise amplifier (LNA) and a variable gain amplifier. The amplified signal is converted to digital domain using an 8-bit SAR ADC, features are digitally extracted and used for classification by a DSP.
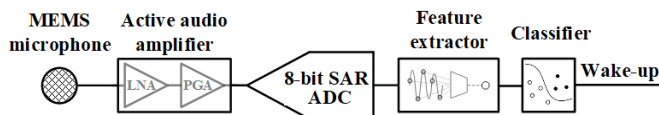
Fig. 8. Block schematic of the wake-up detector presented in [34].

The DSP uses the targeted events' frequency sparsity to replace the conventionally used FFT by a reduced DFT algorithm to further reduce power consumption. The detector operates with a power consumption of 12 nW, successfully detecting events with SNR as low as 3 dB.

A wearable digital always-on camera wake-up detector is presented in [53]. It wakes up a more complex wearable system for video recording upon detecting aggressive stance or behavior of a human The detector is a restricted Boltzmann machine-based artificial neural network implemented on a commercial FPGA platform, with a power consumption of 19.18 mW and an 85% detection accuracy. The input is acquired by a low-power camera, converted into raw pixel data, then the silhouette is extracted through background subtraction, and finally the posture is classified, and potentially aggressive posture is determined.

In [54] a reconfigurable general-purpose multi-stage digital CMOS ASIC wake-up detector is presented (Fig. 9). The input signal is converted to digital domain by a level-crossing ADC.

The feature extractor extracts the spectro-temporal instant rate of change (integral of input signal derivation) and evaluates the input signal's amplitude and duration. If the amplitude and duration point to an event of interest, a feature memory chip is activated to store the feature extractor's data. Finally, a convolutional neural network classifier uses the data from the feature memory to classify the event.
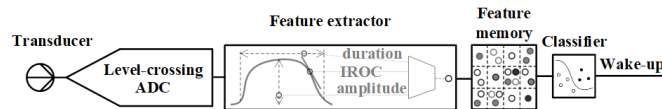
Fig. 9. Block schematic of the wake-up detector presented in [54].

The wake-up detector has a power consumption of 148 nW and its detection accuracy and false positive rate vary with application.

A digital CMOS ASIC keyword-spotting wake-up detector is presented in [10]. It consists of a serial FFT-based Mel-frequency cepstral coefficients (MFCC) feature extractor and a binarized depth-wise separable convolutional neural network. Utilizing serial FFT significantly reduces the required system memory and power consumption compared to conventional parallel FFT. The detector has a power consumption of 510 nW and a detection accuracy of 97.3%.

In [55] a multi-level digital ASIC wake-up detector for wearable motion sensors is proposed. The system features a tiered (or hierarchical) scheme where a higher precision and higher power consumption event detection block is activated only if the previous lower level determines the potential presence of an event of interest. This means that only the initial level, with lowest precision and lowest power consumption is always active. Each level preforms cross correlation template matching, utilizing a template stored in a memory, a multiplier, an adder, an accumulator, and a comparator, with a predefined threshold (defining the comparison precision). To enable each sequentially activated stage to operate with the same signal, an input buffer is employed. The authors also consider optimal sequences of level activations, depending on previous level activity to further lower power consumption by potentially skipping unnecessary comparisons. This leads to a power consumption ranging from 0.64 nW to 1.02 nW with true positive detection rate of 94.3%.

In Table II an overview of digital wake-up systems is given, considering power consumption, detection accuracy, implementation, and application.

TABLE II – Overview of digital wake-up systems

Ref.	Power (µW)	Detection accuracy (%)	Impl.	Feature extraction	Application
[34]	0.012	96 – 98	CMOS ASIC	spectro-temporal power	acoustic event recognition (car, truck generator)
[54]	0.148	85 – 99	CMOS ASIC	spectro-temporal derivation	multi-purpose
[10]	0.510	97.3	CMOS ASIC	spectro-temporal MFCC	keyword spotting
[52]	0.835	> 90	CMOS ASIC	autocorrelation	acoustic surveillance (vehicle detection)
[49]	8.5 – 24.4	55 – 95	CMOS ASIC	autocorrelation and spectro-temporal energy	voice activity detector
[50]	~100	> 90	CMOS ASIC	spectro-temporal energy	voice activity detector
[51]	50 – 4500	not specified	FPGA	spectro-temporal energy	multi-purpose
[53]	19180	85	FPGA	silhouette recognition	posture recognition

As there are no universally applicable sensor nodes or wake-up detectors, the power consumption greatly varies (as seen in Table II), depending on the sensor modality. However, it is also clear form Table II that detectors implemented as ASICs have significantly lower power consumption than those utilizing commercial off-the-shelf (COTS) components (as much as several orders of magnitude).

2) *Mixed-signal and analog active wake-up detectors*

In [56]–[58] embedded low-power wake-up detectors are developed utilizing COTS components (Fig. 10). They detect the event of interest by performing frequency decomposition and extracting the envelope in each frequency band of interest and matching the activity of each frequency band to a predefined template. The detector presented in [56] acquires the acoustic signal using a microphone (or hydrophone), filters it using an analog second order general impedance converter (GIC) bandpass filter with adjustable central frequency and bandwidth, and extracts the frequency band's envelope using an active voltage doubler (consisting of an operational amplifier and two diodes). After the envelope is digitized using a comparator, the pattern of comparator output high states is compared to a predefined template to determine the presence of an event of interest. The systems presented in [57], [58] perform the same set of operations, just replacing the active filter and envelope detector of [56] with an envelope detector (also acting as a filter) utilizing either a mechanically [58] or electrically switched inductor [57]. The detector presented in [58] utilizes zero-power feature extraction.
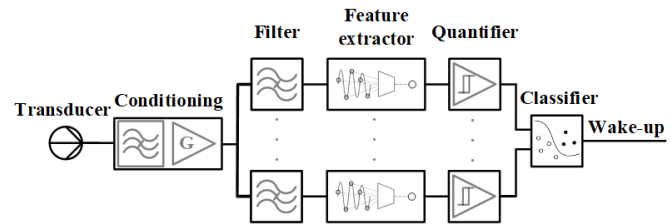
Fig. 10. Generalized block schematic of the spectro-temporal decomposition-based wake-up detector. The input signal is (optionally) preprocessed, filtered, a feature of interest is extracted (envelope, power, energy), quantified and the detected event is classified. This principle, with minor variations, is utilized in multiple reported circuits.

In [6], [38] similar wake-up detectors based on frequency decomposition are presented (Fig. 10). The detectors also perform frequency decomposition using an active adjustable second order GIC bandpass filter, an active envelope detector and a comparator. The reported power consumption of the detectors is 26.89 µW with detection accuracy ranging from 98.67% to 100%, while the false positive rate is 14% for the detector from [6] and 0% for the one from [38].

Frequency decomposition is again employed in the analog ASIC wake-up detector presented in [59] (Fig. 10). The detector consists of two 8-channel filter banks which can be used separately (even combining different sensing modalities, like acoustic and seismic) or jointly, on a single input sensor. After filtering, magnitude detectors consisting of a peak detector and a smoothing filter are utilized to determine each frequency band's magnitude. The magnitude detector outputs are connected to two comparators, allowing multi-level quantization of each band. The comparator outputs are fed into a programmable logic array that performs template matching and generates a wake-up signal. The detector consumes 46.67 µW with a detection accuracy between 70% and 90%.

An ultrasonic wake-up plant drought detector is presented in [60] (Fig. 11). The detector conditions the transducer impedance, amplifies the input signal, and converts it into differential. After conditioning, the signal is sent to a triggering circuit consisting of a comparator and a monostable, that generates a wake-up signal for the microcontroller when an ultrasonic emission is detected. The power consumption of the wake-up detector is around 2.575 mW (with an additional 2.2 mW for the microcontroller and ADC in sleep mode).
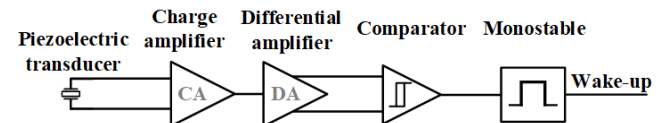

Fig. 11. Block schematic of the wake-up detector presented in [60].

In [61] the authors present an ASIC low-power wake-up voice detector (Fig. 10). The system operates with a power consumption of 6 µW detecting in-band energy of up to 16 frequency bands and has an average detection accuracy of 89% at 12 dB SNR. This system incorporates two interesting concepts. Firstly, it is a two-stage hierarchical wake-up detector, in which the microphone signal is sensed by a comparator and only when activity over a certain level is detected is the analog feature extraction activated. The features are extracted, sent to a mixed-signal classifier and, if the classifier recognizes the event as voice, it wakes up a

This article has been accepted for publication in IEEE Sensors Journal. This is the author's version which has not been fully edited and content may change prior to final publication. Citation information: DOI 10.1109/JSEN.2022.3162319

Marko Gazivoda *et al*.: Always-on sparse event wake-up detectors: A Review

5

microcontroller for more sophisticated operation. Secondly, it features context-aware sensing, meaning that, depending on the context (noise level or target event) this system can adjust the number of active channels (up to a maximum of 16) that it utilizes to classify the event, greatly increasing detection accuracy, while only increasing power consumption when necessary.

A mixed-signal wake-up detector based on a custom-made field-programmable analog array (FPAA) is presented in [62]. The 10-stage FPAA consists of a set of computational analog blocks, analog switches, digital look-up tables and flip flops, all interconnected by an internal serial peripheral interface. The analog blocks include bandpass filters, peak detectors, adaptive-time-constant filters and operational transconductance amplifiers. The connections between the functional blocks are programable, so the FPAA functionality can be adjusted according to the use scenario. The authors declare that the detector operates with a power consumption of 43 µW and a vehicle detection accuracy of 100%. Upon complete detection and classification, the detector wakes up a microcontroller to perform a more detailed and less resource-constrained classification.

In [3] a multi-purpose low-power acoustic event detection system is developed, featuring low-power always-on control circuits that activate more power-hungry components only when there is activity on the microphone. This system combines scheduled duty cycling and wake-up functionalities into a two-level hierarchical power-up, by having the microphone amplifier, which provides input for the wake-up circuit, active only 1% of the time (1 ms in each 100 ms) and then having the wake-up circuit power up the phase-locked loop and power amplifier only if an event is detected. The wake-up circuitry has a power consumption around 58 µW.

An embedded analog wake-up detector featuring COTS components and based on frequency detection is presented in [18] (Fig. 12). The input signal passes through a hysteresis comparator. Each time a predefined level is crossed, the change of comparator output triggers a monostable, which drives a current mirror to charge a capacitor. This means that the capacitor is charged depending on the number of level crossings, i.e., the frequency spectrum of the input signal. After a predefined interval, the capacitor voltage is passed over to a set of comparator pairs to determine if the voltage level is within certain bounds (and thus determining the input signal frequency). The capacitor is afterwards discharged and the whole process starts again.
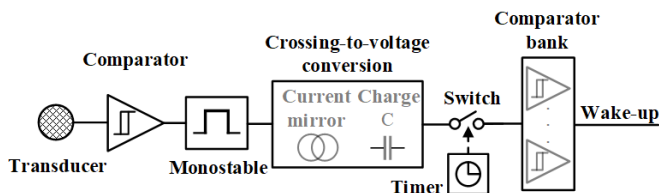
Fig. 12. Block schematic of the wake-up detector presented in [18].

The detector's power consumption is 34 µW, which is a fraction of the 600 µW power consumption of the same concept implemented digitally by the same authors in [63]. A similar analog embedded detector which uses COTS components was developed and presented in [64], with a detection accuracy of 100% (at SNR > 5 dB) and a power consumption of 9.1 µW.

In [65] authors report a mixed-signal event-triggered acoustic emission wake-up detector (Fig. 13). The three-part system consists of an acoustic sensor interface, which consumes 1.2 µW in standby mode and 38.5 µW in active mode, an acoustic event characterization part, which consumes 2.5 µW in standby mode and 150.8 µW in active mode and a multi-hop event dissemination part which has a power consumption of 52.8 µW in standby mode and 3.6 mW in active mode.
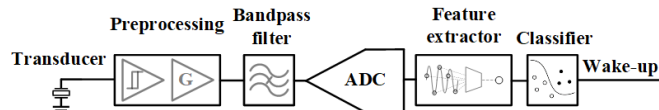
Fig. 13. Block schematic of the wake-up detector presented in [65].

The system was implemented as an analog acoustic front-end followed by two processors, one for event characterization and the other for communication. The input signal is compared to a preset threshold by a comparator and if it surpasses the threshold, a latch is activated to maintain power supply to the analog amplification and filtering stage and ensure the input signal for the ADC. Then, after a digital feature extraction and classification, if an event is detected a signal is sent to wake up communication hardware.

In [8] the authors present a 16-channel mixed-signal ASIC wake-up VAD with a 1 µW power consumption and a detection accuracy of 84.4%/85.4% (speech/non-speech) (Fig. 14).
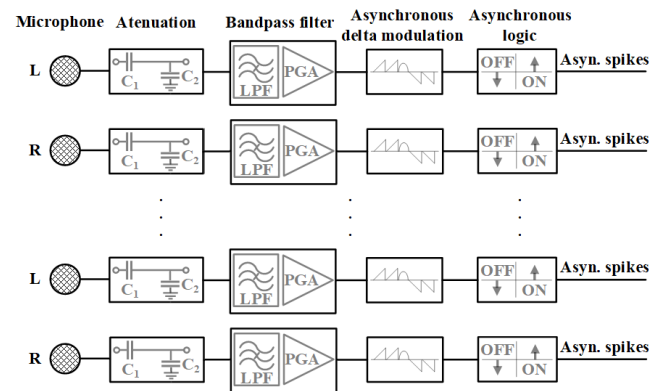

Fig. 14. Block schematic of the wake-up detector presented in [8].

The system preforms analog feature extraction and digital event classification. The signal is acquired by a microphone, amplified by an LNA, filtered by a second order super-source-follower bandpass filter, rectified by a full-wave rectifier and converted to the digital domain by the integrate-and-fire encoder. The encoder integrates its input until a threshold is reached and then generates a pulse, allowing overall power consumption reduction utilizing the so-called event-driven AD conversion (an ADC operating only when input signal is present). The information on each passband envelope is stored in the pulse frequency. The detector utilizes a 143-neuron deep neural network classifier to classify the detected event as speech/non-speech. A previous 128-channel version of this detector was used as basis for an event-driven silicon cochlea, with a 55 µW power consumption [66].

An ASIC mixed-signal wake-up detector presented in [67] utilizes analog amplification by an LNA and a programmable gain amplifier, frequency down-conversion (from 4 kHz to < 500 Hz) and digital spectro-temporal power extraction and

voice activity detection by a neural network classifier. The detector features an 8-bit SAR ADC. In addition to the ultra-low-power (ULP) channel described above, the detector also uses a high-power (HP) channel, which does not use frequency down-conversion (Fig. 15).
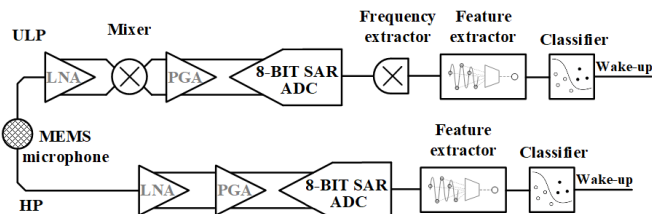

Fig. 15. Block schematic of the wake-up detector presented in [67].

The power consumption of the ULP is 142 nW and speech/non-speech detection accuracy is 91.5%/90% with 10 dB SNR. Upon speech recognition, the active channel wakes up a microcontroller to record the audio signal.

An ultra-low-power human body motion detector is presented in [68] (Fig. 16), as a wake-up circuit for a more power-hungry motion sensor system.
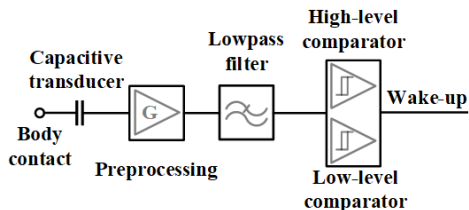
Fig. 16. Block schematic of the wake-up detector presented in [68].

The detector relies on the capacitive coupling between the human body and its surroundings, measuring the voltage across a capacitor whose one side is connected to the body and the other is a small local ground plane on the sensor board. The voltage sensed on the body is amplified so that the full-scale range of motions observed for normal actions generate voltages from rail to rail. Then an active Sallen-Key third order Butterworth lowpass filter with a 10 Hz corner frequency is used to filter out the 60 Hz the power lines noise. Finally, the filtered signal is sent to two comparators to determine if it is within the predefined bounds and, if so, a wake-up signal is generated. The wake-up detector has a detection accuracy of around 90% and a power consumption of 9.3 μW.

In [69] an analog low-power wake-up event detector is proposed, used to wake up a more power-hungry microcontroller upon detecting seismic signals from footsteps (Fig. 10). The input signal is filtered using a capacitively coupled current conveyor (C4) bandpass filter and then passed through an operational transconductance amplifier-based envelope detector, consisting of a full wave rectifier followed by a peak detector. A comparator is then used to detect whether a certain threshold has been passed. If the voltage peaks from both bands are higher than a threshold, a wake-up signal is generated. To avoid background noise triggering the detector, a subtractor, divider and an averaging circuit are added to compare the voltage amplitude and background noise. The final circuit was not physically implemented in this work, but simulation results showed a power consumption of 7.8 nW.

An ultrasonic wake-up detector for proximity detection is presented in [70]. The system features a relatively simple wake-up circuit which uses a piezoelectric transducer (sensitive in ultrasonic frequency range) to acquire the input signal, followed by an operational amplifier (with a gain of 1000), a comparator and an integrator (Fig. 17). If the amplified signal from the transducer is over a predefined level, the comparator charges the integrator. Once the integrator output reaches a certain level, the microcontroller is woken up.
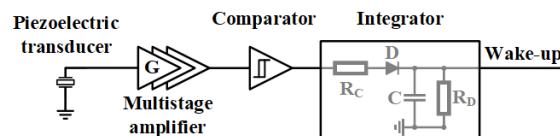
Fig. 17. Block schematic of the wake-up detector presented in [70].

These detectors are used for detecting the presence of other nodes and estimating the distance between them. To be able to emit the pulses used in mutual sensor node detection, the input transducer also functions as an ultrasonic pulse emitter, with the input and output functionality determined by a predefined schedule. The system has a power consumption of 19 μW and the wake-up system detection accuracy is not stated (only the 95% accuracy of distance estimation).

An ASIC analog wake-up detector based on envelope periodicity detection was presented in [71] (Fig. 18). It detects voice or engine activity based on their periodic components. Its input is a preamplified and prefiltered microphone signal. The detector extracts the signal's envelope using a peak detector, and a spike generator produces voltage spikes at the envelope peaks. Next, the inter-spike intervals are linearly converted to voltage by the interval-to-voltage stage, using a controlled voltage ramp. This voltage is then sampled and compared to the previous one (stored in an analog memory). If three or five consecutive voltages (and therefore inter-peak intervals) are the same, envelope periodicity is established, and an event of interest is detected. If two consecutive voltages are not sufficiently alike, the counter resets. Additionally, an interval limiter circuit is employed, which confines the detection to signals of interest.
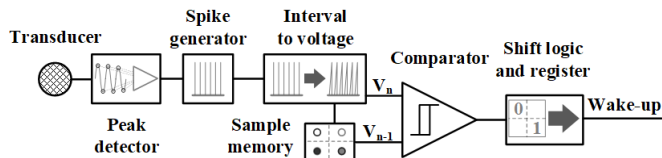

Fig. 18. Block schematic of the wake-up detector presented in [71].

All sections of the presented detector are custom made and the detector's power consumption is around 1.8 μW. The authors state that with appropriate threshold settings 100% detection accuracy with no false alarms can be achieved.

A complex disaster event detection system featuring multiple wake-up sensor modalities is presented in [23]. The system envisions a sensor network of upper and lower sensor nodes placed on the ceilings and floors of subway tunnels, featuring hydrostatic pressure sensors for water ingress detection, a combination of temperature and photoelectric gas sensors for detecting fire and passive acoustic sensors for explosion detection. The upper nodes consist of temperature, gas and acoustic sensors and consume 7.8 μW and the lower nodes use hydrostatic pressure sensors and consume 35.9 μW. The sensor nodes communicate regular status information during train passing, while exceptional communication, not

synchronized with train passing, is a wake-up signal if one of the nodes detects one of the described disaster events.

In [72] an energy-efficient gas recognition system is reported, which employs the wake-up concept to power up the power-hungry gas sensors only when an analog wake-up circuit detects activity on the transducer. The paper does not present specifics on the event-driven wake-up circuit.

Table III gives an overview of analog and mixed-signal wake-up systems, showing power consumption, detection accuracy, implementation, extracted feature, and application.

TABLE III – Overview of analog and mixed-signal wake-up detectors

Ref.	Power (µW)	Detection accuracy (%)	Impl.	Feature extraction	Application
[62]	43	100	custom-made FPAA	spectro-temporal envelope	acoustic vehicle detection
[71]	1.8	100	ASIC	envelope periodicity	voice or acoustic engine detection
[64]	9.1	100	COTS	frequency detection	acoustic vehicle detection
[6], [38]	62.86	98.67 – 100	COTS	spectro-temporal envelope	multiple acoustic events detection
[67]	0.142	90 – 91.5	ASIC	spectro-temporal power	voice detection
[56], [58], [57]	3.2 – 34.92	90.91	custom made & COTS	spectro-temporal envelope	acoustic vehicle detection
[68]	9.3	90	COTS	capacitive coupling estimation	human motion detection
[59]	46.67	70 – 90	ASIC	spectro-temporal envelope	acoustic vehicle detection
[61]	6	89	ASIC	spectro-temporal envelope	voice detection
[8]	1	84.4 – 85.4	ASIC	spectro-temporal envelope	multiple acoustic events detection
[3]	58	not specified	ASIC	threshold detection	multiple acoustic events detection
[18]	34	not specified	COTS	frequency detection	multiple acoustic events detection
[65]	1.2	not specified	COTS	threshold detection	acoustic emissions in rock walls
[60]	2575	not specified	COTS	threshold detection	ultrasonic plant drought detection
[69]	0.0078	not specified	ASIC model	spectro-temporal peak voltage	seismic activity detection
[70]	19	not specified	COTS	threshold detection	ultrasonic proximity detection

3) Summary

In this subsection we present a summary of the SOTA wake-up detector analysis, emphasizing the conclusions on trends and ideas regarding implementations and functionalities to serve as guidelines for future wake-up detector developers.

The data presented in Tables II, III and IV is shown in a visualization of a design plane defined by the detector's power consumption and its accuracy (Fig. 19). The detectors are separated into four groups, depending on their signal processing domain (digital and analog) and their implementation (utilizing COTS or custom-made components).
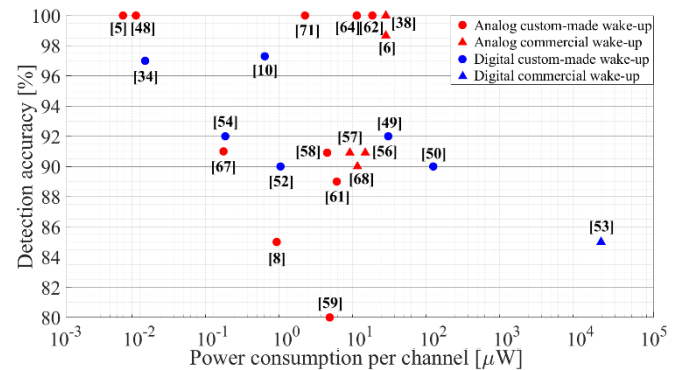
Fig. 19. A visual representation of the wake-up detector design plane defined by detectors' power consumption and detection accuracy.

The visualization in Fig. 19 points to several conclusions. There are more mixed-signal and analog than digital wake-up detectors. While wake-up detectors utilizing COTS components are cheaper to develop and produce, they generally have higher power consumptions than custom-made ones. A typical wake-up detector has a detection accuracy around or over 90%. Seeing how each detector's power consumption is defined by its application, events of interest and applicable transducers the power consumption range for typical wake-up detectors is broad and spans from around a few hundreds of nW to around few tens of µW.

Table IV presents the power consumptions of the three commonly used wake-up detector functional blocks (Fig. 2 a).

TABLE IV – Power consumption breakdown for the analog and mixed-signal wake-up detectors

Ref.	Power consumption (µW)		
	Preprocessing (per channel)	Feature extraction (per channel)	Classification
[56]	not utilized	11.52	0.36
[57]	not utilized	6.97	0.36
[58]	not utilized	3.24	0.36
[6], [38]	not utilized	22.59	0.036
[59]	2.168	0.093	1.643
[60]	2533	45	2286
[61]	0.96	~0.105	1.05 – 3.8
[62]	5.375		9.45
[18]	not utilized	29.7	4.422
[65]	5.87	2.5	
[8]	0.088	0.017	0.63
[67]	0.073	0.069	
[68]	3.3	6	

As we can see from Table IV, a considerable amount of a wake-up detector's power consumption is used for

preprocessing (around 30% – 50%) and classification (usually over 30%).

The SOTA analysis also shows that the majority of wake-up detectors utilize acoustic transducers, because acoustic signals contain a lot of easily extractable information [34], [38], [62], making them ideal for simple, low-power detectors. Furthermore, these detectors predominantly detect events utilizing spectro-temporal decomposition and features like spectro-temporal envelope, magnitude, or energy.

4) *Guidelines*

Following the summary, a set of guidelines for wake-up detector design is presented.

- If the event of interest can be detected using multiple sensor modalities, carefully chose the sensor modality to optimize detection accuracy and energy efficiency – mechanical (acoustic and vibrational) sensors present a favorable choice due to high detection accuracy and energy efficiency

- Chose appropriate features of the signal to be used for events recognition – some features allow for simpler, more efficient and accurate event detection

- If possible, with regards to price and deployment specifics for a given application, use custom integrated design to achieve lower power consumption and higher (or at least the same) detection accuracy

- Put special emphasis on the classification scheme, as this could allow for a significant power consumption reduction

Finally, the SOTA also pointed to several techniques and ideas that could serve as potential guidelines to improve the very concept of wake-up detectors.

- Multi-level hierarchical wake-up with tiered activation [34], [55]

- Context- and cost-aware wake-up which selects features based on knowledge of current operating conditions and available resources [61]

- Combination of scheduled duty cycling and a wake-up detector [3]

IV. WAKE-UP DETECTOR APPLICATIONS

A. Wake-up in Speech and Voice Activity Detection

Most complex voice and speech analysis systems (be it voice control systems, artificial cochlea, or others) feature always-on wake-up detectors [8], [10], [49], [50], [73] that power the rest of the system up only upon detecting potential voice or speech patterns in the audio signal, making this one of the most utilized wake-up detector applications.

The fact that voice activity can relatively easily be distinguished from background noise, either by its caried energy or spectrum, allows these wake-up systems to be simple,

and accurate while operating with a low power consumption.

B. Wake-up in Surveillance and Monitoring Systems

Another frequent application of wake-up detectors is in surveillance and monitoring systems [3], [23], [53], [56], [69], [74], because these systems must be continuously active to detect any unauthorized entry or violation, and have a high detection accuracy because of the potentially high price of missed events (people safety, material price and so on). This also presents a fitting application for wake-up detectors because of the clear distinction between the regular environment state and the onset of events of interest, allowing simple detector design. Finally, the events of interest should be rare compared to a regular system state. All of this contributes to these being among the simplest and most reliable wake-up detectors that can continuously and reliably monitor and detect events of interest with low power consumption.

There are many different monitoring scenarios and targets of interest for these detectors, from human or animal step detection [69], [74], vehicle detection [56], [74], detection of aggressive behavior [53], to detection of disasters, such as explosions, floods or terrorist attacks [23]. While these detectors most often employ some form of acoustic transducers [3], [23], [56], [74] due to the density of easily accessible information in acoustic signals, other transducer modalities such as seismic [69], gas, temperature, pressure [23], magnetic, infrared [74], or even video [53] are also utilized.

Stemming from the interest to understand and preserve our surroundings, a special subgroup of these monitoring wake-up detectors is emerging, meant to observe the natural environment [7], with a goal to protect it from pollution, illegal activities and so on.

C. Wake-up in Biomedicine and Health Monitoring

A somewhat surprisingly well developed wake-up detector field of application is in biomedical and health monitoring devices [12], [55], [60], [68]. This area of wake-up detectors is very broad and encompasses multiple transducer modalities. Applications vary from asthmatic wheeze detection [12] utilizing acoustic transducers, plant drought detection [60] utilizing ultrasonic transducers, to body position and movement detection utilizing capacitive transducers [68] and accelerometers, gyroscopes and magnetometers [55].

Stemming from a more complex manifestation of the event of interest, these detectors generally have higher power consumptions than other wake-up detectors as they require more signal processing and a more complex feature extraction scheme. Also, seeing how they interact with living beings, special care must be taken in their design to make them safe for their subjects and additional restrictions might be imposed on their design (limited weight, size, dissipated heat, special shape and so on). In certain biomedical applications missed events can also be life-threatening, meaning that these systems must provide very consistent and reliable event detection.

D. Other Wake-up Applications

There are several other wake-up detector utilizations, which showcase the currently sparsely explored potential application fields where wake-up detectors can improve performance and sensor applicability.

This article has been accepted for publication in IEEE Sensors Journal. This is the author's version which has not been fully edited and content may change prior to final publication. Citation information: DOI 10.1109/JSEN.2022.3162319

Marko Gazivoda *et al.*: Always-on sparse event wake-up detectors: A Review

5

In [70] an on-demand localization application of the wake-up detector is explored, providing a low-power wearable solution, requiring no additional infrastructure, making the whole system a lot more practical and portable.

In [72] a wake-up detector is added to a usually power-hungry task of gas detection and recognition, enabling continuous low-power gas sensing. A zero-power piezoelectric flow velocity wake-up detector was developed in [75]. In [45] a multi-purpose near-zero-power piezoelectric wake-up detector was developed for detecting predefined patterns in acceleration, rotation and magnetic field signals.

Additionally, some authors develop multi-purpose wake-up detectors applicable in multiple event detection scenarios [18], [34], [51], [54], [63].

E. Wake-up Applications Summary

The visual summary of wake-up detector applications shown in Fig. 20 presents comments regarding detector power consumption, design complexity and implementation.
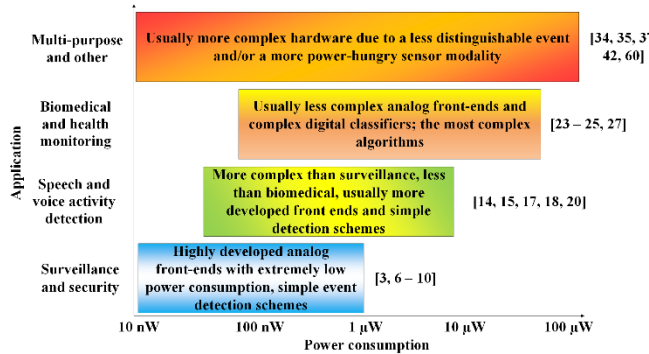
Fig. 20. Wake-up detector application overview.

V. CONCLUSION

In this paper we presented a review of the wake-up detectors applied for sensor node activation. We explained the wake-up concept and presented its advantages of increased responsiveness (less missed events) and greater prolongation of sensor node lifetime compared to duty cycling. We determined the power consumption, detection accuracy and false positive rate as parameters of interest for wake-up detectors. We presented a SOTA analysis, grouping the detectors based on their power consumption and implementation. The analysis shows that SOTA wake-up detectors achieve detection accuracies over 90%. The detectors' power consumptions vary greatly from a few nW to few tens of μW, due to their application, events of interest and transducer modalities. The analysis also shows that SOTA wake-up detectors most frequently utilize acoustic transducers, because the information rich acoustic signals allow for simple detector design utilizing spectro-temporal features. The analysis also points to future trends in wake-up detector design going towards custom-made mixed-signal circuits, employing MEMS and NEMS, allowing further lowering of the power consumption, while maintaining high detection accuracies. Additionally, in the SOTA analysis, several techniques and ideas are presented, like hierarchical wake-up, context-aware detection, or combination of wake-up with duty cycling, which could be used to further improve the

wake-up detector concept. The presented application analysis pointed to surveillance, security, voice detection, biomedical and health monitoring as the most common wake-up detector applications. The volume of research focusing on wake-up detectors presented in this review confirms the wake-up detectors' position as a ubiquitous component in future low-power sensor node design.

REFERENCES

[1] M. Alioto, "IoT: Bird's Eye View, Megatrends and Perspectives," in *Enabling the Internet of Things*, M. Alioto, Ed. Cham: Springer International Publishing, pp. 1–45, 2017., DOI:10.1007/978-3-319-51482-6

[2] N. Goux and F. Badets, "Review on event-driven wake-up sensors for ultra-low power time-domain design," *Midwest Symp. Circuits Syst.*, vol. 2018-August, pp. 554–557, 2019., DOI:10.1109/MWSCAS.2018.8623935.

[3] Y. Wang, R. Zhou, Z. Liu, and B. Yan, "A Low-Power CMOS Wireless Acoustic Sensing Platform for Remote Surveillance Applications," *Sensors*, vol. 20, no. 1, pp. 1–15, 2020., DOI:10.3390/s20010178.

[4] B. Thoen *et al.*, "Saving energy in WSNs for acoustic surveillance applications while maintaining QoS," *SAS 2017 - 2017 IEEE Sensors Appl. Symp. Proc.*, pp. 1–6, 2017., DOI:10.1109/SAS.2017.7894109

[5] V. Pinrod *et al.*, "Zero Power, Tunable Resonant Microphone with Nanowatt Classifier for Wake-Up Sensing," *Proc. IEEE Sensors*, vol. 2018-Octob, 2018., DOI:10.1109/ICSENS.2018.8589792

[6] P. Mayer, M. Magno, and L. Benini, "Self-Sustaining Acoustic Sensor with Programmable Pattern Recognition for Underwater Monitoring," *IEEE Trans. Instrum. Meas.*, vol. 68, no. 7, pp. 2346–2355, 2019., DOI:10.1109/TIM.2018.2890187

[7] G. Mois, S. Folea, and T. Sanislav, "Analysis of Three IoT-Based Wireless Sensors for Environmental Monitoring," *IEEE Trans. Instrum. Meas.*, vol. 66, no. 8, pp. 2056–2064, 2017., DOI:10.1109/TIM.2017.2677619

[8] M. Yang, C. H. Yeh, Y. Zhou, J. P. Cerqueira, A. A. Lazar, and M. Seok, "Design of an Always-On Deep Neural Network-Based 1-μ W Voice Activity Detector Aided with a Customized Software Model for Analog Feature Extraction," *IEEE J. Solid-State Circuits*, vol. 54, no. 6, pp. 1764–1777, 2019., DOI:10.1109/JSSC.2019.2894360

[9] J. E. G. Medeiros, L. A. P. Chrisostomó, G. Meira, Y. C. R. Toledo, M. Pimenta, and S. A. P. Haddad, "A fully analog low-power wavelet-based Hearing Aid Front-end," *2013 IEEE Biomed. Circuits Syst. Conf. BioCAS 2013*, pp. 242–245, 2013., DOI:10.1109/BioCAS.2013.6679684

[10] W. Shan *et al.*, "A 510-nW Wake-Up Keyword-Spotting Chip Using Serial-FFT-Based MFCC and Binarized Depthwise Separable CNN in 28-nm CMOS," *IEEE J. Solid-State Circuits*, vol. 56, no. 1, pp. 151–164, Jan. 2021., DOI:10.1109/JSSC.2020.3029097

[11] D. Oletic and V. Bilas, "Energy-efficient respiratory sounds sensing for personal mobile asthma monitoring," *IEEE Sens. J.*, vol. 16, no. 23, pp. 8295–8303, 2016., DOI:10.1109/JSEN.2016.2585039

[12] D. Oletic, B. Arsenali, and V. Bilas, "Low-power wearable respiratory sound sensing," *Sensors (Switzerland)*, vol. 14, no. 4. pp. 6535–6566, 2014., DOI:10.3390/s140406535

[13] A. Page, C. Sagedy, E. Smith, N. Attaran, T. Oates, and T. Mohsenin, "A flexible multichannel EEG feature extractor and classifier for seizure detection," *IEEE Trans. Circuits Syst. II Express Briefs*, vol. 62, no. 2, pp. 109–113, 2015., DOI:10.1109/TCSII.2014.2385211

[14] C. Tschope, F. Duckhorn, C. Richter, P. Bl, and M. Wolff, "An Embedded System for Acoustic Pattern Recognition," in *2017 IEEE SENSORS*, 2017, pp. 1–3., DOI:10.1109/ICSENS.2017.8234380

[15] M. Delgado Prieto, D. Zurita Millan, W. Wang, A. Machado Ortiz, J. A. Ortega Redondo, and L. Romeral Martinez, "Self-powered wireless sensor applied to gear diagnosis based on acoustic emission," *IEEE Trans. Instrum. Meas.*, vol. 65, no. 1, pp. 15–24, 2016., DOI:10.1109/TIM.2015.2476274

[16] S. Moazzeni, M. Sawan, and G. E. R. Cowan, "An ultra-low-power energy-efficient dual-mode wake-up receiver," *IEEE Trans. Circuits Syst. I Regul. Pap.*, vol. 62, no. 2, pp. 517–526, 2015., DOI:10.1109/TCSI.2014.2360336

[17] H. Fuketa, S. O'Uchi, and T. Matsukawa, "A 0.3-V 1- µw Super-Regenerative Ultrasound Wake-Up Receiver with Power Scalability," *IEEE Trans. Circuits Syst. II Express Briefs*, vol. 64, no. 9, pp. 1027–1031, 2017., DOI:10.1109/TCSII.2016.2621772

[18] M. Fourniol *et al.*, "Analog Ultra Low-Power Acoustic Wake-Up System Based on Frequency Detection," in *2018 IEEE International Conference on Internet of Things and Intelligence System (IOTAIS)*, 2018, pp. 109–115., DOI:10.1109/IOTAIS.2018.8600849

[19] H. Khodr, N. Kouzayha, M. Abdallah, J. Costantine, and Z. Dawy, "Energy Efficient IoT Sensor With RF Wake-Up and Addressing Capability," *IEEE Sensors Lett.*, vol. 1, no. 6, pp. 1–4, 2017., DOI:10.1109/LSENS.2017.2762918

[20] S. Kodali, P. Hansen, N. Mulholland, P. Whatmough, D. Brooks, and G.-Y. Wei, "Applications of Deep Neural Networks for Ultra Low Power IoT," *2017 IEEE Int. Conf. Comput. Des.*, pp. 589–592, 2017., DOI:10.1109/ICCD.2017.102

[21] DARPA Microsystems Technology Office, "Near Zero Power RF and Sensor Operations," *Broad Agency Announc.*, 2015.

[22] T. Frank, G. Gerlach, and A. Steinke, "Binary Zero-Power Sensors: An alternative solution for power-free energy-autonomous sensor systems," *Microsyst. Technol.*, vol. 18, no. 7–8, pp. 1225–1231, 2012., DOI:10.1007/s00542-012-1547-4

[23] J. Vincke, S. Kempf, N. Schnelle, C. Horch, and F. Schäfer, "Ultra-Low Power Sensor System for Disaster Event Detection in Metro Tunnel Systems," *Sensors & Transducers*, vol. 212, no. 5, p. 7, 2017.,

[24] K. Mikhaylov and J. Tervonen, "Experimental Evaluation of Alkaline Batteries's Capacity for Low Power Consuming Applications," in *2012 IEEE 26th International Conference on Advanced Information Networking and Applications*, 2012, pp. 331–337., DOI:10.1109/AINA.2012.99

[25] M. Alioto, "From Less Batteries to Battery-Less Alert Systems with Wide Power Adaptation down to nWs—Toward a Smarter, Greener World," *IEEE Des. Test*, vol. 38, no. 5, pp. 90–133, Oct. 2021., DOI:10.1109/MDAT.2021.3069087

[26] Q. He, Z. Ni, F. Chen, J. Wang, and X. Li, "Sub-g Vibration-threshold Triggered Dual Functions of Energy-harvesting and Vibration-sensing," pp. 5–7, 2016., DOI:10.1109/ICSENS.2016.7808557

[27] S.-Y. Park, K. Lee, H. Song, and E. Yoon, "Simultaneous Imaging and Energy Harvesting in CMOS Image Sensor Pixels," *IEEE Electron Device Lett.*, vol. 39, no. 4, pp. 1–1, 2018., DOI:10.1109/LED.2018.2811342

[28] I. Lee *et al.*, "System-On-Mud: Ultra-Low Power Oceanic Sensing Platform Powered by Small-Scale Benthic Microbial Fuel Cells," *IEEE Trans. Circuits Syst. I Regul. Pap.*, vol. 62, no. 4, pp. 1126–1135, 2015, DOI:10.1109/TCSI.2015.2390559

[29] G. Rovere, S. Fateh, and L. Benini, "A 2.2-µW Cognitive Always-On Wake-Up Circuit for Event-Driven Duty-Cycling of IoT Sensor Nodes," *IEEE J. Emerg. Sel. Top. Circuits Syst.*, vol. 8, no. 3, pp. 543–554, 2018., DOI:10.1109/jetcas.2018.2828505

[30] R. H. Olsson, R. B. Bogoslovov, and C. Gordon, "Event driven persistent sensing: Overcoming the energy and lifetime limitations in unattended wireless sensors," *Proc. IEEE Sensors*, pp. 1–3, 2016., DOI:10.1109/ICSENS.2016.7808398

[31] D. D. Wentzloff, A. Alghaihab, and J. Im, "Ultra-Low Power Receivers for IoT Applications: A Review," in *2020 IEEE Custom Integrated Circuits Conference (CICC)*, 2020, vol. 2020-March, pp. 1–8., DOI:10.1109/CICC48029.2020.9075938

[32] R. Piyare, A. L. Murphy, C. Kiraly, P. Tosato, and D. Brunelli, "Ultra Low Power Wake-Up Radios: A Hardware and Networking Survey," *IEEE Commun. Surv. Tutorials*, vol. 19, no. 4, pp. 2117–2157, 2017., DOI:10.1109/COMST.2017.2728092

[33] H. Bello, Z. Xiaoping, R. Nordin, and J. Xin, "Advances and Opportunities in Passive Wake-Up Radios with Wireless Energy Harvesting for the Internet of Things Applications," *Sensors*, vol. 19, no. 14, p. 3078, Jul. 2019., DOI:10.3390/s19143078

[34] S. Jeong *et al.*, "Always-On 12-nW Acoustic Sensing and Object Recognition Microsystem for Unattended Ground Sensor Nodes," *IEEE J. Solid-State Circuits*, vol. 53, no. 1, pp. 261–274, 2018., DOI:10.1109/JSSC.2017.2728787

[35] T. D. Wickens, *Elementary Signal Detection Theory*. Oxford University Press, 2001., ISBN:9780195092509

[36] D. Liu, Y. Luo, J. Liu, Y. Peng, L. Guo, and M. Pecht, "Lithium-ion battery remaining useful life estimation based on fusion nonlinear degradation AR model and RPF algorithm," *Neural Comput. Appl.*, vol 25, no 3–4, pp 557–572, 2014., DOI:10.1007/s00521-013-1520-x

[37] D. Linden and T. B. Reddy, *Handbook of batteries*, 3rd ed. New York, New York, USA: McGraw-Hill, 2002., ISBN:0071359788

[38] P. Mayer, M. Magno, and L. Benini, "A2Event: A Micro-Watt Programmable Frequency-Time Detector for Always-On Energy-Neutral Sensing," *Sustain. Comput. Informatics Syst.*, vol. 25, p. 100368, Mar. 2019., DOI:10.1016/j.suscom.2019.100368

[39] C. Salazar-García, R. Castro-González, and A. Chacón-Rodríguez, "RISC-V based sound classifier intended for acoustic surveillance in protected natural environments," *LASCAS 2017 - 8th IEEE Lat. Am. Symp. Circuits Syst. R9 IEEE CASS Flagsh. Conf. Proc.*, pp. 1–4, 2017., DOI:10.1109/LASCAS.2017.7948070

[40] D. Widhalm, K. M. Goeschka, and W. Kastner, "An Open-Source Wireless Sensor Node Platform with Active Node-Level Reliability for Monitoring Applications," *Sensors*, vol. 21, no. 22, p. 7613, Nov. 2021., DOI:10.3390/s21227613

[41] C. Titouna, M. Aliouat, and M. Gueroui, "FDS: Fault Detection Scheme for Wireless Sensor Networks," *Wirel. Pers. Commun.*, vol. 86, no. 2, pp. 549–562, Jan. 2016., DOI:10.1007/s11277-015-2944-7

[42] C. Wang, L. Xing, V. M. Vokkarane, and Y. (Lindsay) Sun, "Reliability and lifetime modeling of wireless sensor nodes," *Microelectron. Reliab.*, vol. 54, no. 1, pp. 160–166, Jan. 2014., DOI:10.1016/j.microrel.2013.08.001

[43] S. Kang, V. Rajaram, S. D. Calisgan, A. Risso, Z. Qian, and M. Rinaldi, "Near-Zero Power Integrated Microsystems for the IOT," in *2021 IEEE 34th International Conference on Micro Electro Mechanical Systems (MEMS)*, 2021, vol. 2021-Janua, no. January, pp. 143–148., DOI:10.1109/MEMS51782.2021.9375244

[44] C. Ren *et al.*, "A Self-Powered MEMS Inertial Switch for Potential Zero Power-Consumption Wake-Up Application," *J. Microelectromechanical Syst.*, vol. 30, no. 4, pp. 550–559, Aug. 2021., DOI:10.1109/JMEMS.2021.3081465

[45] V. Pinrod *et al.*, "Zero-power sensors with near-zero-power wakeup switches for reliable sensor platforms," *Proc. IEEE Int. Conf. Micro Electro Mech. Syst.*, pp. 1236–1239, 2017., DOI:10.1109/MEMSYS.2017.7863640

[46] R. W. Reger *et al.*, "Near-zero power accelerometer wakeup system," in *2017 IEEE SENSORS*, 2017, vol. 2017-Decem, pp. 1–3., DOI:10.1109/ICSENS.2017.8234277

[47] E. H. Cook *et al.*, "Low-power resonant acceleration switch for unattended sensor wake-up," *J. Microelectromechanical Syst.*, vol. 27, no. 6, pp. 1071–1081, 2018., DOI:10.1109/JMEMS.2018.2867282

[48] J. J. Bernstein *et al.*, "Resonant Acoustic MEMS Wake-Up Switch," *J. Microelectromechanical Syst.*, vol. 27, no. 4, pp. 625–634, 2018., DOI:10.1109/JMEMS.2018.2830322

[49] M. Price, J. Glass, and A. P. Chandrakasan, "A Low-Power Speech Recognizer and Voice Activity Detector Using Deep Neural Networks," *IEEE J. Solid-State Circuits*, vol. 53, no. 1, pp. 66–75, Jan. 2018., DOI:10.1109/JSSC.2017.2752838

[50] A. Raychowdhury, C. Tokunaga, W. Beltman, M. Deisher, J. W. Tschanz, and V. De, "A 2.3 nJ/Frame Voice Activity Detector-Based Audio Front-End for Context-Aware System-On-Chip Applications in 32-nm CMOS," *IEEE J. Solid-State Circuits*, vol. 48, no. 8, pp. 1963–1969, Aug. 2013., DOI:10.1109/JSSC.2013.2258827

[51] A. Di Mauro, F. Conti, and L. Benini, "An Ultra-Low Power Address-Event Sensor Interface for Energy-Proportional Time-to-Information Extraction," *Proc. 54th Annu. Des. Autom. Conf. 2017 - DAC '17*, pp. 1–6, 2017., DOI:10.1145/3061639.3062201

[52] D. H. Goldberg, A. G. Andreou, P. Julián, P. O. Pouliquen, L. Riddle, and R. Rosasco, "VLSI implementation of an energy-aware wake-up detector for an acoustic surveillance sensor network," *ACM Trans. Sens. Networks*, vol. 2, no. 4, pp. 594–611, 2006., DOI:10.1145/1218556.1218562

[53] S. J. Desai, M. Shoaib, and A. Raychowdhury, "An Ultra-Low Power, 'Always-On' Camera Front-End for Posture Detection in Body Worn Cameras Using Restricted Boltzman Machines," *IEEE Trans. Multi-Scale Comput. Syst.*, vol. 1, no. 4, pp. 187–194, 2015., DOI:10.1109/TMSCS.2015.2513741

[54] Z. Wang *et al.*, "A 148-nW Reconfigurable Event-Driven Intelligent Wake-Up System for AIoT Nodes Using an Asynchronous Pulse-Based Feature Extractor and a Convolutional Neural Network," *IEEE J. Solid State Circ.*, pp 15, 2021., DOI:10.1109/JSSC.2021.3113257

[55] H. Ghasemzadeh and R. Jafari, "Ultra low-power signal processing in wearable monitoring systems," *ACM Trans. Embed. Comput. Syst.*, vol. 13, no. 1, pp. 1–23, 2013., DOI:10.1145/2501626.2501636

This article has been accepted for publication in IEEE Sensors Journal. This is the author's version which has not been fully edited and content may change prior to final publication. Citation information: DOI 10.1109/JSEN.2022.3162319

Marko Gazivoda *et al*.: Always-on sparse event wake-up detectors: A Review
5

[56] D. Oletic, M. Gazivoda, and V. Bilas, "A Programmable 3-Channel Acoustic Wake-Up Interface Enabling Always-On Detection of Underwater Events within 20 µA," in *Proceedings Eurosensors2018*, 2018, vol. 2, no. 13, p. 7. DOI:10.3390/proceedings2130768

[57] M. Gazivoda and V. Bilas, "Low-power sensor interface with a switched inductor frequency selective envelope detector," *Sensors*, vol. 21, no. 6, pp. 1–21, Mar. 2021. DOI:10.3390/s21062124

[58] M. Gazivoda, D. Oletić, C. Trigona, and V. Bilas, "Passive extraction of signal feature using a rectifier with a mechanically switched inductor for low power acoustic event detection," *Sensors (Switzerland)*, vol. 20, no. 18, pp. 1–19, 2020., DOI:10.3390/s20185445

[59] B. Rumberg, D. W. Graham, and V. Kulathumani, "A low-power, programmable analog event detector for resource-constrained sensing systems," in *2012 IEEE 55th International Midwest Symposium on Circuits and Systems (MWSCAS)*, 2012, pp. 338–341., DOI:10.1109/MWSCAS.2012.6292026

[60] D. Oletic and V. Bilas, "Piezoelectric sensor front-end for energy-efficient acquisition of ultrasonic emissions related to water-stress in plants," in *Proceedings of IEEE Sensors*, 2019, vol. 2019-Octob, pp. 1–4., DOI:10.1109/SENSORS43011.2019.8956671

[61] K. M. H. Badami, S. Lauwereins, W. Meert, and M. Verhelst, "A 90 nm CMOS, 6 µW power-proportional acoustic sensing frontend for voice activity detection," *IEEE J. Solid-State Circuits*, vol. 51, no. 1, pp. 291–302, 2016., DOI:10.1109/JSSC.2015.2487276

[62] S. Bhattacharyya, S. Andryzcik, and D. W. Graham, "An Acoustic Vehicle Detector and Classifier Using a Reconfigurable Analog/Mixed-Signal Platform," *J. Low Power Electron. Appl.*, vol. 10, no. 1, p. 6, Feb. 2020. DOI:10.3390/jlpea10010006

[63] M. Fourniol, V. Gies, V. Barchasz, and E. Kussener, "Low-Power Wake-Up System based on Frequency Analysis for Environmental Internet of Things," *Proc. 14th IEEE/ASME Int. Conf. Mechatron. Embed. Syst. Appl*, p 1–6, 2018., DOI:10.1109/MESA.2018.8449164

[64] M. Gazivoda, D. Oletić, and V. Bilas, "Features and Always-On Wake-Up Detectors for Sparse Acoustic Event Detection," *Electron.*, vol. 11, no. 3, p. 14, Feb. 2022., DOI:10.3390/electronics11030478

[65] F. Sutton *et al.*, "The Design of a Responsive and Energy-efficient Event-triggered Wireless Sensing System," in *Proceedings of the 14th Int. Conf. on Embedded Wireless Systems and Networks (EWSN 2017)*, 2017, pp. 144–155., DOI:10.5555/3108009.3108028

[66] M. Yang, C.-H. Chien, T. Delbruck, and S.-C. Liu, "A 0.5V 55µW 64×2-channel binaural silicon cochlea for event-driven stereo-audio sensing," 2016, pp. 388–389., DOI:10.1109/ISSCC.2016.7418070

[67] S. Oh *et al.*, "An Acoustic Signal Processing Chip With 142-nW Voice Activity Detection Using Mixer-Based Sequential Frequency Scanning and Neural Network Classification," *IEEE J. Solid-State Circuits*, vol. 54, no. 11, pp. 3005–3016, Nov. 2019., DOI:10.1109/JSSC.2019.2936756

[68] G. Cohn *et al.*, "An ultra-low-power human body motion sensor using static electric field sensing," *Proc. 2012 ACM Conf. Ubiquitous Comput. - UbiComp*, p. 99, 2012., DOI:10.1145/2370216.2370233

[69] U. Antao, J. Choma, A. Dibazar, and T. Berger, "Low power, long life design for smart Intelligence, Surveillance, and Reconnaissance (ISR) sensors," *2012 IEEE Int. Conf. Technol. Homel. Secur. HST 2012*, pp. 631–636, 2012., DOI:10.1109/THS.2012.6459922

[70] W. Huang, Y.-S. Kuo, P. Pannuto, and P. Dutta, "Opo: A Wearable Sensor for Capturing High-fidelity Face-to-face Interactions," *Proc. 12th ACM Conf. Embed. Netw. Sens. Syst.*, pp. 61–75, 2014., DOI:10.1145/2668332.2668338

[71] H. Abdalla and T. K. Horiuchi, "An analog VLSI low-power envelope periodicity detector," *IEEE Trans. Circuits Syst. I Regul. Pap.*, vol. 52, no. 9, pp. 1709–1720, 2005., DOI:10.1109/LSENS.2017.2762918

[72] C. Y. Huang, P. T. Huang, C. C. Yang, C. Te Chuang, and W. Hwang, "Energy-efficient gas recognition system with event-driven power control," *Int. Syst. Chip Conf.*, vol. 2016-Febru, pp. 245–250, 2016., DOI:10.1109/SOCC.2015.7406956

[73] S. Lauwereins, W. Meert, J. Gemmeke, and M. Verhelst, "Ultra-low-power voice-activity-detector through context- and resource-cost-aware feature selection in decision trees," in *2014 IEEE International Workshop on Machine Learning for Signal Processing (MLSP)*, 2014, pp. 1–6., DOI:10.1109/MLSP.2014.6958918

[74] P. Dutta, M. Grimmer, A. Arora, S. Bibykt, and D. Culler, "Design of a wireless sensor network platform for detecting rare, random, and ephemeral events," *2005 4th Int. Symp. Inf. Process. Sens. Networks, IPSN 2005*, vol. 2005, pp. 497–502, 2005., DOI:10.1109/IPSN.2005.1440983

[75] Y. Tomimatsu, K. Kuwana, T. Kobayashi, T. Itoh, and R. Maeda, "A piezoelectric flow sensor for wake-up switch of wireless sensor network node," *Proc. - 2012 2nd Work. Des. Control Softw. Implement. Distrib. MEMS, dMEMS 2012*, pp. 53–57, 2012., DOI:10.1109/dMEMS.2012.10

Marko Gazivoda (S'17) received the B.Sc. and M.Sc. degrees from the University of Zagreb in 2014 and 2016, respectively, where he is currently pursuing the Ph.D. degree with the Faculty of Electrical Engineering and Computing. His research interests include energy efficient sensors, detectors and interfaces and electronic systems design.
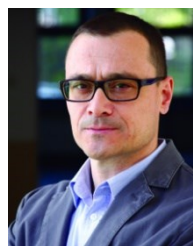
Vedran Bilas (SM'10) is a Professor with the Faculty of Electrical Engineering and Computing and the Head of the Laboratory for Intelligent Sensor Systems with the University of Zagreb. He has over 20 years of research, development, and technology transfer experience in the area of sensors and electronic systems. His research interests are in the field of energy efficient intelligent and networked sensors in various application domains.

Publication 2

Features and Always-On Wake-Up Detectors for Sparse Acoustic Event Detection

Marko Gazivoda *, Dinko Oletić and Vedran Bilas

Faculty of Electrical Engineering and Computing, University of Zagreb, 10000 Zagreb, Croatia;
dinko.oletic@fer.hr (D.O.); vedran.bilas@fer.hr (V.B.)
* Correspondence: marko.gazivoda@fer.hr

Abstract: The need to understand and manage our surroundings has led to increased interest in sensor networks for the continuous monitoring of events and processes of interest. To reduce the power consumption required for continuous monitoring, dedicated always-on wake-up detectors have been designed, with an emphasis on their low power consumption, simple and robust design, and reliable and accurate detection. An especially interesting application of these wake-up detectors is in detecting acoustic signals. In this paper, we present a study on the features and detectors applicable for the detection of sporadic acoustic events. We perform a state-of-the-art acoustic detector analysis, grouping the detectors based on the features they utilize and their implementations. This analysis shows that acoustic wake-up detectors predominantly utilize spectro-temporal (56%) and temporal features (36%). Following the state-of-the-art analysis, we select two detector architecture candidates for a case study on passing motor vehicle detection. We utilize our previously developed spectro-temporal decomposition detector and develop a novel level-crossing rate detector. The results of the case study shows that the proposed level-crossing rate detector has lower component count (44 compared to 70) and power consumption (9.1 μW compared to 34.6 μW) and is an optimal solution for SNRs over 0 dB.

Keywords: low power; state-of-the-art analysis; wake-up detector architecture; embedded electronics; case study; motor vehicle detection

1. Introduction

The growing need to better understand and manage our surroundings has led to increased interest in the continuous monitoring of events and processes, utilizing sensor networks consisting of hundreds or thousands of small, robust sensor nodes [1–4]. However, having a complex system continuously monitoring for events of interest consumes a lot of power [5,6]. To reduce this power consumption, dedicated always-on low-power wake-up detectors have been designed that wake up the more complex circuits with higher power consumption only when an event of interest is detected [3,7]. Such detectors determine the presence of event candidates by performing low-power extraction and analysis of the sensor signal's features [8–11].

The key emphasis in the design of wake-up detectors is on low power consumption, cheap, simple design, and accurate detection [7,11–14] to ensure low false detection rates, even in the most adverse conditions, as false event detections increase the overall system's power consumption by causing unnecessary activations of the main stage.

Wake-up detectors are often employed in acoustic event recognition because acoustic signals contain a lot of easily extracted information [15–17]. Because of this, they have been utilized in many fields, including safety and security [5,18–21], biomedical and health monitoring [22–24], environmental monitoring [12,25–27], Internet of Things (IoT)

applications [2,8], structural health monitoring, non-destructive testing and machinery diagnosis [24], speech or voice activity detection [24,28–33], and others.

In this paper, we present a study on the signal features and wake-up detector architectures applicable for the detection of sporadic, rarely occurring transient acoustic events that appear in the lower end of the acoustic spectrum (up to a few kHz), such as passing motor vehicles.

Our contributions include a review of the state-of-the-art (SOTA) acoustic detectors, the selection of detector architectures of interest, and a comparison of their performance in a case study of motor vehicle (speedboat) detection. A dditionally, we develop a novel implementation of a level-crossing rate acoustic wake-up detector and analyze its performance.

The rest of the paper is organized as follows. Section 2 details the SOTA acoustic wake-up detector analysis. Stemming from the SOTA analysis, in Section 3, the detector selection is performed, and the principles of operation and generalized block schematics of the selected detectors are presented. In Section 4, a case study experiment is presented to evaluate the performance of the selected detectors in the detection of passing motor vehicles. Section 5 concludes the paper and presents future work.

2. State-of-the-Art Acoustic Wake-Up Detector Analysis

2.1. Methodology

To select the applicable detectors, we perform an analysis of SOTA acoustic wake-up detectors. We explore detector implementations, feature extraction domains (analog, digital, or mixed), power consumptions, and detection accuracies (true and false positive rates). The detector implementation is divided into embedded and integrated, and both are further divided into analog, digital, and mixed-signal detectors. The embedded implementations utilize commercial off-the-shelf (COTS) components, while the integrated implementations are custom-made.

In this analysis, we group the detectors by the acoustic signal features they utilize. To enable this grouping, we devise a feature categorization (Table 1) by analyzing the literature on acoustic signal features [34–36]. While a detailed description of each feature used in acoustic event detection would go beyond the scope of this paper, readers interested in a more detailed explanation of any mentioned feature can find detailed explanations in the literature focused on acoustic feature analysis [34–36].

Table 1. Acoustic signal feature categorization.

Temporal	Spectral	Spectro-Temporal	Cepstral	Other
Level-crossing rate-based	Spectral shape-based	Spectro-temporal decomposition-based	Mel-frequency cepstral coefficient-based	Eigenspace-based
Temporal amplitude-based	Brightness-based	Hurst parameter-based	Other cepstral coefficient-based	Acoustic environment-based
Temporal power-based	Tonality-based	MP-based Gabor features	-	-
Rhythm-based	Chroma-based	Sparse coding tensor-based		-
Correlation-based	-	-	-	-

2.2. Results

As we can see from the results of the SOTA acoustic wake-up detector analysis (presented in Table 2), six of the categorized acoustic feature subgroups are used in power-constrained wake-up detector event detection.

The spectro-temporal decomposition feature subgroup implies the filtering of the input signals into sub-bands, and the continuous extraction of each sub-band's feature of interest (envelope, energy, power, root mean square (RMS)). After extraction, the feature

values are quantified and converted into a binarized spectro-temporal template. A classifier determines this template's resemblance to a preset template, defined by the event of interest. These detectors are usually implemented as mixed-signal detectors, with feature extraction and processing performed in the analog and classification in the digital domain.

The level-crossing rate feature subgroup entails converting the input signal's crossings of a predefined level into pulses of fixed length and amplitude, estimating the number of those pulses in a defined time interval, quantifying it and, therefore, quantifying the level crossing rate and determining if it is within the bounds of level-crossing rates specific for the event of interest. These detectors are usually implemented fully digitally, but they can also be implemented completely in the analog domain.

The correlation subgroup requires the input signal to be compared to a delayed version of itself (autocorrelation) or to a preset template representing the event of interest (cross-correlation). Autocorrelation can also be employed to estimate the input signal's spectral content by examining and locating the local maxima of the autocorrelation function, which appear at delay times equal to periods of the input signal's dominant spectral components. These detectors are usually implemented as digital, because of the impracticality of the analog implementation of some required elements, such as delay lines or memories for storing templates.

The short-time energy feature subgroup implies measuring the input signal's energy in short time windows and comparing it to a preset template. While the SOTA detector utilizing this feature subgroup ([31]) is implemented as digital, a mixed-signal implementation similar to the spectro-temporal decomposition could also be considered.

The spectral shape feature subgroup requires the signal spectrum to be determined, and then for certain parameters of its shape to be examined and quantified. To obtain a detailed enough spectrum representation, these detectors must be implemented as digital.

The cepstral coefficients entail estimating the signal's spectrum, calculating the logarithm of the spectral amplitude, and then performing the discrete cosine transformation on it, generating a cepstrum. The amplitudes of the cepstrum peaks represent cepstral coefficients. Detectors utilizing these features can be implemented as mixed-signal detectors, employing analog domain filtering specific for the cepstral coefficients of interest, followed by digital domain cepstral coefficient estimation.

Table 2. Acoustic wake-up detectors.

Feature group	Feature subgroup	Feature	Ref.	Detector Implementation	Feature Extraction Domain	Power (μW)	Detection Accuracy	
							TP (%)	FP (%)
Spectro-temporal	**Spectro-temporal decomposition**	Spectro-temporal envelope	[37,38]	Embedded mixed	Analog	7.33; 34.92	90.91	Not stated
			[8,15]	Embedded mixed	Analog	26.89	98.67; 100	14; 0
			[16]	Integrated mixed	Analog	43	100	0
		Spectro-temporal energy	[39]	Integrated mixed	Analog	1.01	Not stated	Not stated
			[32]	Integrated digital	Digital	~ 100	96.63	2.33
		Spectro-temporal power	[40]	Integrated mixed	Mixed	0.142	90–91.5	Not stated
		Spectro-temporal RMS	[41]	Integrated mixed	Analog	6	89	Not stated
		Spectro-temporal (absolute) voltage	[17]	Integrated mixed	Digital	0.012	96 – 98	0
			[30]	Integrated analog	Analog	2.5	Not stated	Not stated

			[28,42]	Integrated mixed	Analog	1; 27.77	~85; ~80	Not stated; 0
		Spectro-temporal instant rate of change	[43]	Integrated digital	Digital	0.148	85 – 99	1 – 18
Temporal	**Level-crossing rate**	Zero-crossing rate	[13]	Embedded analog	Analog	34	Not stated	Not stated
		Zero-crossing rate	[8]	Embedded digital	Digital	~ 600	Not stated	Not stated
		Zero-crossing rate with peak amplitude (ZCPA)	[44]	Integrated digital	Digital	Not stated	98	Not stated
		Zero-crossing with short-time magnitude difference	[45]	Embedded digital	Digital	30.71	91	Not stated
	Correlation	Autocorrelation	[31]	Integrated digital	Digital	24.4	55 – 95	5 – 20
		Autocorrelation	[46]	Integrated mixed	Digital	0.835	97	0
		Cross-correlation	[47]	Integrated mixed	Mixed	1.5	92	7
	Short-time energy	Short-time energy difference	[31]	Integrated digital	Digital	8.5	55 – 95	5 – 20
	Multiple	Rise time, min/max, energy	[48]	Embedded mixed	Digital	8.7	100	Not stated
Spectral	**Spectral shape**	Power spectrum density	[49]	Integrated mixed	Digital	4.7	Not stated	Not stated
Cepstral	**Cepstral coefficients**	Mel-frequency CC	[33]	Integrated digital	Digital	0.51	97.3	2 – 2.3

2.3. Discussion

As can be seen from Table 2, most acoustic wake-up detectors utilize spectro-temporal (56% of all analyzed detectors) and, to a lesser extent, temporal features (36% of all analyzed detectors). Furthermore, of those detectors, spectro-temporal-decomposition-based (61%), level-crossing rate-based (17%) and correlation-based (13%) detectors constitute the majority.

Next, we can see that the integrated custom designs account for 68% of all analyzed wake-up detector designs, while embedded implementations utilizing COTS components constitute around 32%.

There is approximately the same number of detectors that extract the features in the analog and digital domains, with only a few detectors extracting features in both domains simultaneously (8%).

Acoustic wake-up detectors have high detection accuracies (over 90% true positives and under 15% false positives, where stated) and their power consumptions vary from around 10 nW to around 600 μW, greatly depending on the detector implementation and utilized feature. Integrated mixed-signal and digital spectro-temporal decomposition detectors can reach sub-μW power consumptions, while embedded level-crossing rate detectors reach tens or even hundreds of μW.

3. Wake-Up Detector Selection

3.1. Criteria

Motivated by the passing motor vehicle use case scenario, we aim to develop a wake-up detector of sporadic, transient acoustic events, lasting for several seconds, with the bandwidth spanning up to 2 kHz.

We focus on wake-up detector architectures implementable with COTS components, operating on analog-domain signals, designed for direct interfacing with acoustic sensors with little or no amplification, and avoiding power-hungry analog-to-digital (AD) conversion [16]. Hence, the detector should be able to reliably operate with weak electric input signals (on the order of 10 mV).

Finally, a wake-up detector must have high detection accuracy, both in terms of high true positive rates, as a detector should not miss events, and low false positive rates, as false detections lead to wasting power due to unnecessary activations of the power-hungry main stage.

3.2. Results

As we can see from Table 3, wake-up detectors utilizing level-crossing rate and spectro-temporal decomposition meet all our selection criteria.

Table 3. Detector Selection.

Detectors Utilizing	Criteria			
	Applicable for Signals of Interest	Embedded Implementation	No AD Conversion	Detection Accuracy
Autocorrelation / cross-correlation	✓	✗	✗	✓
Level-crossing rate	✓	✓	✓	✓
Spectro-temporal decomposition	✓	✓	✓	✓
Other features	✓	✗	✗	✓

3.3. Selected Detectors

3.3.1. Spectro-Temporal Decomposition

The generalized architecture of the spectro-temporal decomposition wake-up detector is shown in Figure 1.
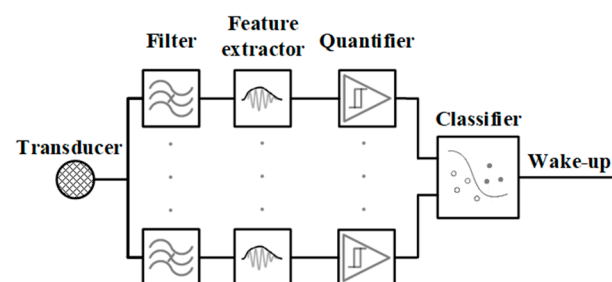
Figure 1. Spectro-temporal decomposition wake-up detector generalized architecture.

The spectro-temporal decomposition detector consists of a filter for spectral decomposition, a feature extractor, a quantifier for quantifying the extracted features, and a classifier to determine if the input signal is from an event of interest. It is usually implemented with multiple channels.

3.3.2. Level-Crossing Rate

The level-crossing rate wake-up detector general architecture is shown in Figure 2.
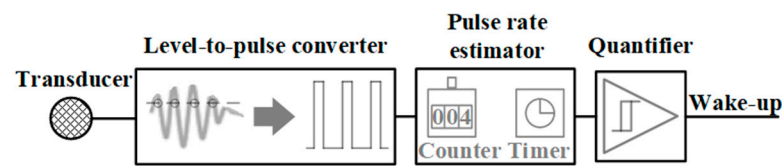
Figure 2. Level-crossing rate wake-up detector generalized architecture.

The level-crossing rate detector consists of a level-to-pulse converter that detects level crossings and converts them into pulses, a pulse rate estimator for estimating the level-crossing rate, and a quantifier for quantifying the level-crossing rate. It is usually implemented as a single-channel detector.

4. Motor Vehicle Passing Detection

In this section, we present a case study in which we evaluate the performance of the two selected detectors in the detection of passing motor vehicles through the analysis of their power consumption, minimal input voltage, detection accuracy, and component count (estimate of hardware complexity).

4.1. Motor Vehicle Passing Event and Signal

For our dataset, we used 11 prerecorded signals of a twin-engine speedboat passing over a hydrophone submerged approximately 1 m under the surface in shallow water [50]. A representative signal and its spectrogram are shown in Figure 3a and 3b, respectively.

(a)

(b)
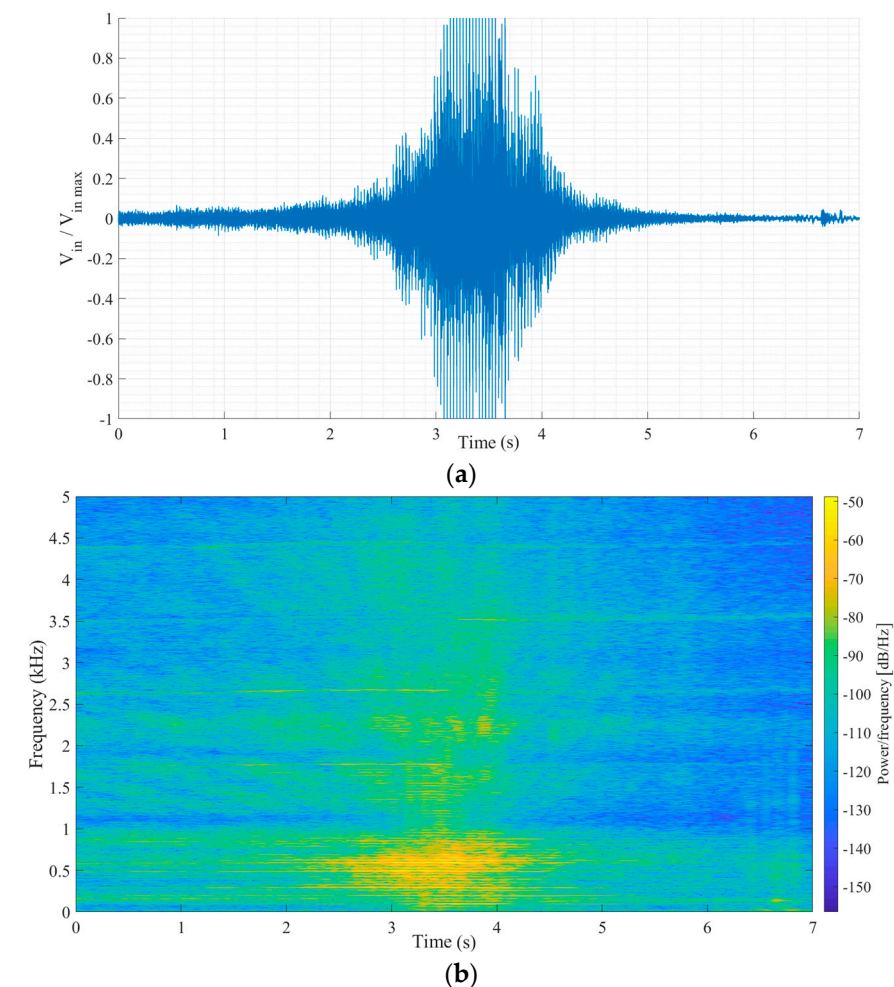
Figure 3. (**a**) Speedboat passing signal and (**b**) its spectrogram.

In case of the wake-up detector utilizing spectro-temporal decomposition, the passage of the speedboat can be detected by detecting and tracking the duration of the presence of the signal in the characteristic frequency band (e.g., 100 Hz to 1 kHz for typically 0.5 s – 5 s). On the other hand, a similar type of information is obtained by the level-crossing wake-up detector by tracking the rate at which the signal passes a predefined level in a set time interval.

4.2. Detector Implementations

4.2.1. Spectro-Temporal Decomposition Detector Implementation

We utilize an embedded spectro-temporal decomposition detector that we first presented in [38] (schematic and photograph shown in Figure 4).

(**a**)   (**b**)
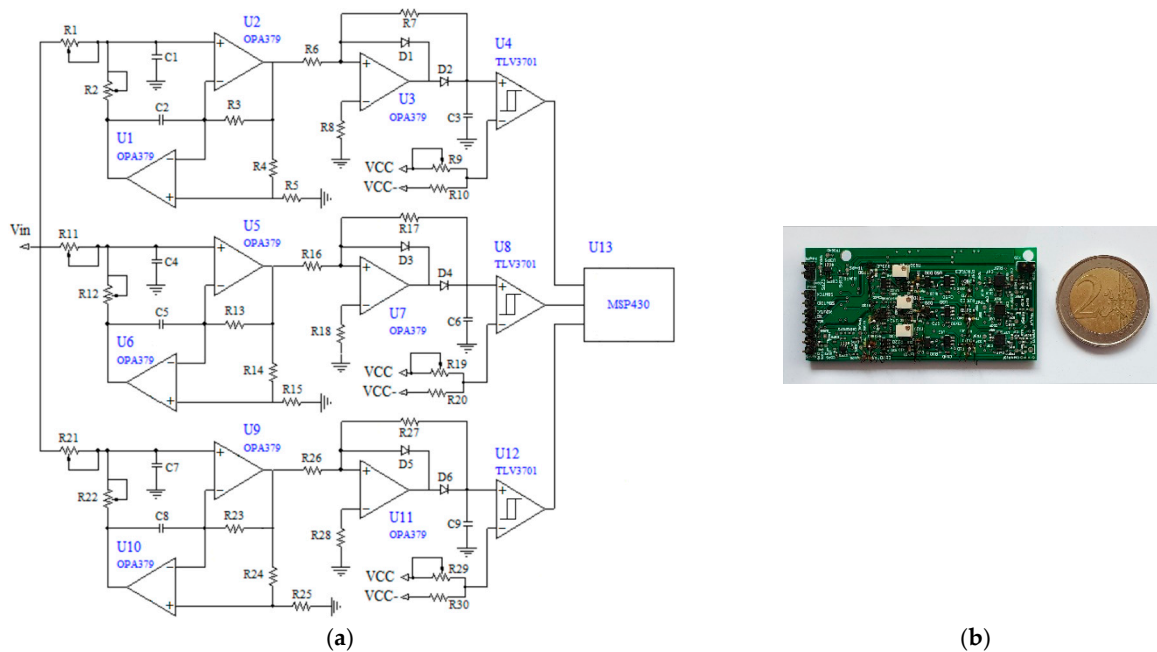
Figure 4. Spectro-temporal decomposition wake-up detector from [38]: (**a**) schematic and (**b**) photograph.

As can be seen from Figure 4a, the implemented detector consists of three channels. Each channel extracts information on signal presence within its frequency band. Each channel filters the input signal by a digitally programmable active bandpass filter in the general impedance converter (GIC) topology, implemented with two MCP6142 operational amplifiers. The first channel spans the frequency range from 200 Hz to 500 Hz, the second from 500 Hz to 1 kHz, and the third from 1 kHz to 2.5 kHz. The central frequency and bandpass are programmable (within set limits) in 256 steps by digitally adjustable AD5144 potentiometers.

After filtering, the envelope is extracted utilizing an active voltage doubler, consisting of an MCP6141 operational amplifier and two diodes. The envelope is then quantified using a TLV3701 comparator, with a digitally adjustable threshold, adjusted by another AD5144 potentiometer.

Classification is implemented by binary template matching. A template representing the signal of interest is programed into an MSP430F2013 low-power microcontroller, which also implements a three-channel digital sequence recognition state machine. If the spectro-temporal envelopes' relations match the predefined template, a wake-up signal triggers a more power-hungry digital audio signal processing stage. To achieve this, the microcontroller implements a state machine, which in each state S_0, …, S_k compares the binary outputs of the three comparators to the prestored three-channel template. The

change from S_0 to S_1 is asynchronous, and occurs upon the first change of comparator state (started by an interrupt), while S_1 to S_k each last 0.5 s up to the maximal sequence length. A more detailed explanation on the basics of the state machine implementation can be found in [9]. For this experiment, the sequence either ends without a wake-up after 7 seconds (in S_{14}) if there is no template match, or with a wake-up signal if all three channels' comparators are simultaneously in a high state for a duration between 0.5 s and 4 s (preset template). This sequence description leads to the state machine implementation with states S_0 to S_{14}. The state machine functionality is also illustrated in Figure 5.

(a)

(b)
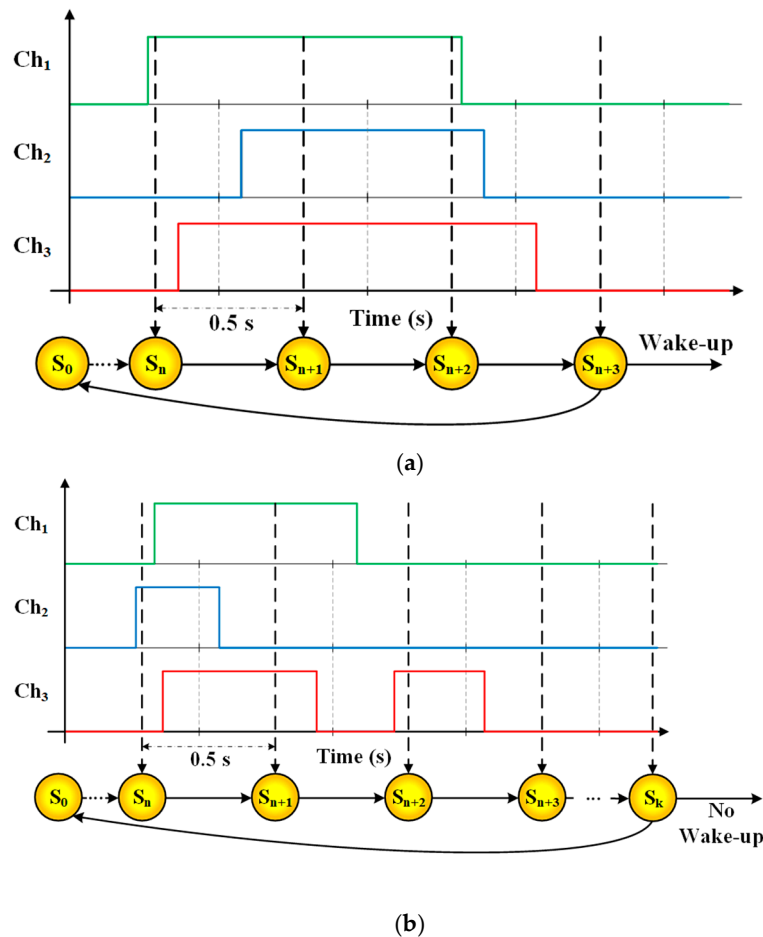
Figure 5. Microcontroller state machine implementation and event detection scheme. Ch_1 to Ch_3 and the three colored lines (green, blue and red) represent each channel's comparator output, and S_0 to S_k are the state machine states, each lasting 0.5 s. (**a**) Event detected: at least 2 and no more than 9 consecutive states have all 3 comparator outputs in a high state, and a wake-up signal is generated. (**b**) No event detected: the total S_0 to S_{14} sequence passes without meeting the detection condition, no wake-up signal is generated.

4.2.2. Level-Crossing Rate Detector Implementation

We developed and utilized a novel embedded level-crossing rate detector, which is an adapted version of a similar detector presented in [13] (schematic and photograph shown in Figure 6).

The level-crossing detector consists of three main parts. In the first part, each level-crossing is detected with a TLV3701 comparator. The level is set by adjusting the comparator threshold and, for this experiment, it is set to 2.2 mV. Every time the comparator output changes to a high state, a monostable (consisting of two SN74AUP1G02 NOR gates) is triggered to generate a fixed-length pulse. These pulses are summed by a passive RC circuit, whose output, thus, represents the number of level crossings.

The second part is the timer that consists of a capacitor connected to a TLV3701 comparator with an adjustable threshold. The capacitor is charged by a fixed voltage source over a trimmer resistor. The trimmer resistor and comparator threshold values determine the capacitor charge time, which is set to around 600 ms for this experiment. When the capacitor voltage reaches the comparator threshold, the comparator output changes and closes the S1 switch (TMUX1101) to propagate the RC circuit voltage to the final detector part. After an interval determined by the delay line, the reset switches S2 and S3 (TMUX1101) of the RC circuit and the timer close, allowing their capacitors to discharge to the ground. During the reset, the switch S1 opens, disconnecting the RC circuit from the final detector part. After the RC circuit and timer resets are complete, the reset switches open, and a new level crossing counting interval starts. For this experiment, the delay of the reset signal is set to around 5 ms.

(**a**)

(**b**)
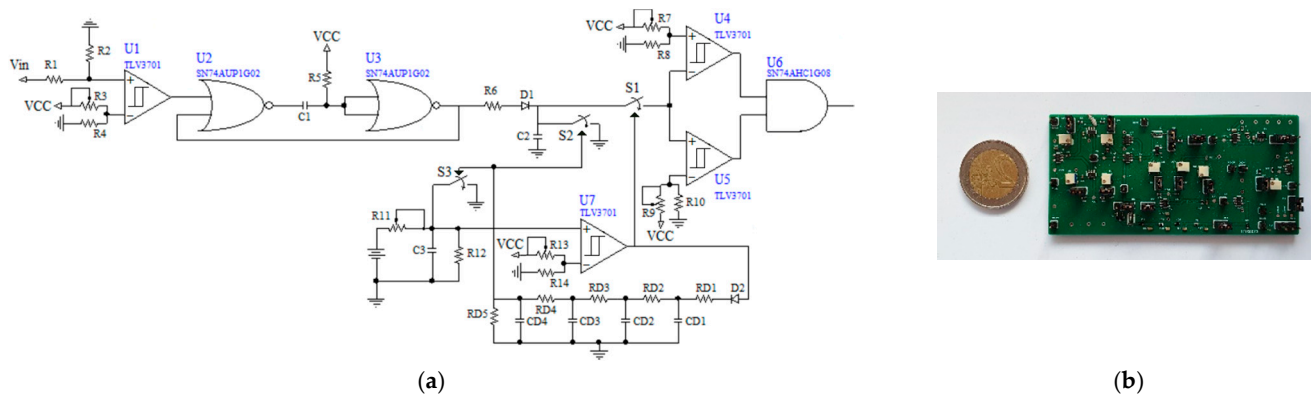
Figure 6. Novel level-crossing rate wake-up detector: (**a**) schematic and (**b**) photograph.

The final part consists of two TLV3701 comparators with adjustable thresholds and an AND logic gate. If the RC circuit voltage is both higher than the lower threshold and lower than the higher one, the level-crossing rate is within the set bounds, an event of interest is detected, and a wake-up pulse is generated at the AND gate output. For this experiment, the lower and upper bounds are set to 100 mV and 625 mV, respectively.

4.3. Experimental Setup and Procedure

4.3.1. Experimental Setup

The experimental setup utilized in this case study is shown in Figure 7.
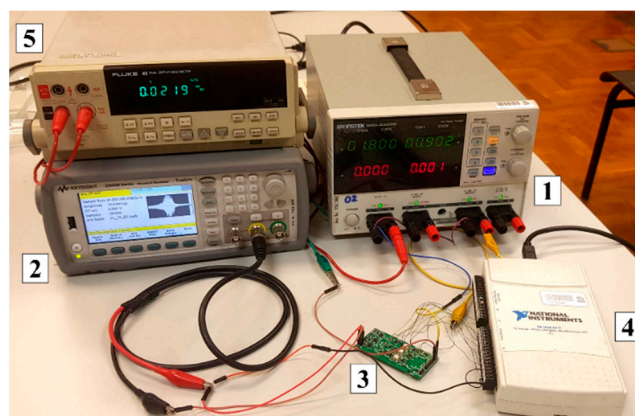
Figure 7. Experimental setup, with marked components: (1) power source, (2) waveform generator, (3) tested detector PCB, (4) data acquisition card, and (5) multimeter.

The experimental setup (Figure 7) consists of a GW INSTEK GPD-4303S power source (1), a Keysight 33500B waveform generator (2), the tested detector PCBs (spectro-temporal decomposition or level-crossing rate detector) (3), a National Instruments USB-6211 data acquisition card (4), and a Fluke 45 multimeter (5).

4.3.2. Experimental Procedure

The prerecorded speedboat signals were processed in MATLAB, cropped to a duration of 7 s, and then attenuated to determine the lowest input signal with which each detector is operational. Then, for the detection accuracy test, the input signals are scaled to 10 mV and 20 mV peak-to-peak for the level-crossing and spectro-temporal detector, respectively. This voltage scaling adjusts the input signal peak-to-peak voltages to adequately represent the signals generated by passing speedboats on passive hydrophones. Additionally, both detectors are operational with higher voltage levels, with threshold adjustments. However, if the approximate expected voltage levels are not known for a given application, or the input signal dynamic range would expectedly exceed around 40 dB, an additional automatic gain control (AGC) amplifier would have to be added to each detector's input to ensure correct operation.

To compare the performance of the two wake-up detectors, different levels of white noise were added to each signal to achieve signal-to-noise ratio (SNR) levels from −15 dB to 15 dB with a 5 dB step. Such signals were then stored in the waveform generator used as a signal source for the detectors. The detector outputs are recorded by a data acquisition card, and the recordings are processed using MATLAB.

For the spectro-temporal detector, a successful wake-up was recorded when its comparator outputs matched the predefined binary template and the detector generated a wake-up signal. On the other hand, for the level-crossing rate detector, successful detection is recorded if the RC circuit capacitor voltage was within predefined bounds, generating a wake-up signal.

The detector's power consumption was assessed by measuring its supply current (using a multimeter) and multiplying it with the detector's supply voltage, consumed in the steady state, while listening for the acoustic event.

4.4. Results

In Table 4 and Figure 8, we present the case study results, showing each detector's power consumption, minimal input voltage, component count, and detection accuracy.

Table 4. Wake-up detector's power consumption, minimal input voltage and component count.

Detector	Power (μW)	Minimal Input Voltage (mVpp)	Number of Components			
			Active	Passive	Diode	Total
Spectro-temporal envelope detector	34.6	20	12 + μC	51	6	70
Level-crossing rate detector	9.1	10	7	35	2	44
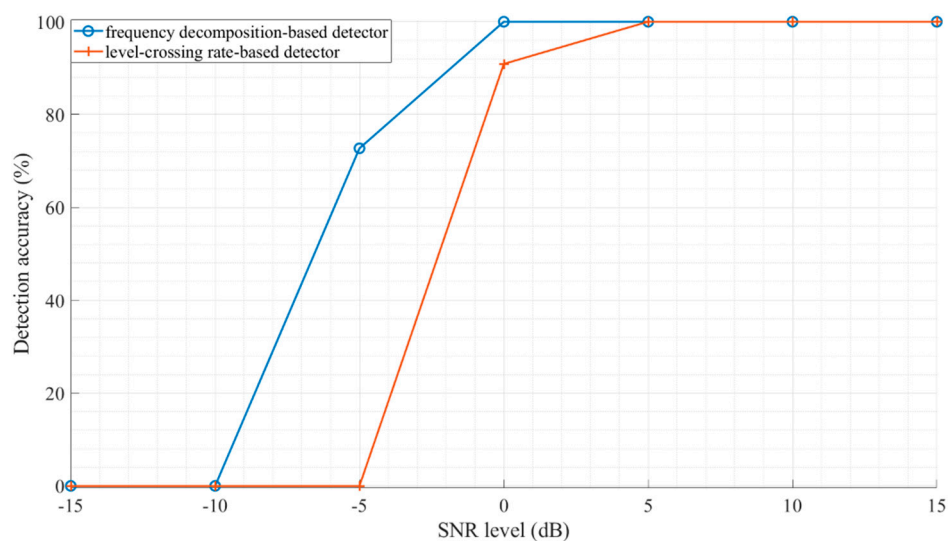
Figure 8. Comparison of speedboat passing detections at given SNR with selected detectors.

As we can see from Table 4 and Figure 8, the level-crossing rate detector has a significantly lower component count and would require around a 40% smaller area to implement (hardware complexity), has lower power consumption, and is operational with lower input voltages, while the spectro-temporal detector has slightly better performance with low-SNR signals, being operational even with −5 dB SNR, as opposed to the level-crossing rate one, which requires at least an SNR of 0 dB for the examined implementation.

5. Conclusions

In this paper, we presented a study on low-power always-on sporadic acoustic event wake-up detector designs. To determine the employable detectors and features for this application, we performed a SOTA acoustic wake-up detector analysis, which showed that most acoustic wake-up detectors utilize spectro-temporal (56%) and temporal features (36%), and that the dominant detector implementation is integrated custom-made detectors (68%). Following the SOTA analysis, we presented criteria and selected spectro-temporal decomposition and level-crossing rate as features that allow for the design of a low-power, embedded, always-on wake-up detector operating in the analog domain. These two wake-up detector designs were compared on a case study on passing marine motor vehicle detection. This case study showed that the level-crossing rate detector can be made with a significantly lower component count (44 compared to 70) and power consumption (9.1 µW compared to 34.6 µW), but a slightly narrower SNR range of operation (minimum of 0 dB SNR compared to -5 dB) than the spectro-temporal detector. In future work, the possibilities of utilizing features not utilized previously in wake-up detectors will be examined, and a more detailed study of the novel level-crossing rate detector will be performed.

References

1. Alioto, M. From Less Batteries to Battery-Less Alert Systems with Wide Power Adaptation down to nWs—Toward a Smarter, Greener World. *IEEE Des. Test* **2021**, *38*, 90–133. https://doi.org/10.1109/MDAT.2021.3069087.

2. Alioto, M. IoT: Bird's Eye View, Megatrends and Perspectives. In *Enabling the Internet of Things*; Alioto, M., Ed.; Springer International Publishing: Cham, Switzerland, 2017; pp. 1–45, ISBN 978-3-319-51480-2.

3. Goux, N.; Badets, F. Review on event-driven wake-up sensors for ultra-low power time-domain design. *Midwest Symp. Circuits Syst.* **2018**, *2018*, 554–557. https://doi.org/10.1109/MWSCAS.2018.8623935.

4. Zikria, Y.B.; Ali, R.; Afzal, M.K.; Kim, S.W. Next-Generation Internet of Things (IoT): Opportunities, Challenges, and Solutions. *Sensors* **2021**, *21*, 1174. https://doi.org/10.3390/s21041174.

5. Thoen, B.; Ottoy, G.; Rosas, F.; Lauwereins, S.; Rajendran, S.; De Strycker, L.; Pollin, S.; Verhelst, M. Saving energy in WSNs for acoustic surveillance applications while maintaining QoS. In Proceedings of the 2017 IEEE Sensors Applications Symposium, Glassboro, NJ, USA, 13–15 March 2017; pp. 1–6. https://doi.org/10.1109/SAS.2017.7894109.

6. Rovere, G.; Fateh, S.; Benini, L. A 2.2-μW Cognitive Always-On Wake-Up Circuit for Event-Driven Duty-Cycling of IoT Sensor Nodes. *IEEE J. Emerg. Sel. Top. Circuits Syst.* **2018**, *8*, 543–554. https://doi.org/10.1109/jetcas.2018.2828505.

7. Olsson, R.H.; Bogoslovov, R.B.; Gordon, C. Event driven persistent sensing: Overcoming the energy and lifetime limitations in unattended wireless sensors. In Proceedings of the 2016 IEEE SENSORS, Orlando, FL, USA, 30 October–3 November 2016; pp. 1–3. https://doi.org/10.1109/ICSENS.2016.7808398.

8. Fourniol, M.; Gies, V.; Barchasz, V.; Kussener, E. Low-Power Wake-Up System based on Frequency Analysis for Environmental Internet of Things. In Proceedings of the 2018 14th IEEE/ASME International Conference on Mechatronic and Embedded Systems and Applications (MESA), Oulu, Finland, 2–4 July 2018; pp. 1–6. https://doi.org/10.1109/MESA.2018.8449164.

9. Oletic, D.; Korman, L.; Magno, M.; Bilas, V. Time-frequency pattern wake-up detector for low-power always-on sensing of acoustic events. In Proceedings of the 2018 IEEE International Instrumentation and Measurement Technology Conference (I2MTC), Houston, TX, USA, 14–17 May 2018; pp. 1–6. https://doi.org/10.1109/I2MTC.2018.8409577.

10. Anastasopoulos, A.A. Signal Processing and Pattern Recognition of Ae Signatures. In *Experimental Analysis of Nano and Engineering Materials and Structures*; Springer: Dordrecht, The Netherlands, 2007; pp. 929–930. https://doi.org/10.1007/978-1-4020-6239-1_462.

11. Jensen, U.; Kugler, P.; Ring, M.; Eskofier, B.M. Approaching the accuracy–cost conflict in embedded classification system design. *Pattern Anal. Appl.* **2016**, *19*, 839–855. https://doi.org/10.1007/s10044-015-0503-1.

12. Mayer, P.; Magno, M.; Benini, L. Self-Sustaining Acoustic Sensor with Programmable Pattern Recognition for Underwater Monitoring. *IEEE Trans. Instrum. Meas.* **2019**, *68*, 2346–2355. https://doi.org/10.1109/TIM.2018.2890187.

13. Fourniol, M.; Gies, V.; Barchasz, V.; Kussener, E.; Barthelemy, H.; Vauche, R.; Glotin, H. Analog Ultra Low-Power Acoustic Wake-Up System Based on Frequency Detection. In Proceedings of the 2018 IEEE International Conference on Internet of Things and Intelligence System (IOTAIS), Bali, Indonesia, 1–3 November 2018; pp. 109–115. https://doi.org/10.1109/IOTAIS.2018.8600849.

14. Astapov, S.; Preden, J.S.; Ehala, J.; Riid, A. Object detection for military surveillance using distributed multimodal smart sensors. In Proceedings of the 2014 19th International Conference on Digital Signal Processing, Hong Kong, China, 20–23 August 2014; pp. 366–371. https://doi.org/10.1109/ICDSP.2014.6900688.

15. Mayer, P.; Magno, M.; Benini, L. A2Event: A Micro-Watt Programmable Frequency-Time Detector for Always-On Energy-Neutral Sensing. *Sustain. Comput. Inform. Syst.* **2019**, *25*, 100368. https://doi.org/10.1016/j.suscom.2019.100368.

16. Bhattacharyya, S.; Andryzcik, S.; Graham, D.W. An Acoustic Vehicle Detector and Classifier Using a Reconfigurable Analog/Mixed-Signal Platform. *J. Low Power Electron. Appl.* **2020**, *10*, 6. https://doi.org/10.3390/jlpea10010006.

17. Jeong, S.; Chen, Y.; Jang, T.; Tsai, J.M.L.; Blaauw, D.; Kim, H.S.; Sylvester, D. Always-On 12-nW Acoustic Sensing and Object Recognition Microsystem for Unattended Ground Sensor Nodes. *IEEE J. Solid-State Circuits* **2018**, *53*, 261–274. https://doi.org/10.1109/JSSC.2017.2728787.

18. Wang, Y.; Zhou, R.; Liu, Z.; Yan, B. A Low-Power CMOS Wireless Acoustic Sensing Platform for Remote Surveillance Applications. *Sensors* **2020**, *20*, 178. https://doi.org/10.3390/s20010178.

19. Kucukbay, S.E.; Sert, M.; Yazici, A. Use of Acoustic and Vibration Sensor Data to Detect Objects in Surveillance Wireless Sensor Networks. In Proceedings of the 2017 21st International Conference on Control Systems and Computer Science (CSCS), Bucharest, Romania, 29–31 May 2017; pp. 207–212. https://doi.org/10.1109/CSCS.2017.35.

20. Salazar-García, C.; Castro-González, R.; Chacón-Rodríguez, A. RISC-V based sound classifier intended for acoustic surveillance in protected natural environments. In Proceedings of the 2017 IEEE 8th Latin American Symposium on Circuits & Systems (LASCAS), Bariloche, Argentina, 20–23 February 2017; pp. 1–4. https://doi.org/10.1109/LASCAS.2017.7948070.

21. Delgado Prieto, M.; Zurita Millan, D.; Wang, W.; Machado Ortiz, A.; Ortega Redondo, J.A.; Romeral Martinez, L. Self-powered wireless sensor applied to gear diagnosis based on acoustic emission. *IEEE Trans. Instrum. Meas.* **2016**, *65*, 15–24. https://doi.org/10.1109/TIM.2015.2476278.

22. Oletic, D.; Bilas, V. Asthmatic Wheeze Detection from Compressively Sensed Respiratory Sound Spectra. *IEEE J. Biomed. Health Inform.* **2018**, *22*, 1406–1414. https://doi.org/10.1109/JBHI.2017.2781135.

23. Oletic, D.; Bilas, V. Energy-efficient respiratory sounds sensing for personal mobile asthma monitoring. *IEEE Sens. J.* **2016**, *16*, 8295–8303. https://doi.org/10.1109/JSEN.2016.2585039.

24. Tschope, C.; Duckhorn, F.; Richter, C.; Bl, P.; Wolff, M. An Embedded System for Acoustic Pattern Recognition. In Proceedings of the 2017 IEEE SENSORS, Glasgow, UK, 29 October–1 November 2017; pp. 1–3. https://doi.org/10.1109/ICSENS.2017.8234380.

25. Mois, G.; Folea, S.; Sanislav, T. Analysis of Three IoT-Based Wireless Sensors for Environmental Monitoring. *IEEE Trans. Instrum. Meas.* **2017**, *66*, 2056–2064. https://doi.org/10.1109/TIM.2017.2677619.

26. Luo, L.; Qin, H.; Song, X.; Wang, M.; Qiu, H.; Zhou, Z. Wireless Sensor Networks for Noise Measurement and Acoustic Event Recognitions in Urban Environments. *Sensors* **2020**, *20*, 2093–2113. https://doi.org/10.3390/s20072093.

27. Peckens, C.; Porter, C.; Rink, T. Wireless Sensor Networks for Long-Term Monitoring of Urban Noise. *Sensors* **2018**, *18*, 3161. https://doi.org/10.3390/s18093161.

28. Yang, M.; Yeh, C.H.; Zhou, Y.; Cerqueira, J.P.; Lazar, A.A.; Seok, M. Design of an Always-On Deep Neural Network-Based 1-μ W Voice Activity Detector Aided with a Customized Software Model for Analog Feature Extraction. *IEEE J. Solid-State Circuits* **2019**, *54*, 1764–1777. https://doi.org/10.1109/JSSC.2019.2894360.

29. Lauwereins, S.; Meert, W.; Gemmeke, J.; Verhelst, M. Ultra-low-power voice-activity-detector through context- and resource-cost-aware feature selection in decision trees. In Proceedings of the 2014 IEEE International Workshop on Machine Learning for Signal Processing (MLSP), Reims, France, 21–24 September 2014; pp. 1–6. https://doi.org/10.1109/MLSP.2014.6958918.

30. Medeiros, J.E.G.; Chrisostomó, L.A.P.; Meira, G.; Toledo, Y.C.R.; Pimenta, M.; Haddad, S.A.P. A fully analog low-power wavelet-based Hearing Aid Front-end. In Proceedings of the 2013 IEEE Biomedical Circuits and Systems Conference (BioCAS), Rotterdam, The Netherlands, 31 October–2 November 2013; pp. 242–245. https://doi.org/10.1109/BioCAS.2013.6679684.

31. Price, M.; Glass, J.; Chandrakasan, A.P. A Low-Power Speech Recognizer and Voice Activity Detector Using Deep Neural Networks. *IEEE J. Solid-State Circuits* **2018**, *53*, 66–75. https://doi.org/10.1109/JSSC.2017.2752838.

32. Raychowdhury, A.; Tokunaga, C.; Beltman, W.; Deisher, M.; Tschanz, J.W.; De, V. A 2.3 nJ/Frame Voice Activity Detector-Based Audio Front-End for Context-Aware System-On-Chip Applications in 32-nm CMOS. *IEEE J. Solid-State Circuits* **2013**, *48*, 1963–1969. https://doi.org/10.1109/JSSC.2013.2258827.

33. Shan, W.; Yang, M.; Wang, T.; Lu, Y.; Cai, H.; Zhu, L.; Xu, J.; Wu, C.; Shi, L.; Yang, J. A 510-nW Wake-Up Keyword-Spotting Chip Using Serial-FFT-Based MFCC and Binarized Depthwise Separable CNN in 28-nm CMOS. *IEEE J. Solid-State Circuits* **2021**, *56*, 151–164. https://doi.org/10.1109/JSSC.2020.3029097.

34. Alías, F.; Socoró, J.C.; Sevillano, X. A review of physical and perceptual feature extraction techniques for speech, music and environmental sounds. *Appl. Sci.* **2016**, *6*, 143. https://doi.org/10.3390/app6050143.

35. Serizel, R.; Bisot, V.; Essid, S.; Richard, G. Acoustic Features for Environmental Sound Analysis. In *Computational Analysis of Sound Scenes and Events*; Springer International Publishing: Cham, Switzerland, 2018; pp. 71–101. https://doi.org/10.1007/978-3-319-63450-0_4.

36. Chu, S.; Narayanan, S.; Kuo, C.J. Environmental Sound Recognition with Time–Frequency Audio Features. *IEEE Trans. Audio Speech. Lang. Processing* **2009**, *17*, 1142–1158. https://doi.org/10.1109/TASL.2009.2017438.

37. Gazivoda, M.; Bilas, V. Low-Power Sensor Interface with a Switched Inductor Frequency Selective Envelope Detector. *Sensors* **2021**, *21*, 2124. https://doi.org/10.3390/s21062124.

38. Oletic, D.; Gazivoda, M.; Bilas, V. A programmable 3-channel acoustic wake-up interface enabling always-on detection of underwater events within 20 μA. In Proceedings of the Eurosensors 2018 Conference, Graz, Austria, 9–12 September 2018; pp. 1–7. https://doi.org/10.3390/proceedings2130768.

39. Gutierrez, E.; Perez, C.; Hernandez, F.; Hernandez, L. VCO-based Feature Extraction Architecture for Low Power Speech Recognition Applications. In Proceedings of the 2019 IEEE 62nd International Midwest Symposium on Circuits and Systems (MWSCAS), Dallas, TX, USA, 4–7 August 2019; pp. 1175–1178. https://doi.org/10.1109/MWSCAS.2019.8885088.

40. Oh, S.; Kim, H.-S.; Sylvester, D.; Cho, M.; Shi, Z.; Lim, J.; Kim, Y.; Jeong, S.; Chen, Y.; Rothe, R.; et al. An Acoustic Signal Processing Chip With 142-nW Voice Activity Detection Using Mixer-Based Sequential Frequency Scanning and Neural Network Classification. *IEEE J. Solid-State Circuits* **2019**, *54*, 3005–3016. https://doi.org/10.1109/JSSC.2019.2936756.

41. Badami, K.M.H.; Lauwereins, S.; Meert, W.; Verhelst, M. A 90 nm CMOS, 6 μW power-proportional acoustic sensing frontend for voice activity detection. *IEEE J. Solid-State Circuits* **2016**, *51*, 291–302. https://doi.org/10.1109/JSSC.2015.2487276.

42. Rumberg, B.; Graham, D.W.; Kulathumani, V. A low-power, programmable analog event detector for resource-constrained sensing systems. In Proceedings of the 2012 IEEE 55th International Midwest Symposium on Circuits and Systems (MWSCAS), Boise, ID, USA, 5–8 August 2012; pp. 338–341. https://doi.org/10.1109/MWSCAS.2012.6292026.

43. Wang, Z.; Liu, Y.; Zhou, P.; Tan, Z.; Fan, H.; Zhang, Y.; Shen, L.; Ru, J.; Wang, Y.; Ye, L.; et al. A 148-nW Reconfigurable Event-Driven Intelligent Wake-Up System for AIoT Nodes Using an Asynchronous Pulse-Based Feature Extractor and a Convolutional Neural Network. *IEEE J. Solid-State Circuits* **2021**, *56*, 3274–3288. https://doi.org/10.1109/JSSC.2021.3113257.

44. Kim, C.M.; Lee, S.Y. A digital chip for robust speech recognition in noisy environment. In Proceedings of the 2001 IEEE International Conference on Acoustics, Speech, and Signal Processing. Proceedings (Cat. No.01CH37221), Salt Lake City, UT, USA, 7–11 May 2001; Volume 2, pp. 1089–1092. https://doi.org/10.1109/ICASSP.2001.941109.

45. He, F. *A Portable Low-Power Electronic Adherence Monitoring System for Cystic Fibrosis*; University of Sheffield: Sheffield, UK, 2019.

46. Goldberg, D.H.; Andreou, A.G.; Julián, P.; Pouliquen, P.O.; Riddle, L.; Rosasco, R. VLSI implementation of an energy-aware wake-up detector for an acoustic surveillance sensor network. *ACM Trans. Sens. Netw.* **2006**, *2*, 594–611. https://doi.org/10.1145/1218556.1218562.

47. Habibi, M.; Shakarami, M.; Khoddami, A.A. A low power mixed signal correlator for power efficient sound signature detection and template matching. *Sens. Rev.* **2017**, *37*, 213–222. https://doi.org/10.1108/SR-06-2016-0098.

48. Sutton, F.; Forno, R.D.; Gschwend, D.; Gsell, T.; Lim, R.; Beutel, J.; Thiele, L. The Design of a Responsive and Energy-efficient Event-triggered Wireless Sensing System. In Proceedings of the 14th International Conference on Embedded Wireless Systems and Networks (EWSN 2017), Uppsala, Sweden, 20–22 February 2017; pp. 144–155. https://doi.org/10.5555/3108009.3108028.

49. Cho, M.; Oh, S.; Jeong, S.; Zhang, Y.; Lee, I.; Kim, Y.; Chuo, L.-X.; Kim, D.; Dong, Q.; Chen, Y.-P.; et al. A $6 \times 5 \times 4$ mm^3 general purpose audio sensor node with a 4.7 μW audio processing IC. In Proceedings of the 2017 Symposium on VLSI Circuits, Kyoto, Japan, 5–8 June 2017; pp. C312–C313. https://doi.org/10.23919/VLSIC.2017.8008521.

50. Underwater Video of Twin Engine Boat Props High Speed. Available online: https://www.youtube.com/watch?v=6uQ7IDqb-mAE (accessed on 7 June 2018).

Publication 3

Gazivoda, M., Bilas, V., "Low-Power Sensor Interface with a Switched Inductor Frequency Selective Envelope Detector", *Sensors*, Vol. 21, Issue 6, pp 21, 2021, doi:10.3390/s21062124

Marko Gazivoda * and **Vedran Bilas**

Faculty of Electrical Engineering and Computing, University of Zagreb, 10000 Zagreb, Croatia; vedran.bilas@fer.hr
* Correspondence: marko.gazivoda@fer.hr

Abstract: With the growing need to understand our surroundings and improved means of sensor manufacturing, the concept of Internet of Things (IoT) is becoming more interesting. To enable continuous monitoring and event detection by IoT, the development of low power sensors and interfaces is required. In this work we present a novel, switched inductor based acoustic sensor interface featuring a bandpass filter and envelope detector, perform a sensitivity, frequency selectivity, and power consumption analysis of the circuit, and present its design parameters and their qualitative influence on circuit characteristics. We develop a prototype and present experimental characterization of the interface and its operation with input signals up to 20 mV peak-to-peak, at low acoustic frequencies from 100 Hz to 1 kHz. The prototype achieves a sensitivity of approximately 2 mV/mV in the passband, a four times lower sensitivity in the stopband, and a power consumption of approximately 3.31 μW. We compare the prototype interface to an interface consisting of an active bandpass filter and a passive voltage doubler using a prerecorded speedboat signal.

Keywords: sensor signal conditioning circuit; event detection application; switched inductor filter; weak signal detection

1. Introduction

The growing need to understand and manage our surroundings, coupled with advances in sensor technologies and manufacturing processes [1], has led to an increased interest in the concept of Internet of Things (IoT), which envisions sensor networks consisting of hundreds of thousands of small, robust sensor nodes utilized to continuously monitor real-world events and processes [2–4]. Continuous monitoring and event detection emphasize the need for low-power sensors and sensor signal conditioning circuits which enable the node to achieve long life-times, even when powered by small batteries [3–5].

Acoustic sensors present an attractive choice for IoT applications because they generate signals that are rich in information and can be processed using relatively simple hardware [6–8] that powers up the rest of the sensor node only upon detection of an event of interest [4,5], thereby reducing the power consumption of an acoustic sensor node. These wake-up sensor interfaces utilize bandpass filtering, envelope detection, quantization, and some rudimentary form of classification to determine if an event of interest occurred. Implementations of the wake-up interface with an active bandpass filter, diode envelope detector, and microcontroller-based classification are presented in [9,10]. The power consumption of the bandpass filter and the envelope detector is reported as 8.25 μW in [9] and 20.74 μW in [10].

The envelope detector is one of the critical elements in the weak signal front ends in various applications (sensing, communications, energy harvesting) due to its power-consumption to sensitivity trade-off [11–16]. In [17] we studied the impact of the envelope detector on sensitivity and power consumption of the wake-up sensor interface in the lower audio frequency range. Based on the mechanically switched inductor energy harvester [16],

in [18] we demonstrated that a piezoelectric energy harvester can be used as a vibration sensor utilizing a mechanically switched inductor driven by the sensed vibrations.

In order to increase the sensitivity of low-power acoustic wake-up sensor interfaces, and at the same time lower their power consumption, in this work we propose a novel approach, utilizing an electrically switched inductor as a replacement for conventionally used bandpass filter and envelope detector functional blocks. Using this approach, inspired by the switched inductor bandpass filter [19,20], and the switched inductor energy harvester [12,13,16], we devise a novel, low-power wake-up sensor interface, operational with weak input signals (around 5 mV) in the low acoustic frequency range (100 Hz–1 kHz) and applicable in low-power always-on acoustic event detectors.

With this work we present several contributions: a novel, frequency-selective, voltage-boosting, low-power, weak-signal acoustic sensor interface; a sensitivity, frequency selectivity and power consumption analysis of the circuit; design parameter selection, and their influence on interface characteristics; experimental characterization of a prototype, and its comparison to an interface consisting of an active bandpass filter and a passive voltage doubler.

The rest of this paper is organized as follows: Section 2 presents related circuits and principles of operation. Section 3 shows the proposed interface characteristics and design parameters. Section 4 presents a simulation study of the sensor interface, determining its key design parameters and desired functionality. Section 5 shows the developed prototype and its experimental characterization. In Section 6 a set of design recommendations for interface synthesis are given. Section 7 presents a comparison of the novel sensor interface and interface presented in [9,18] and Section 8 states the concluding remarks of the paper and presents future work.

2. Related Circuits and Principles of Operation

The proposed sensor interface utilizes the switched inductor for filtering the sensor signal and extracting and boosting its envelope. This concept was inspired by two previous lines of work, the switched inductor filter and the switched inductor energy harvester.

2.1. Switched Inductor Filter

The switched inductor filter (shown in Figure 1a) consisting of a capacitor, C_f, inductor, L_f, and two switches S_{f1} and S_{f2}, is used in power electronics to electrically tune the frequency characteristic of inverter outputs, suppressing unwanted harmonics [19,20]. Figure 1b shows the electrically tunable frequency characteristic of such a filter and the impact of the switch control function duty cycle as its tuning parameter. The input signal frequency was normalized with regards to the filter central frequency and the output voltage root mean square (RMS) was normalized with regards to the maximal filter output RMS voltage (obtained with the 90% duty cycle when the input signal frequency was equal to the filter central frequency).
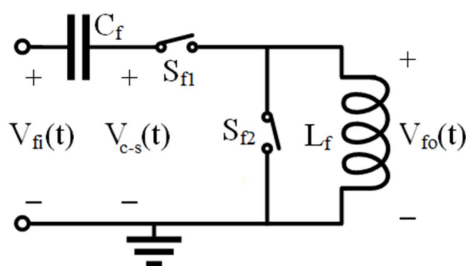
(a)

Figure 1. *Cont.*
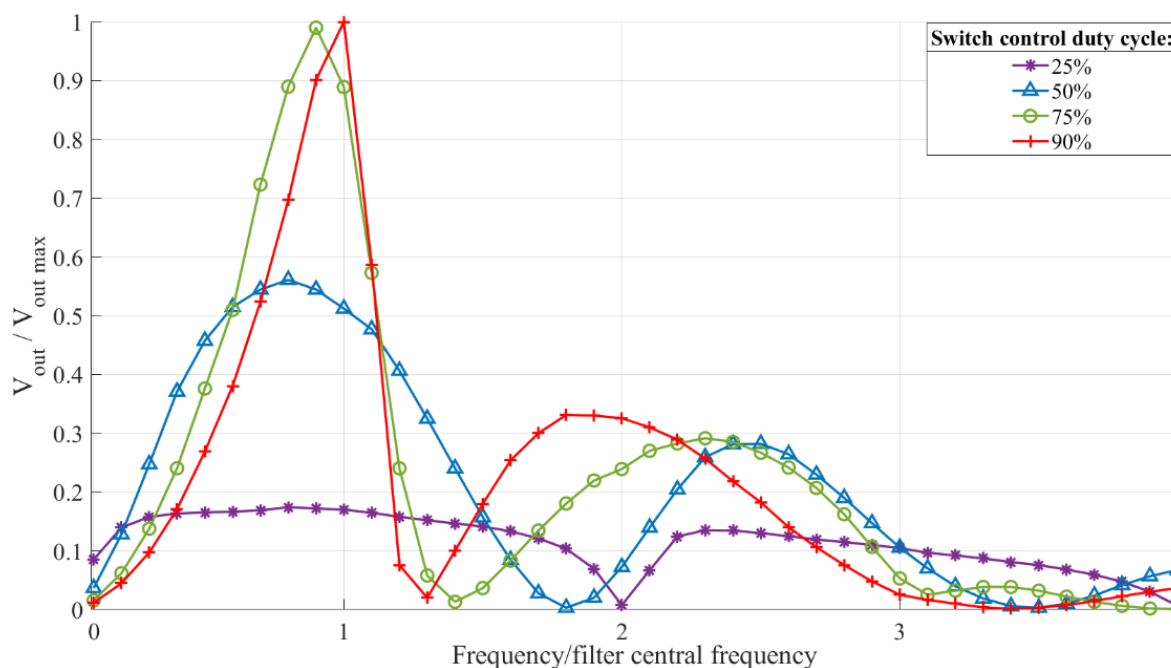
(b)

Figure 1. (**a**) Switched inductor filter and (**b**) its qualitative frequency characteristic with the duty cycle of 25% (purple), 50% (blue), 75% (green), and 90% (red). Filter output voltage RMS is normalized with regards to maximal output voltage RMS (obtained with the 90% duty cycle at the input frequency equal to filter central frequency), input signal frequency normalized with regards to the filter's central frequency.

The passive LC filter has a resonant frequency, f_{res}:

$$f_{res} = \frac{1}{2\pi\sqrt{L_f C_f}} \tag{1}$$

where L_f and C_f are the values of inductance and capacitance, respectively. By switching the inductor on and off, its effective value, L_{feff}, seen at the circuit input, is changed, which changes the filter's frequency characteristics. The two switches, S_{f1} and S_{f2}, (Figure 1a) are driven by two antiparallel square signals, with switch S_{f2} closing when S_{f1} opens to provide a discharge current path for the inductor. The switching function $F_1(t)$ of the switch S_1 is given as [20]:

$$F_1(t) = A_0 + 2\sum_{n=1}^{\infty} \frac{\sin\left(n\omega\frac{d}{2}\right)}{n\pi} \cos(n\omega t - n\theta) \tag{2}$$

where t denotes time, d and θ are the pulse duration and the phase delay of the switch control function, respectively, ω is the angular frequency of the switch control signal, n is a positive integer, and A_0 is the average value of the switching function on its single period T. The average value of the switching function is determined by its duty cycle, i.e., the ratio of the duration of the function's high state and its period, $A_0 = d/T$. The switching function takes on the value of 1 when the switch is closed and 0 when it is open.

The authors of [19,20] do not analyze the influence of the switch control function frequency on the filter functionality. They only state that it should be higher than input signal frequency f_{in}.

The filter output voltage, $V_{fo}(t)$, is determined by the voltage of the node between the filter capacitor C_f and switch S_{f1}, $V_{c-s}(t)$, and the switching function $F_1(t)$:

$$V_{fo}(t) = F_1(t) \cdot V_{c-s}(t) \tag{3}$$

From Equations (2) and (3) and a few steps presented in [20], it can be determined that the effective value of the filter inductance L_{feff} is proportional to:

$$L_{feff} \propto \frac{L_f}{A_0{}^2} \tag{4}$$

and therefore, dependent on the average value of the switching function, which is, as shown previously, determined by the switching function's duty cycle that can be used to tune the filter's frequency characteristic, as shown in Figure 1b.

2.2. Switched Harvester on Inductor

The switched harvester on inductor (one version shown in Figure 2a) is used to increase the efficiency in energy harvesting, by boosting the harvester's transducer voltage, $V_{tr}(t)$, prior to rectification (as shown in Figure 2b) [12,13,16].

(a)

(b)
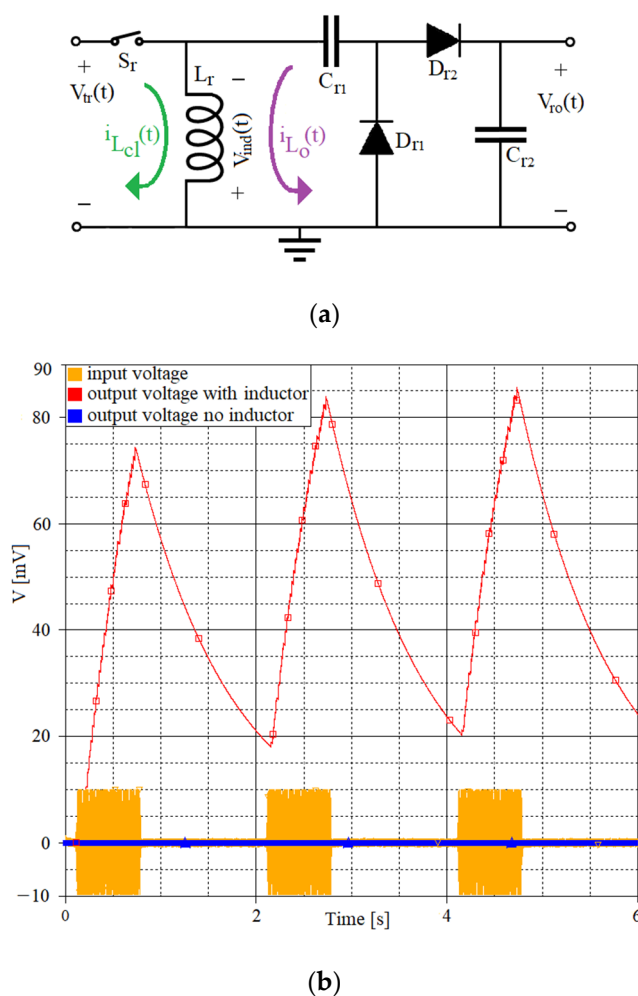
Figure 2. (**a**) Switched harvester on inductor with marked inductor current, $i_{Lcl}(t)$ (green) and $i_{Lo}(t)$ (purple) with the switch closed and opened, respectively. (**b**) Switched harvester on inductor output signal waveform (red) compared to a rectifier without the switched inductor (blue). Input signal (yellow): 500 ms of sinusoidal signal, 20 mV peak-to-peak, 100 Hz, followed by a 1.5 s pause. $C_{r1} = C_{r2} = 1$ μF, $L_r = 100$ mH, switch control frequency $f_{switch} = 256$ Hz, duty cycle 50%.

While the switch S_r is closed, the energy of the harvester's transducer signal is stored in the magnetic field of the inductor, L_r, changing the inductor's current by Δi_L with:

$$\Delta i_L = \frac{1}{L_r} \int_{t_1}^{t_2} V_{tr}(t)dt \tag{5}$$

where t_1 and t_2 are, respectively, the beginning and ending moment of observing the storing of energy in the inductor's magnetic field, and $V_{tr}(t)$ is the harvester's transducer voltage.

At the moment t_o, when the switch opens, the energy stored in the inductor generates an induced voltage, V_{ind}:

$$V_{ind} = L_r \left. \frac{di_L(t)}{dt} \right|_{t=t_o} \tag{6}$$

We can approximate the time derivation of the inductor current at the moment t_o as:

$$\left. \frac{di_L(t)}{dt} \right|_{t=t_o} = \frac{i_L(t_O)}{\Delta t} = \frac{\frac{1}{L_r}\int_{t_C}^{t_O} V_{tr}(t)dt}{\Delta t} \tag{7}$$

where $i_L(t_o)$ is the inductor current at the instant of the switch opening, t_c the time instant when the switch is closed, and Δt is the time required for the inductor current to fall to zero.

If the voltages induced on the inductor are high enough to pass over the diodes, they will charge the output capacitor to the steady state voltage:

$$V_{ro\_ss} = 2 \cdot \left(\frac{\int_{t_C}^{t_O} V_{tr}(t)dt}{\Delta t} - V_D \right) \tag{8}$$

where V_D is the diode threshold voltage.

Neglecting energy losses, the maximal obtainable rectifier output voltage V_{ro_max} depends on the inductance L_r, capacitance $C_{r1,2}$, and the current through the inductor at the instant the switch opens, $i_L(t_o)$ (9) [21].

$$V_{ro\_max} = i_L(t_O) \cdot \sqrt{\frac{L_r}{C_{r1,2}}} \tag{9}$$

The output capacitor C_{r2} gradually discharges when no signal is coming from the harvester's transducer (as seen in Figure 2b) because of the leakage currents of the reversely polarized diodes, or the input impedance of the next interface stage.

3. Proposed Sensor Interface Characteristics and Design Parameters

Combining the two functionalities explored in the literature, in this work we devise a low-power, frequency selective, voltage boosting sensor interface (Figure 3a), capable of operating with signals under 5 mV peak-to-peak and in the low acoustic frequency range, from 100 Hz to 1 kHz. For the interface to meet these demands, several of its characteristics should be considered. The first is the interface's sensitivity (Figure 3c), the ratio of output headroom voltage and input voltage, with the headroom voltage defined as the voltage difference between the interface output voltage with no input and the interface lowest steady-state output voltage with a given input, as shown in Figure 3b. The stopband sensitivity should also be considered, as the maximal expected stopband voltage defines the lowest passband voltage levels with which the interface can operate (spurious-free range, Figure 3c). This leads to the next characteristic, the frequency selectivity, i.e., the difference between its passband and stopband sensitivities (Figure 3c,d). The final characteristic is the power consumption.

(**a**)

(**b**)

(**c**)

(**d**)
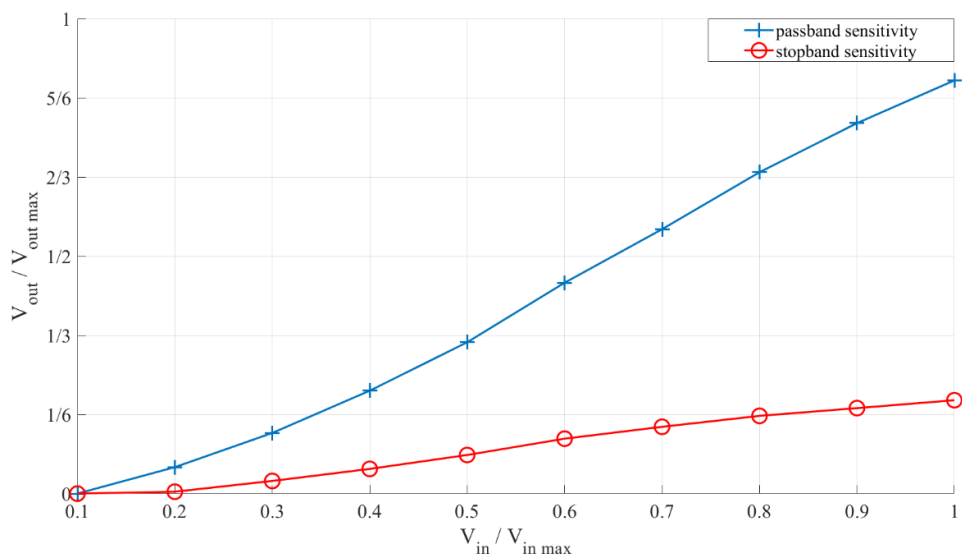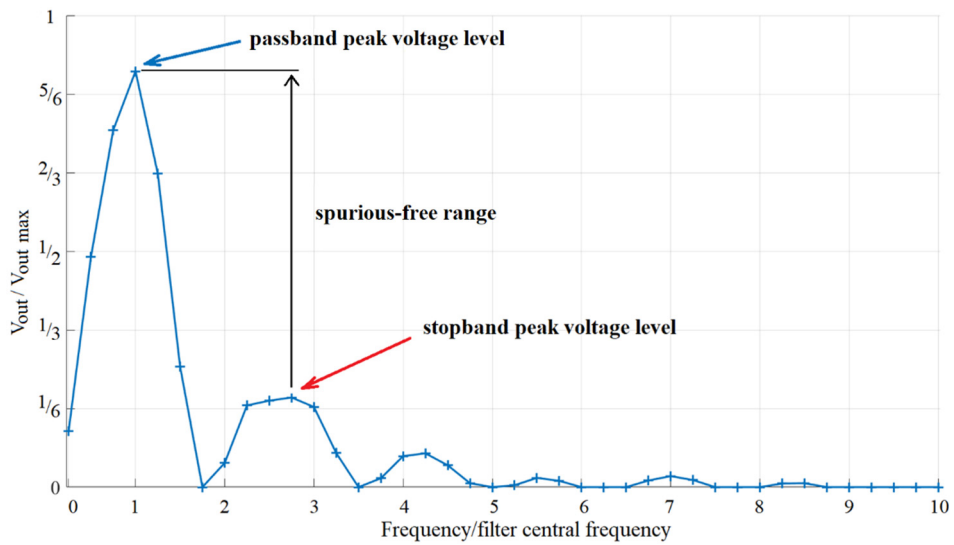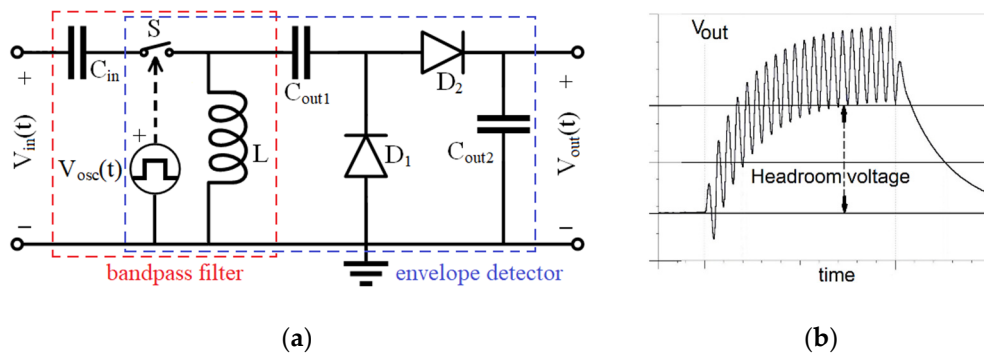
Figure 3. (**a**) Proposed sensor interface (with marked bandpass filter and envelope detector functional blocks), (**b**) output signal waveform (with marked headroom voltage), (**c**) normalized frequency characteristic and (**d**) normalized output headroom voltage with input voltage.

From the presented principles of operation and the desired characteristics of the proposed interface, we determined its key design parameters that can be divided in two groups: switch control signal parameters and passive component values.

The switch control signal parameters of interest are: switch control signal frequency, duty cycle, and delay between the switch control and input signal (the switch is controlled by an independent voltage signal $V_{osc}(t)$, as shown in Figure 3a).

The passive components of interest are: input capacitor C_{in}, inductor L, Q factor of the input switched inductor filter, and output capacitors, C_{out1} and C_{out2}, which we analyzed in detail in our previous work [17,18]. The diodes were also chosen based on previous work analyzing their influence on weak-signal rectifier performance [14,22].

4. Proposed Sensor Interface Simulation Study

4.1. Simulation Model

In order to both characterize the proposed sensor interface and narrow the parameter selection for the prototype realization, a SPICE model has been implemented and simulated in Texas Instruments' PSpice (Dallas, Texas, TX, USA) following the schematic shown in Figure 3a. The obtained simulation results were further processed and presented using MathWorks' MATLAB® (Natick, Massachusetts, MA, USA).

The following parameters were varied to determine their influence on the output voltage characteristics and power consumption: switch control signal frequency and duty cycle, delay between the switch control signal and input signal, input capacitor, C_{in}, inductor, L, and resistance, R_L, filter quality factor, Q, defined as:

$$Q = \frac{1}{R_L} \cdot \sqrt{\frac{L}{C_{in}}} \tag{10}$$

The output capacitors, C_{ou1} and C_{out2} were both 1 μF, following previous research conclusions and the diodes chosen for the simulation model were the HSMS-282x (Agilent Technologies, Santa Clara, California, CA, USA), because of their low forward voltage, low reverse current, and high saturation current. For simulation analyses showing the frequency characteristics, the input, $V_{in}(t)$, was a sinusoidal signal with frequency varied from 50 Hz to 2000 Hz, with a 50 Hz step and 20 mV peak-to-peak, while the simulation analyses showing the sensitivity were done with an input sinusoidal signal of a fixed frequency in the range from 100 Hz to 600 Hz and voltage from 1 mV to 20 mV peak-to-peak with a 1 mV step.

4.2. Simulation Results

4.2.1. Switch Control Signal Parameters—Duty Cycle and Frequency

Figure 4a,b show the interface frequency characteristic and the relation of output headroom voltage and input voltage with switch control signal duty cycle. The filter central frequency was 512 Hz (C_{in} = 1 μF, L = 100 mH, R_L = 66.6 Ω (Q = 4.8335)). The switch control signal frequency was 1024 Hz and duty cycles were 25%, 33%, 50%, 66%, and 75%.

From Figure 4a,b we see that increasing the switch control signal duty cycle leads to an increased sensitivity and a narrower frequency characteristic, both of which are desired traits. It also increases the central frequency of the interface passband towards the one of a fixed passive LC filter. These results adhere to the theoretical switched inductor filter performance presented in Section 2.1 and Figure 1b. We can also conclude that duty cycles under 50% should not be utilized, as they lead to low sensitivity and poorer frequency selectivity.
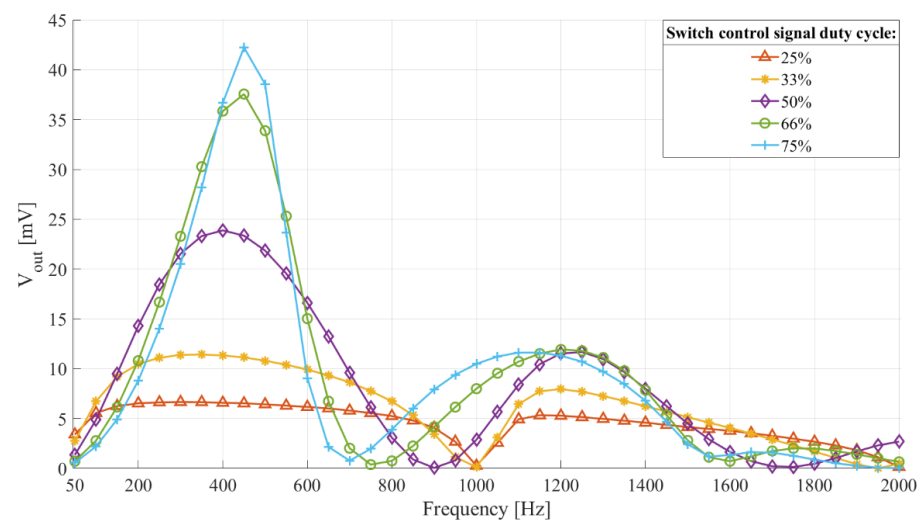
(**a**)
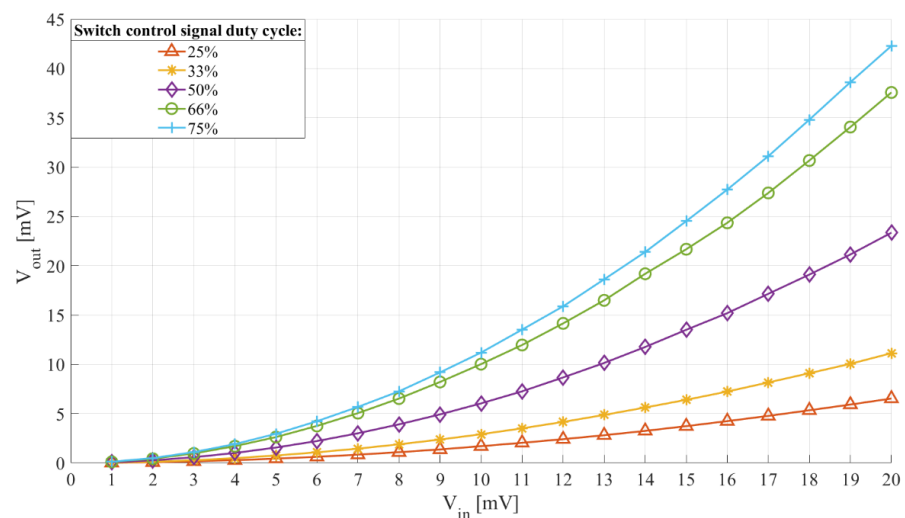
(**b**)

Figure 4. (**a**) Frequency characteristic and (**b**) output headroom voltage to input voltage relation of the sensor interface with switch control signal duty cycle. Filter central frequency 512 Hz (L = 100 mH, C_{in} = 1 μF, R_L = 66.6 Ω). Switch control signal frequency f_{switch} = 1024 Hz and duty cycle from 25% to 75%. (**a**) Input voltage 20 mV peak-to-peak and frequency from 50 Hz to 2000 Hz with a 50 Hz step. (**b**) Input signal voltage from 1 mV to 20 mV with a 1 mV step. Input signal frequency 450 Hz.

However, increasing the duty cycle leads to longer periods of time in which the sensor drives the interface, leading to an increased sensor current. This is shown in Figure 5, which depicts the inductor current with switch control signal duty cycle. The simulation model was the same as for Figure 4a,b, and the switch control signal duty cycle was 25%, 50%, and 75%.
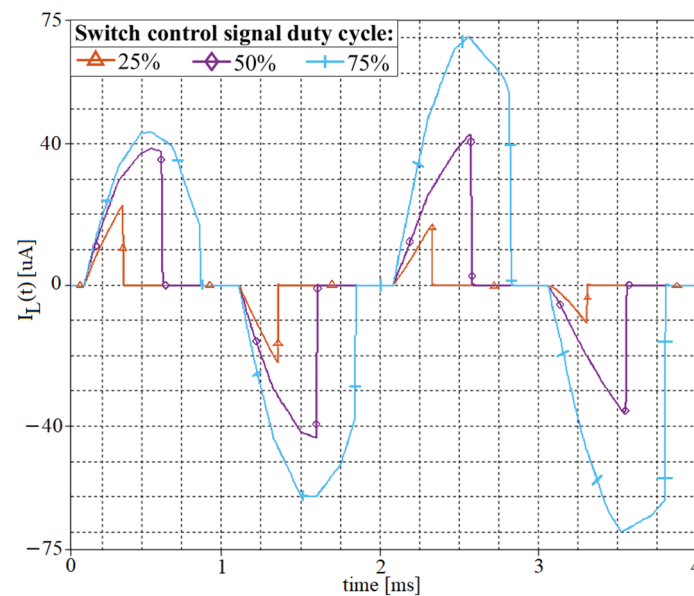
Figure 5. Inductor current of the sensor interface with switch control signal duty cycle. Filter central frequency 512 Hz (L = 100 mH, C_{in} = 1 μF, R_L = 66.6 Ω). Switch control signal frequency f_{switch} = 1024 Hz and duty cycle 25%, 50%, and 75%. Input signal voltage 20 mV peak-to-peak and frequency 450 Hz.

As we can see from Figure 5, both peak and mean inductor currents are determined by the switch control signal duty cycle. The peak and mean currents were around 23 μA peak and 2.88 μA mean for 25% duty cycle, 42 μA peak, and 10.5 μA mean for 50% duty cycle, and 70 μA peak and 26.25 μA mean for 75% duty cycle.

Figure 6 shows the interface frequency characteristics with switch control signal frequency, f_{switch}. The filter central frequency was 512 Hz (C_{in} = 1 μF, L = 100 mH, R_L = 66.6 Ω (Q = 4.8335)). The switch control frequency was 256 Hz, 512 Hz, 1024 Hz, and 2048 Hz. The switch control signal duty cycle was 75%.
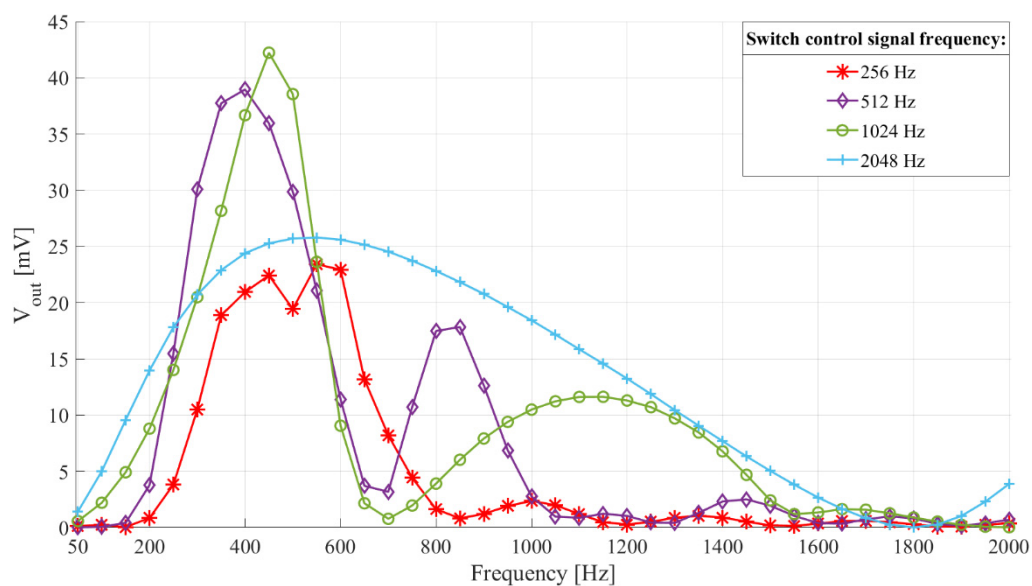
Figure 6. Frequency characteristics of the sensor interface with switch control frequency. Filter central frequency 512 Hz (L = 100 mH, C_{in} = 1 μF, R_L = 66.6 Ω). Input voltage 20 mV peak-to-peak and frequency from 50 Hz to 2000 Hz with a 50 Hz step. Switch control signal frequency, f_{switch}, 256 Hz, 512 Hz, 1024 Hz, and 2048 Hz and duty cycle 75%.

Looking at Figure 6 we see that there is a switch control signal frequency that, with a given filter central frequency and *Q* factor, leads to the most frequency selective interface, with the highest sensitivity (in this case it is 1024 Hz, i.e., double the filter central frequency).

The dependency of the frequency characteristic and sensitivity on the switch control frequency can be explained by energy transfer from the input LC circuit to the output capacitors.

The maximal energy transfer occurs if the switch opens twice per inductor current period, precisely at maximal positive and negative inductor current values. The switch control signal frequency should be set slightly above double the frequency of the input signal of interest, to avoid the influence of time delay between the input and switch control signal on the output voltage (explained in the following text).

More than two switch openings per inductor current period cause more generations of induced voltage, but of lower value, which reduces the overall energy transfer efficiency, because of the exponential dependency of the diode current on the voltage on it, i.e., the induced voltage. Having more than two openings per input signal period also leads to a broader frequency characteristic (output voltage less dependent on the switch opening instant).

Finally, when considering the switch control signal parameters, it should be mentioned that the proposed sensor interface output voltage can also be influenced by the time delay between the input signal onset and the switch control signal. This effect explains the small discontinuities, like the one visible in Figure 6 at 500 Hz, on the red curve. However, this delay can substantially influence the interface output voltage only if the input signal frequency matches the switch control signal frequency or one of its specific rational multipliers (1/4, 1/2, 2, 3 . . .). For all other input signals, this time delay can change the output voltage by no more than 10%. Therefore, this effect will not substantially impact the device's application and performance with transducer inputs (which consist of frequencies of interest, other frequencies, noise, and interference).

4.2.2. Passive Component Selection—Capacitor and Inductor

From Equation (1) it is clear that the same central frequency can be obtained with different values of inductance, *L*, and capacitance, *C*. This is shown in Figure 7a,b, which present the frequency characteristics and the relation of the output headroom voltage and input voltage of interfaces with different inductance and capacitance. The filter central frequency was 512 Hz, the switch control frequency was 1080 Hz, and the duty cycle was 75%. *L* were 100 mH, 350 mH, and 590 mH, and C_{in}, were 1 µF, 276 nF, and 164 nF, respectively. The *Q* factor was kept constant (*Q* = 267.3) by setting the resistance, R_L, to 1.2 Ω, 4.2 Ω, and 7.1 Ω, respectively.

From Figure 7a,b we see that interfaces with filters set to the same central frequency, have lower sensitivity the higher their inductance is. Furthermore, if we compare the results from Figure 4b with the results from Figure 7b we can see that an interface with a significantly lower *Q* factor (Figure 4b, *Q* = 4.8335) still has higher sensitivity than the two interfaces with higher inductances and higher *Q* factor (Figure 7b, *Q* = 267.3).
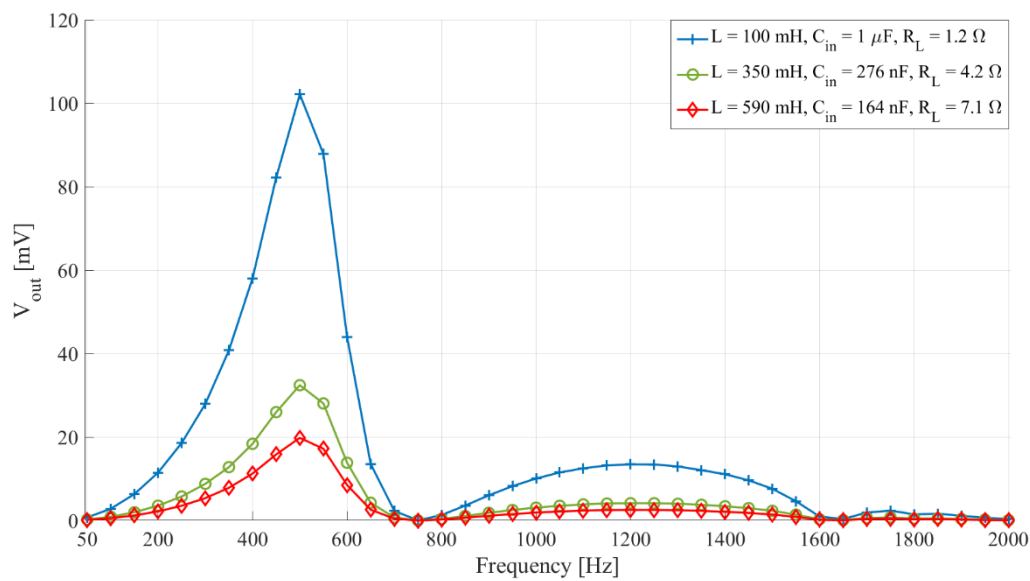
(**a**)
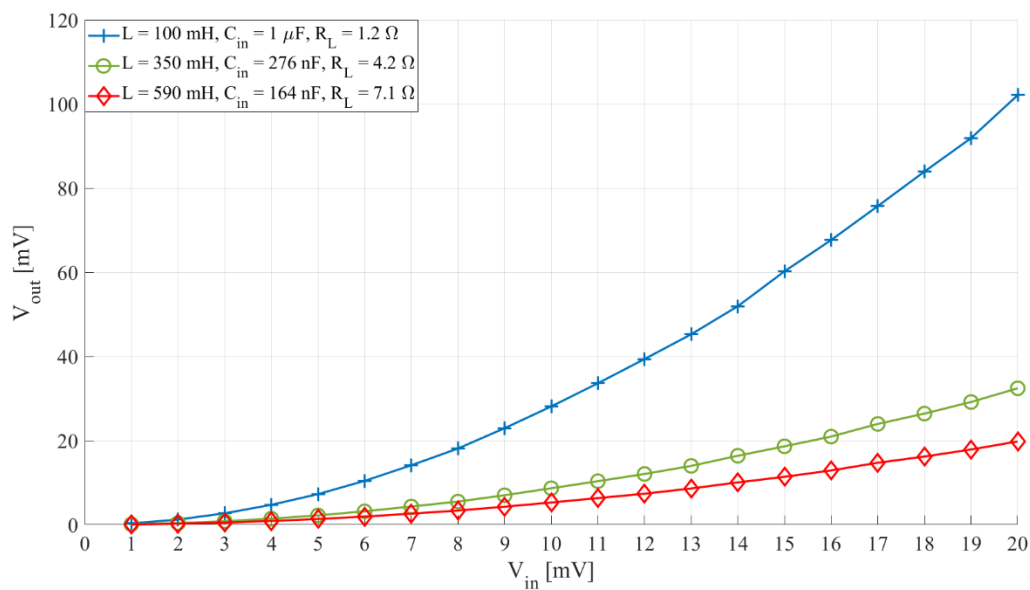
(**b**)

Figure 7. (**a**) Sensor interface frequency characteristic and (**b**) the relation of output headroom voltage and input voltage with *L*. The switch control frequency, f_{switch}, 1080 Hz and duty cycle 75%, *Q* = 267.3. (**a**) Input signal voltage 20 mV peak-to-peak, frequency from 50 Hz to 2000 Hz with a 50 Hz step. (**b**) Input signal frequency 500 Hz and voltage from 1 mV to 20 mV peak-to-peak with a 1 mV step.

5. Proposed Sensor Interface Experimental Characterization

The goal of these measurements was to provide experimental verification of the simulation results and characterize the proposed sensor interface prototype in terms of frequency selectivity, sensitivity, and power consumption.

5.1. Measurement Setup

Figure 8a shows a photograph of the measurement setup. The measurement setup consisted of a Keysight 33500B waveform generator (Keysight Technologies, Santa Rosa, California, CA, USA) for generating the input and switch control signal, the prototype

sensor interface (shown in Figure 8b), and an NI USB-6211 (National Instruments, Austin, Texas, TX, USA) data acquisition card connected to a PC for recording the output voltage. The power consumption of the interface was measured using a Fluke 45 multimeter (Fluke Corporation, Everett, Washington, WA, USA). The interface was powered by a DP832 power source from RIGOL (RIGOL Technologies, Beijing, China).

(**a**)　　　　　　　　　　　　　　　　(**b**)
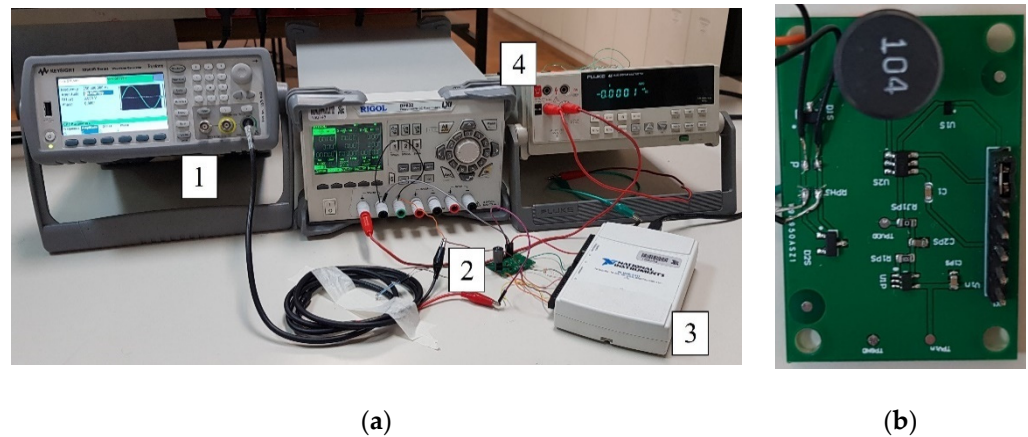
Figure 8. (**a**) A photograph of the measurement setup. (1) Keysight 33500B waveform generator, (2) sensor interface prototype, (3) NI USB-6211 data acquisition card. (4) Power supply (RIGOL DP832) and a multimeter for supply current measurement (Fluke 45). (**b**) Proposed frequency-selective voltage-boosting sensor interface prototype.

The prototype of the proposed frequency-selective voltage-boosting sensor interface was designed according to the schematic in Figure 3a, with components shown in Table 1.

Table 1. Prototype components.

Integrated Components				
Component	**Manufacturer**	**Supply Voltage**	**Supply Current (Typical)**	**Transition Times (Typical)**
switch TMUX1101	Texas Instruments	1.8 V	3 nA	12 ns
oscillator SiT1569	SiTime	1.8 V	1.7 μA–3.3 μA	200 ns
Discrete Semiconductor Components				
Component	**Manufacturer**	**Reverse Current (at 1V)**	**Saturation Current**	**Forward Voltage (Maximal)**
diodes HSMS-282x	Agilent	100 nA	22 nA	0.34 V
Discreet Passive Components				
Component		**Value**		**Type**
Output capacitors		$C_{out_1} = C_{out2} = 1$ μF		Multilayer ceramic
Input capacitors		$C_{in_1} = 100$ nF, $C_{in2} = 1$ μF, $C_{in3} = 2.2$ μF		Multilayer ceramic
Inductors		$L_1 = 100$ mH, $R_{L1} = 66.6$ Ω		Air-core
		$L_2 = 590$ mH, $R_{L2} = 7.1$ Ω		Ferrite-core

5.2. Measurement Procedure and Results

The measurement results were recorded by a National Instruments NI USB-6211 data acquisition card. The data acquisition control, data processing, and presentation were implemented using MathWorks' MATLAB® (Natick, Massachusetts, MA, USA).

5.2.1. Frequency Selectivity

The goal was to characterize the sensor interface frequency selectivity with different input capacitors, C_{in}, inductors, L, and switch control signal frequencies.

The filter central frequencies were: 139 Hz (C_{in3}, L_2), 211 Hz (C_{in2}, L_2), 512 Hz (C_{in2}, L_1), and 655 Hz (C_{in1}, L_2). The switch control signal duty cycle was 50% and the frequency was 256 Hz, 278 Hz, 422 Hz, 512 Hz, 1024 Hz, and 1310 Hz. The input signal voltage was 20 mV peak-to-peak and the frequency was ranging from 50 Hz to 2000 Hz, with a 50 Hz step.

Figure 9 shows the frequency characteristics of the interface with four filter central frequencies and Figure 10 shows the frequency characteristics of an interface with a filter central frequency of 512 Hz and three different switch control signal frequencies. In addition to the measurement results, both figures show the simulation results for the same setups.
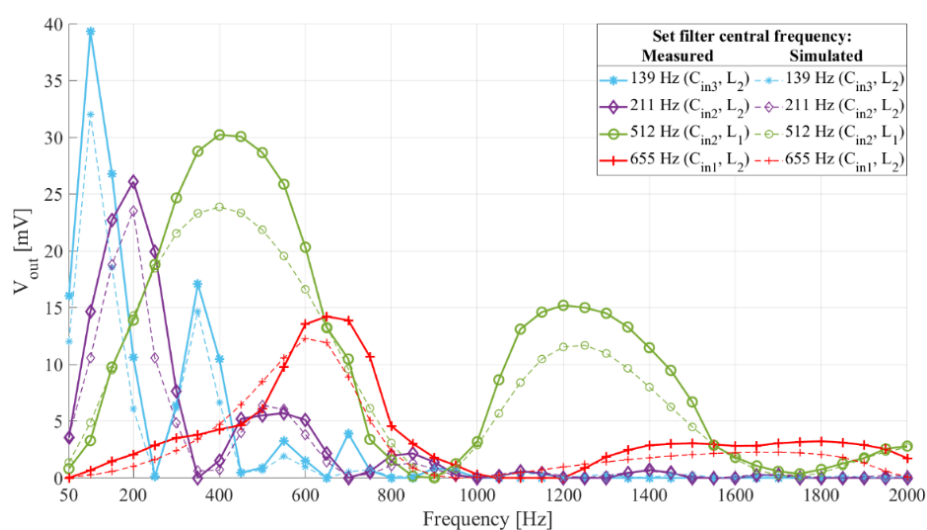
Figure 9. Frequency characteristic of the sensor interface prototype with different C_{in}, L and R_L. The switch control duty cycle 50%. The switch control frequencies were 278 Hz (blue), 422 Hz (purple), 1024 Hz (green), and 1310 Hz (red). The dashed lines show simulation results, paired with the experimental results by color and same markers.
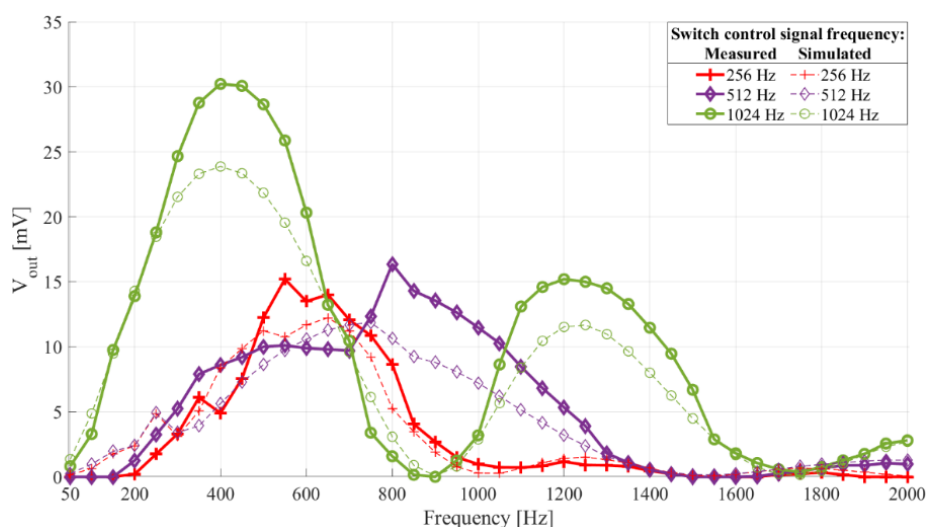
Figure 10. Frequency characteristic of the sensor interface prototype with the filter central frequency 512 Hz (C_{in2}, L_1). Switch control duty cycle 50%, frequency 256 Hz, 512 Hz, and 1024 Hz. The dashed lines show simulation results, paired with the experimental results by color and same markers.

Comparing the experimental and simulation results shown in Figures 9 and 10, we see the frequency characteristics of the prototype interface match those of the simulated interfaces.

In [6,23] the authors presented the idea of reducing power consumption of wake-up interfaces and increasing their flexibility with reconfigurability, while in [10] digital setting of the filter central frequency was presented as an interesting feature for a wake-up interface. From the results in Figure 9, the filter central frequency of this interface can be digitally set by simultaneously selecting the input capacitor and switch control frequency. The settling time of the reconfigurable switched inductor circuit can be shorter than of that of a circuit utilizing an operational amplifier-based active bandpass filters.

5.2.2. Sensitivity

The goal was to determine the sensor interface sensitivity with different filter central frequencies (different input capacitors, C_{in}, and inductors, L) and switch control signal frequencies.

The prototype setup was identical to the one described for frequency selectivity measurement. The input signal frequency was 100 Hz, 200 Hz, 450 Hz, and 650 Hz and, the voltage was ranging from 2 mV peak-to-peak to 20 mV peak-to-peak with a 2 mV step.

Figure 11 shows the measured and simulated output headroom voltage with input voltage of the interface whose frequency characteristics are shown in Figure 9, while Figure 12 shows the measured passband and stopband output-to-input voltage relation of two setups of the interface, with an input signal frequency of 200 Hz and 500 Hz for the 211 Hz filter central frequency setup, and 450 Hz and 1200 Hz for the 512 Hz filter central frequency setup.
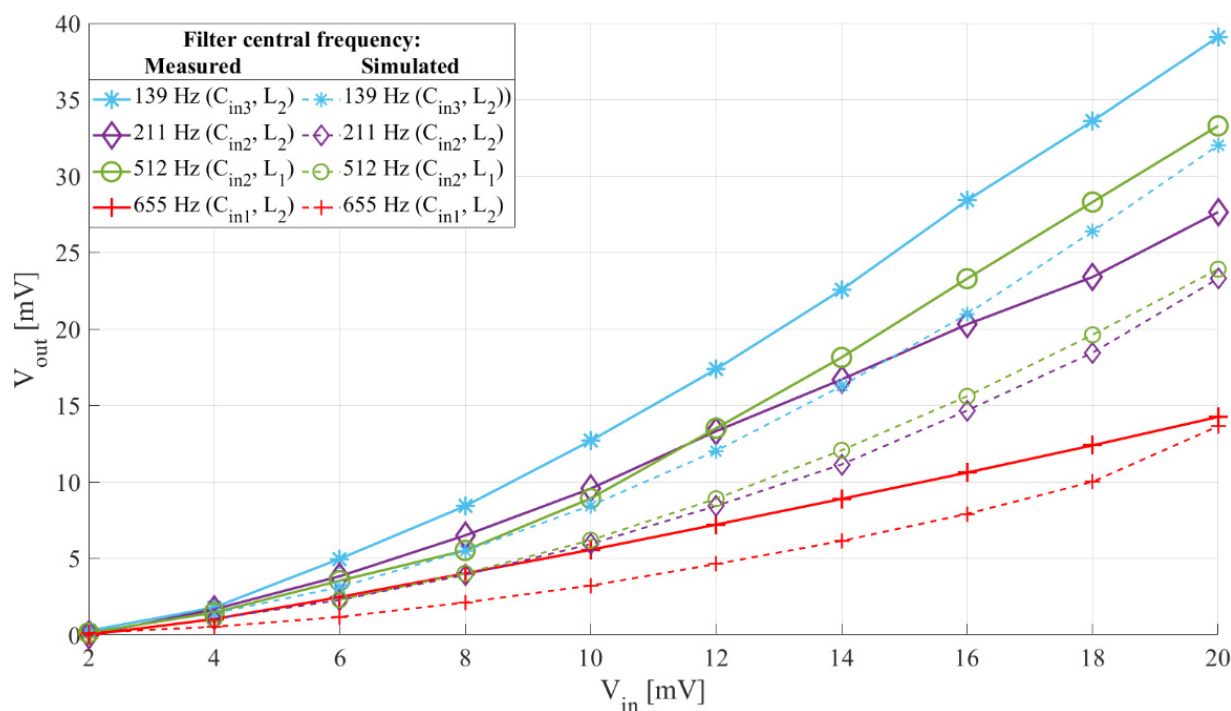
Figure 11. Sensor interface output headroom voltage to input voltage relation with different C_{in}, and L. Switch control frequency 278 Hz (blue), 422 Hz (purple), 1024 Hz (green), and 1310 Hz (red), and duty cycle 50%. Input signal frequency 100 Hz (blue), 200 Hz (purple), 450 Hz (green) and 650 Hz (red), and voltage from 2 mV to 20 mV peak-to-peak with a 2 mV step. The dashed lines show simulation results, paired with the experimental results by color and same markers.
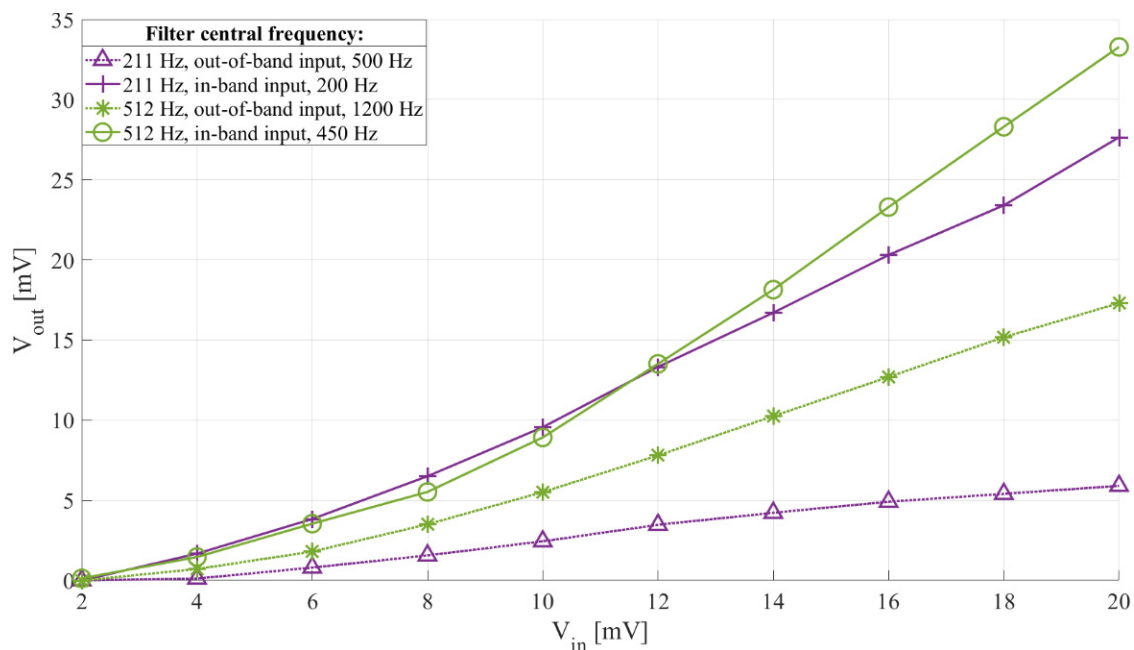
Figure 12. Sensor interface passband and stopband output and input voltage relation with C_{in}, and L. Filter central frequency 211 Hz (C_{in2}, L_2) and 512 Hz (C_{in2}, L_1). The switch control frequency 422 Hz and 1024 Hz, respectively, and the duty cycle 50%. Input signal frequency 200 Hz and 500 Hz for the 211 Hz interface, and 450 Hz and 1200 Hz for the 512 Hz setting, and voltage from 2 mV to 20 mV peak-to-peak with a 2 mV step.

From Figure 11 we can see that the sensitivity of the proposed sensor interface reaches up to approximately 2 mV/mV and it can be adjusted by choosing the input capacitor, C_{in}, inductor, L, and switch control signal frequency. Comparing the experimental and simulation results shown in Figure 11, we see that the sensitivities and their trends of the developed prototype match those of the simulated interfaces.

From Figure 12 we can see that when the interface filter is set to 512 Hz, the interface has a higher passband sensitivity (around 1.66 mV/mV) than when it is set to 211 Hz (around 1.38 mV/mV), but also, due to the lower Q factor, it leads to a higher stopband sensitivity (0.87 mV/mV compared to around 0.3 mV/mV), making the 211 Hz interface setting more than twice more frequency selective than the 512 Hz one.

5.2.3. Power Consumption

The goal was to determine the power consumption of the proposed sensor interface prototype with selected components: the 1024 Hz SiT1569 oscillator, the input capacitor C_{in2} and inductor L_1. The power consumption was determined by multiplying the interface supply voltage of 1.8 V with its supply current, measured by a Fluke 45 multimeter.

The measured interface current consumption, consisting of the oscillator and switch current consumptions, was 1.84 µA, with a 1.8 V power supply, resulting in a power consumption of 3.31 µW.

The overall power consumption was predominantly defined by the oscillator, further emphasizing the crucial role of the switch control signal generator selection in achieving low power consumption.

6. Design Recommendations

Following the numerical and experimental analyses of the interface's functionality and design parameters, this section presents a set of recommendations for interface synthesis.

The interface synthesis is performed in a series of steps:

1. Choosing the output capacitors C_{out1} and C_{out2} to ensure the desired output signal waveform and its key parameters (more details in [17,18]).

2. Determining the wanted frequency characteristic of the interface, by choosing its resonant frequency, f_{res}, (and angular frequency $\omega_{res} = 2\pi f_{res}$) and Q factor. This choice is made considering the frequency characteristic of the input signal of interest.

3. Setting the desired sensitivity at the resonant frequency.

When considering Equation (9) for determining the maximal obtainable output voltage of the proposed interface, the inductor current can be expressed using the input voltage and input circuit impedance, Z_{in}:

$$V_{out} = \frac{V_{in}}{|Z_{in}|} \sqrt{\frac{L_r}{C_{out1,2}}} \tag{11}$$

with Z_{in} given as:

$$|Z_{in}| = \sqrt{\left(\omega_{in}{\cdot}L - \frac{1}{\omega_{in}{\cdot}C_{in}}\right)^2 - R_L{}^2} \tag{12}$$

where ω_{in} is the input signal angular frequency.

From this, we can get an expression for the maximal sensitivity (at the resonant frequency):

$$\frac{V_{out}}{V_{in}} = \frac{1}{\sqrt{L}} \cdot \frac{Q}{\omega_{res}{\cdot} \sqrt{C_{out1,2}}} \tag{13}$$

where ω_{res} is the input circuit resonant angular frequency, and Q the quality factor, given in Equation (10).

From Equation (13), it is clear that, with a chosen output capacitance, input circuit resonant frequency and Q factor, the interface sensitivity at the resonant frequency is set by choosing the appropriate inductance value.

4. Setting the switch control signal duty cycle to 50%, as this provides a suitable sensitivity, frequency selectivity and power consumption. Small increases of the duty cycle can be considered for slight central frequency tuning, despite of increasing the design complexity, but not over 60%, due to increased power consumption.

5. Setting the switch control signal frequency, f_{switch}, to around 2% to 5% higher than double of the frequency of the input signal of interest.

$$f_{switch} = (1.02 \ \sim \ 1.05){\cdot}2f_{in} \tag{14}$$

To conclude this set of design guidelines, an exemplary evaluation of the maximal obtainable sensitivity is shown for one interface setup utilized in the experiments and simulations. With a filter central frequency of f_{res} = 512 Hz, a Q factor of around 4.8, an inductor of L = 100 mH, and output capacitors of $C_{out1,2}$ = 1 μF, we get a maximal obtainable interface sensitivity of around 4.7 mV/mV.

7. Functional Test and Comparison

7.1. Measurement Setup

The measurement setup for comparison of the proposed interface and one consisting of an active bandpass filter and a passive voltage doubler [9] was the same as for the experimental characterization of the proposed sensor interface (Figure 8a).

The proposed sensor interface's (Figure 3a) filter central frequency was 512 Hz with a 400 Hz bandwidth (C_{in} = 1 μF, L = 100 mH, R_L = 66.6 Ω). Its switch control signal duty cycle was 50% and the frequency was 1024 Hz. The output capacitors, C_{out1} and C_{out2}, were 1 μF, and the HSMS-282x diodes, the TMUX1101 switch, and the SiT1569 1024 Hz oscillator were used.

It was compared to a sensor interface consisting of an active general impedance converter (GIC) bandpass filter and a passive two-diode voltage doubler, as shown in Figure 13 [9,18]. The filter central frequency was 500 Hz, with a passband bandwidth of

around 300 Hz. The rectifier capacitors C_{r1} and C_{r2} were 22 nF, to allow the capacitor to fully charge and achieve maximal headroom voltage during each event of interest [17,18].
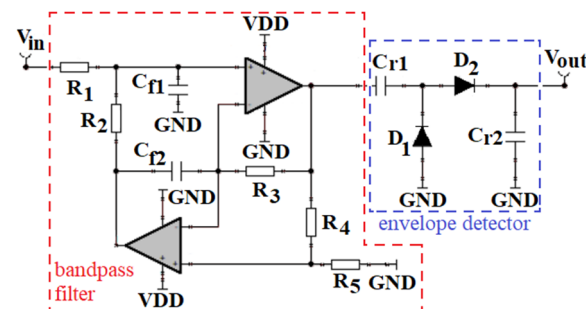
Figure 13. Schematic of the sensor interface consisting of an active GIC bandpass filter and a passive two-diode voltage doubler [9,18].

7.2. Measurement Procedure

The two compared interfaces consist of the same two functional blocks (bandpass filter and envelope detector) and perform the same function of frequency signal decomposition and envelope extraction. To establish if the previously developed interface can be replaced by the one proposed in this work, a comparison of their output headroom voltages (Figure 3b) was performed, using a prerecorded speedboat signal input (twin-engine speedboat passing over a hydrophone submerged approximately 1 m under the surface in shallow water) [24].

The signal waveform with normalized amplitudes and its spectrogram are shown in Figure 14a,b, respectively. The input signal is periodical, each period consisting of approximately 3 seconds of the passing speedboat, followed by around 3seconds of pause. The maximal input signal voltage was scaled from 2 mV to 20 mV peak-to-peak, in steps of 2 mV.

7.3. Results

The two sensor interfaces' comparison with the prerecorded speedboat signal input is shown in Figure 15.

The results show that the proposed sensor interface outperforms the previously developed one, being able to operate with signals around 5 mV peak-to-peak, while the previously developed one required over 20 mV peak-to-peak. The 1.5 mV/mV sensitivity of the proposed interface stems from the increased rectification efficiency provided by the switched inductor.

In addition to the mentioned improvements, it should also be noted that the proposed sensor interface has a power consumption of 3.31 μW compared to 8.25 μW consumed by the previously developed one, which represents a reduction of around 60%. This means that replacing the previously developed interface with the interface proposed in this work, would either extend the sensor node life-time, or allow for more sensors with the same power budget, leading to increased event detection accuracy.

To conclude the demonstration of applicability of the proposed interface in low-power analog acoustic event detection, Table 2 shows a comparison of its functionality and power consumption to state-of-the-art similar interfaces.
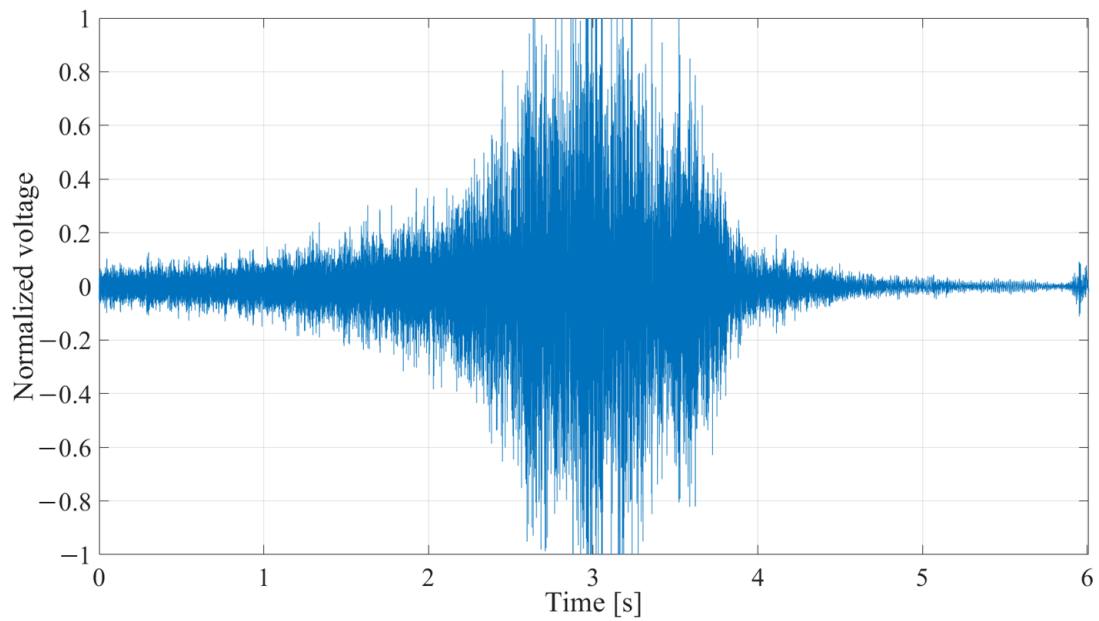
(**a**)
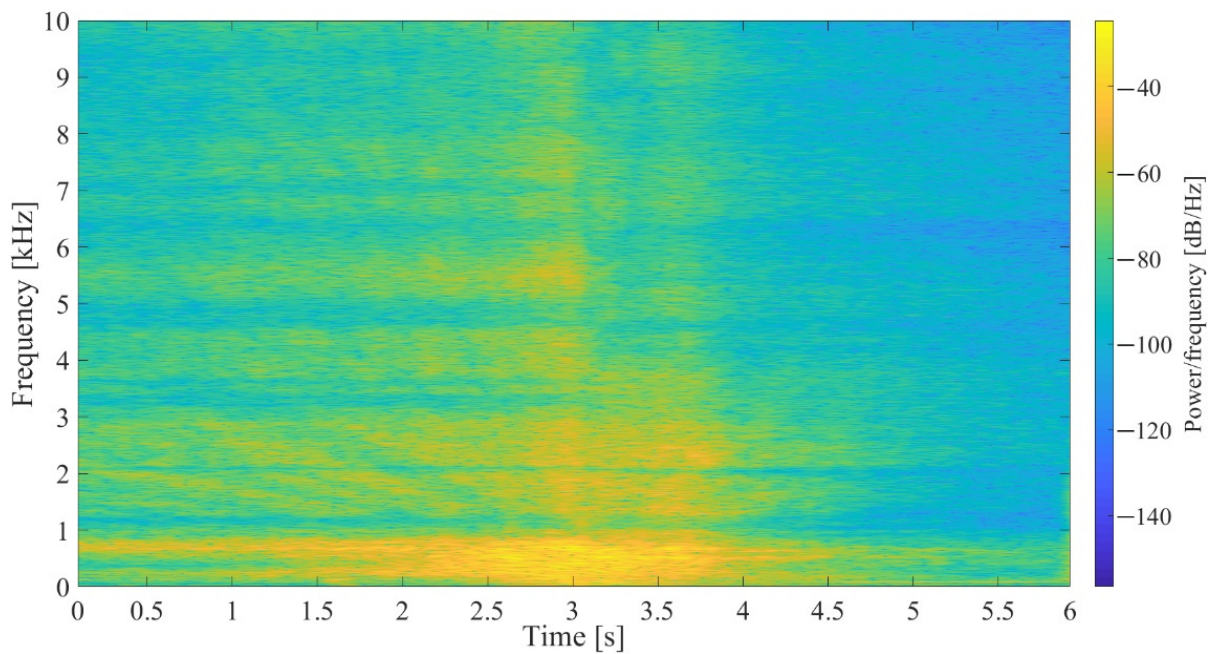
(**b**)

Figure 14. (**a**) Waveform of the prerecorded input signal, V_{in}, with a duration of approximately 3 s, followed by around 3 s of pause. The voltage shown was normalized with regards to maximal value. (**b**) Spectrogram of the prerecorded input signal [18].
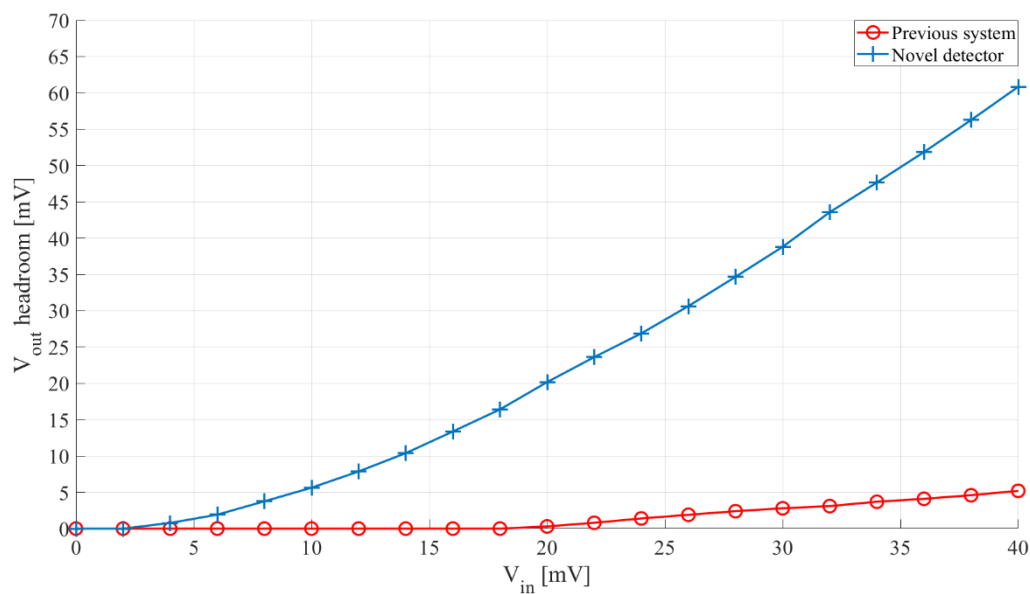
Figure 15. Comparison of outputs of the proposed sensor interface and one consisting of a bandpass filter and a passive voltage doubler. Input—prerecorded speedboat signal, 3 s of signal, 3 s of pause, scaled from 0 mV peak-to-peak to 40 mV peak-to-peak.

Table 2. Per channel power consumption comparison of state-of-the-art acoustic event detector sensor interfaces with the proposed interface.

Reference	Technology	Functionality	Power Consumption (μW)
This work	Embedded design, COTSC	frequency decomposition and envelope detection	3.31
[10]	Embedded design, COTSC	frequency decomposition, envelope detection, 1-bit quantization (adjustable)	22.59
[9]	Embedded design, COTSC	frequency decomposition, envelope detection, 1-bit quantization (adjustable)	11.52
[25]	Embedded design, COTSC	frequency decomposition, amplification, template matching (adjustable)	9.32
[6]	Custom FPAA	frequency decomposition, amplification, peak detection, quantization, pattern recognition (programmable)	5.38
[26]	ASIC	energy threshold detection, 16 feature extraction based on amplification, filtering and absolute value detection, and classification	6
[27]	ASIC	frequency decomposition, magnitude detection, quantization, template matching	2.92

COTSC—commercial of-the-shelf components; FPAA—field-programmable analog array; ASIC—application specific integrated circuit.

8. Conclusions

Low-power analog sensors and interfaces present a necessity in IoT development. Following previous research on switched inductor filters and energy harvesters, a novel switched inductor frequency selective sensor interface is proposed. A simulation study was done to determine the key design parameters and characterize the interface performance with input signals up to 20 mV peak-to-peak, at low acoustic frequencies from 100 Hz to 1 kHz. A prototype interface was developed and characterized, achieving the maximal sensitivity of approximately 2 mV/mV in the passband, four times lower sensitivity in the stopband, and a power consumption of approximately 3.31 μW. The novel sensor interface can operate with inputs around 5 mV compared to over 20 mV needed for

the one consisting of an active bandpass filter and a passive voltage doubler, having around 60% lower power consumption (3.31 µW compared to 8.25 µW), thus enabling life-time extension or improved detection. The future work will focus on reconfigurable switched inductor sensor interfaces and lowering the power consumption of the switch control oscillator.

Author Contributions: Conceptualization, M.G. and V.B.; data curation, M.G.; investigation, M.G.; methodology, M.G. and V.B.; project administration, V.B.; supervision, V.B.; visualization, M.G.; writing—original draft, M.G. and V.B. Both authors have read and agreed to the published version of the manuscript.

Institutional Review Board Statement: Not applicable.

Informed Consent Statement: Not applicable.

Data Availability Statement: Not applicable.

Conflicts of Interest: The authors declare no conflict of interest. The funders had no role in the design of the study; in the collection, analyses, or interpretation of data; in the writing of the manuscript, or in the decision to publish the results.

References

1. Kalsoom, T.; Ramzan, N.; Ahmed, S.; Ur-Rehman, M. Advances in Sensor Technologies in the Era of Smart Factory and Industry 4.0. *Sensors* **2020**, *20*, 6783. [CrossRef] [PubMed]
2. Zikria, Y.B.; Ali, R.; Afzal, M.K.; Kim, S.W. Next-Generation Internet of Things (IoT): Opportunities, Challenges, and Solutions. *Sensors* **2021**, *21*, 1174. [CrossRef] [PubMed]
3. Alioto, M. (Ed.) *Enabling the Internet of Things*; Springer International Publishing: Cham, Switzerland, 2017; pp. 1–45, ISBN 978-3-319-51480-2.
4. Goux, N.; Badets, F. Review on Event-Driven Wake-Up Sensors for Ultra-Low Power Time-Domain Design. *Midwest Symp. Circuits Syst.* **2019**, 554–557. [CrossRef]
5. Olsson, R.H.; Bogoslovov, R.B.; Gordon, C. Event Driven Persistent Sensing: Overcoming the Energy and Lifetime Limitations in Unattended Wireless Sensors. *Proc. IEEE Sens.* **2016**, 1–3. [CrossRef]
6. Bhattacharyya, S.; Andryzcik, S.; Graham, D.W. An Acoustic Vehicle Detector and Classifier Using a Reconfigurable Analog/Mixed-Signal Platform. *J. Low Power Electron. Appl.* **2020**, *10*, 6. [CrossRef]
7. Mayer, P.; Magno, M.; Benini, L. A2Event: A Micro-Watt Programmable Frequency-Time Detector for Always-On Energy-Neutral Sensing. *Sustain. Comput. Inform. Syst.* **2019**, *25*, 100368. [CrossRef]
8. Jeong, S.; Chen, Y.; Jang, T.; Tsai, J.M.L.; Blaauw, D.; Kim, H.S.; Sylvester, D. Always-On 12-nW Acoustic Sensing and Object Recognition Microsystem for Unattended Ground Sensor Nodes. *IEEE J. Solid-State Circuits* **2018**, *53*, 261–274. [CrossRef]
9. Oletic, D.; Gazivoda, M.; Bilas, V. A Programmable 3-Channel Acoustic Wake-Up Interface Enabling Always-On Detection of Underwater Events Within 20 µA. In Proceedings of the Eurosensors 2018 Conference, Graz, Austria, 9–12 September 2018; pp. 1–7.
10. Mayer, P.; Magno, M.; Benini, L. Self-Sustaining Acoustic Sensor with Programmable Pattern Recognition for Underwater Monitoring. *IEEE Trans. Instrum. Meas.* **2019**, *68*, 2346–2355. [CrossRef]
11. Galante-Sempere, D.; Ramos-Valido, D.; Lalchand, K.S.; del Pino, J. Low-Power RFED Wake-Up Receiver Design for Low-Cost Wireless Sensor Network Applications. *Sensors* **2020**, *20*, 6406. [CrossRef] [PubMed]
12. Lu, S.; Boussaid, F. A Highly Efficient P-SSHI Rectifier for Piezoelectric Energy Harvesting. *IEEE Trans. Power Electron.* **2015**, *30*, 5364–5369. [CrossRef]
13. Wu, L.; Zhu, P.; Xie, M. A Self-Powered Hybrid SSHI Circuit with a Wide Operation Range for Piezoelectric Energy Harvesting. *Sensors* **2021**, *21*, 615. [CrossRef] [PubMed]

14. Alex-Amor, A.; Moreno-Núñez, J.; Fernández-González, J.M.; Padilla, P.; Esteban, J. Parasitics Impact on the Performance of Rectifier Circuits in Sensing RF Energy Harvesting. *Sensors* **2019**, *19*, 4939. [CrossRef] [PubMed]

15. Gak, J.; Miguez, M.; Alvarez, E.; Arnaud, A. Integrated Ultra-Low Power Precision Rectifiers for Implantable Medical Devices. In Proceedings of the 2019 Argentine Conference on Electronics (CAE), Mar del Plata, Argentina, 14–15 March 2019; pp. 27–30. [CrossRef]

16. Trigona, C.; Giuffrida, S.; Andò, B.; Baglio, S.; Elettrica, I.; Doria, V.A. Micromachined "Random Mechanical Harvester on Inductor " to Recovery Energy from Very Low-Amplitude Vibrations with Zero-Voltage Threshold. In Proceedings of the 2016 IEEE SENSORS, Orlando, FL, USA, 30 October–3 November 2016; pp. 2–4. [CrossRef]

17. Gazivoda, M.; Oletic, D.; Bilas, V. Characterization and Comparison of Envelope Detectors for Wake-up Sensor Interfaces at Audio Frequencies. In Proceedings of the 2020 IEEE International Instrumentation and Measurement Technology Conference (I2MTC), Dubrovnik, Croatia, 25–28 May 2020; pp. 1–6. [CrossRef]

18. Gazivoda, M.; Oletić, D.; Trigona, C.; Bilas, V. Passive Extraction of Signal Feature Using a Rectifier with a Mechanically Switched Inductor for Low Power Acoustic Event Detection. *Sensors* **2020**, *20*, 5445. [CrossRef] [PubMed]

19. Argyrou, M.C.; Marouchos, C.C.; Darwish, M.; Iosif, E.; Paterakis, F. Investigation of the Switched Inductor Circuit for Harmonics Compensation. In Proceedings of the 2017 52nd International Universities Power Engineering Conference, UPEC 2017, Heraklion, Greece, 28–31 August 2017; Volume 2017, pp. 1–5. [CrossRef]

20. Marouchos, C.C. *The Switching Function: Analysis of Power Electronic Circuits*; The Institution of Engineering and Technology: London, UK, 2006; ISBN 0896038890.

21. Ott, H.W. *Noise Reduction Techniques in Electronic Systems*; Wiley-Interscience: Livingston, NJ, USA, 1988; ISBN 0-471-85068-3.

22. Ming, Y.; Ziping, C.; Jun, L. Characterization the Influences of Diodes to Piezoelectric Energy Harvester. *Int. J. Smart Nano Mater.* **2018**, *9*, 151–166. [CrossRef]

23. Thoen, B.; Ottoy, G.; Rosas, F.; Lauwereins, S.; Rajendran, S.; De Strycker, L.; Pollin, S.; Verhelst, M. Saving Energy in WSNs for Acoustic Surveillance Applications while Maintaining QoS. In Proceedings of the 2017 IEEE Sensors Applications Symposium (SAS), Glassboro, NJ, USA, 13–15 March 2017; pp. 1–6. [CrossRef]

24. Underwater Video of Twin Engine Boat Props High Speed. Available online: https://www.youtube.com/watch?v=6uQ7IDqbmAE (accessed on 7 June 2018).

25. Sutton, F.; Da Forno, R.; Gschwend, D.; Gsell, T.; Lim, R.; Beutel, J.; Thiele, L. The Design of a Responsive and Energy-efficient Event-triggered Wireless Sensing System. In Proceedings of the 2017 International Conference on Embedded Wireless Systems and Networks, Uppsala, Sweden, 20–22 February 2017; pp. 144–155, ISBN 978-0-9949886-1-4.

26. Badami, K.M.H.; Lauwereins, S.; Meert, W.; Verhelst, M. A 90 nm CMOS, 6 µW Power-Proportional Acoustic Sensing Frontend for Voice Activity Detection. *IEEE J. Solid-State Circuits* **2016**, *51*, 291–302. [CrossRef]

27. Rumberg, B.; Graham, D.W.; Kulathumani, V. A Low-Power, Programmable Analog Event Detector for Resource-Constrained Sensing Systems. In Proceedings of the 2012 IEEE 55th International Midwest Symposium on Circuits and Systems (MWSCAS), Boise, ID, USA, 5–8 August 2012; pp. 338–341. [CrossRef]

Publication 4

Gazivoda, M., Oletić, D., Trigona, C., Bilas, V., "Passive Extraction of Signal Feature Using a Rectifier with a Mechanically Switched Inductor for Low Power Acoustic Event Detection", *Sensors*, Vol. 20, Issue 18, pp 19, 2020, doi:10.3390/s20185445

Passive Extraction of Signal Feature Using a Rectifier with a Mechanically Switched Inductor for Low Power Acoustic Event Detection

Marko Gazivoda [1,]*[ORCID]**, Dinko Oletić** [1][ORCID]**, Carlo Trigona** [2] **and Vedran Bilas** [1,]*

[1] Faculty of Electrical Engineering and Computing, University of Zagreb, 10000 Zagreb, Croatia;
   dinko.oletic@fer.hr
[2] Department of Electrical, Electronic and Computer Engineering, University of Catania, 95100 Catania, Italy;
   carlo.trigona@dieei.unict.it
[*] Correspondence: marko.gazivoda@fer.hr (M.G.); vedran.bilas@fer.hr (V.B.)

check for updates

Abstract: Analog hardware used for signal envelope extraction in low-power interfaces for acoustic event detection, owing to its low complexity and power consumption, suffers from low sensitivity and performs poorly under low signal to noise ratios (SNR) found in undersea environments. To overcome those problems, in this paper, we propose a novel passive electromechanical solution for the signal feature extraction in low frequency acoustic range (200–1000 Hz), in the form of a piezoelectric vibration transducer, and a rectifier with a mechanically switched inductor. A simulation study of the novel solution is presented, and a proof-of-concept device is developed and experimentally characterized. We demonstrate its applicability and show the advantages of the passive electromechanical device in comparison to the active electrical solution in terms of operation with lower input signals (<20 mV compared to 40 mV), and higher robustness in low SNR conditions (output voltage loss for −10 dB ≤ SNR < 40 dB of 1 mV, compared to 10 mV). In addition to the signal processing performance improvements, compared to our previous work, the utilization of the presented novel passive feature extractor would also decrease power consumption of a detector's channel by over 76%, enabling life-time extension and/or increased quality of detection with larger number of channels. To the best of our knowledge, this is the first solution presented in the literature that demonstrates the possibility of using a passive electromechanical feature extractor in a low-power analog wake-up event detector interface.

Keywords: wake-up interface; acoustic vibrations; pattern recognition; low SNR; passive electromechanical transducer

1. Introduction

The recognition of infrequent events is of interest in many fields (environmental monitoring [1–5], safety and security [6–13], communication [14–16], agriculture, health monitoring [17]). It requires continuous operation of an electronic system comprising sensing, detection and recognition functions, which are power-hungry tasks [7,18]. The power consumption can be reduced by introduction of always-on low-power interfaces that wake up the main processing stage upon detection of an event of interest [19,20].

Many acoustic events can be recognized based on their time-frequency pattern [5], which can be approximated by an ordered sequence of discrete time-frequency states (Figure 1a). The extraction of these patterns in wake-up systems is usually performed by processing in the time domain utilizing a low-power multichannel analog detector [21]. The event detector consists of multiple channels to allow for simultaneous analog frequency decomposition, with each channel requiring a feature extractor to

extract features from a designated frequency band from the signal of interest. To make the detector simple and efficient it is crucial to choose an appropriate feature and its extraction method. Features that can be used in these detectors can either be instantaneous ones (envelope) or related to the signal integral (root mean square (RMS), power, energy) [22–24]. Most of low-power event detection systems use instantaneous signal features because of their simple extraction (shown in Figure 1b). In our previous work [25], we developed such a system, with a power consumption of 11.52 µW per channel. In this work, we will focus on the feature extraction part of the acoustic event detection system.

(a)

(b)

(c)

Figure 1. *Cont.*

(d)
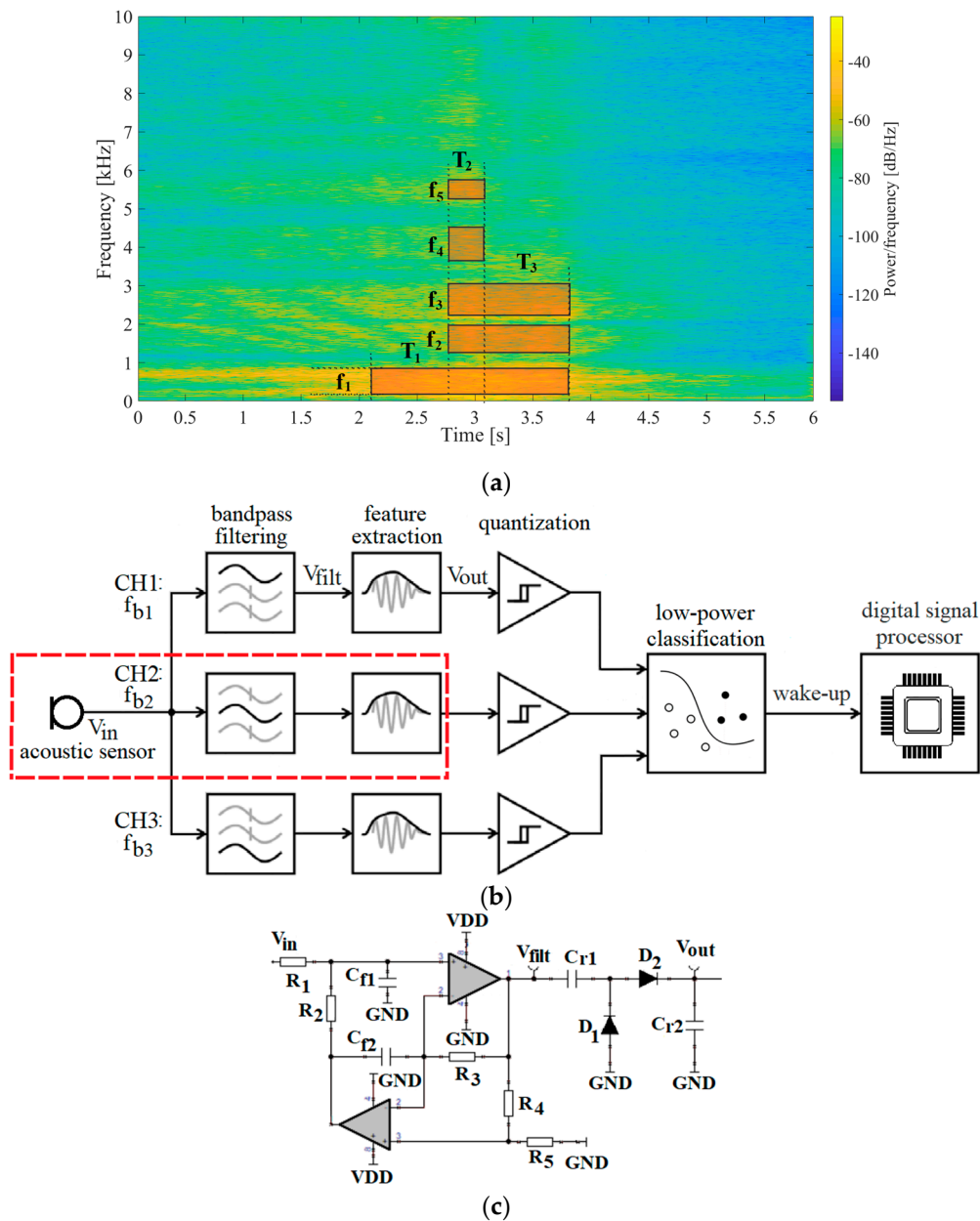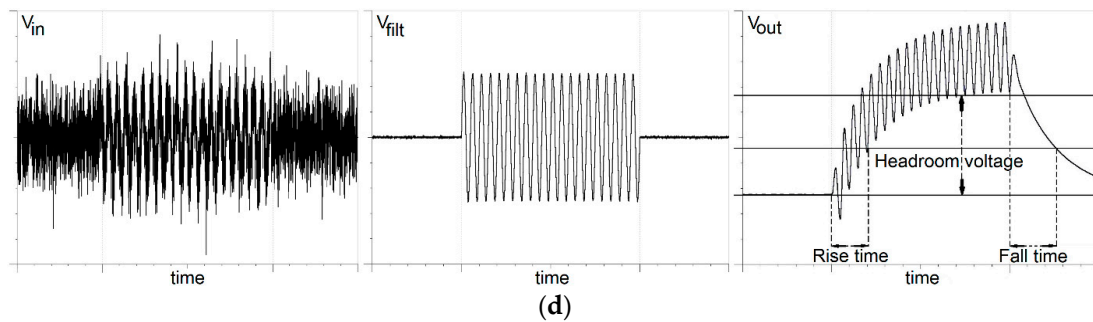
Figure 1. (**a**) An example of a spectrogram of a signal of interest. T_1, T_2, T_3, represent durations, f_{b1}, f_{b2}, f_{b3} frequency bands and E_1, E_2, E_3 energy (feature) of states within the time-frequency pattern. (**b**) Block diagram of an analog multichannel pattern recognition-based event detection system. The marked part of the system is the active electrical feature extractor (in this case the feature is signal envelope in a set frequency band). (**c**) A schematic of the active electrical feature extractor (AE FE). (**d**) Characteristic signals of the detector—at transducer (V_{in}), after filter (V_{filt}) and at output (V_{out}). The values of interest in the feature extractor's output voltage are marked—headroom voltage, rise and fall time.

Despite the envelope having the advantage of being one of the simplest features to extract in terms of hardware complexity and power consumption, a serious drawback of the envelope is its poorer performance in low signal to noise ratios (SNR) conditions [26].

Following an idea of using electromechanical components to improve low-power event detector functionality [20], our goal in this work was to evaluate a passive electromechanical feature extractor that utilizes a piezoelectric transducer and a rectifier with a mechanically switched inductor, inspired by the Random Mechanical Switching Harvester on Inductor (RMSHI) [27–29], as an alternative for active electrical feature extractor (Figure 1c), consisting of an active bandpass filter and a passive rectifier used for detecting slowly evolving acoustic events in low SNR conditions in frequency range from 200 Hz to 1 kHz.

In [30], we analyzed the applicability of a rectifier with a mechanically switched inductor (part of RMSHI) used with an active bandpass filter forming an active feature extractor. The goal of this work was to develop and characterize a novel, fully passive electromechanical feature extractor (PEM FE) implementing a transducer, a mechanical filter and a rectifier with a mechanically switched inductor, to be utilized in an acoustic event detection.

In this paper we make several contributions. We present a simulation model of the passive electromechanical feature extractor as part of an acoustic event detector and present simulation results. We develop a proof-of-concept extractor and, with it, provide experimental verification of the simulation results. We demonstrate applicability and advantages of the extractor in extraction of features under low SNR. To the best of our knowledge, this is the first solution presented in the literature that shows a low-power acoustic event detector utilizing a passive electromechanical feature extractor. This work represents a step towards a fully passive, or self-sustaining, infrequent acoustic event detector.

The rest of the paper is organized as follows: Section 2 shows an event detector architecture, describing the passive electromechanical feature extractor. Section 3 shows the simulation model and simulation results of the passive electromechanical feature extractor. Section 4 shows experimental results and characterization of the developed extractor. Section 5 presents comparison of an active electrical and passive electromechanical feature extractor. Section 6 concludes the paper and shows future research.

2. Event Detector Architecture

2.1. Time-Frequency Signal Pattern and Event Detection System

A spectrogram of a passing ship with marked time-frequency states and a pattern recognition-based event detector are shown in Figure 1a,b, respectively [25]. The detector entails three analog-domain filtering channels decomposing the transducer's signal (V_{in}) into arbitrary frequency bands. Intervals of signal presence within individual filtering channels (V_{filt}) are localized in time by extracting features of filtered signals, and then performing single-bit quantization using comparators. Temporal relations between comparator responses are finally analyzed by a 3-channel digital sequence recognition state-machine, which wakes-up the digital signal processor DSP [21]. A schematic of detector's active electrical feature extractor (AE FE) is shown in Figure 1c.

Detailed characterization of this detector utilizing an active general impedance converter (GIC)-based dual operational amplifier bandpass filter was performed in [25] and a study on rectifier topologies for envelope extraction was presented in [31]. Such a combination of an active bandpass filter and passive diode rectifier developed in previous work showed several constraints on this detector's feature extractor performance and output signal (Figure 1d). The rise and fall times determine the detector's ability to distinguish two consecutive time-frequency states. Based on our previous study, rise and fall times around 1 s are acceptable for slow-evolving acoustic events of interest. The output headroom voltage of the envelope extractor shows variations in the feature of interest. The headroom voltage required for event detection is dependent on the selected comparator. In this work, we consider a level of 1 mV to be acceptable.

In this work, we intend to replace the active electrical feature extractor (AE FE), consisting of an active bandpass filter and a passive rectifier (Figure 1c), with a passive electromechanical feature extractor (PEM FE) that features a rectifier with a mechanically switched inductor (Figure 3), to reduce power consumption and improve performance in high background noise environments.

2.2. Passive Electromechanical Feature Extractor

The mechanical structure of the proposed passive electromechanical feature extractor (PEM FE) (Figure 2) is based on Random Mechanical Switching Harvester on Inductor (RMSHI). The RMSHI was developed for vibration energy harvesting utilizing a piezoelectric transducer. Its key advantage is high efficiency of converting vibration into electrical energy, which is 0.622%, compared to the 0.022% for resonant harvesters with single-frequency excitation, and 0.126% compared to 0.001% for broad frequency excitation [32]. The greater energy conversion efficiency of the RMSHI stems from: non-resonant frequency response and utilization of a mechanically switched inductor.
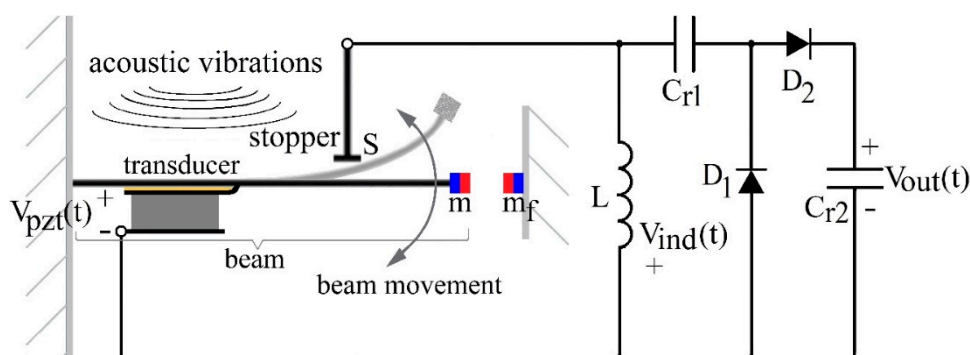
Figure 2. Block diagram of the passive electromechanical feature extractor (PEM FE). *S*—switch, *m*—magnet at the beam end, m_f—fixed magnet, *L*—inductor, C_{r1}, C_{r2}—rectifier capacitors, D_1, D_2—rectifier diodes. $V_{pzt}(t)$—voltage generated at piezoelectric transducer, $V_{ind}(t)$—voltage induced at the inductor *L*, $V_{out}(t)$—extractor output voltage.

The RMSHI consists of a metal cantilever beam having a permanent magnet at its free end, a metal stopper that forms a mechanical switch with the cantilever, and a fixed permanent magnet that modifies elasticity of vibration driven movement of the cantilever. A piezoelectric transducer is mounted on a metal cantilever beam that transforms input vibrations into an electrical signal. An inductor is switched by the cantilever movement and connected to a rectifier that conditions the electric signal (a mechanically switched inductor).

Due to the RMSHI featuring a stopper and a pair of magnets exerting repulsive force on each other (as shown in Figure 2), the movement of the RMSHI cantilever beam can be considered a movement of two beams attached to one another, with an initial magnetic force bias placing the beam in contact with the stopper when no external force is applied. While the beam is in contact with the stopper, only its part in front of the stopper moves. Once the overall external force on beam overcomes the magnetic force bias, the beam detaches from the stopper and the entire beam moves. This two-part movement causes the beam to have a non-resonant, broader frequency characteristic. Further explanation on this can be found in [27,32].

The utilization of the mechanically switched inductor provides further increase in harvester efficiency in conditions of weak vibrations, generating signals under the diode threshold.

When the beam and the stopper are in contact, the switch S is closed, and the energy of the signal generated by the piezoelectric transducer is stored in the inductor's magnetic field (Figure 3, red details). When the switch opens, the energy stored in the inductor's (L) magnetic field, E_L, is transferred over the rectifier to the capacitor's (C_{r2}) electric field energy, E_C, charging the capacitor to V_{out} (Figure 3, blue details). Neglecting energy losses, voltage V_{out} depends on the current through the inductor at that instant of time, I_{open}, and the values of inductance L and capacitance C_{r1-2} (1) [33]

$$V_{out} = I_{open} \cdot \sqrt{\frac{L}{C_{r1-2}}} \tag{1}$$
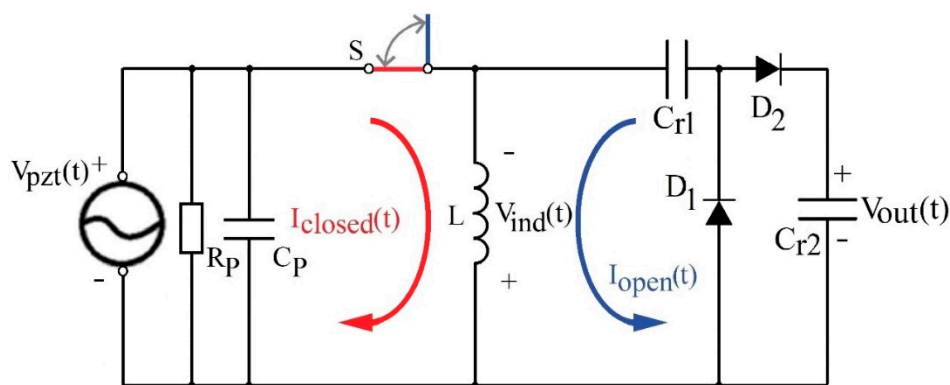
Figure 3. Schematic of the proposed passive electromechanical feature extractor (PEM FE). Red—current $I_{closed}(t)$—passing through the PEM FE while the switch S is closed. Blue—current $I_{open}(t)$ passing through the PEM FE when the switch S opens. L—inductor and C_{r1}, C_{r2}—rectifier capacitors, D_1, D_2—rectifier diodes. R_P and C_P—parasitic resistance and capacitance of piezoelectric transducer, respectively. $V_{pzt}(t)$—voltage generated at piezoelectric transducer, $V_{ind}(t)$—voltage induced at the inductor, $V_{out}(t)$—extractor output voltage.

The switching of the inductor induces voltage, $V_{ind}(t)$, higher than the voltage generated by the piezoelectric transducer, $V_{pzt}(t)$, and the diode threshold, making the switched inductor a voltage booster. A detailed description of the process is presented in [27,28,32].

The exact physical implementation of the extractor used in this study, with transducer and switch parameters will be presented in the Measurement Setup subsection in Section 4.

3. Passive Electromechanical Feature Extractor Simulation Model and Simulation Results

3.1. Simulation Model

In order to evaluate the use of the passive electromechanical feature extractor (PEM FE) in a set frequency band, an analytical model has been implemented and simulated in MathWorks' MATLAB® Simulink (Natick, MA, USA).

The mechanics of the PEM FE can be modeled by a second order non-linear differential equation:

$$m\ddot{x} + d\dot{x} + \frac{\partial U_T}{\partial x} = F(t)\Big|_{U_T = \delta x^4} \tag{2}$$

where m is the mass of the beam with the magnet and d is its damping coefficient. Term x is the displacement of the tip of the beam and the dotted terms represent the first and second derivate of the displacement (velocity and acceleration of the cantilever, respectively). U_T is the potential energy function, which is non-linear due to the stopper and permanent magnet positions, which act as adjustable factors, allowing fine adjustments within ranges determined by the physical dimensions of the device (beam length, l and mass, m). The magnet's contribution is expressed with the term δ.

The voltage generated on the piezoelectric transducer ($V_{pzt}(t)$) on the cantilever beam, is:

$$V_{pzt}(t) = \int (\Pi\dot{x} - V_{pzt}(t)/\tau)dt \tag{3}$$

where Π is the coupling constant and τ is the time constant of the piezoelectric material. In detail, all parameters describing the previous equations are listed and their values, originated by the model, experiments and the literature, are indicated in Table 1.

Table 1. List of used parameters.

Parameter	Unit	Value	Method of Estimation
m	kg	0.00082	Model
d	kg/s	0.001	Experiment
δ	kg m^{-2} s^{-2}	300,000	Model
Π	V/m	1.13	Experiment
τ	s	162	Literature [27]

The analytical considerations presented by Equations (2) and (3) constitute the basis for the development of the simulation model (simplified version is shown in Figure 4). The topology of the electric circuit used in the model is the same as shown in Figure 3. The inductor L used for the simulation model was 1 mH and the diodes were modeled to fit the D1N4148 diode characteristics. The rectifier capacitances, C_{r1-2}, used in the simulations were: 33 nF, 100 nF, 470 nF and 1 μF. The physical parameters of the PEM FE models, beam length (l), beam and magnet mass (m) and magnet position (δ) were varied to achieve different frequency characteristics, while the parameters concerning the piezoelectric transducer (Π and τ) were fixed to simulate the behavior of the used piezoelectric transducer as closely as possible.

$$mx\ddot{} + dx\dot{} + \frac{\partial U_T}{\partial x} = F(t)\Big|_{U_T = \delta x^4} \qquad V_{pzt}(t) = \int (\Pi \dot{x} - V_{pzt}(t)/\tau)dt$$
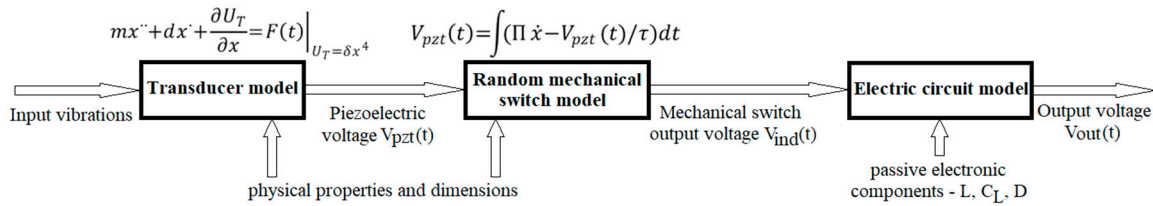
Figure 4. Simplified simulation model of the passive electromechanical feature extractor (PEM FE). It consists of simulation models of the piezoelectric transducer, the mechanical switch and the electric circuit.

Using the simulation model, the following analyses were done: the relation between the input energy (E_{in}) and the RMS value of the output voltage (V_{out}) (transfer characteristic of the passive electromechanical feature extractor), the frequency selectivity of the extractor and the rectifier capacitances' (C_{r1-2}) influence on the output voltage (V_{out}) waveform.

3.2. Simulation Results

The simulation analysis of PEM FE frequency selectivity shows that its frequency characteristic can be adjusted to fit a selected band within the lower acoustic frequencies of interest (up to around 1 kHz) by changing its physical parameters explained in Section 3.1 and shown in Figure 4. The results in Figure 5. show three feature extractors for different selected frequency bands. Rectifier capacitances were set to $C_{r1-2} = 33$ nF and an inductor of $L = 1$ mH was used. Input vibration frequency changed by 5 Hz from 270 Hz to 350 Hz, from 400 Hz to 495 Hz and from 880 Hz to 1060 Hz for each extractor, respectively. Input vibration energy was set to 1.6 nJ.
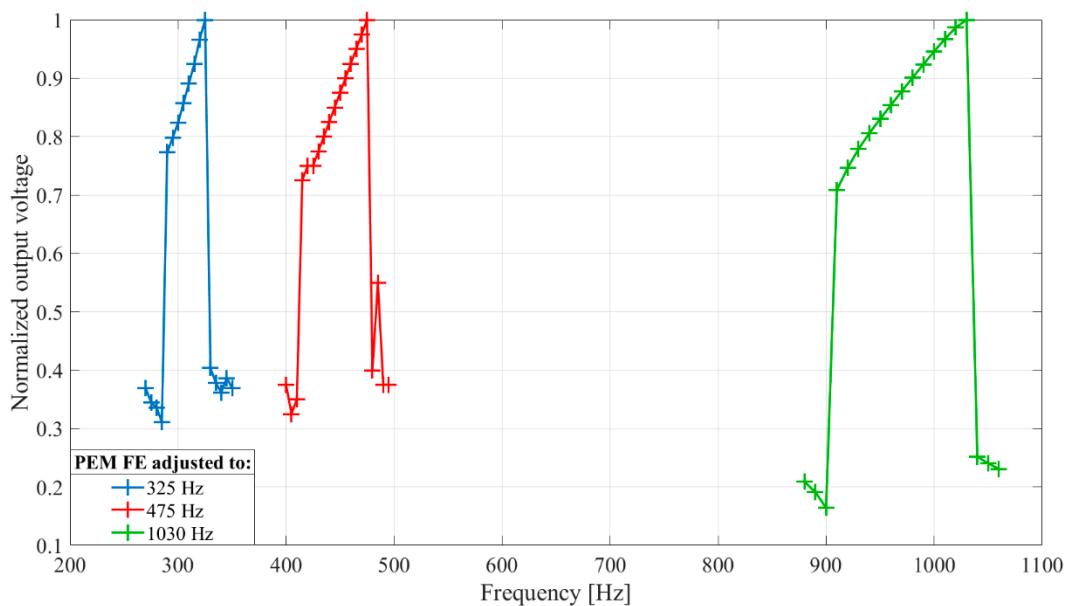
Figure 5. Frequency selectivity of passive electromechanical feature extractor (PEM FE) obtained by change of its physical dimensions (beam length (*l*), beam and magnet mass (*m*), magnet position (*δ*)). The output voltage was normalized with regards to maximal value. Rectifier capacitances $C_{r1-2} = 33$ nF. Inductor $L = 1$ mH. Input vibration frequency changed by 5 Hz from 270 Hz to 350 Hz, from 400 Hz to 495 Hz and from 880 Hz to 1060 Hz for each PEM FE setting, respectively. Input vibration energy set to 1.6 nJ.

The simulation analysis of the relation between input vibration energy and output voltage shows (Figure 6) that a PEM FE can operate with sufficiently high sensitivity of 2 mV/nJ in a frequency band

around 325 Hz, and with input vibration levels of interest (from 0.1 nJ to 1.6 nJ), proving it can be used as a feature extractor in an acoustic event detector channel. The measurement resolution of ±1 nJ can be achieved. The analysis also shows the sensitivity with different input vibration frequencies, around the passband central frequency of 325 Hz (dashed lines in Figure 6). Rectifier capacitances were set to C_{r1-2} = 33 nF and the inductor was set to L = 1 mH.
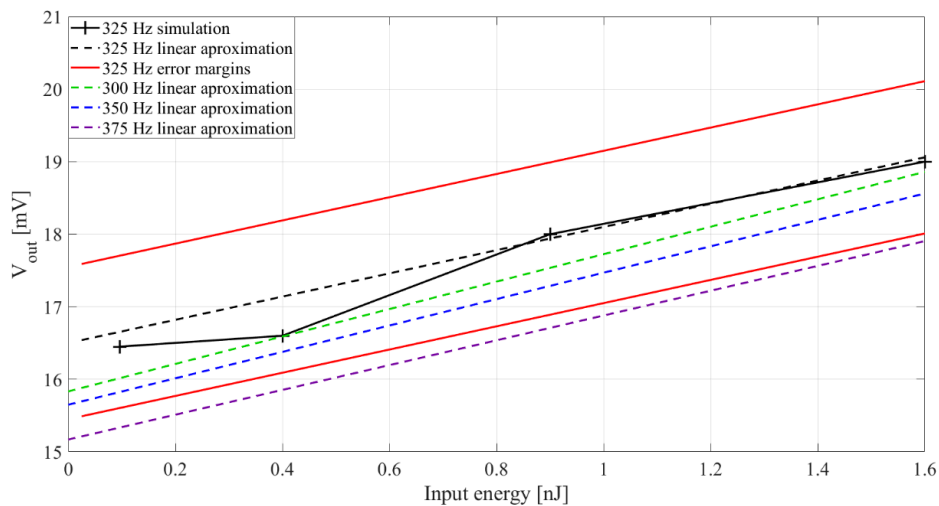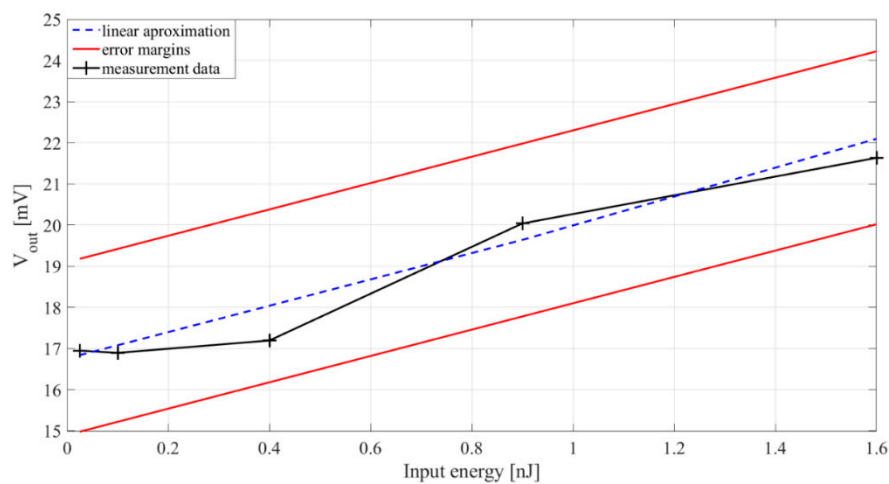

Figure 6. Extractor output voltage (V_{out}) with input signal energy, E_{in}. Rectifier capacitance C_{r1-2}= 33 nF. Inductor L = 1 mH. Input vibration energy was set to 0.1 nJ, 0.4 nJ, 0.9 nJ and 1.6 nJ, respectively. The black line with pluses represents the simulation results, the black dashed line the linear approximation and the red lines represent the error margins (explained in more detail in the experimental part) for 325 Hz input vibration frequency. The green, blue and purple dashed lines represent linear approximations for 300 Hz, 350 Hz and 375 Hz input vibration frequency, respectively.

The simulation analysis concerning rectifier capacitances shows the influence the rectifier capacitance has on PEM FE's output voltage waveform. For higher values of the rectifier capacitances a decrement in output voltage (V_{out}) ripple can be observed from around ± 33 mV to around ± 2.5 mV (Figure 7b), increasing the headroom voltage (Figure 1d), but this is counterbalanced with an increment in rise and fall times (Figure 1d) from around 1 s to around 10 s (Figure 7a).

(a)

(b)
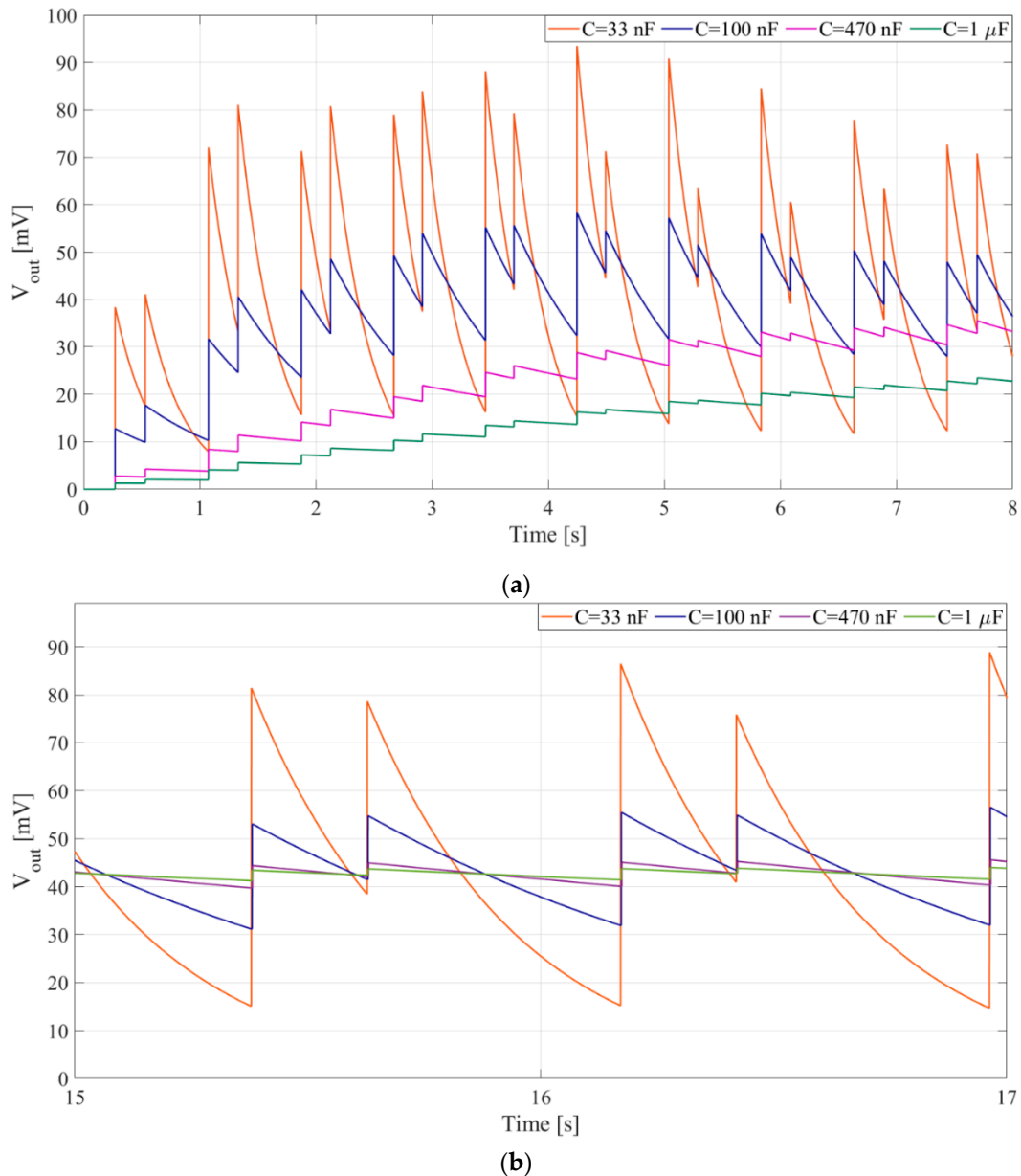
Figure 7. Waveform of the output voltage, V_{out}, for several values of rectifier capacitances: 33 nF, 100 nF, 470 nF, 1 µF. Input vibrations at 325 Hz generate 50 mV peak-to-peak at the piezoelectric transducer. Inductor L = 1 mH. (**a**) At beginning of capacitor charging, (**b**) In stationary conditions.

4. Experimental Characterization of Passive Electromechanical Feature Extractor

4.1. Measurement Setup

The goal of these measurements was to provide experimental verification of the simulation results and characterize the passive electromechanical feature extractor in terms of selectivity and sensitivity and to confirm design parameters.

A photograph of the measurement setup can be seen in Figure 8a. The measurement setup consisted of a waveform generator (Keysight 33500B) that drives the shaker (Smart Material Energy Harvesting Kit 1.2.) used both to generate the voltage on a piezoelectric transducer and to open and close the switch in the extractor. The output voltage was acquired by a National Instruments data acquisition card (NI USB-6211) connected to a PC.

(a)　　　　　　　　　　　　　　(b)
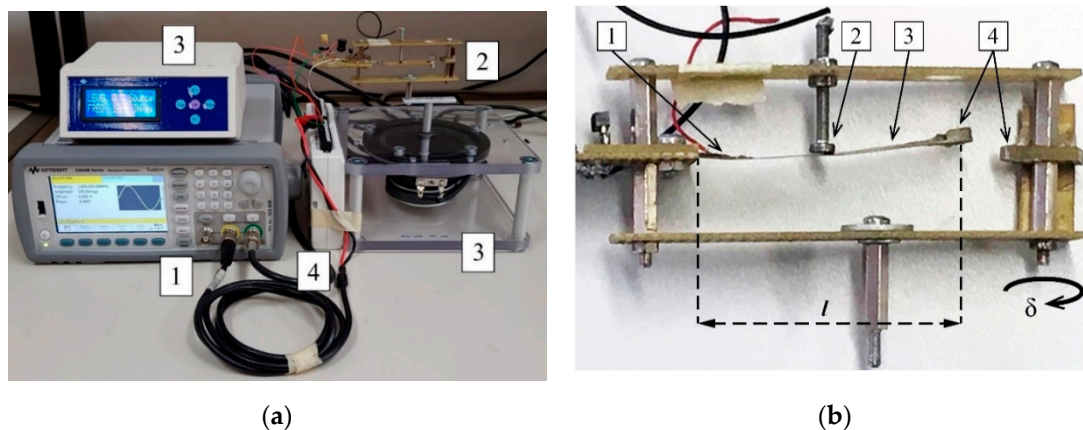
Figure 8. (**a**) A photograph of the measurement setup. (1) Keysight 33500B waveform generator, (2) PEM FE,(3) Smart Material Energy Harvesting Kit 1.2. shaker, (4) NI USB-6211 data acquisition card. (**b**) Physical realization of the PEM FE (without the rectifier). (1) Piezoelectric transducer, (2) stopper, (3) cantilever beam, (4) fixed magnet (right) and adjustable magnet (left). The mass of the beam (*m*) is approximated by the mass of the magnet at its end. δ is the magnet position adjustment parameter. Length of the beam is marked by *l*.

Figure 8b shows the physical realization of the PEM FE used in this study. The piezoelectric element was bonded to the cantilever in part of the beam where maximal strain was measured. The piezoelectric material used in this study is a 7BB-12-9 piezoelectric diaphragm (Murata), with an external diameter of 12 mm and thickness of 0.22 mm, [34]. The electromechanical switch used in this study is composed of a brass beam with a length (*l*) of about 55 mm, width of about 8.3 mm and thickness of about 0.2 mm, with the distance (l_1) between the anchor of the cantilever and the stopper of about 28 mm. This choice is correlated with an optimization process as shown in [35].

4.2. Measurement Procedure

4.2.1. Transfer Characteristics

The goal was to characterize the PEM FE's output voltage sensitivity to input vibration energy. Rectifier capacitors, C_{r1-2}, are set to 33 nF. The inductor, *L*, of 100 mH was chosen. The extractor was adjusted to have the highest output voltage at frequency of 315 Hz. The frequency of the input signal was 315 Hz, and its energy was set to 0.05 nJ, 0.1 nJ, 0.4 nJ, 0.9 nJ and 1.6 nJ, respectively. The energy level is estimated as external applied force (mass of the extractor multiplied by its acceleration) multiplied by the displacement of the beam [32]. For each input energy level, 10 measurements were done, in duration of 5 s each, and output voltage V_{out} RMS value was averaged for each energy level. The measurement error ε was calculated as:

$$\varepsilon = 3A = 3\sqrt{\frac{std^2(RMS1, RMS2, \ldots, RMS10)}{10}} \tag{4}$$

where *A* is the uncertainty and *std* is the standard deviation of the voltage values of the 10 measurements.

4.2.2. Frequency Selectivity

The goal was to determine the relation of output voltage and input vibration frequency, within the selected frequency band. Rectifier capacitors, C_{r1-2}, are set to 33 nF. Inductor, *L*, of 100 mH is chosen. The frequency of the input signal was swept from 150 Hz to 210 Hz with increment of 10 Hz for one developed extractor and from 290 Hz to 330 Hz with increment of 5 Hz for the other. For each input signal frequency, the output voltage was recorded in duration of 20 s. The recorded waveforms were processed in MATLAB® to obtain normalized RMS values of output voltage for each frequency.

4.2.3. Design Parameters

The goal was to select the rectifier capacitors C_{r1-2} considering output voltage ripple and response times. The frequency of the input signal was set for maximal output voltage (to 315 Hz), and to generate a voltage on the piezoelectric transducer of 100 mV peak-to-peak. Input vibrations were gated, with 0.75 s of signal, followed by 4 s of pause. The output voltage was measured for capacitors of 33 nF, 100 nF, 470 nF and 1 µF. The inductor, *L*, of 100 mH was used for the experiment.

4.3. Measurement Results

The experimental characterization of the passive electromechanical feature extractor verifies the simulation results shown in Section 3. Figure 9 shows the transfer characteristic of the PEM FE. The sensitivity of the proposed device is around 2 mV/nJ. As can be seen from the maximal measurement error, the measurement resolution is around ±1 nJ.

Figure 9. Relation of extractor output voltage (V_{out}) and input signal energy, E_{in}. Rectifier capacitances $C_{r1-2} = 33$ nF. Inductor $L = 100$ mH. Black pluses—measurement data, blue line—linear interpolation, red lines—error margins.

Figure 10 shows frequency characteristics of two developed PEM FEs with central frequencies in two different frequency bands of interest for the application in an acoustic detector. This provides verification of the simulation results shown in Figure 5 for three different frequency bands of interest. The number of points in the measured frequency characteristics is lower than in the simulated characteristics for practical reason, and the difference in shapes of the two sets of frequency characteristics is most likely a consequence of the numerical inaccuracies of the simulated model at transitions from the out-of-band to passband frequencies.
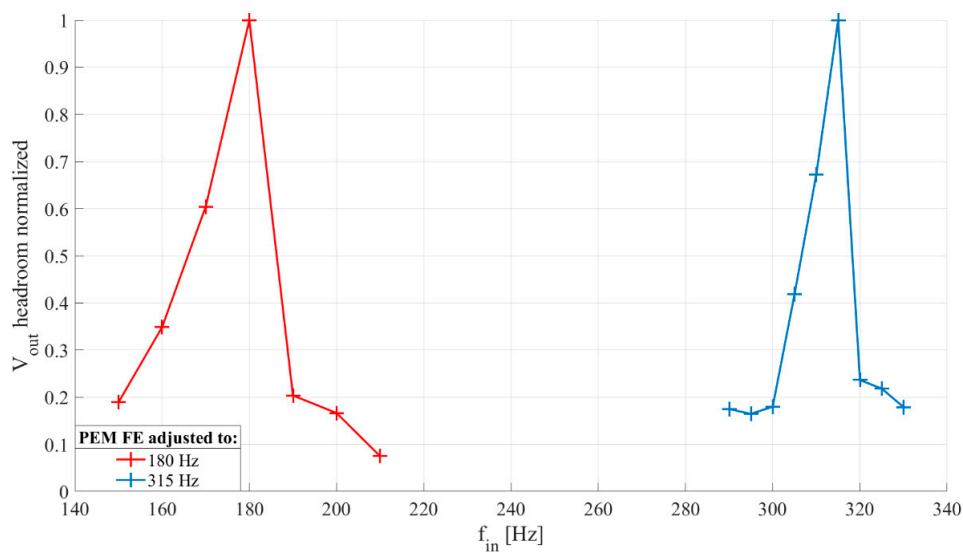
Figure 10. Frequency selectivity of passive electromechanical feature extractor (PEM FE) obtained by change of physical dimensions (beam length (l), beam and magnet mass (m), magnet position (δ)). The output voltage was normalized with regards to maximal value. Input vibrations generate 50 mV peak-to-peak at piezoelectric transducer, input vibration frequency changed by 10 Hz from 150 Hz to 210 Hz and by 5 Hz from 290 Hz to 330 Hz for each developed PEM FE, respectively. Rectifier capacitance $C_{r1-2} = 33$ nF, inductor $L = 100$ mH.

It is clear from the waveforms shown in Figure 11 that increasing rectifier capacitances decreases output voltage ripple, but prolongs rise and fall times.
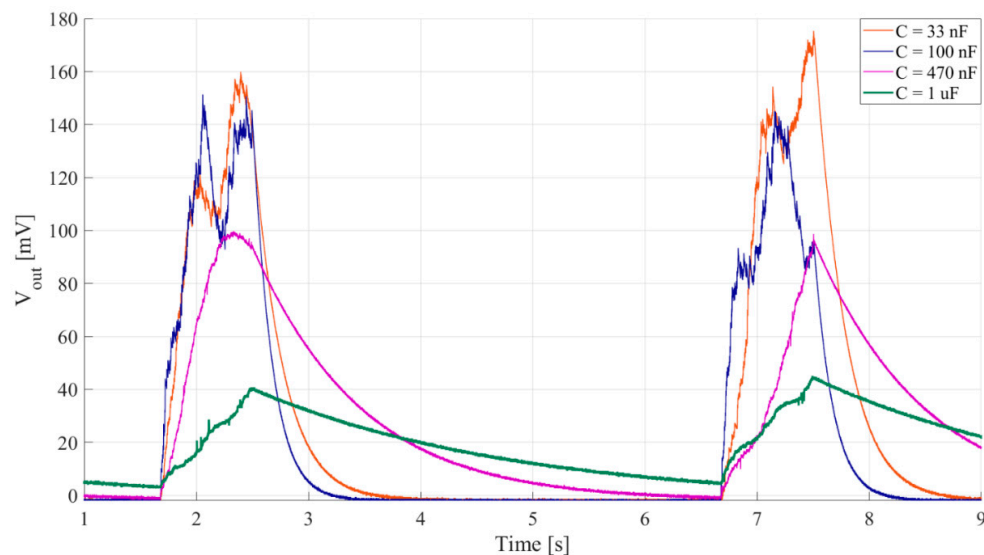
Figure 11. Waveform of the output voltage for different values of rectifier capacitances C_{r1-2}. Voltage generated at the piezoelectric transducer, $V_{pzt}(t)$, is 100 mV peak-to-peak, frequency 315 Hz. Input vibrations are gated, 0.75 s of signal followed by 4 s of pause. Inductor $L = 100$ mH.

5. Comparison of Active Electrical and Passive Electromechanical Feature Extractor

The feature extractors comparison was done using two types of signal: synthetic gated sinusoidal signals with added white noise and a prerecorded speedboat signal.

5.1. Measurement Setup

The measurement setups for passive electromechanical and active electrical feature extractors are shown in Figures 8a and 12, respectively.
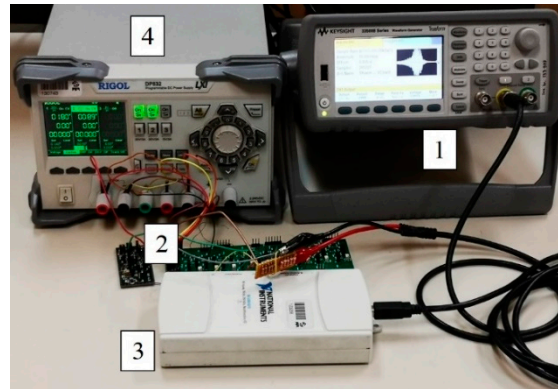
Figure 12. A photograph of the measurement setup for active electrical feature extractor [25,31] measurements. (1) Keysight 33500B waveform generator, (2) active electrical feature extractor, (3) National Instruments (NI) USB-6211 data acquisition card, (4) Rigol DP832 power supply.

The passive electromechanical feature extractor (PEM FE), shown in Figure 3, was adjusted to generate the highest output voltages at input vibration frequency of 180 Hz. The rectifier capacitors, C_{r1} and C_{r2}, were both set to 1 µF. The inductor, L, was set to 100 mH.

The active electrical feature extractor (AE FE) consisted of an active GIC bandpass filter and a passive two-diode voltage doubler, as shown in Figure 1c. The filter central frequency was set to 200 Hz (by R_1, C_{f1} and C_{f2}), with a pass bandwidth of 200 Hz (set by $R2$, R_3, C_{f1} and C_{f2}). The rectifier capacitors C_{r1} and C_{r2} were both set to 22 nF, to allow the capacitor to fully charge and achieve maximal headroom voltage during each event of interest [25,31].

The measurement setup consisted of the input signal generator (Keysight 33500B), the feature extractor and a data acquisition card (National Instruments NI USB-6211) connected to a PC. The vibrations for the passive electromechanical feature extractor operation were generated by a shaker (Smart Material Energy Harvesting Kit 1.2.) driven by the waveform generator.

5.2. Measurement Procedure

The goal of these measurements was to compare the headroom voltages of the active electrical (AE FE) and passive electromechanical feature extractor (PEM FE) in two steps. In the first step, a characterization with synthetic signals of varying amplitudes and signal to noise ratios (SNRs) was performed, while the second step provided verification using a prerecorded speedboat signal.

The vibrations driving the passive electromechanical feature extractor were set to generate peak-to-peak voltage at the piezoelectric transducer, V_{pzt}, equal to the peak-to-peak voltage at the output of the filter, V_{filt}, of the active electrical feature extractor, for the same input signal waveform. The voltage amplitudes ranged from 10 mV to 70 mV peak-to-peak, in steps of 10 mV.

5.2.1. Synthetic Signal

The synthetic signal was a gated 180 Hz sinusoidal signal of varying amplitude lasting for 3 s, followed by 5 s of pause. White noise was added to the signal to achieve SNRs of −10 dB, 0 dB and 10 dB. The 0 dB SNR signal waveform with normalized amplitudes and its spectrogram are shown in Figure 13a,b, respectively.

(a)

(b)
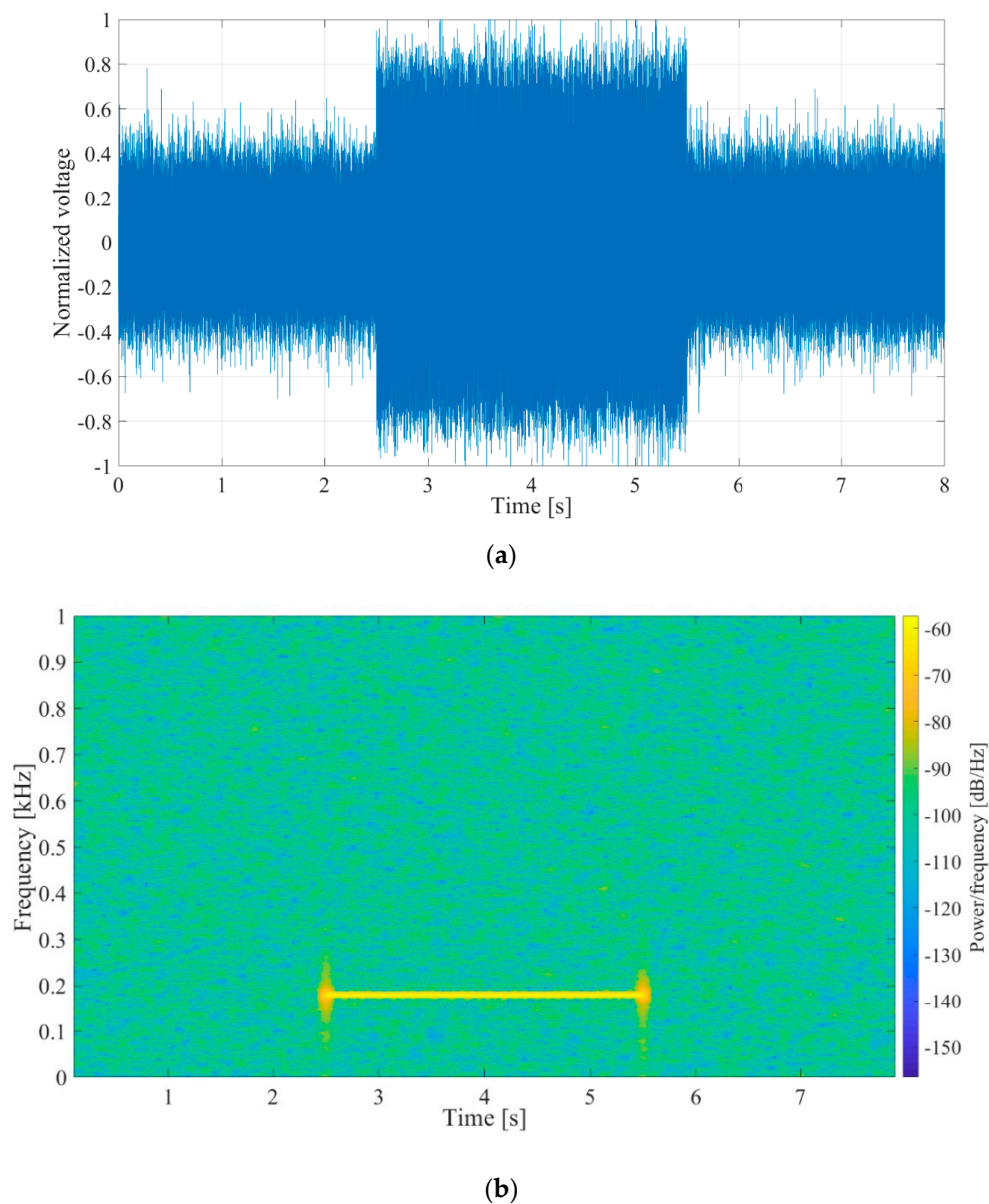
Figure 13. (**a**) Waveform of the synthetic input signal, V_{in}, 3 s of 180 Hz sinus, followed by 5 s pause, 0 dB signal to noise ratio (SNR). The voltage shown was normalized with regards to maximal value. (**b**) Spectrogram of the synthetic input signal.

5.2.2. Prerecorded Signal

The prerecorded signal was a signal of a twin-engine speedboat passing over a hydrophone submerged approximately 1 m under the surface in shallow water [36]. The signal waveform with normalized amplitudes and its spectrogram are shown in Figure 14a,b, respectively. Signal duration is approximately 3 s, followed by around 3 s of pause.
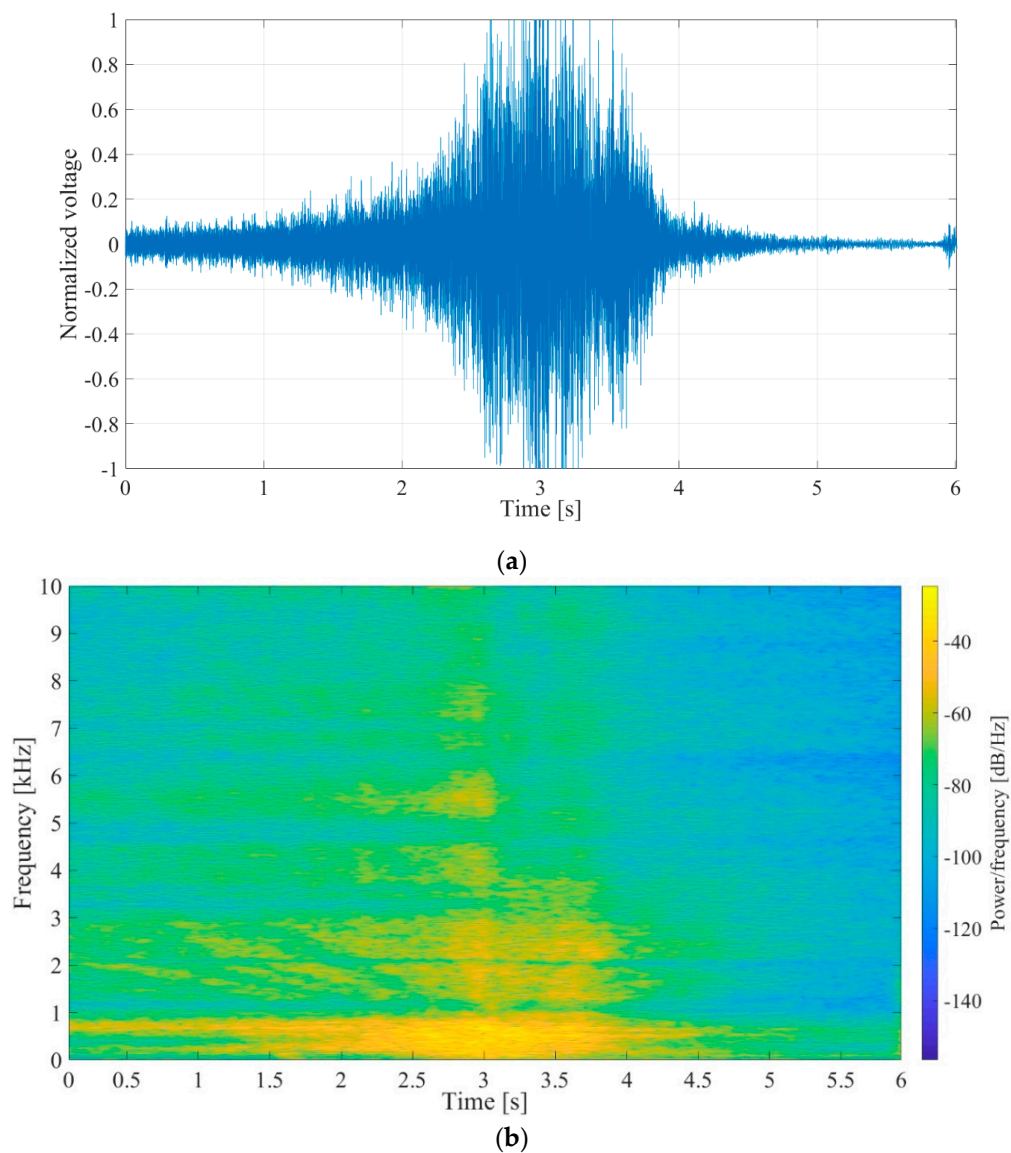
(a)

(b)

Figure 14. (**a**) Waveform of the prerecorded input signal, V_{in}, with a duration of approximately 3 s, followed by around 3 s of pause. The voltage shown was normalized with regards to maximal value. (**b**) Spectrogram of the prerecorded input signal.

5.3. Results

The obtained comparison for synthetic signals and prerecorded speedboat signal are shown in Figure 15a,b, respectively.

(a)

(b)
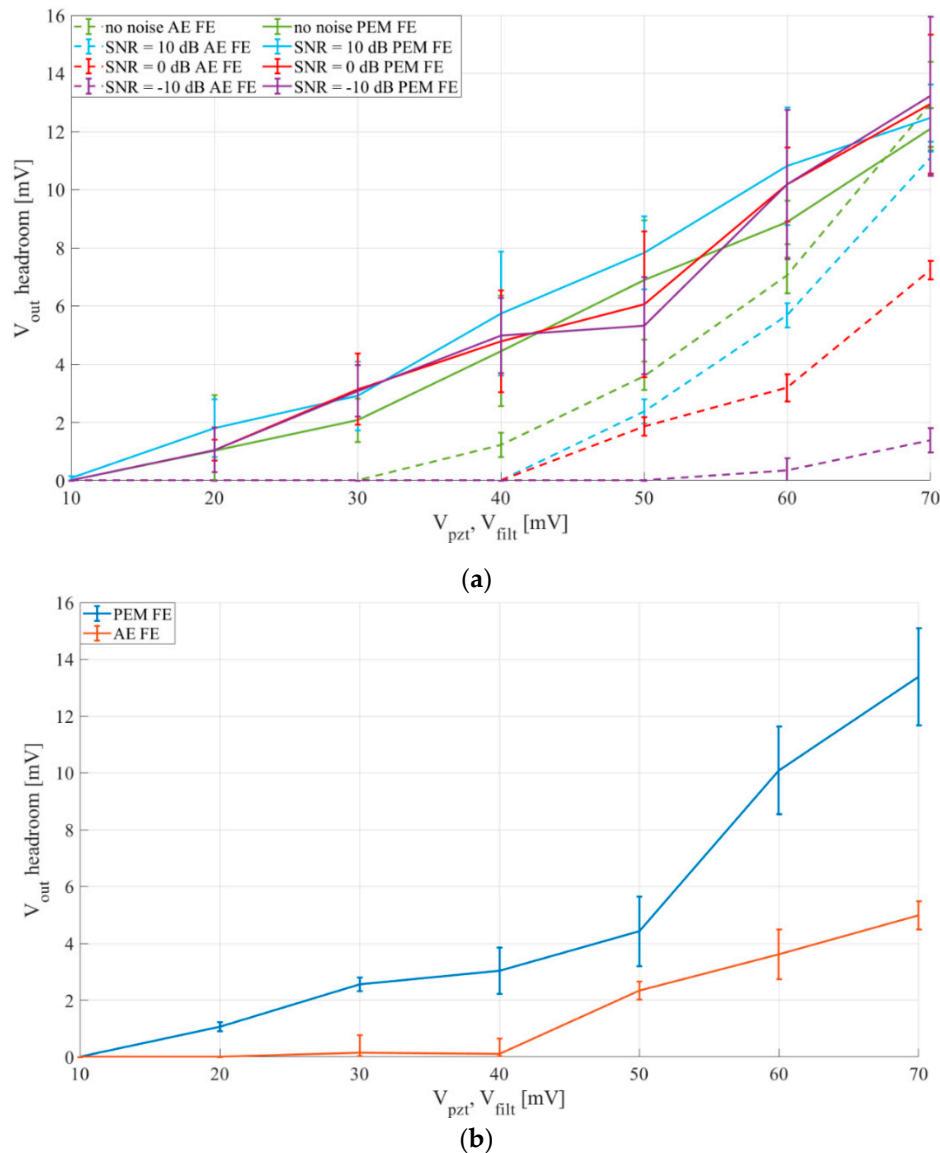
Figure 15. Comparison of outputs of a passive electromechanical feature extractor (PEM FE) and an active electrical feature extractor (AE FE). Rectifier capacitances for AE FE C_{r1-2} = 22 nF, for PEM FE C_{r1-2} = 1 µF. PEM FE inductor L = 100 mH. (**a**) Synthetic input signals, 3 s of sinus, 180 Hz, 5 s of pause, filter and piezoelectric transducer output, V_{filt}, V_{pzt}—10–70 mV peak-to-peak, (**b**) Prerecorded speedboat signal, 3 s of signal, 3 s of pause, filter and piezoelectric transducer output, V_{filt}, V_{pzt}—10–70 mV peak-to-peak.

The results show that the passive electromechanical feature extractor (PEM FE) outperforms the active electrical feature extractor (AE FE), with inputs up to 70 mV, for both synthetic and prerecorded speedboat signal inputs.

The higher headroom voltages of the PEM FE stem from the increase of rectifier efficiency provided by utilization of the mechanically switched inductor. This increased sensitivity allows a detector utilizing the PEM FE to detect events generating signals under 20 mV peak-to-peak, while a detector using the AE FE could only detect events generating signals of more than 40 mV peak-to-peak.

The results also show that the PEM FE is far more resistant to noise than AE FE, as for the input signal SNR ranging from signal with no noise down to an SNR of −10 dB the PEM FE loses less than 1 mV of headroom voltage, while the AE FE loses more than 10 mV of headroom voltage in the same SNR range.

In addition to the mentioned performance improvements, it should also be emphasized that, unlike the previously developed AE FE, the novel feature extractor is fully passive. The previously developed AE FE consists of an adjustable bandpass filter and an envelope tracker, and consumes 8.25 μW of the total 11.52 μW consumed by each channel [25], meaning that replacing it with a fully passive feature extractor, as proposed in this work, would reduce each channel's power consumption by around 72%, proving that utilizing this method would either greatly extend the detector's life-time, or allow us to put in more channels with the same power budget, further increasing the detection accuracy.

6. Conclusions

Acoustic infrequent events can be recognized from an ordered sequence of discrete time-frequency states obtained from a low-power multichannel detector comprising filtering, envelope extraction and single bit quantization. The envelope is simple to extract in terms of hardware complexity and power consumption, but the extractor has poor performance in low SNR conditions that are common in undersea environments. The goal of this work was to present and characterize a novel passive electromechanical feature extractor utilizing a mechanically switched inductor, based on RMSHI, as an alternative solution for feature extraction in an acoustic event detector in frequency range from 200 Hz to 1 kHz. Through presented simulation and experimental characterization of the passive extractor we confirmed its applicability for the signals of interest and determined the key design parameters. We demonstrated advantages of the passive electromechanical extractor in comparison to the active electrical version in terms of operation with lower input signal levels (under 20 mV, compared to 40 mV), and higher robustness in low SNR conditions (1 mV output voltage loss compared to 10 mV). In addition to outperforming the signal processing performances, compared to our previous work, utilization of the passive extractor would also decrease the power consumption of a detector's channel by 72%, enabling life-time extension and/or increased quality of detection with larger number of channels. This work represents the basis for future research towards a fully passive, or self-sustaining infrequent acoustic event detector channel design utilizing an electromechanical device with an emphasized threshold.

References

1. Peckens, C.; Porter, C.; Rink, T. Wireless Sensor Networks for Long-Term Monitoring of Urban Noise. *Sensors* **2018**, *18*, 3161. [CrossRef] [PubMed]
2. Luo, L.; Qin, H.; Song, X.; Wang, M.; Qiu, H.; Zhou, Z. Wireless Sensor Networks for Noise Measurement and Acoustic Event Recognitions in Urban Environments. *Sensors* **2020**, *20*, 2093. [CrossRef] [PubMed]
3. Mayer, P.; Magno, M.; Benini, L. Self-Sustaining Acoustic Sensor with Programmable Pattern Recognition for Underwater Monitoring. *IEEE Trans. Instrum. Meas.* **2019**, *68*, 2346–2355. [CrossRef]
4. Mois, G.; Folea, S.; Sanislav, T. Analysis of Three IoT-Based Wireless Sensors for Environmental Monitoring. *IEEE Trans. Instrum. Meas.* **2017**, *66*, 2056–2064. [CrossRef]

5. Fourniol, M.; Gies, V.; Barchasz, V.; Kussener, E. Low-Power Wake-Up System based on Frequency Analysis for Environmental Internet of Things. In Proceedings of the 14th IEEE/ASME International Conference on Mechatronic and Embedded Systems and Applications, Oulu, Finland, 2–4 July 2018; pp. 1–6. [CrossRef]

6. Wang, Y.; Zhou, R.; Liu, Z.; Yan, B. A Low-Power CMOS Wireless Acoustic Sensing Platform for Remote Surveillance Applications. *Sensors* **2020**, *20*, 178. [CrossRef] [PubMed]

7. Thoen, B.; Ottoy, G.; Rosas, F.; Lauwereins, S.; Rajendran, S.; De Strycker, L.; Pollin, S.; Verhelst, M. Saving energy in WSNs for acoustic surveillance applications while maintaining QoS. In Proceedings of the SAS 2017—2017 IEEE Sensors Applications Symposium, Glassboro, NJ, USA, 13–15 March 2017; pp. 1–6. [CrossRef]

8. Kucukbay, S.E.; Sert, M.; Yazici, A. Use of Acoustic and Vibration Sensor Data to Detect Objects in Surveillance Wireless Sensor Networks. In Proceedings of the 21st International Conference on Control Systems and Computer Science (CSCS), Bucharest, Romania, 29–31 May 2017; pp. 207–212. [CrossRef]

9. Salazar-García, C.; Castro-González, R.; Chacón-Rodríguez, A. RISC-V based sound classifier intended for acoustic surveillance in protected natural environments. In Proceedings of the 2017 IEEE 8th Latin American Symposium on Circuits & Systems (LASCAS), Bariloche, Argentina, 20–23 February 2017; pp. 1–4. [CrossRef]

10. Prieto, M.D.; Millan, D.Z.; Wang, W.; Ortiz, A.M.; Redondo, J.A.O.; Martinez, L.R. Self-powered wireless sensor applied to gear diagnosis based on acoustic emission. *IEEE Trans. Instrum. Meas.* **2016**, *65*, 15–24. [CrossRef]

11. Fu, H.; Sharif-Khodaei, Z.; Aliabadi, M.H.F. An energy-efficient cyber-physical system for wireless on-board aircraft structural health monitoring. *Mech. Syst. Signal Process.* **2019**, *128*, 352–368. [CrossRef]

12. Solimine, J.; Niezrecki, C.; Inalpolat, M. An experimental investigation into passive acoustic damage detection for structural health monitoring of wind turbine blades. *Struct. Health Monit.* **2020**, 1–15. [CrossRef]

13. Gong, L.; Zhao, Y.; Xiang, C.; Li, Z.; Qian, C.; Yang, P. Robust Light-Weight Magnetic-Based Door Event Detection with Smartphones. *IEEE Trans. Mob. Comput.* **2019**, *18*, 2631–2646. [CrossRef]

14. Bello, H.; Zeng, X.; Nordin, R.; Jian, X. Advances and opportunities in passive wake-up radios with wireless energy harvesting for the internet of things applications. *Sensors* **2019**, *19*, 3078. [CrossRef] [PubMed]

15. Sánchez, A.; Blanc, S.; Yuste, P.; Perles, A.; Serrano, J.J. An ultra-low power and flexible acoustic modem design to develop energy-efficient underwater sensor networks. *Sensors* **2012**, *12*, 6837–6856. [CrossRef] [PubMed]

16. Fuketa, H.; O'Uchi, S.; Matsukawa, T. A 0.3-V 1-μw Super-Regenerative Ultrasound Wake-Up Receiver with Power Scalability. *IEEE Trans. Circuits Syst. II Express Briefs* **2017**, *64*, 1027–1031. [CrossRef]

17. Oletic, D.; Bilas, V. Energy-efficient respiratory sounds sensing for personal mobile asthma monitoring. *IEEE Sens. J.* **2016**, *16*, 8295–8303. [CrossRef]

18. Rovere, G.; Fateh, S.; Benini, L. A 2.2-μW Cognitive Always-On Wake-Up Circuit for Event-Driven Duty-Cycling of IoT Sensor Nodes. *IEEE J. Emerg. Sel. Top. Circuits Syst.* **2018**, *8*, 543–554. [CrossRef]

19. Goux, N.; Badets, F. Review on event-driven wake-up sensors for ultra-low power time-domain design. In Proceedings of the 2018 IEEE 61st International Midwest Symposium on Circuits and Systems (MWSCAS), Windsor, ON, Canada, 5–8 August 2018; pp. 554–557. [CrossRef]

20. Olsson, R.H.; Bogoslovov, R.B.; Gordon, C. Event driven persistent sensing: Overcoming the energy and lifetime limitations in unattended wireless sensors. In Proceedings of the 2016 IEEE Sensors, Orlando, FL, USA, 30 October–3 November 2016; pp. 1–3. [CrossRef]

21. Oletic, D.; Korman, L.; Magno, M.; Bilas, V. Time-frequency pattern wake-up detector for low-power always-on sensing of acoustic events. In Proceedings of the 2018 IEEE International Instrumentation and Measurement Technology Conference (I2MTC), Houston, TX, USA, 14–17 May 2018; pp. 1–6. [CrossRef]

22. Alías, F.; Socoró, J.C.; Sevillano, X. A review of physical and perceptual feature extraction techniques for speech, music and environmental sounds. *Appl. Sci.* **2016**, *6*, 143. [CrossRef]

23. Carmel, D.; Yeshurun, A. Detection of alarm sounds in noisy environments. In Proceedings of the 25th European Signal Processing Conference (EUSIPCO), Kos, Greece, 28 August–2 September 2017; pp. 1839–1843. [CrossRef]

24. Alvarez-Rosario, A.; Padovese, L.R. Real-time performance of energy based underwater acoustic event detectors embedded in a single-board computer. In Proceedings of the 2015 IEEE/OES Acoustics in Underwater Geosciences Symposium (RIO Acoustics), Rio de Janeiro, Brazil, 29–31 July 2015; pp. 1–5. [CrossRef]

25. Oletic, D.; Gazivoda, M.; Bilas, V. A programmable 3-channel acoustic wake-up interface enabling always-on detection of underwater events within 20 μA. *Proc. Eurosensors* **2018**, *2*, 768. [CrossRef]

26. Moctezuma, F.P.; Prieto, M.D.; Martinez, L.R. Performance Analysis of Acoustic Emission Hit Detection Methods Using Time Features. *IEEE Access* **2019**, *7*, 71119–71130. [CrossRef]

27. Giusa, F.; Giuffrida, A.; Trigona, C.; Andò, B.; Bulsara, A.R.; Baglio, S. "Random mechanical switching harvesting on inductor": A novel approach to collect and store energy from weak random vibrations with zero voltage threshold. *Sens. Actuators A Phys.* **2013**, *198*, 35–45. [CrossRef]

28. Trigona, C.; Giuffrida, S.; Andò, B.; Baglio, S.; Elettrica, I.; Doria, V.A. Micromachined "Random Mechanical Harvester on Inductor" to recovery energy from very low-amplitude vibrations with zero-voltage threshold. In Proceedings of the 2016 IEEE Sensors, Orlando, FL, USA, 30 October–3 November 2016; pp. 2–4. [CrossRef]

29. Bradai, S.; Naifar, S.; Trigona, C.; Baglio, S.; Kanoun, O. Electromagnetic transducer with bistable-RMSHI for energy harvesting from very weak kinetic sources. In Proceedings of the 2018 IEEE International Instrumentation and Measurement Technology Conference (I2MTC), Houston, TX, USA, 14–17 May 2018; pp. 1–5. [CrossRef]

30. Gazivoda, M.; Oletic, D.; Trigona, C.; Bilas, V. Measurement of Weak Signal Energy at Acoustic Frequencies by using RMSHI as a Passive Conditioning Circuit. In Proceedings of the 2019 IEEE International Instrumentation and Measurement Technology Conference (I2MTC), Auckland, New Zealand, 20–23 May 2019; pp. 1735–1739. [CrossRef]

31. Gazivoda, M.; Oletic, D.; Bilas, V. Characterization and comparison of envelope detectors for wake-up sensor interfaces at audio frequencies. In Proceedings of the 2020 IEEE International Instrumentation and Measurement Technology Conference (I2MTC), Dubrovnik, Croatia, 25–28 May 2020; pp. 1–6. [CrossRef]

32. Trigona, C.; Andò, B.; Baglio, S. Performance Measurement Methodologies and Metrics for Vibration Energy Scavengers. *IEEE Trans. Instrum. Meas.* **2017**, *66*, 3327–3339. [CrossRef]

33. Ott, H.W. *Noise Reduction Techniques in Electronic Systems*; Wiley-Interscience: Livingston, NJ, USA, 1988; ISBN 0-471-85068-3.

34. Vinolo, C.; Toma, D.; Manuel, A.; Del Rio, J. Sea motion electrical energy generator for low-power applications. In Proceedings of the 2013 MTS/IEEE OCEANS-Bergen, Bergen, Norway, 10–14 June 2013. [CrossRef]

35. Giuffrida, A.; Giusa, F.; Trigona, C.; Andò, B.; Baglio, S. Optimal Parameters Selection for Novel Low-Voltage Vibration Energy Harvesters. In *Sensors Microsystems, Proceedings of the 17th National Conference, Brescia, Italy, 5–7 February 2013*; Springer: Cham, Switzerland, 2014; Volume 268, pp. 313–316. [CrossRef]

36. Underwater Video of Twin Engine Boat Props High Speed. Available online: https://www.youtube.com/watch?v=6uQ7IDqbmAE (accessed on 7 June 2018).

Publication 5

Oletić, D., **Gazivoda, M.**, Bilas, V., "A Programmable 3-Channel Acoustic Wake-Up Interface Enabling Always-On Detection of Underwater Events Within 20 µA", *Proceedings of the 32nd Eurosensors Conference*, Graz, Austria, pp. 1-7, 2018, doi:10.3390/proceedings2130768

A Programmable 3-Channel Acoustic Wake-Up Interface Enabling Always-On Detection of Underwater Events within 20 μA [†]

Dinko Oletic, Marko Gazivoda and Vedran Bilas *

Faculty of Electrical Engineering and Computing, University of Zagreb, Unska 3, 10000 Zagreb, Croatia; dinko.oletic@fer.hr (D.O.); marko.gazivoda@fer.hr (M.G.)

* Correspondence: vedran.bilas@fer.hr; Tel.: +385-1-6129-974

† Presented at the Eurosensors 2018 Conference, Graz, Austria, 9–12 September 2018.

Abstract: We present an always-on acoustic wake-up sensor interface, designed for prolonging the autonomy of energy-hungry hardware for underwater acoustic surveillance. Proposed design enables the detection of a passing ship by simultaneous listening up to three arbitrarily defined frequency-bands within the 2.5 kHz range, and generates a wake-up signal upon finding a match with a digitally preset template describing signal's discriminatory time-frequency features. In this paper, we propose the architecture of such fully programmable, multichannel, mixed-signal wake-up circuit. We show the implementation of a PCB prototype, characterize its sensitivity, analyze its current consumption, and verify its response on real-world hydrophone recordings. It is demonstrated that the design consumes only 6.4 μA per channel (in total <20 μA) with ultra-low-power COTS components, while listening.

Keywords: acoustic event detection; underwater surveillance; always-on sensor interface; DSP

1. Introduction

In a variety of underwater passive acoustic surveillance applications (security, marine-biology, environmental science etc.), bandwidth of signals of interest often spans up to 100 kHz. This requires continuous, high-fidelity signal acquisition, at sample rates as high as 100–200 kHz, real-time digital processing, and storage of terabytes of data. State-of-the-art underwater acoustic surveillance equipment typically requires 10–100 mW of power for such tasks [1,2], consequently suffering from either limited autonomy, or requiring bulky energy-storage units (batteries).

In order to miniaturize the passive acoustic surveillance equipment, prolong its autonomy, and lower the required data-storage capacity, an ultra-low-power always-on "wake-up" circuitry can be used [3] to trigger the signal acquisition and storage only in the presence of potential acoustic events of interest. In spite of significant research of always-on acoustic wake-up interfaces for terrestrial applications [4–6], limited work has been done in the context of detection of underwater acoustic events. Even then, most of the research efforts address asynchronous underwater communications by acoustic modems [2].

Here we demonstrate a design of an ultra-low-power acoustic wake-up interface for underwater detection of passing naval vessels (boats, ships) by analyzing the time-frequency signatures [7] of ship's engine and propeller noise. Our key contributions w.r.t. the previous work [7] include the end-to-end design of a fully-programmable multichannel mixed-signal wake-up circuit, its implementation with state-of-the-art COTS components yielding minimal power consumption, characterization of circuit's design parameters, and verification of its detection performance on hydrophone recordings of passing ships [8].

2. Materials and Methods

The design entails three analog-domain filtering channels decomposing the hydrophone's signal (V_{in}) into arbitrary frequency bands (Figure 1a). Each channel consists of a digitally programmable active band pass filter. Each filter is designed in general impedance convertor (GIC) topology, and implemented using a pair of single-supply, CMOS, 100 kHz gain-bandwidth, 600 nA amplifiers (MCP6142, Figure 1b). Channel CH1 is designed to cover 200–500 Hz, CH2 for range between 500–1000 Hz, and CH3 1.0–2.5 kHz. Within these limits, each channel's central frequency (f_c), and pass-band bandwidth (B), are digitally programmable in 256 steps using I^{2}C potentiometers R_{fc}, R_b (AD5144).

Intervals of signal presence within individual filtering channels (V_{filt}) are localized in time first by extracting the envelopes (V_{env}) of filtered signals with active envelope trackers (MCP6141), and then performing single-bit quantization using comparators (TLV3701). Each channel's comparator threshold voltage (V_{comp}) is set by a digital potentiometer R_{tr} (AD5144).

Temporal relations between comparator responses (V_{out}) are finally analyzed by a 3-channel digital sequence recognition state-machine [7] (MSP430F2013), which wakes-up the DSP. Event's template—an ordered sequence of discrete spectro-temporal states describing the vessel's acoustic signature, is programmed into the MSP430F2013 by I^{2}C as well. Consumption of MSP430F2013 is minimized by aggressive frequency scaling (11 kHz) and extensive use of low-power modes (LPM4, LPM3).

A PCB prototype implementation of the described wake-up circuit with proposed COTS components (Figure 2a) was used for experimental characterization of design parameters, testing of detection performance, and power consumption measurements.

(a)
(b)
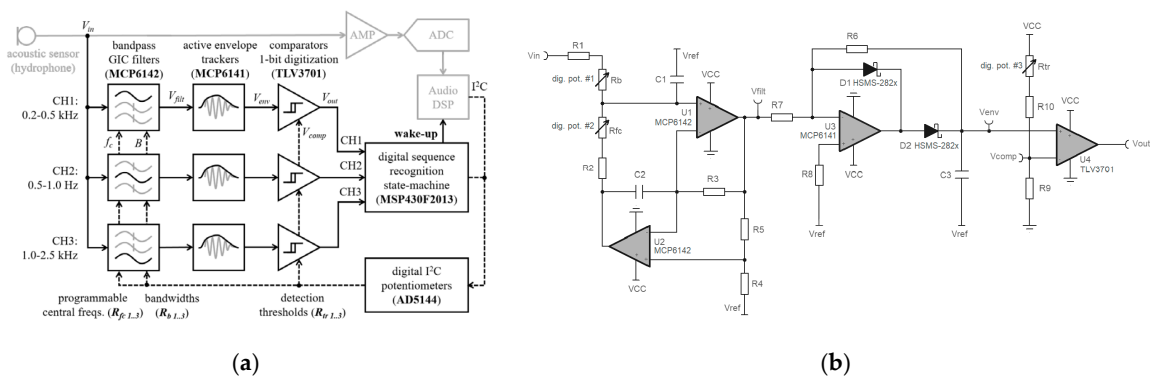
Figure 1. The 3-channel always-on wake-up interface. (**a**) Architecture; (**b**) Design of an individual analog channel (GIC filter, active envelope tracker, comparator).

(**a**)

(**b**)

(**c**)

(**d**)

(**e**)

(**f**)
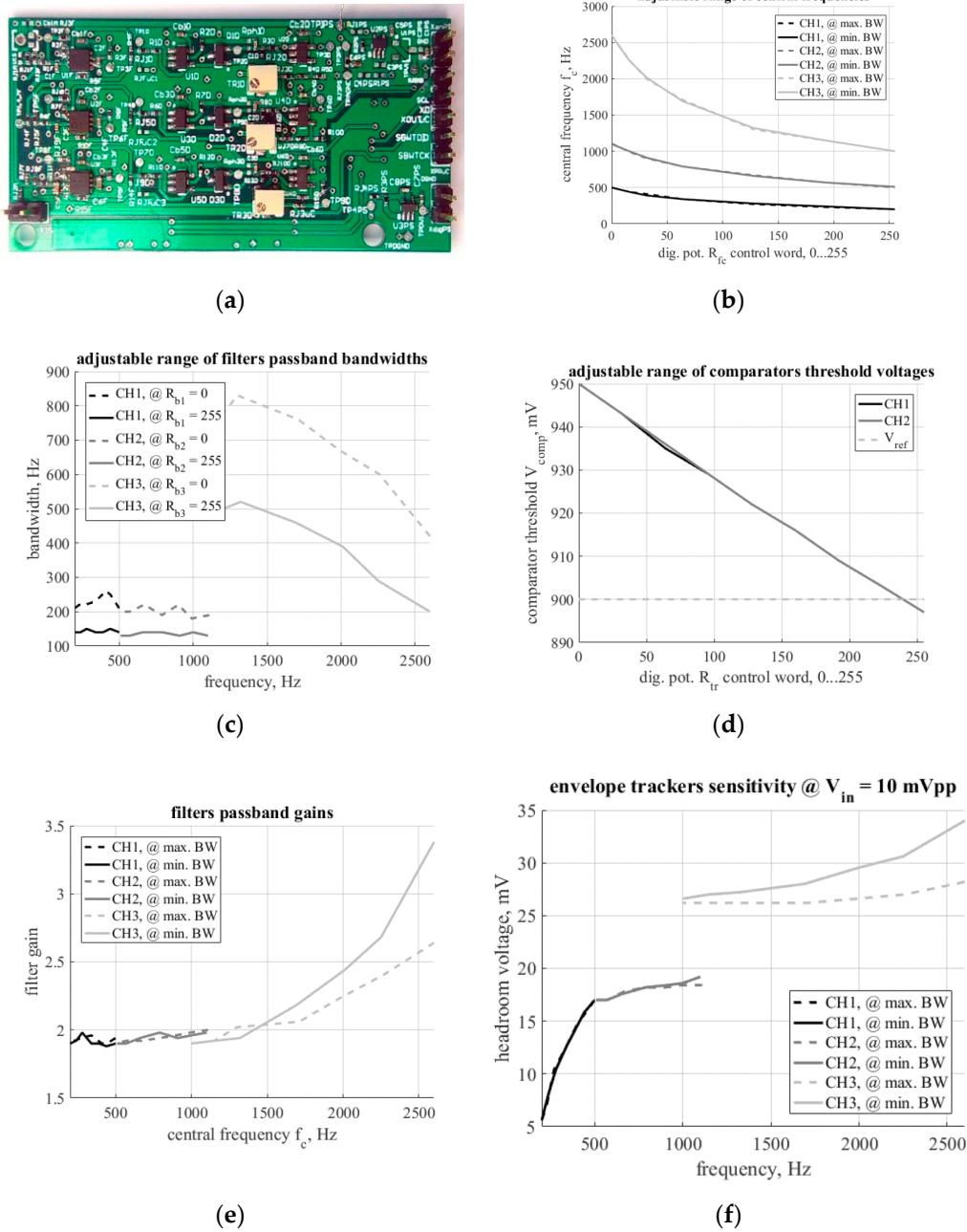
Figure 2. Design characterization. (**a**) PCB; (**b**) Range of filters central frequencies (adjusted by R_{fc}), (**c**) bandwidths (set by R_b), and (**d**) span of comparators thresholds (R_{tr}); (**e**) Filters' gains (V_{filt}/V_{in}); (**f**) Envelope trackers' sensitivities (V_{env}).

3. Results

Results of characterization of the PCB prototype are summarized in Figure 2. First, adjustable ranges of each channel's programmable parameters are shown in Figure 2b–d. Range of filtering channels' central frequencies f_c against digital potentiometers R_{fc} are verified in Figure 2b: CH1 200–500 Hz, CH2 500–1100 Hz, and CH3 1.0–2.6 kHz. $RB's$ are tuned for narrow, 150–200 Hz pass-bandwidths B at low and mid-frequency channels CH1 and CH2 (Figure 2c), and CH3 is enables extraction of broader bands of 500–800 Hz at the f_c = 1.0 kHz, and 200–500 Hz at the maximal f_c = 2.6 kHz. R_{tr} enables setting the comparator's threshold voltage within approximately 50 mV (Figure 2d) around the envelope detector's output voltage baseline (V_{env}), sitting on V_{ref} = 0.9 V.

Ideally, gains of GIC filtering stages is 2 (Figure 2e). Frequency-dependent gain increase at the CH3 helps detection of high-frequency signal, typically exhibiting lower power-spectrum density (amplitude) than the signals at low frequencies (CH1, CH2). Sensitivity of the complete analog signal chain was measured at the envelope detector's output, as a ripple-free headroom between the V_{env} and the signal's baseline, floating around V_{ref} (Figure 2f). V_{env} ripple affects the sensitivity at low frequencies at most. Sensitivity to input signals as low as $V_{in} < 5$ mV, enables direct coupling of the wake-up circuit to the sensor.

Event detection performance was tested on underwater recordings of 12 passes of an identical speedboat over an acoustic sensor submerged approx. 1 m under the surface in shallow water [8]. Signals were rescaled to yield max. $V_{in} = \{20\ldots5\}$ mV amplitude at pass-over. For each V_{in}, thresholds R_{tr} were trained on a single signal, and then tested on the remaining 11. A spectrogram of a training-pass is shown in Figure 3a. The associated circuit response, including a successful wake-up upon the simultaneous detection of uninterrupted 500 ms signal within all three arbitrarily set bands of interest (CH1 200–350 Hz, CH2 580–720 Hz, and CH3 1460–1920 Hz) is shown in Figure 3b. In the testing-phase, circuit was able to detect 8/11 speedboat passes with the V_{in} amplitude = 10 mV.

(a)

(b)
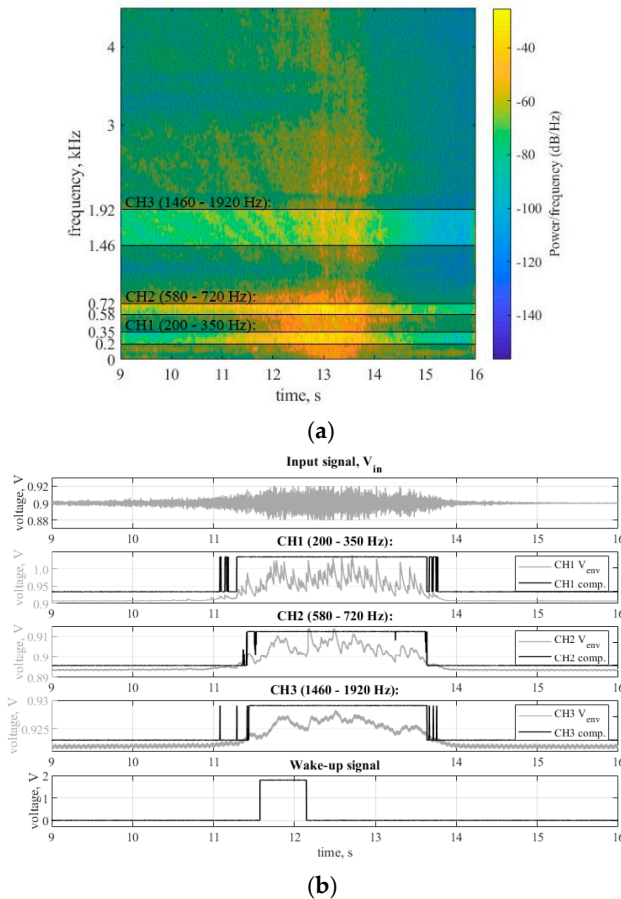
Figure 3. An acoustic event detection with the always-on wake-up circuit. (**a**) A typical underwater spectrogram signature of a passing speedboat [8]; (**b**) The associated wake-up circuit response (V_{in} = 20 mV). DSP processing may be initiated on the rising edge of the wake-up signal.

Current consumption was measured at 1.8 V. GIC filtering within 2.5 kHz implemented with MCP6142, costs 3.5 µA/channel. Each active envelope tracker contributes by 0.8 µA. Full-programmability, implemented with three digital potentiometers per channel (AD5144), adds 0.3 µA. Each comparator costs 1.8 µA, mostly due to the current flowing through the programmable resistor-divider network defining the V_{comp}. Digital state machine implemented in MSP430F2013 consumes only 0.2 µA in listening [7]. This totals 6.4 µA/channel, or 19.4 µA for the three-channel prototype.

4. Discussion

Comparison with functionally and architecturally related state-of-the-art acoustic wake-up designs is given in Table 1. Consuming only 20 μA, the presented design (Figure 2a) achieves the best tradeoff between functionality (signal analysis capabilities), bandwidth and programmability, among COTS designs [3–5] (Table 1). An analogous ASIC design [6] shows potential for 100-fold power reduction.

Table 1. Current consumption breakdown (V_{CC} = 1.8 V), and comparison to the related acoustic wake-up designs. (Legend: - feature not present; ✓ feature present, but consumption not reported).

Ref.	Techn.	Functionality	Band-Width	Filter/ch.	Envelope Tracking/ch.	1-bit Digitizer/ch.	Program Mability/ch.	Classifi-Cation	Single Channel	Total (all ch.)
[3]	COTS	Fixed, single ch. Acoustic modem with address decoding	150 kHz	✓	✓	✓	-	-	4.5 µA	-
this	**COTS**	**dig. programmable 3 ch. filtering, 1-bit envelope digit., time-freq. template matching**	**2.5 kHz**	**3.5 µA**	**0.8 µA**	**1.8 µA**	**0.3 µA**	**0.2 µA**	**6.4 µA**	**19.4 µA**
[4]	COTS	fixed, single-ch., 1-bit digit., periodicity detection in FPGA	380 Hz	4.2 µA	-	1.1 µA	-	20 µA	-	85 µA
[5]	COTS	Fixed, single ch., detection by amplitude thresholding	20 kHz	-	-	3.2 µA	-	-	3.2 µA	-
[6]	ASIC	multi-ch. filtering, env. Peak detect vs amb. noise	100 Hz	0.34 nA	✓	✓	-	-	4.3 nA	-

5. Conclusions

We demonstrated a prototype of an always-on, multichannel, mixed-signal, fully-programmable wake-up sensor interface, consuming less than 20 μA, while listening for time-frequency signature of the acoustic event. Usage of the proposed circuit for on-demand triggering of the conventional underwater acoustic surveillance equipment [1,2], may reduce its average power consumption for more than two orders of magnitude. Apart from underwater security, diver safety, and marine biology, the circuit is applicable in many terrestrial event detection applications, including acoustic emission monitoring in industry and agriculture.

Conflicts of Interest: The authors declare no conflict of interest. The founding sponsors had no role in the design of the study; in the collection, analyses, or interpretation of data; in the writing of the manuscript, and in the decision to publish the results.

References

1. Caldas-Morgan, M.; Alvarez-Rosario, A.; Padovese, L.R. An Autonomous Underwater Recorder Based on a Single Board Computer. *PLoS ONE* **2015**; *10*, 1–18.
2. Develogic Subsea Systems: Acoustic Recorder and Signal Analyzer—Sono.Vault. Available online: http://www.develogic.de/products/ss-r/sonovault/ (accessed on 7 June 2018).
3. Sanchez, A.; Blanc Clavero, S.; Yuste Pérez, P.; Piqueras Gozalbes, I.R.; Serrano Martín, J.J. Advanced Acoustic Wake-up System for Underwater Sensor Networks. In *Communications in Information Science and Management Engineering*; World Academic Publishing: Birmingham, UK, 2012; Volume 2, pp. 1–10.
4. Mays, B.T. *Design Report for Low Power Acoustic Detector ARL-TR-6552*; Army Research Lab., Sensors and Electron Devices Directorate: Adelphi, MD, USA, 2013.
5. Sutton, F.; Da Forno, R.; Gschwend, D.; Gsell, T.; Lim, R.; Beutel, J.; Thiele, L. The Design of a Responsive and Energy-efficient Event-Triggered Wireless Sensing System. In Proceedings of the International Conference on Embedded Wireless Systems and Networks (EWSN 2017), Uppsala, Sweden, 20–22 February 2017; pp. 144–155
6. Uldric, A.; John, C.; Alireza, D.; Theodore, W.B. Low Power, Long Life Design for Smart Intelligence, Surveillance, and Reconnaissance (ISR) Sensors. In Proceedings of the IEEE Conference on Technologies for Homeland Security (HST), Boston, MA, USA, 13–15 November 2012; pp. 631–636
7. Oletic, D.; Korman, L.; Magno, M.; Bilas, V. Time-Frequency Pattern Wake-up Detector for Low-power Always-on Sensing of Acoustic Events. In Proceedings of the 2018 IEEE International Instrumentation and Measurement Technology Conference (I2MTC 2018), Houston, TX, USA, 14–17 May 2018; pp. 1273–1278
8. Underwater Video of Twin Engine Boat Props High Speed. Available online: https://www.youtube.com/watch?v=6uQ7IDqbmAE (accessed on 7 June 2018).

Publication 6

Gazivoda, M., Oletić, D., Trigona, C., Bilas, V., "Measurement of Weak Signal Energy at Acoustic Frequencies by using RMSHI as a Passive Conditioning Circuit", *Proceedings of the 2019 IEEE International Instrumentation and Measurement Technology Conference (I2MTC)*, Auckland, New Zealand, pp. 1735–1739, 2019, doi:10.1109/I2MTC.2019.8827042

Measurement of Weak Signal Energy at Acoustic Frequencies by using RMSHI as a Passive Conditioning Circuit

Marko Gazivoda, Dinko Oletic, Vedran Bilas
Faculty of Electrical Engineering and Computing,
University of Zagreb
Zagreb, Croatia
marko.gazivoda@fer.hr, dinko.oletic@fer.hr, vedran.bilas@fer.hr

Carlo Trigona
Department of Electrical, Electronic and Computer Engineering
University of Catania
Catania, Italy
carlo.trigona@dieei.unict.it

Abstract—To enable low-power recognition of slowly evolving acoustic events generated by weak acoustic sources, we investigate always-on circuit architectures for extraction of signal energy at arbitrarily selected bands of acoustic frequencies. To improve sensitivity and power consumption of existing always-on low-power acoustic event detectors, we consider the application of passive electromechanical systems. In this paper we investigate the Random Mechanical Switching Harvester on Inductor (RMSHI) for rectification of the weak sensor signal and measurement of its energy. The proof-of-concept system has been realized, functionally tested and characterized in terms of sensitivity and resolution. The sensitivity of the presented circuit is around 3 mV/nJ and the resolution is ±0.66 nJ. The active part of the system consumes 6.3 µW. The validity of the approach encourages us towards an integrated weak sensor signal measurement device, using a MEMS switch driven by the acoustic energy.

Keywords—weak signal energy measurement, low-power, acoustic event, frequency selective, wake-up, RMSHI

I. INTRODUCTION

Recognition of infrequent acoustic events is of interest in many fields (environmental monitoring [1], safety and security [2]–[4], agriculture, health monitoring [5]). However, this is a power-hungry task as it requires continuous operation of the wireless embedded system [2]. Power consumption can be lowered by adding an always-on frontend which wakes up a wireless embedded system only upon detection of some specific signature [6]–[9].

Many acoustic events can be recognized based on their time-frequency signature [1], which can be approximated by an ordered sequence of discrete time-frequency states (Fig 1.a). Each state is defined by an arbitrarily chosen time interval, frequency band, and some feature, which quantifies the signal within it [6]. In our previous work we investigated instantaneous envelope as a feature quantifying the signal [10]. However, it is shown in [11] that for very slow evolving acoustic events from weak signal sources, integral signal features may be more suitable. Hence, here we explore energy as a feature quantifying the signal within each time-frequency state.

Always-on wake-up frontends for acoustic event recognition typically incorporate weak sensor signal amplification, filtering, rectification, quantization and rudimentary classification [10]. To lower power consumption of these processing blocks, research has been done towards implementing them as zero-power electromechanical systems [12].

To improve sensitivity and power consumption of our current always-on low-power acoustic event detector [11], we look for application of an electromechanical system in rectification of the weak input signals. It should be noted that the diode bridge rectifier works only in presence of input waveforms having higher amplitude in respect the diode threshold. Furthermore, active rectifiers increase and affect the total budget of the entire converter [13]. A promising approach, applied for the similar problem in energy harvesting, is Random Mechanical Switching Harvester on Inductor (RMSHI). There, energy from a weak vibration source drives a magnetically biased electromechanical switch. Its random switching action boosts the inductor's voltage over the diodes rectifier's threshold, enabling the rectification of very weak signals with a fully passive architecture. Also, being non-resonant, the RMSHI has a broad frequency range of operation [14], [15].

In this paper we investigate the application of the RMSHI for rectification of such weak sensor signals and measurement of their energy, at arbitrarily selected bands of frequencies within the acoustic frequency spectrum. The presented system consists of a preamplifier, a band-pass filter and a macro model of an electromechanical switch operating at the same frequency band, an inductor and a rectifier.

The proof-of-concept system has been realized, functionally tested and characterized, and the validity of the approach has been shown. To the best of our knowledge, this is the first solution presented in the literature, which demonstrates the possibility of using the RMSHI as a low-power passive conditioning circuit for weak signals. This paves the road to the realization of a micromechanical measurement structure able to continuously listen for surrounding acoustic sources and recognize them based on the time-frequency distribution of signal's energy.

The paper is organized as follows: Section II describes the proposed solution. Section III reports the experimental setup and the measurement method. The results are presented in Section IV, while the concluding remarks are given in Section V.

II. Proposed Circuit Description

The proposed circuit has to be able to extract selected frequency bands from the input signal and then measure the energy contained in them. The circuit consists of three main processing blocks, as can be seen in Fig. 1. A more detailed schematic of each processing block is given in Fig. 2.
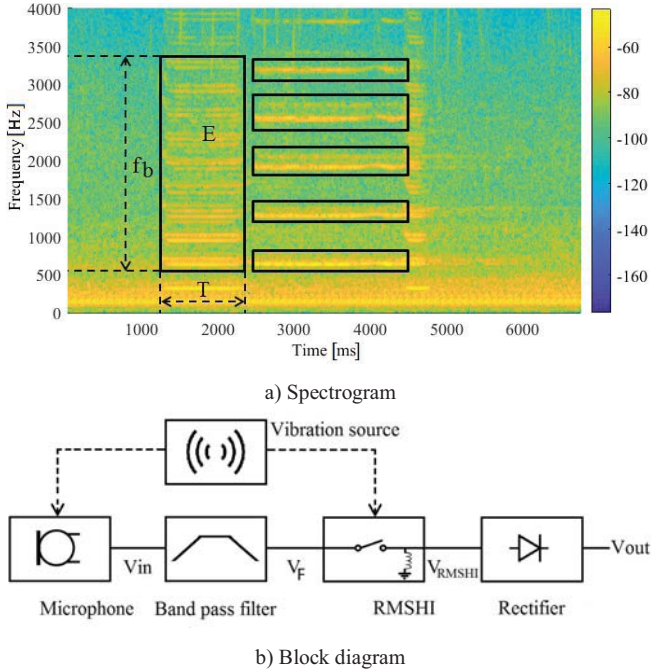

a) Spectrogram

b) Block diagram

Fig. 1. a) Example of a spectrogram of a signal of interest. T represents the duration, f_b the frequency band and E the energy of each state within the time-frequency pattern. b) Block diagram of the presented approach. The energy measurement circuit consists of a band pass filter, an RMSHI and a diode rectifier.

The frequency band of interest is extracted from the input signal by a low-power programmable active analog band pass filter, see Fig. 2.a. The filter has been developed in the general impedance converter (GIC) topology, using a dual low-power operational amplifier (MCP6142). This topology enables independent tuning of the central frequency and bandwidth of the filter spanning between 200 Hz and 2.5 kHz. The current consumption of the filter is 3.5 µA, making it suitable for use in a low power circuit. A more detailed description and characterization of this filter can be found in [11].

The energy contained in the extracted band is measured by using a passive architecture featuring Random Mechanical Switching Harvester on Inductor (RMSHI) [14]. It consists of an electromechanical switch, an inductor, a diode bridge and a load capacitor (see Fig. 2.a).

The electromechanical switch is composed of a cantilever beam having a stopper on the upper part and a tunable magnetic system able to modify the elastic factor and, as consequence, the spectral response of the system as function of the input signal, as shown in Fig. 2.b and Fig. 2.c. Mathematically, this transducer can be modeled using a second order nonlinear differential equation that can be written as follows:

$$mx'' + dx' + \frac{\partial U_T}{\partial x} = F(t)\Big|_{U_T = \delta x^4} \quad (1)$$

Where m and d are the mass and the damping coefficient respectively. The term x is the displacement of the tip of the beam and the dotted terms represent the first and the second derivate of the displacement (velocity and acceleration of the cantilever respectively). U_T is the potential energy function which is nonlinear taking into the account the stopper and the external magnet which acts as tunable factor. This latter contribution is expressed with the term δ. In presence of external vibration source the beam will move and two main conditions will appear: 1) when the beam touches the stopper S_s, all the current provided by the low power filter flows through the inductor L, (see Fig. 2.a); 2) when the contact between both is open, the residual current cannot be instantaneously canceled, so it generates an overvoltage peak across the inductor that overcomes the thresholds of the diodes. In this case it is possible to convert the low level signals into a DC voltage across the load capacitor C_L in order to give the information of the input signal energy.

In particular the electromechanical switch used in this study is composed of a brass beam with a length (l) of about 55 mm, width of about 8.3 mm and thickness of about 0.2 mm, with the distance (l_1) between the anchor of the cantilever and the stopper of about 28 mm, as shown in Fig. 2.c.

a) Proposed circuit schematic

b) Random mechanical switch principle

c) Random mechanical switch photograph
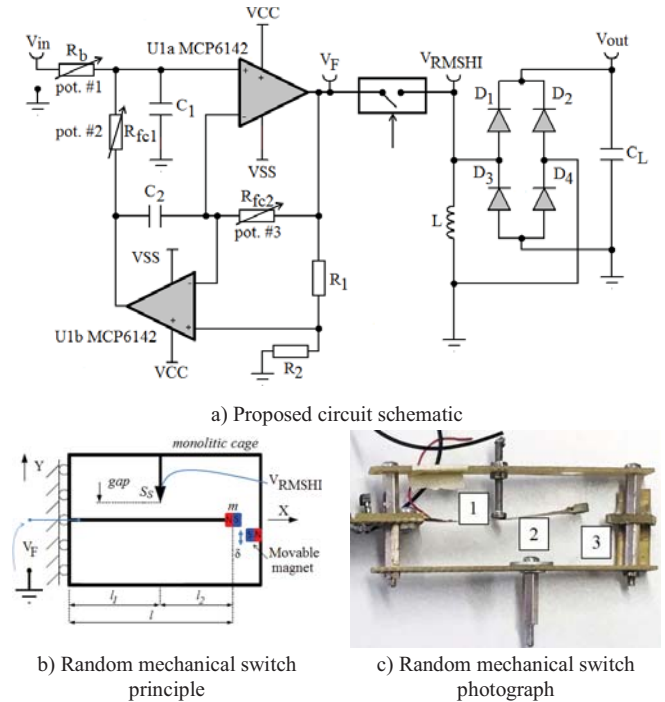
Fig. 2. a) A detailed schematic of the energy measurement circuit. It consists of an active programmable analog band pass filter, an RMSHI part, a full bridge rectifier and a load capacitor C_L. b) Principle of the random mechanical switch used as part of the conditioning circuit for measurements of very weak input sources. c) A photograph of the random mechanical switch. 1) Stopper, 2) Cantilever beam, 3) Movable magnet.

III. Measurement Setup and Procedure

The goal of these measurements was to perform a functional test of the proposed circuit, to select design parameters and to characterize its sensitivity and resolution.

A. Measurement Setup

For all the following measurements the circuit was adjusted in the following way. The central frequency of the

filter was tuned to 300 Hz by setting the values of the trimmer resistors R_{fc1} and R_{fc2} (as shown in Section II, Fig. 2.a) and its pass band width was set to 200 Hz using the trimmer resistor R_b. The magnet opposite to the switch's cantilever beam, Fig. 2.b, was used to set the frequency at which the switch has the highest output voltage to match the central frequency of the filter.

The block diagram and a photograph of the measurement setup can be seen in Fig. 3. and Fig. 4. respectively. The measurement setup consisted of a function generator (Voltcraft FG-506) connected to the input of the circuit. The energy measurement part of the circuit was positioned on a shaker (Smart Material Energy Harvesting Kit 1.2.). In order to decouple the input signal used for the characterization and the RMSHI, we have used a second function generator (Agilent 33250 A) to drive the shaker and to move the mechanical transducer operating with the same waveform and frequency. The output voltage was acquired by a digital oscilloscope (Rigol MSO4014) in duration from 5 s to 20 s.
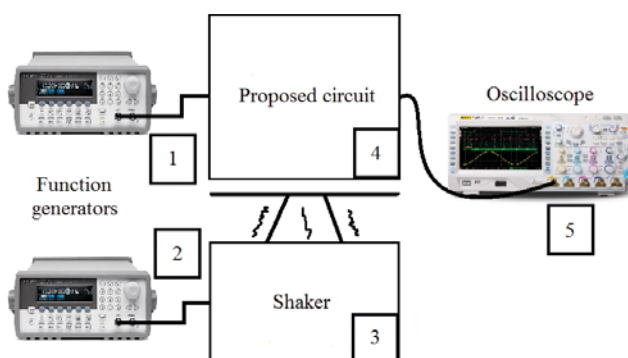
Fig. 3. Block diagram of the measurement setup which consists of the proposed circuit, a pair of function generators, a shaker and a digital oscilloscope.
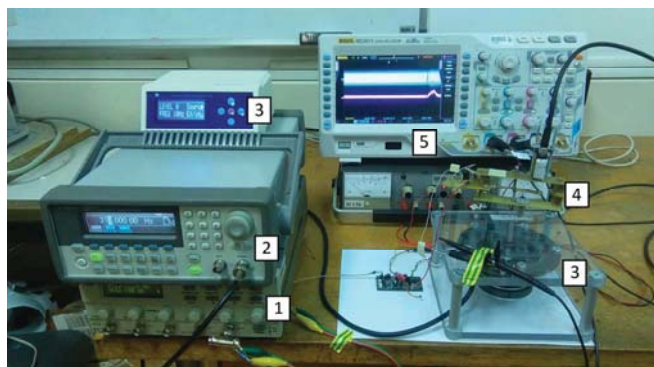
Fig. 4. A photograph of the measurement setup. 1) Voltcraft FG-506 function generator, 2) Agilent 33250 A function generator, 3) Smart Material Energy Harvesting Kit 1.2. shaker, 4) Proposed circuit, 5) Rigol MSO4014 oscilloscope.

B. Measurement Procedure

1) Design parameter selection

The goal was to select the load capacitor C_L in regards to output signal ripple and response time. A higher capacitance means reduction of ripple, but it also causes longer response time. Frequency of the input signal was set for maximal output voltage (to 315 Hz) and peak-to-peak input voltage was set to 50 mV. The output voltage was measured for capacitors of 10 nF, 33 nF, 100 nF, 470 nF and 1 μF.

2) Sensitivity of circuit to input signal frequency within the selected frequency band

The goal was to determine the relation of output signal voltage to change of input signal frequency, within the selected frequency band. The load capacitor of 33 nF was chosen. The frequency of the input signal was swept from 290 Hz to 330 Hz with increment of 5 Hz. The input signal peak-to-peak voltage was set to 5 mV, 10 mV, 20 mV, 30 mV, 40 mV and 50 mV. For each combination of input signal frequency and voltage, output voltage was recorded in duration of 20 s. The recorded waveforms were processed in MATLAB to obtain the RMS value of the output voltage.

3) Energy measurement characterization

The goal was determination of the proposed circuit's energy measurement performance. The frequency of the input signal was 315 Hz, at which the RMSHI has the maximal output voltage. The peak-to-peak values of the input voltage were set at 5 mV, 10 mV, 20 mV, 30 mV and 40 mV respectively. For each input voltage value, 10 measurements in duration of 5 s were done. After acquisition the measurement data was processed in MATLAB. The output of the energy measurement circuit was given as the maximal output voltage during the 5 s period, averaged over 10 consecutive measurements. The measurement error ε was calculated as:

$$\varepsilon = 3A = 3\sqrt{\frac{std^2(Max1, Max2, \dots, Max10)}{10}} \tag{2}$$

Where A is the uncertainty and std is the standard deviation of the maximal voltage values of the 10 measurements.

The input signal energy E in nJ was calculated from peak-to-peak value of the input signal voltage V_{in}, circuit input resistance R_{in} and measurement duration T_m, as shown in (3).

$$E = \frac{V_{in}^2}{R_{in}}T_m \tag{3}$$

IV. RESULTS

The obtained results are organized in two sections. First section covers functional tests and the second characterization of the proposed circuit.

A. Functional Test

The result of the functional test in Fig. 5. shows the waveform of the proposed circuit's output voltage with and without use of the RMSHI. It can be seen that using the RMSHI increases the output voltage of the proposed circuit, which validates the principle and indicates its usefulness in low-power devices for energy measurement. Also, as the RMSHI adds no additional active components to the circuit, the only active part of the circuit remains the band-pass filter. Thus the overall power consumption of the proposed circuit is 6.3 μW (3.5 μA at 1.8 V supply).
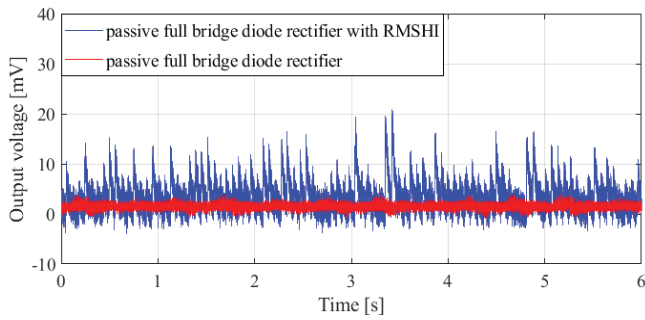
Fig. 5. The waveform of the output voltage with (blue) and without (red) the mechanical switch operational. Input signal voltage peak-to-peak 50 mV, frequency 315 Hz, load capacitance C_L = 33 nF.

B. Circuit Characterization

1) Design parameter selection

As described in Section III, analyses in terms of load capacitors have been pursued. It is clear from the waveforms shown in Fig. 6. that the 33 nF load capacitor works well for our application in both terms of output voltage ripple and response time.
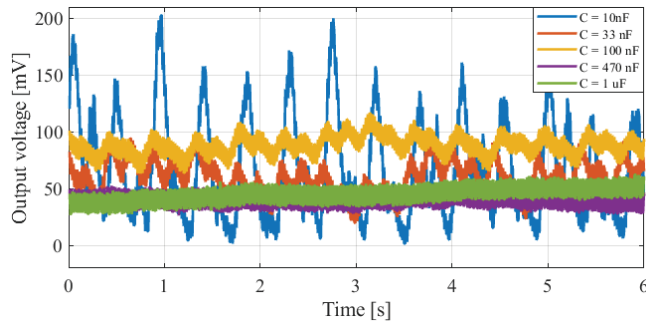

Fig. 6. The waveform of the output voltage for different values of load capacitance C_L. Input signal voltage peak-to-peak 50 mV, frequency 315 Hz.

2) Sensitivity of circuit to input signal frequency within the selected frequency band

Fig. 7. shows that the electromechanical switch has the maximal output voltage for the excitation vibration frequency of around 315 Hz, this result is a consequence of a tuning procedure of δ (see Section II, eq.1). That motivates us to use this as the central frequency for the other sets of measurements.
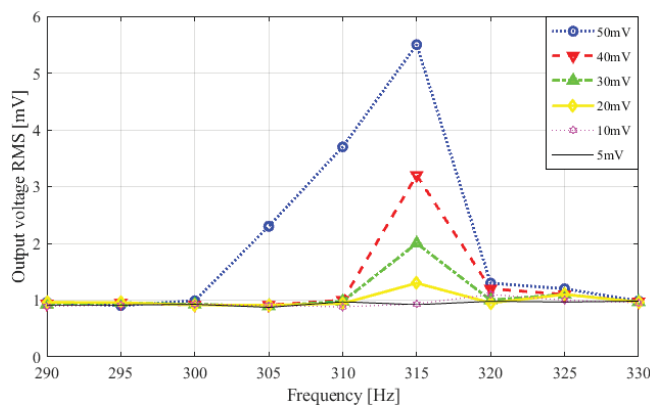
Fig. 7. Sensitivity of circuit to input signal frequency within the selected frequency band. The output RMS voltage is shown. Input signal voltage peak-to-peak from 5 mV to 50 mV, frequency changed by 5 Hz from 290 Hz to 330 Hz, load capacitance C_L = 33 nF.

3) Energy measurement characterization

In Fig. 8. the relation between the input energy and output voltage is shown. It can be seen that the maximum measurement error (deviation from the linear interpolation) is around -2 mV, measured at input energy of 0.4 nJ.
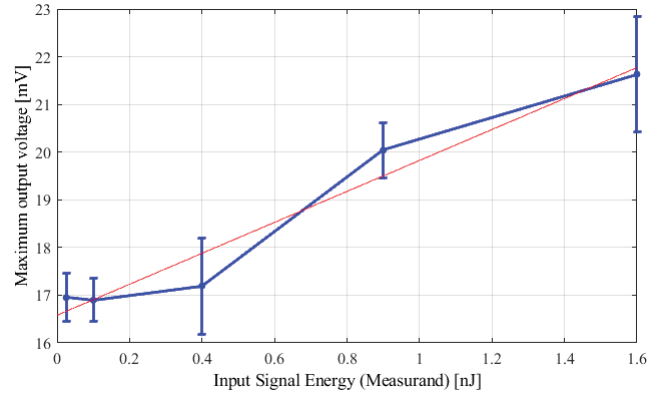
Fig. 8. Output voltage maximum value versus input signal energy. Input signal frequency 315 Hz, load capacitance C_L = 33 nF. The dots and the blue line represent actual measurement data. The red line represents a linear interpolation.

Fig. 9. shows the calibration curve of the proposed circuit. The sensitivity of the measurement circuit is around 3 mV/nJ and the resolution is around ±0.66 nJ.
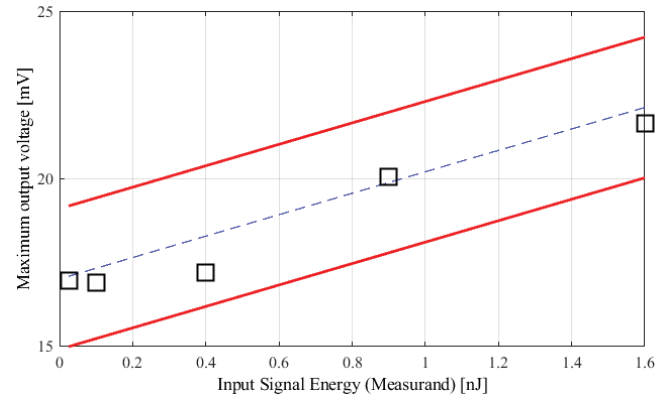
Fig. 9. The calibration curve of the energy measurement circuit. The black squares are the measurements. The blue line represents the linear interpolation. The two red lines represent the maximum measurement error.

V. CONCLUSION

In this paper a proof-of-concept system featuring the RMSHI as a passive conditioning circuit for rectification and measurement of weak signal energy was presented. Using energy as a feature enhances detection of very slow evolving acoustic phenomena. The advantage of the proposed approach is that the single mechanical structure can be tuned to various frequency bands within acoustic frequency spectrum. Thanks to utilization of the RMSHI, we accomplished sensitivity of the presented circuit is around 3 mV/nJ. With the maximum measurement error in mind, the resolution is around ±0.66 nJ. The active part of the system consumes around 6.3 µW.

This work represents the first step towards an integrated weak sensor signal measurement device, using a MEMS switch driven by the acoustic energy. The results presented here shall be used in modeling and development of the future integrated device.

REFERENCES

[1] M. Fourniol, V. Gies, V. Barchasz, and E. Kussener, "Low-Power Wake-Up System based on Frequency Analysis for Environmental Internet of Things," in *2018 14th IEEE/ASME International Conference on Mechatronic and Embedded Systems and Applications (MESA)*, pp. 1–6, 2018.

[2] B. Thoen *et al.*, "Saving energy in WSNs for acoustic surveillance applications while maintaining QoS," *SAS 2017 - 2017 IEEE Sensors Appl. Symp. Proc.*, pp. 1–6, 2017.

[3] S. E. Kucukbay, M. Sert, and A. Yazici, "Use of Acoustic and Vibration Sensor Data to Detect Objects in Surveillance Wireless Sensor Networks," *Proc. - 2017 21st Int. Conf. Control Syst. Comput. CSCS 2017*, pp. 207–212, 2017.

[4] C. Salazar-García, R. Castro-González, and A. Chacón-Rodríguez, "RISC-V based sound classifier intended for acoustic surveillance in protected natural environments," *LASCAS 2017 - 8th IEEE Lat. Am. Symp. Circuits Syst. R9 IEEE CASS Flagsh. Conf. Proc.*, pp. 1–4, 2017.

[5] D. Oletic and V. Bilas, "Energy-efficient respiratory sounds sensing for personal mobile asthma monitoring," *IEEE Sens. J.*, vol. 16, no. 23, pp. 8295–8303, 2016.

[6] D. Oletic, L. Korman, M. Magno, and V. Bilas, "Time-frequency pattern wake-up detector for low-power always-on sensing of acoustic events," *I2MTC 2018 - 2018 IEEE Int. Instrum. Meas. Technol. Conf. Discov. New Horizons Instrum. Meas. Proc.*, pp. 1–6, 2018.

[7] C. Tschope, F. Duckhorn, C. Richter, P. Bl, and M. Wolff, "An Embedded System for Acoustic Pattern Recognition," in *2017 IEEE SENSORS*, pp. 1–3, 2017.

[8] S. Chu, S. Narayanan, and C. J. Kuo, "Environmental Sound Recognition With Time–Frequency Audio Features," *IEEE Trans. Audio. Speech. Lang. Processing*, vol. 17, no. 6, pp. 1142–1158, 2009.

[9] C. V. Cotton and D. P. W. Ellis, "Spectral vs. spectro-temporal features for acoustic event detection," *IEEE Work. Appl. Signal Process. to Audio Acoust.*, pp. 69–72, 2011.

[10] D. Oletic, V. Bilas, M. Magno, N. Felber, and L. Benini, "Low-power multichannel spectro-temporal feature extraction circuit for audio pattern wake-up," *2016 Des. Autom. Test Eur. Conf. Exhib.*, pp. 355–360, 2016.

[11] D. Oletic, M. Gazivoda, and V. Bilas, "A programmable 3-channel acoustic wake-up interface enabling always-on detection of underwater events within 20 µA," in *Eurosensors 2018, 32nd Conference*, pp. 1–7, 2018.

[12] R. H. Olsson, R. B. Bogoslovov, and C. Gordon, "Event driven persistent sensing: Overcoming the energy and lifetime limitations in unattended wireless sensors," *Proc. IEEE Sensors*, pp. 1–3, 2016.

[13] T. Kaho, R. Kishikawa, A. Miyachi, and S. Kawasaki, "Design of C-band Rectitler with Watt-Class DC Output U sing 0.18µm CMOS and GaN Diode," in *Wireless Power Transfer Conference (WPTC), 2016 IEEE*, pp. 1–4, 2016.

[14] F. Giusa, A. Giuffrida, C. Trigona, B. Andò, A. R. Bulsara, and S. Baglio, "'Random mechanical switching harvesting on inductor': A novel approach to collect and store energy from weak random vibrations with zero voltage threshold," *Sensors Actuators, A Phys.*, vol. 198, pp. 35–45, 2013.

[15] S. Bradai, S. Naifar, C. Trigona, S. Baglio, and O. Kanoun, "Electromagnetic transducer with bistable-RMSHI for energy harvesting from very weak kinetic sources," *I2MTC 2018 - 2018 IEEE Int. Instrum. Meas. Technol. Conf. Discov. New Horizons Instrum. Meas. Proc.*, pp. 1–5, 2018.

Publication 7

Gazivoda, M., Trigona, C., Bilas, V., "Weak Signal Detection Utilizing a Mechanically Switched Inductor", *Proceedings of the 8th International Workshop on Advances in Sensors and Interfaces*, Otranto, Italy, 215-220, 2019, doi:10.1109/IWASI.2019.8791307

Weak Signal Detection Utilizing a Mechanically Switched Inductor

Marko Gazivoda
Faculty of Electrical Engineering and Computing,
University of Zagreb
Zagreb, Croatia
marko.gazivoda@fer.hr

Carlo Trigona
Department of Electrical, Electronic and Computer Engineering
University of Catania
Catania, Italy
carlo.trigona@dieei.unict.it

Vedran Bilas
Faculty of Electrical Engineering and Computing,
University of Zagreb
Zagreb, Croatia
vedran.bilas@fer.hr

Abstract— **These days an increasing number of applications have a need for always-on sensor interfaces for processing and analysis of sensor signals. One function most of these interfaces have in common is signal rectification. Seeing how these interfaces are always on, their parts should have low power consumption. This leads us to the idea of an electromechanical rectifier for weak signal rectification that could increase the rectified voltage levels with no additional power consumption, as it would get the energy needed for its operation from the very phenomenon that is observed. Motivated by this application scenario, an electrical analysis of the weak signal detection utilizing a mechanically switched inductor was done, considering a low-impedance weak signal source. After the theoretical analysis, simulations of the proposed electromechanical topology were presented. Finally, an experimental demonstration was done utilizing an RMSHI circuit corroborating the applicability of this concept in weak signal detector for an always-on interface. The experimental results show that it is possible to detect a minimal input voltage between 40 mV and 50 mV peak-to-peak for the macroscopic RMSHI device.**

Keywords— weak sensor signal, low-impedance source, electromechanical detector, rectifier, switching control, RMSHI

I. INTRODUCTION

These days the number of systems used for recognition and detection of infrequent events is increasing at a high pace. This has therefore become a topic of interest in many fields (environmental monitoring [1], safety and security [2], [3], agriculture, health monitoring [4]). However, this is a power-hungry task which requires continuous operation of the wireless embedded system [2]. Power consumption can be lowered by adding a low-power always-on frontend to wake up a more power hungry wireless embedded system only upon detection of some specific signature [5]–[7].

These always-on frontends typically incorporate signal processing blocks, such as amplification, filtering, rectification, quantization and rudimentary classification [8]. To lower power consumption of these processing blocks, extensive research is being done towards implementing them as near-zero-power electromechanical systems [9].

To improve sensitivity and power consumption of our always-on low-power interface, reported in [10], we consider

using an electromechanical detector comprised of a mechanically switched inductor, a diode rectifier bridge and a parallel of a capacitor and resistor. Utilizing a mechanically switch inductor provides voltage levels that can be rectified using a passive diode bridge rectifier. The mechanical switch would get the energy required for its operation from the very phenomenon (vibrations) that the always-on frontend interface observes. This is the key advantage of this topology compared to active rectifiers [11], [12].

Motivated by this application scenario, in this paper we present an analysis and experimental demonstration of detection of weak signals from low-impedance sources, utilizing a mechanically switched inductor. A similar problem was analyzed in detail in previous works regarding energy harvesting [13], with a difference that those works dealt with high-impedance sources [14].

This paper is organized as follows: Section II presents the application of the detector in an always-on interface. Section III presents the theoretical analysis of the mechanically switched inductor. Section IV presents simulations of the detector operation. The experimental demonstration is presented in Section V. The concluding remarks are given in Section VI.

II. DETECTOR APPLICATION IN AN ALWAYS-ON INTERFACE

The structure of the always-on interface with the proposed switched inductor detector can be seen in Fig. 1.
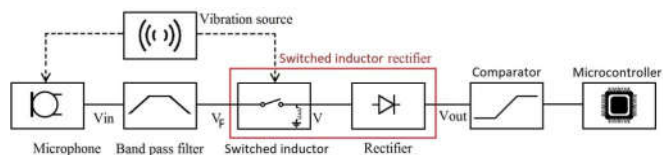

Fig. 1. Structure of the always-on interface with the switched inductor detector

In the always-on interface, the proposed detector is connected to an active bandpass filter. This means that the filter amplifier should be capable of driving the inductor of the proposed detector.

The detector's output is connected to a low-power comparator. The comparator input voltage limits define the required detector output.

A detailed description of the always-on interface can be found in [5], [10].

III. PRINCIPLE OF OPERATION

The proposed weak signal electromechanical detector, shown in Fig. 2., consists of three main elements: a parallel

215

mechanically switched inductor, a diode bridge full wave rectifier and a parallel of a capacitor and a resistor.
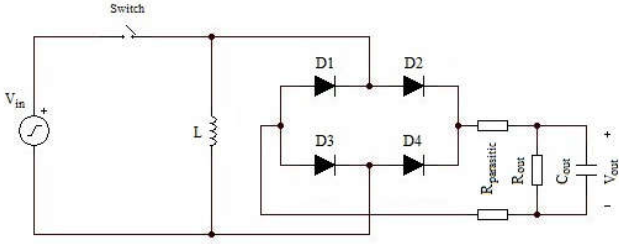

Fig. 2. The schematic of the proposed signal detector used for theoretical analysis

A. Circuit Operation with the Switch Closed

As this is a weak signal detector, the input voltage *Vin* is low (up to tens of millivolts) and under the threshold voltage of the diode bridge. This means that while the switch is closed, current i_L given by (1) flows only through the inductor.

$$i_L(t) = \frac{1}{L} \int_{t_C}^{t_O} V_{in}(t)dt \qquad (1)$$

t_C is the moment when the switch is closed and t_o the moment the switch is opened.

B. Circuit Operation with the Switch Opened

At the moment t_o when the switch opens a voltage V_L is induced across the inductor:

$$V_L = L \frac{di_L}{dt}\Big|_{t=t_O} \qquad (2)$$

We can consider the time derivation of the current at t_o to be:

$$\frac{di_L}{dt}\Big|_{t=t_O} = \frac{i_L(t_O)}{\Delta t}, \qquad (3)$$

with $i_L(t_O)$ being the current at the instant of opening of the switch and Δt the time required for the switch to open and the current through the inductor to fall to zero.

If the voltage induced on the inductor is high enough to pass over the diode bridge, it will charge the capacitor. The output voltage of the detector V_{out} is given with (4) when the capacitor is being charged and (5) while the voltage level is stable:

$$V_{out}(t) = \left(\frac{\int_{t_C}^{t_O} V_{in}(t)dt}{\Delta t} - 2V_D \right)\left(1 - e^{-\frac{t}{\tau_c}} \right), \qquad (4)$$

$$V_{out}(t) = \frac{\int_{t_C}^{t_O} V_{in}(t)dt}{\Delta t} - 2V_D. \qquad (5)$$

With V_D being the diode threshold voltage and τ_C being the charging time constant, defined as:

$$\tau_C = R_d * C_{out}, \qquad (6)$$

with R_d being the resistance of the conducting diodes. It should also be noted that the capacitor must be allowed time to fully discharge for the previously detected event not to affect the next event detection. The discharge time constant, τ_D is:

$$\tau_D = (R_s + R_{out}) * C_{out}, \qquad (7)$$

with R_s being the combined resistance of the capacitor and the wires.

IV. SIMULATIONS

The presented simulations were done using TINA-TI, a Texas Instruments SPICE-based analog simulator, with the simulation model shown in Fig. 3.
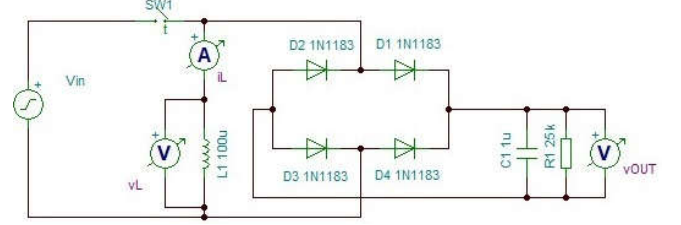
Fig. 3. Switched inductor detector simulation model

Some simulation results were further processed using MATLAB. The following text presents simulations related to output capacitor, switch operation and influence of input interference and noise. The simulations were done for a sinusoidal input voltage with amplitude from 1 mV to 20 mV peak-to-peak and frequency 200 Hz, with inductance of 100 µH and output resistance of 25 kΩ.

A. Selection of Output Capacitor

The output circuit time constant should be set to such a value that an acceptable charge and discharge time and output voltage ripple is achieved. The output voltage waveform for two different time constants can be seen in Fig. 4. The switch was opened for a very short time (20 µs), twice per period, at peak values of inductor current. A time constant around 25 ms fulfils the requirements of application of this detector in an always-on interface.
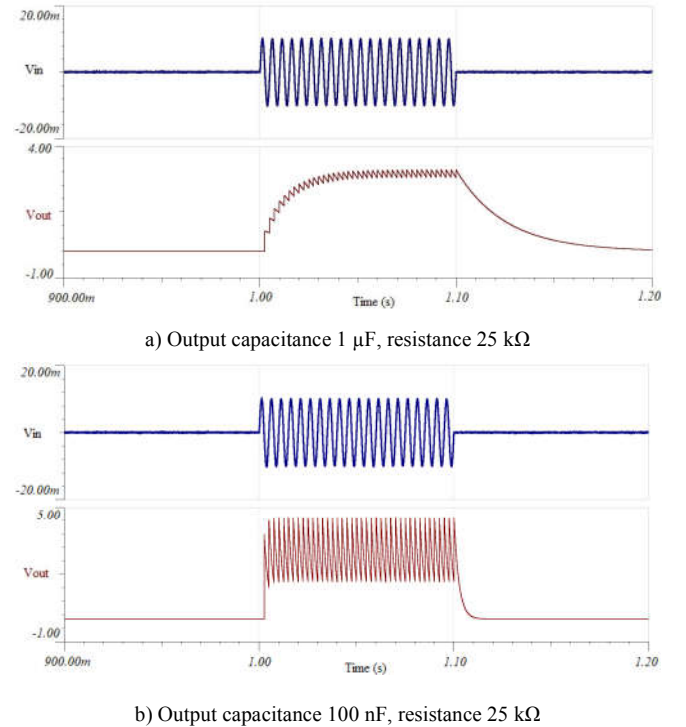

a) Output capacitance 1 µF, resistance 25 kΩ

b) Output capacitance 100 nF, resistance 25 kΩ

Fig. 4. Detector input voltage (blue) and output voltage (red) waveforms for time constant of τ_1=25 ms and τ_2=2.5 ms

B. Switch Operation

The voltage induced on the inductor depends on the integral of the input voltage during the time the switch was closed. We simulated the induced voltage for different switch opening instants, while keeping the same duration of the switch closed state. Results are presented in Fig. 5. The closed state duration was T/16 with the opening instants set from 0 to T/4, with a step of T/16. The opening of the switch lasts around 5.5 μs.
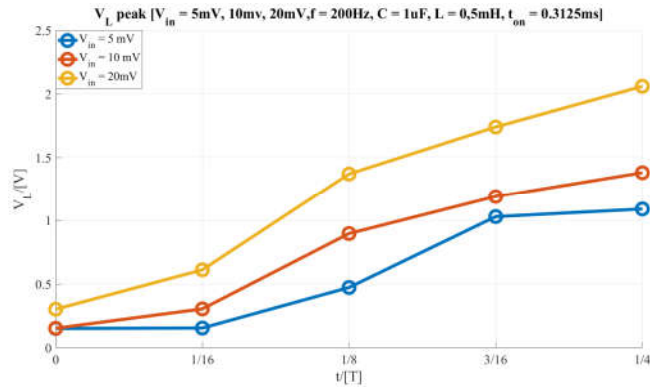

Fig. 5. Inductor induced voltage depending on the switch opening instant for the same switch closed state duration. (Input signal amplitudes 5 mV, 10 mV and 20 mV peak-to-peak).

Fig. 6 presents the induced inductor voltage at the opening instant (T/2-0.02) ms for switch closed state duration from T/16 to T/2, with a step of T/16.
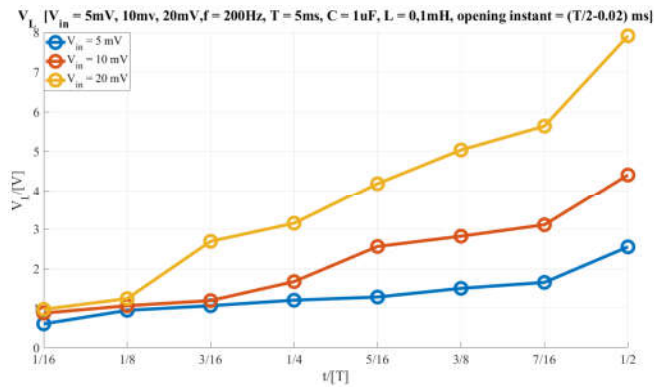
Fig. 6. Inductor induced voltage at the opening instant pi for switch closed state duration from pi/16 to pi/2, with a step of pi/16 (Input signal amplitudes from 5 mV, 10 mV and 20 mV peak-to-peak)

Fig. 6. shows that, if the moment of the switch opening is kept the same, while changing the time it was closed prior to that opening we get a change in the output voltage, which is easily explained by looking at equation (5). If we change the time the switch is in a closed state, we change the time we spend integrating the input signal, meaning the integral is different and therefore so is the output voltage.

C. Influence of Noise and Interference

Thanks to the integral dependence between the induced voltage and the input voltage the influence of the high-frequency harmonic interference and noise can be reduced as shown in Fig. 7.
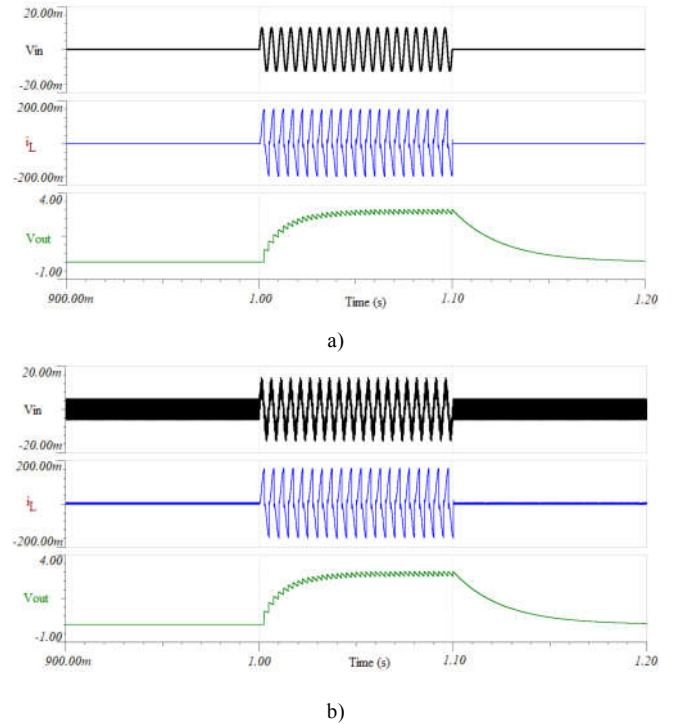
Fig. 7. Input voltage (black), inductor current (blue), output voltage (green) for: a) input signal 200 Hz, 10 mV peak-to-peak and b) added interference of 2 kHz, 5 mV peak-to-peak.

V. EXPERIMENTAL DEMONSTRATION

A. Measurement Setup

The block diagram and a photograph of the measurement setup can be seen in Fig. 8. and Fig. 9. respectively. The measurement setup consisted of a waveform generator (Keysight 33500B) with one channel connected to the input of the rectifier and the other used to drive the shaker (Smart Material Energy Harvesting Kit 1.2.) that was used to open and close the switch in the Random Mechanical Switching Harvester on Inductor (RMSHI) circuit. The output voltage was acquired by a National Instruments data acquisition card (NI USB-6211) connected to a PC.
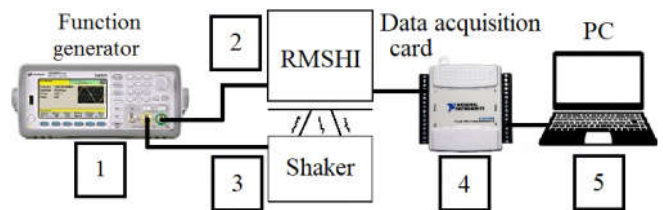

Fig. 8. Block diagram of the measurement setup which consists of a function generator (1), the RMSHI circuit (2), a shaker (3) and a data acquisition card (4) connected to a PC (5).
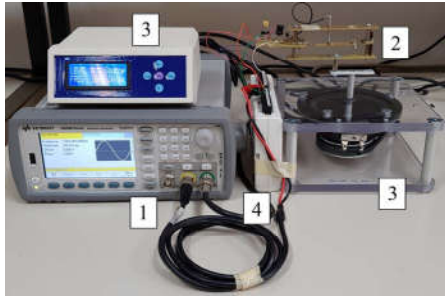
Fig. 9. A photograph of the measurement setup. 1) Keysight 33500B waveform generator, 2) RMSHI circuit, 3) Smart Material Energy Harvesting Kit 1.2. shaker, 4) NI USB-6211 data acquisition card.

The RMSHI circuit consists of an electromechanical switch, an inductor, a diode bridge and a load capacitor. The electromechanical switch is composed of a cantilever beam having a stopper on the upper part and a tunable magnetic system able to modify the elastic factor and, as consequence, the spectral response of the system as function of the input signal, as shown in Fig. 10. Mathematically, this transducer can be modeled using a second order nonlinear differential equation that can be written as follows:

$$m\ddot{x} + d\dot{x} + \frac{\partial U_T}{\partial x} = F(t)\Big|_{U_T = \delta x^4} \tag{8}$$

where m and d are the mass and the damping coefficient respectively. The term x is the displacement of the tip of the beam and the dotted terms represent the first and the second derivate of the displacement (velocity and acceleration of the cantilever respectively). U_T is the potential energy function which is nonlinear taking into the account the stopper and the external magnet which acts as tunable factor. This latter contribution is expressed with the term δ.

The electromechanical switch used in this study is composed of a brass beam with a length (l) of about 55 mm, width of about 8.3 mm and thickness of about 0.2 mm, with the distance (l_1) between the anchor of the cantilever and the stopper of about 28 mm, as shown in Fig. 10.a. Further information about the RMSHI can be found in [13], [15] and [16]. The vibrations generated by the shaker bend the beam, opening and closing the contact between the beam and the stopper and therefore opening and closing the switch.

a) Random mechanical switch principle

b) Random mechanical switch photograph
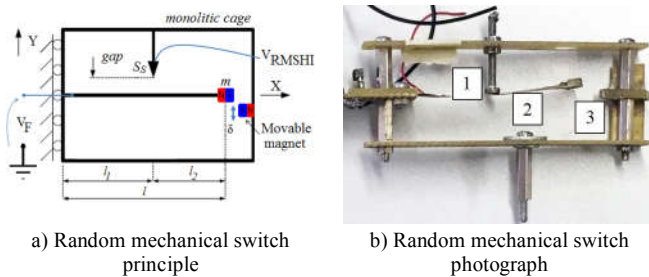
Fig. 10. a) Principle of the random mechanical switch used as part of the conditioning circuit for measurements of weak input sources. b) A photograph of the random mechanical switch. 1) Stopper, 2) Cantilever beam, 3) Movable magnet.

B. Measurement Procedure

The goal of these measurements was to demonstrate the use of RMSHI in weak signal detection and potentially in the always-on interface. The measurements were done in the following three sets.

1) Switch behaviour

The goal was to record the used RMSHI switch timing parameters. A 50 mV signal was connected to the switch input. Voltage at the switch input was measured. The shaker (speaker) was driven by a 212 Hz, 3.5 V peak-to-peak square wave.

2) Design parameter selection

The goal was to select the load capacitor C_{out} with regards to output signal ripple and response time. The input signal was a square waveform of 50 mV high state (lasting 800 ms) and 0 mV low state (lasting 1.2 s). The output voltage was measured for ceramic capacitors of 2 nF, 10 nF, 22 nF, 68 nF, 100 nF and 400 nF.

3) Input voltage detection

The goal was determination of the proposed circuit's voltage detection. The input signal was set to a square waveform with the high state lasting 800 ms and the low state lasting 1.2 s. The values of the input voltage high states were set at 10 mV, 20 mV, 30 mV, 40 mV and 50 mV respectively, while the low state was always 0 mV. For each input voltage value, the output voltage waveform was recorded.

C. Results

The obtained results are organized in three sections. First section shows the RMSHI switch operation, the second covers design parameter selection and the third shows the applicability of the proposed detector topology utilizing an RMSHI switch in the always-on interface.

1) RMSHI switch operation

The used RMSHI switch operation is shown in Fig. 11. The complexity of such a system's operation can be seen from the changing duration of switch open and closed states.
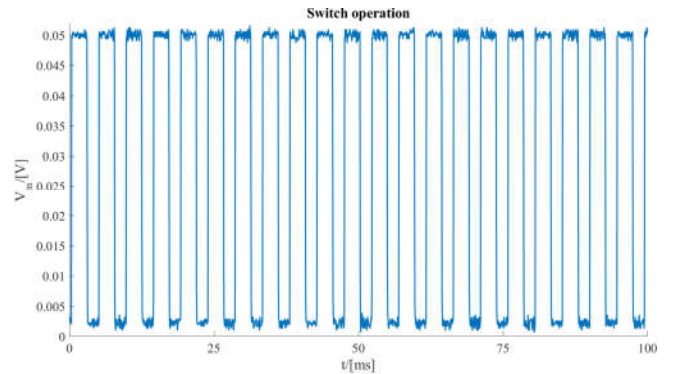

Fig. 11. RMSHI switch operation under the drive conditions used for the rest of the experiments.

2) Design parameter selection

As described in Section IV, analysis in terms of load capacitors has been pursued. As Fig. 12. shows a higher capacitance means reduction of ripple, but causes longer response time. The waveforms shown in Fig. 12. show that the 10 nF load capacitor ($\tau = 6.65$ ms) works well for this setup.
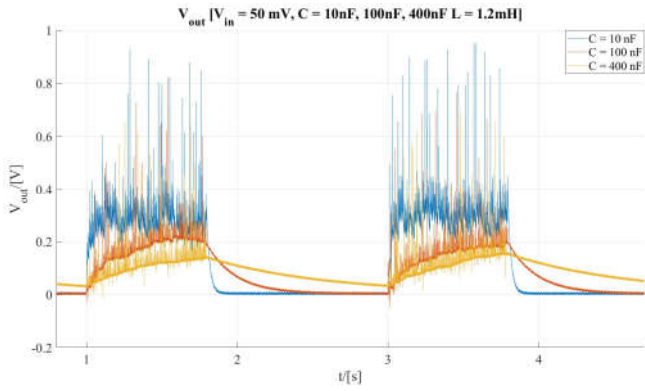
Fig. 12. The waveform of the output voltage for different values of load capacitance C_{out}. (Input signal square wave, voltage 50 mV peak-to-peak, 25 mV offset, 800 ms high state, 1200 ms low state.)

3) Input voltage detection

Fig. 13. shows the detector output voltage utilizing an RMSHI circuit as its switch. The lowest output voltage value of 28 mV and 128 mV were measured for the input voltages of 40 mV and 50 mV peak-to-peak respectively, with a time constant of 6.65 ms. The RMSHI circuit used in this experiment represents a highly complex system, which cannot easily be described by a simple model and the basic concepts described in previous sections. However, from a phenomenological point of view it is clear that such a detector can be used in an always-on interface, warranting further research in the subject.
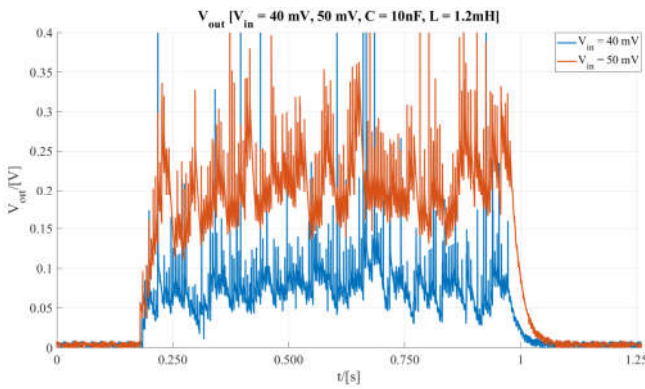
Fig. 13. Output voltage waveform for input voltage V_{in} 40 mV peak-to-peak (blue) and 50 mV peak-to-peak (red).Output capacitance 10 nF, detector inductance 1.2 mH.

4) Comparison to current solutions

Table I. shows a comparison of our proposed system with current solutions for active envelope detectors used in signal processing.

TABLE I. PROPOSED DETECTOR COMPARED TO CURRENT SOLUTIONS

Reference	Power consumption	Minimal input voltage
[10]	1.44 μW	~20 mVpp
[17]	100 nW	~140 mVpp
[18]	2.365 nW	~2 mVpp
[19]	1 – 10 nW	~150 mVpp (1.5 V bias)
this work	–	~40 mVpp

VI. CONCLUSION

In this paper we studied the application of a mechanically switched inductor detector in an always-on weak sensor signal interface. We have shown the importance of switch operation timing. We've done a preliminary simulation study and experimental demonstration of the detector with a random mechanically switched inductor.

The experimental results show that it is possible to detect a minimal input voltage between 40 mV and 50 mV peak-to-peak for the macroscopic RMSHI device.

Further work will be focused on a better understanding of switch operation and optimization of the detector sensitivity.

REFERENCES

[1] M. Fourniol, V. Gies, V. Barchasz, and E. Kussener, "Low-Power Wake-Up System based on Frequency Analysis for Environmental Internet of Things," in *2018 14th IEEE/ASME International Conference on Mechatronic and Embedded Systems and Applications (MESA)*, pp. 1–6, 2018.

[2] B. Thoen *et al.*, "Saving energy in WSNs for acoustic surveillance applications while maintaining QoS," *SAS 2017 - 2017 IEEE Sensors Appl. Symp. Proc.*, pp. 1–6, 2017.

[3] S. E. Kucukbay, M. Sert, and A. Yazici, "Use of Acoustic and Vibration Sensor Data to Detect Objects in Surveillance Wireless Sensor Networks," *Proc. - 2017 21st Int. Conf. Control Syst. Comput. CSCS 2017*, pp. 207–212, 2017.

[4] D. Oletic and V. Bilas, "Energy-efficient respiratory sounds sensing for personal mobile asthma monitoring," *IEEE Sens. J.*, vol. 16, no. 23, pp. 8295–8303, 2016.

[5] D. Oletic, L. Korman, M. Magno, and V. Bilas, "Time-frequency pattern wake-up detector for low-power always-on sensing of acoustic events," *I2MTC 2018 - 2018 IEEE Int. Instrum. Meas. Technol. Conf. Discov. New Horizons Instrum. Meas. Proc.*, pp. 1–6, 2018.

[6] C. Tschope, F. Duckhorn, C. Richter, P. Bl, and M. Wolff, "An Embedded System for Acoustic Pattern Recognition," in *2017 IEEE SENSORS*, pp. 1–3, 2017.

[7] S. Chu, S. Narayanan, and C. J. Kuo, "Environmental Sound Recognition With Time–Frequency Audio Features," *IEEE Trans. Audio. Speech. Lang. Processing*, vol. 17, no. 6, pp. 1142–1158, 2009.

[8] D. Oletic, V. Bilas, M. Magno, N. Felber, and L. Benini, "Low-power multichannel spectro-temporal feature extraction circuit for audio pattern wake-up," *2016 Des. Autom. Test Eur. Conf. Exhib.*, pp. 355–360, 2016.

[9] R. H. Olsson, R. B. Bogoslovov, and C. Gordon, "Event driven persistent sensing: Overcoming the energy and lifetime limitations in unattended wireless sensors," *Proc. IEEE Sensors*, pp. 1–3, 2016.

[10] D. Oletic, M. Gazivoda, and V. Bilas, "A programmable 3-channel acoustic wake-up interface enabling always-on detection of underwater events within 20 μA," in *Eurosensors 2018, 32nd Conference*, pp. 1–7, 2018.

[11] A. S. Herbawi, O. Paul, and T. Galchev, "An ultra-low-power active AC-DC CMOS converter for sub-1V integrated energy harvesting applications," *Proc. IEEE Sensors*, pp. 1–4, 2013.

[12] K. G. Sun, K. Choi, and T. N. Jackson, "Low-power double-gate ZnO TFT active rectifier," *IEEE Electron Device Lett.*, vol. 37, no. 4, pp. 426–428, 2016.

[13] F. Giusa, A. Giuffrida, C. Trigona, B. Andò, A. R. Bulsara, and S. Baglio, "'Random mechanical switching harvesting on inductor': A novel approach to collect and store energy from weak random vibrations with zero voltage threshold," *Sensors Actuators, A Phys.*, vol. 198, pp. 35–45, 2013.

[14] N. Krihely and S. Ben-Yaakov, "Self-contained resonant rectifier for piezoelectric sources under variable mechanical excitation," *IEEE Trans. Power Electron.*, 2011.

[15] S. Bradai, S. Naifar, C. Trigona, S. Baglio, and O. Kanoun, "Electromagnetic transducer with bistable-RMSHI for energy harvesting from very weak kinetic sources," *I2MTC 2018 - 2018*

219

IEEE Int. Instrum. Meas. Technol. Conf. Discov. New Horizons Instrum. Meas. Proc., pp. 1–5, 2018.

[16] M. Gazivoda, D. Oletic, C. Trigona, and V. Bilas, "Measurement of Weak Signal Energy at Acoustic Frequencies by using RMSHI as a Passive Conditioning Circuit," *I2MTC 2018 - 2018 IEEE Int. Instrum. Meas. Technol. Conf. Proc.*, (in press), 2019.

[17] K. M. H. Badami, S. Lauwereins, W. Meert, and M. Verhelst, "A 90 nm CMOS, 6 μW power-proportional acoustic sensing frontend for voice activity detection," *IEEE J. Solid-State Circuits*, vol. 51, no. 1, pp. 291–302, 2016.

[18] U. Antao, J. Choma, A. Dibazar, and T. Berger, "40nW subthreshold event detector chip for seismic sensors," *2015 IEEE Int. Symp. Technol. Homel. Secur. HST 2015*, pp. 1–6, 2015.

[19] B. Rumberg, D. W. Graham, V. Kulathumani, and R. Fernandez, "Hibernets: Energy-efficient sensor networks using analog signal processing," *IEEE J. Emerg. Sel. Top. Circuits Syst.*, vol. 1, no. 3, pp. 321–334, 2011.

Publication 8

Gazivoda, M., Oletić, D., Bilas, V., "Characterization and Comparison of Envelope Detectors for Wake-up Sensor Interfaces at Audio Frequencies", *Proceedings of the 2020 IEEE International Instrumentation and Measurement Technology Conference (I2MTC)*, Dubrovnik, Croatia, pp. 1–6., 2020, doi:10.1109/I2MTC43012.2020.9128810

Characterization and comparison of envelope detectors for wake-up sensor interfaces at audio frequencies

Marko Gazivoda
Faculty of Electrical Engineering and
Computing, University of Zagreb
Zagreb, Croatia
marko.gazivoda@fer.hr

Dinko Oletić
Faculty of Electrical Engineering and
Computing, University of Zagreb
Zagreb, Croatia
dinko.oletic@fer.hr

Vedran Bilas
Faculty of Electrical Engineering and
Computing, University of Zagreb
Zagreb, Croatia
vedran.bilas@fer.hr

Abstract— **Ultra-low-power analog hardware interfaces are becoming often used for continuous monitoring of weak, rarely and randomly occurring (spurious) acoustic events. Detection often requires interfaces for analog-domain time-frequency decomposition. These interfaces most often have a generic structure incorporating the same processing blocks, such as amplification, filtering, rectification, quantization and rudimentary classification. A critical processing block of the wake-up sensor interface is the envelope detector. In this paper we select four envelope detector topologies and show simulation and measurement results of their key parameters for their application in wake-up sensor interfaces. The selected envelope detectors must have short transient times (< 100 ms), used to rectify weak input signals (under 10 mV) in the lower audio frequency range and have a low power consumption to make them applicable in wake-up sensor interfaces.**

Keywords— *passive envelope detector, switched inductor envelope detector, weak-signal envelope detection*

I. INTRODUCTION

The research of low-power circuits is becoming more prominent because of their wide range of applications from IoT [1], communication systems [2], wake-up systems [3], detectors and monitoring systems [4], wearable and biomedical electronics [5] and many others. One of the most interesting applications of low-power circuits, that is providing solutions in many fields, are low-power wireless sensor networks. These networks require specific low-power, weak-signal embedded sensors most often used for continuous monitoring of spurious events, occurring randomly and rarely throughout the monitoring time.

Detection of spurious events based on time-frequency pattern recognition requires a set of signal processing operations and most sensor interfaces for this application have a structure incorporating processing blocks, such as amplification, filtering, rectification, quantization and rudimentary classification [6], [7]. The block schematic of the structure is shown in Fig. 1.
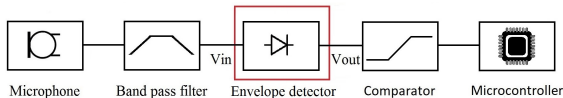

Fig. 1. An always-on wake-up sensor interface for spurious event detection based on time-frequency signal decomposition

A critical processing block of the wake-up sensor interface is the envelope detector, which is connected to the comparator input. The comparator must be able to respond quickly to the event and distinguish two events close in time. Therefore, the envelope detector must have a short rise and fall times (Fig. 2), estimated under 100 ms for the wanted application [7].

The comparator should also be able to distinguish as low levels of voltage as possible. So, the output headroom voltage (Fig. 2.) of the envelope detector should be at least 5 mV for the wake-up sensor interface application [7].
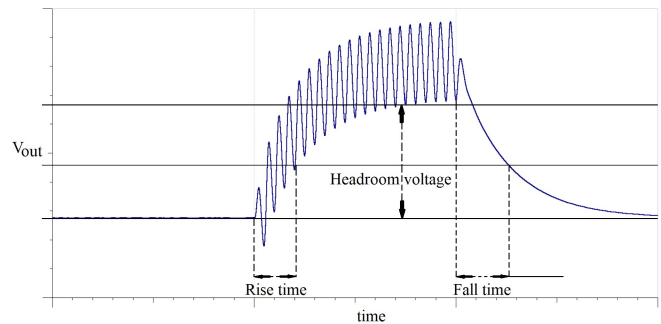

Fig. 2. A graphic representation of the values of interest in simulation and measurement – headroom voltage, rise and fall time

There are several other demands on wake-up sensor interface envelope detectors stemming from their application – working with input voltages under the diode threshold and having a low power consumption.

In this paper we will focus on envelope detectors operating in the lower audio frequency range, as this frequency range is rich in easily extracted useful information about the phenomena of interest. A lot of work has recently been done in development of appropriate envelope detection solutions. In [8] the authors present a fully passive envelope detector that works with input signals as low as 100 mV at frequencies from DC to 100 MHz. In [9] a low-power envelope detector is presented with power consumption of just 10 nW, operational with an input as low as 50 mV at 50 Hz. In [10] an envelope detector with around 100 nW power consumption is presented, that can work with input signals over 100 mV at a low frequency of only 4 Hz. It should be noted that the envelope detectors presented in [8]–[10] are integrated, unlike the prototypes in this paper, which are made of commercially available components.

In vibration energy harvesting the problem of low generated voltages (under the diode threshold) is solved by utilizing the concept of envelope detectors with a switched inductor, such as SSHI (synchronous switched harvester on inductor) to increase the envelope detector's efficiency [11], [12].

In this paper we characterize and compare four envelope detector topologies and show simulation and experimental results of key parameters for their app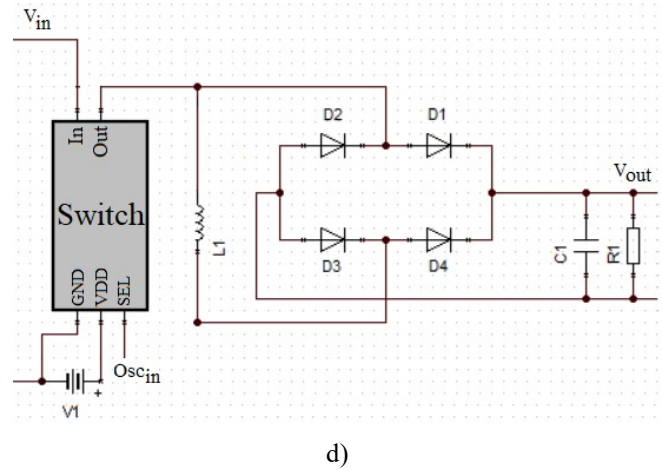lication in low-power embedded wake-up sensor interfaces. The selected envelope detector topologies are: passive single-diode half-wave envelope detector, passive two-diode half-wave voltage doubler (Greinacher circuit), active two-diode half-wave voltage doubler utilizing an operational amplifier and an active full-wave envelope detector utilizing a switched inductor (switched by an electrical switch driven by an oscillator).

This paper is organized as follows: Section II presents a simulation study of the envelope detectors, showing the simulation models and results, Section III presents the experimental setup and results measured using the developed prototypes, Section IV presents a summary comparison of the envelope detectors and Section V presents the concluding remarks of the paper, along with possible future work.

II. SIMULATION STUDY

The goals of the simulation study were the selection of passive and active components for envelope detector realization and preliminary insight into parameters of interest (headroom voltage, rise and fall time). The presented simulations were done using TINA-TI, a Texas Instruments SPICE-based analog simulator.

A. Simulation models and setup

The simulation models are shown in Fig 3. a) through d).
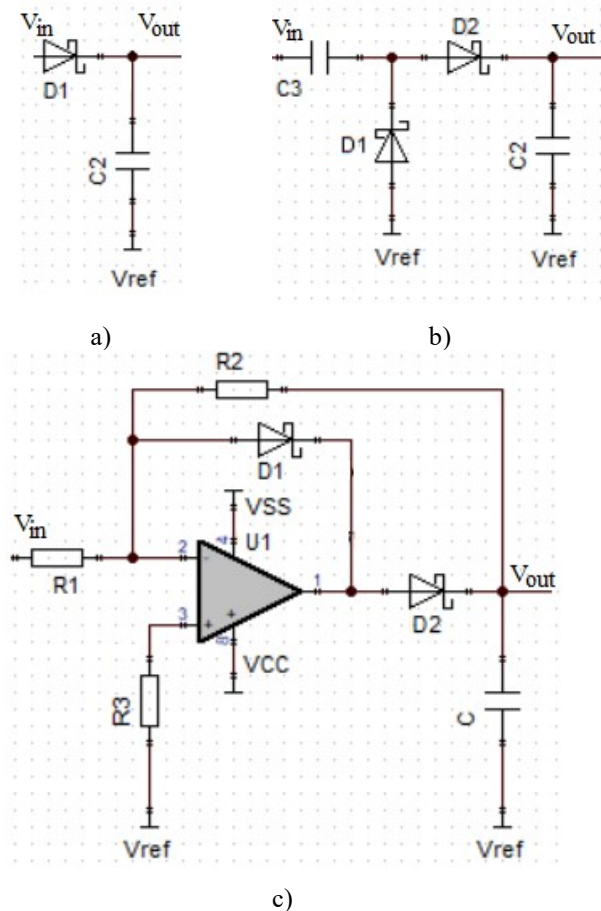

a)

b)

c)

d)

Fig. 3. Envelope detector topologies: a) passive single-diode half-wave envelope detector, b) passive two-diode half-wave voltage doubler (Greinacher circuit), c) active two-diode half-wave voltage doubler utilizing an operational amplifier and d) active full-wave envelope detector utilizing a switched inductor

The envelope detector input signal was a gated sinusoidal signal because that allows both transient times to be measured. The duration of the sinusoidal signal was set to 1.5 s. The set input voltages for all envelope detectors were 1 mV, 2 mV, 3 mV, 5 mV, 7 mV and 10 mV and the input frequencies 128 Hz, 256 Hz and 512 Hz for the switched inductor envelope detector and 200 Hz, 500 Hz and 1000 Hz for the other three topologies. In the simulation model for the switched inductor envelope detector, the electrical switch is triggered by a 256 Hz oscillator (not synchronized with the input signal). The input signals and the oscillator signal (Fig. 3.d)) are made in MATLAB and imported to the TINA-TI simulator.

The load capacitor values were set to 3.3 nF, 6.8 nF, 10 nF, 15 nF, 22 nF, 33 nF, 100 nF, 350 nF and 1 µF. In all the simulations several diodes' performances were compared. In addition, for the active envelope detector with the operational amplifier two amplifiers were compared – the Texas Instruments' OPA379 and Microchip's MCP6141 and for the active envelope detector with the switched inductor the three switches were compared – TPS22916, TPS22976 and TPS22860 from Texas Instruments.

For the active envelope detector utilizing an operational amplifier several values of resistors were tested. Simulations of the switched inductor envelope detector were done with three inductor values: 1 mH, 10 mH and 100 mH.

B. Simulation results

Table I. shows the simulation results for the headroom voltages, rise and fall times of the four proposed envelope detector topologies (for the full range of load capacitor values). Simulation results were processed using MATLAB.

From the simulation results Avago Technology's HSMS-282x diodes were chosen for all the envelope detectors as they allowed for the best headroom voltages and a relatively flat frequency response in the frequency range of interest. For the active envelope detector utilizing the operational amplifier the MCP6141 amplifier was chosen because of its slightly higher headroom voltages and shorter transient times (and lower declared power consumption). For the switched inductor envelope detector, the TPS22860 switch was chosen as it gave a far higher headroom voltage.

single-diode passive envelope detector			
Input signal frequency (Hz)	Headroom (mV)	Rise time (ms)	Fall time (ms)
200	< 2.84	14.86 – 50.29	13.30 – 41.01
500	< 3.16	7.95 – 47.87	6.35 – 33.85
1000	< 2.82	6.05 – 36.12	5.08 – 34.86

two-diode passive voltage doubler			
Input signal frequency (Hz)	Headroom (mV)	Rise time (ms)	Fall time (ms)
200	< 5.25	19.66 – 79.87	16.41 – 89.92
500	< 5.98	11.83 – 52.03	10.77 – 77.28
1000	< 5.46	9.96 – 45.75	8.69 – 73.11

active voltage doubler utilizing an operational amplifier			
Input signal frequency (Hz)	Headroom (mV)	Rise time (ms)	Fall time (ms)
200	< 80.69	2.50 – 5.33	2.67 – 7.61
500	< 78.32	1.20 – 3.62	2.33 – 6.15
1000	< 70.23	1.60 – 4.4	1.61 – 14.23

active envelope detector utilizing a switched inductor			
Input signal frequency (Hz)	Headroom (mV)	Rise time (ms)	Fall time (ms)
128	< 8.53	20.07 – 238.95	27.32 – 251.34
256	< 8.17	20.09 – 238.80	27.36 – 246.80
512	–	–	–

The simulation results also pointed to the fact that larger load capacitor values (100 nF, 350 nF and 1 µF) should be used for the switched inductor envelope detector to reduce the ripple caused by its impulse operation (high pulse values of currents charging the capacitor), which leads to this topology having longer transient times. The remaining topologies should use the lower capacitor values (< 100 nF).

The chosen values for the resistors in the active topology utilizing the operational amplifier were $R_1 = 200$ kΩ, $R_2 = 1$ MΩ and $R_3 = 100$ kΩ and the 100 mH inductor value was chosen in the switched inductor topology, because it gave the highest output voltages with the same input current.

Simulation results have also shown some envelope detectors to be unusable at certain input voltages (passive single-diode envelope detector with lower input voltages), or frequencies (switched inductor envelope detector at 512 Hz).

III. Experimental Study

Prototypes of each envelope detector were made in order to acquire experimental measurement data. In the following subsections the measurement setup and procedure are described, and experimental results presented.

The goal of these measurements was to characterize and compare the four proposed envelope detector topologies from the aspects of headroom voltage, rise time, fall time and power consumption, in order to determine their applicability in a wake-up sensor interface.

A. Experimental setup

The block diagram and a photograph of the measurement setup can be seen in Fig. 8. and Fig. 9. respectively. The measurement setup consisted of a waveform generator (Keysight 33500B) connected to the input of the prototype envelope detector. The output voltage was acquired by a

National Instruments data acquisition card (NI USB-6211) connected to a PC. The switches were powered by a DC power supply (Rigol DP832) and the supply current measured by a multimeter (Fluke 45).
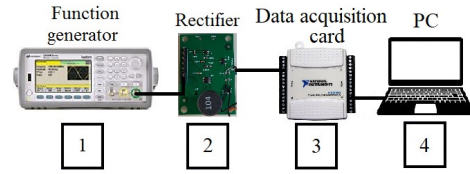

Fig. 4. Block diagram of the measurement setup: a function generator (1), the envelope detector PCB (2) a data acquisition card (3) connected to a PC (4).
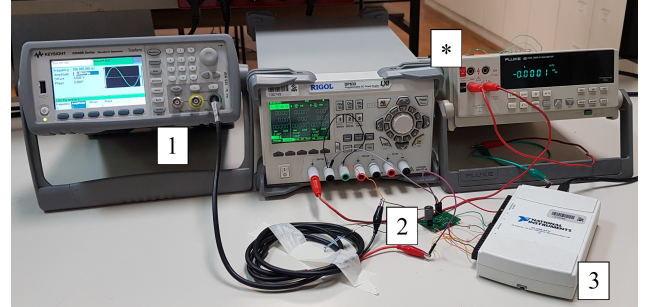

Fig. 5. A photograph of the measurement setup. 1) Keysight 33500B waveform generator, 2) envelope detector prototype, 3) NI USB-6211 data acquisition card, *) Power supply (Rigol DP832) and a multimeter for supply current measurement (Fluke 45).

B. Experimental procedure

The power consumption of the envelope detectors, with a set supply voltage of 1.8 V, was measured by measuring the supply current using a multimeter (Fluke 45). The remaining three parameters were measured simultaneously, by setting the input voltage at the envelope detector input using a waveform generator and measuring the characteristics of the output voltage (Fig. 2.) acquired by a data acquisition card.

The measurements done at three frequencies: 128 Hz, 256 Hz and 512 Hz for the switched inductor envelope detector (switching was controlled by a 256 Hz oscillator) and 200 Hz, 500 Hz and 1000 Hz for the remaining three envelope detectors. For all frequencies six input signal peak-to-peak voltages were set: 1 mV, 2 mv, 3 mV, 5 mV, 7 mV and 10 mV.

The measurements for the switched inductor envelope detector were done with three capacitors: 100 nF, 350 nF and 1 µF. The measurements for the two passive envelope detectors were also done with three capacitors: 10 nF, 15 nF and 33 nF. The measurements for the active envelope detector with an operational amplifier were done with four capacitors: 3.3 nF, 6.8 nF, 10 nF and 15 nF.
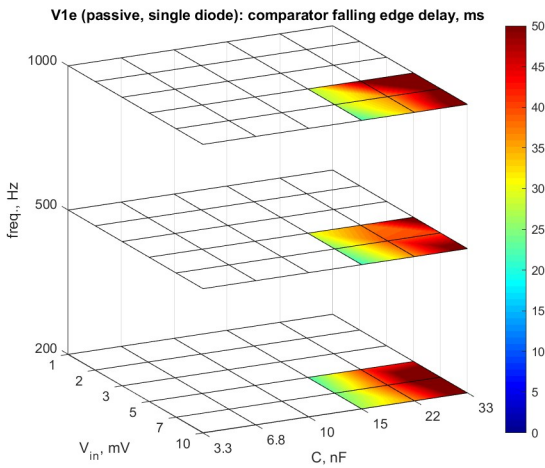
C. Experimental results

The obtained experimental results are shown in Fig. 6-9., one for each of the selected envelope detectors, showing the headroom voltage (a), rise time (b) and fall time (c). The results were processed and presented using MATLAB.
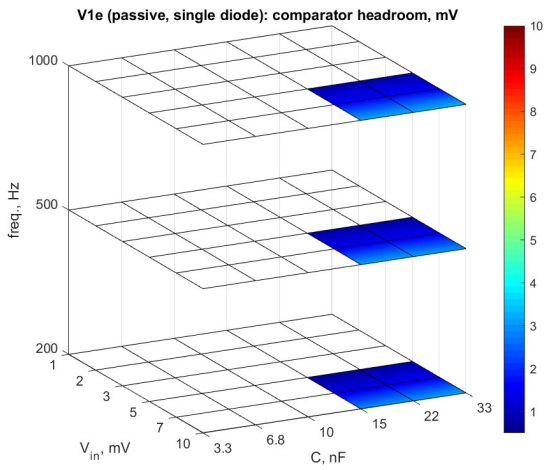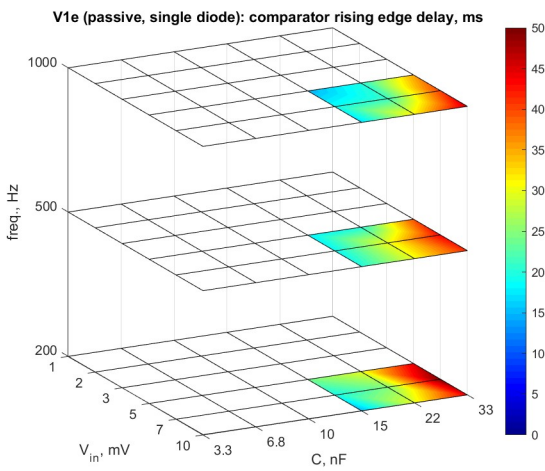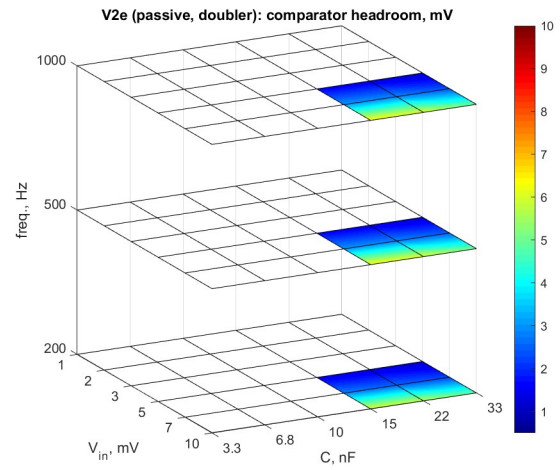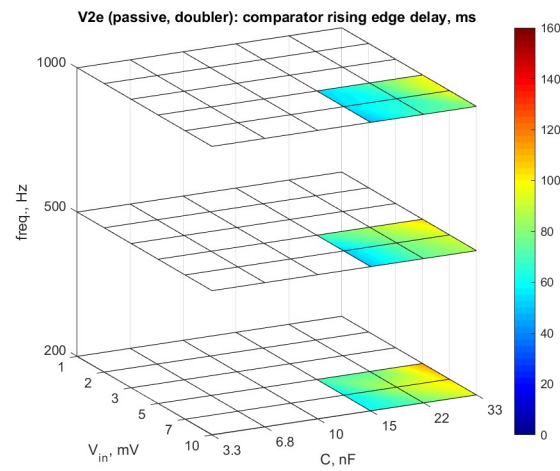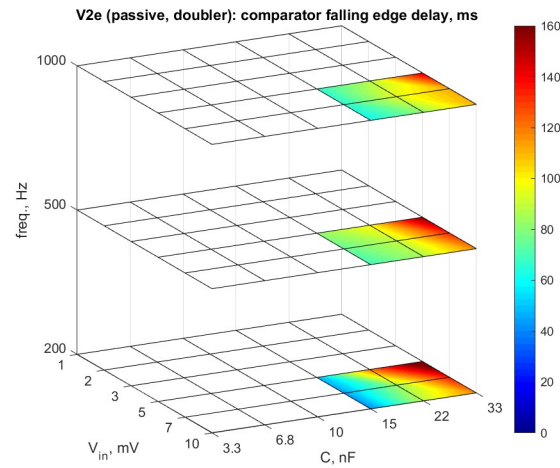
Fig. 6. Experimental results for the passive single diode half-wave envelope detector: a) headroom voltage, b) rise time c) fall time
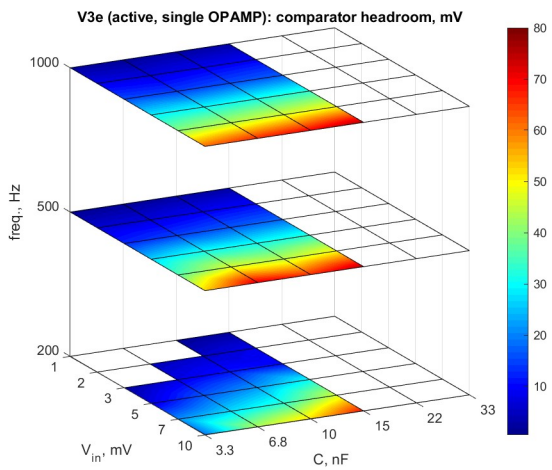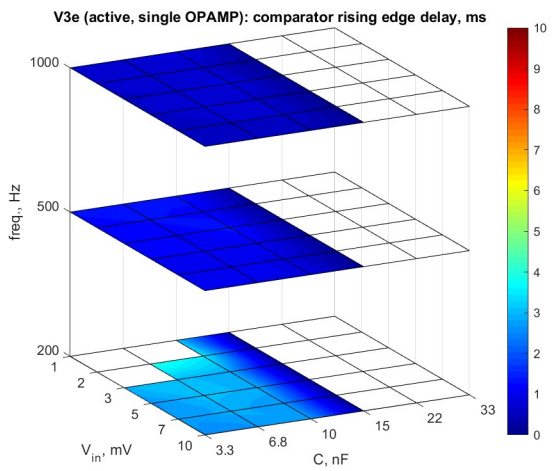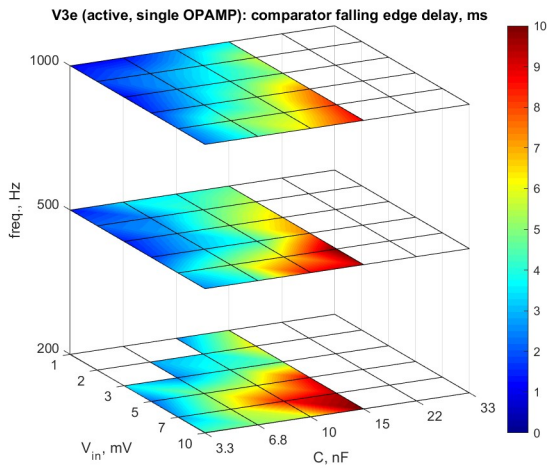

Fig. 7. Experimental results for the passive two-diode half-wave voltage doubler (Greinacher circuit): a) headroom voltage, b) rise time c) fall time
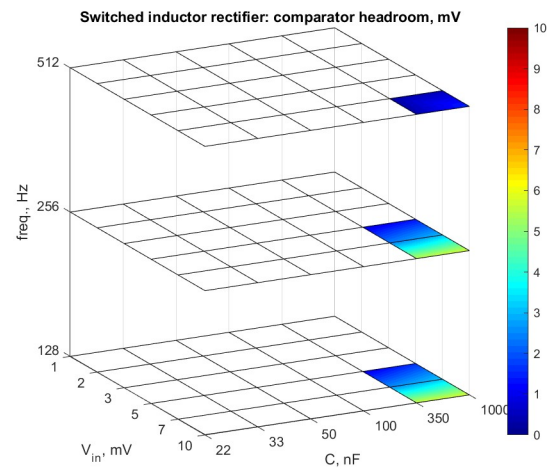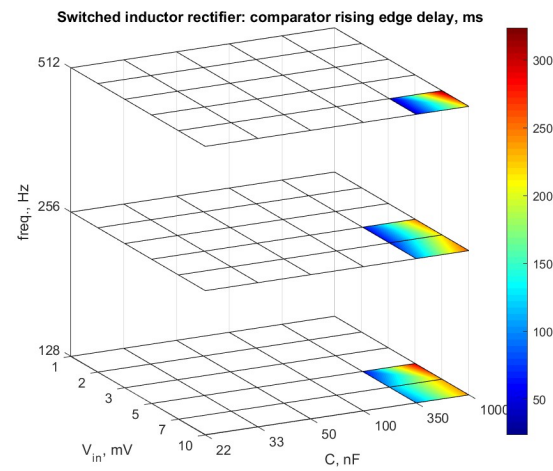
4

a)

b)

c)

Fig. 8. Experimental results for the active two-diode half-wave voltage doubler utilizing an MCP6141 operational amplifier: a) headroom voltage, b) rise time c) fall time
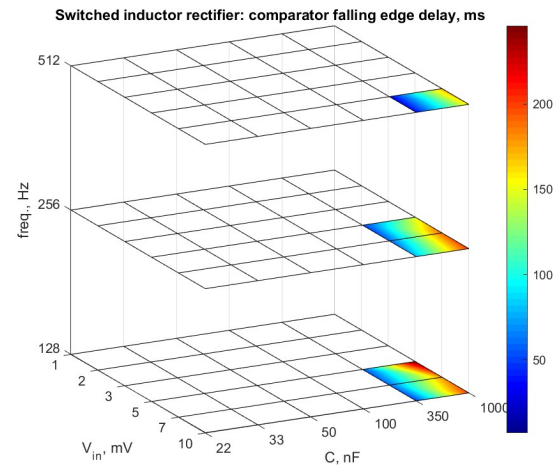
Measurement results for the passive single-diode envelope detector confirm the simulation results and show the headroom voltage to be too low (<2 mV).

a)

b)

c)

Fig. 9. Experimental results for the active full-wave envelope detector utilizing a 100 mH switched inductor: a) headroom voltage, b) rise time c) fall time

The results for the passive voltage doubler show that the headroom voltage is high enough (>5 mV). However, this envelope detector exhibits longer fall times (> 100 ms).

This active envelope detector with the MCP6141 operational amplifier achieves very high headroom voltages (> 70 mV) and short transient times (~10 ms). Its power consumption of 1.44 µW stems from its operational amplifier.

The switched inductor envelope detector utilizing a TPS22860 switch and SiT1569 oscillator shows high enough headroom voltage (> 5 mV), but long rise and fall times (around 250 ms). The relatively high power consumption of 3.42 µW of this envelope detector stems from the oscillator and electrical switch.

Table II. shows a summary comparison of the four selected envelope detectors.

TABLE II.   PROPOSED ENVELOPE DETECTORS SUMMARY COMPARISON

Topology	Power consumption	Headroom voltage	Transition times
one-diode passive	–	< 2 mV	med., < 50 ms
two-diode passive	–	~5.5 mV	long, > 100 ms
active, op. amp.	1.44 µW	~70 mV	short, < 10 ms
active, switched L	3.42 µW	~5.5 mV	long, > 200 ms

IV. CONCLUSION

In this paper we presented a characterization and comparison of four candidate envelope detector topologies for application in wake-up sensor interfaces for lower audio frequencies. From the presented simulation and experimental characterization and comparison data the active half wave voltage doubler utilizing an MCP6141 operational amplifier can be used for application in a wake-up sensor interface and outperforms the switched inductor envelope detector in the selected topology with the selected components.

In future work the switched inductor envelope detector topology will be explored further to devise ways of reducing its power consumption and shortening its transient times.

REFERENCES

[1] M. Alioto, *IoT: Bird's Eye View, Megatrends and Perspectives*. 2017.

[2] H. Fuketa, S. O'Uchi, and T. Matsukawa, "A 0.3-V 1- µw Super-Regenerative Ultrasound Wake-Up Receiver with Power Scalability," *IEEE Trans. Circuits Syst. II Express Briefs*, vol. 64, no. 9, pp. 1027–1031, 2017.

[3] M. Gazivoda, D. Oletic, C. Trigona, and V. Bilas, "Measurement of Weak Signal Energy at Acoustic Frequencies by using RMSHI as a Passive Conditioning Circuit," *I2MTC 2019 - 2019 IEEE Int. Instrum. Meas. Technol. Conf. Proc.*, pp. 1735-1739., 2019.

[4] P. Mayer, M. Magno, and L. Benini, "Self-Sustaining Acoustic Sensor with Programmable Pattern Recognition for Underwater Monitoring," *IEEE Trans. Instrum. Meas.*, vol. 68, no. 7, pp. 2346–2355, 2019.

[5] D. Oletic and V. Bilas, "Energy-efficient respiratory sounds sensing for personal mobile asthma monitoring," *IEEE Sens. J.*, vol. 16, no. 23, pp. 8295–8303, 2016.

[6] N. Goux and F. Badets, "Review on event-driven wake-up sensors for ultra-low power time-domain design," *Midwest Symp. Circuits Syst.*, vol. 2018-Augus, pp. 554–557, 2019.

[7] D. Oletic, V. Bilas, M. Magno, N. Felber, and L. Benini, "Low-power multichannel spectro-temporal feature extraction circuit for audio pattern wake-up," *2016 Des. Autom. Test Eur. Conf. Exhib.*, pp. 355–360, 2016.

[8] R. S. Suri, N. T. Tasneem, and I. Mahbub, "Low-power highly efficient voltage-boosting rectifier for wide-band inductively-coupled power telemetry," *2019 United States Natl. Comm. URSI Natl. Radio Sci. Meet. Usn. NRSM 2019*, no. 1, pp. 1–2, 2019.

[9] J. Gak, M. Miguez, E. Alvarez, and A. Arnaud, "Integrated ultra-low power precision rectifiers for implantable medical devices," *2019 Argentine Conf. Electron. CAE 2019*, pp. 27–30, 2019.

[10] K. G. Sun, K. Choi, and T. N. Jackson, "Low-power double-gate ZnO TFT active rectifier," *IEEE Electron Device Lett.*, vol. 37, no. 4, pp. 426–428, 2016.

[11] S. Du, G. A. J. Amaratunga, and A. A. Seshia, "A Cold-Startup SSHI Rectifier for Piezoelectric Energy Harvesters with Increased Open-Circuit Voltage," *IEEE Trans. Power Electron.*, vol. 34, no. 1, pp. 263–274, 2019.

[12] X. Li and Y. Sun, "An SSHI Rectifier for Triboelectric Energy Harvesting," *IEEE Trans. Power Electron.*, vol. 8993, no. c, pp. 1–15, 2019.

Biography

Marko Gazivoda was born in Zagreb, Croatia, in 1992, where he attended primary and secondary school. After finishing secondary school, he continued his education at the University of Zagreb Faculty of Electrical Engineering, where he graduated in 2016, with highest honor (summa cum laude) and the Josip Lončar bronze plaque award for distinguished results.

Since the end of 2017., he has been employed as a research assistant at the Department of Electronic Systems and Information Processing, Faculty of Electrical Engineering and Computing, University of Zagreb. He participated in one scientific projects of the Croatian Science Foundation (IP-2016-06-8379, SENSIRRIKA), and one scientific project of the U.S. Office of Naval Research Global (ONRG-NICOP-N62909-17-1-2160, AWAKE).

His research interests include low-power sensors, sensor interfaces and instrumentation, sensor interface architectures, and biomedical electronics. He is an author of four journal and three conference papers and a coauthor of one conference paper.

Publications

Journal Papers

1. **Gazivoda, M.**, Bilas, V., "Always-on sparse event wake-up detectors: A Review", *IEEE Sensors Journal*, Vol., Issue, pages, 2022, doi:

2. **Gazivoda, M.**, Oletić, D., Bilas, V., "Features and always-on wake-up detectors for sparse acoustic event detection", *Electronics*, Vol. 11, Issue 3, pp 14, 2022, doi:10.3390/electronics11030478

3. **Gazivoda, M.**, Bilas, V., "Low-Power Sensor Interface with a Switched Inductor Frequency Selective Envelope Detector", *Sensors*, Vol. 21, Issue 6, pp 21, 2021, doi:10.3390/s21062124

4. **Gazivoda, M.**, Oletić, D., Trigona, C., Bilas, V., "Passive Extraction of Signal Feature Using a Rectifier with a Mechanically Switched Inductor for Low Power Acoustic Event Detection", *Sensors*, Vol. 20, Issue 18, pp 19, 2020, doi:10.3390/s20185445

Conference Papers

1. Oletić, D., **Gazivoda, M.**, Bilas, V., "A Programmable 3-Channel Acoustic Wake-Up Interface Enabling Always-On Detection of Underwater Events Within 20 µA", *Proceedings of the 32nd Eurosensors Conference*, Graz, Austria, pp. 1-7, 2018, doi:10.3390/proceedings2130768

2. **Gazivoda, M.**, Oletić, D., Trigona, C., Bilas, V., "Measurement of Weak Signal Energy at Acoustic Frequencies by using RMSHI as a Passive Conditioning Circuit", *Proceedings of the 2019 IEEE International Instrumentation and Measurement Technology Conference (I2MTC)*, Auckland, New Zealand, pp. 1735–1739, 2019, doi:10.1109/I2MTC.2019.8827042

3. **Gazivoda, M.**, Trigona, C., Bilas, V., "Weak Signal Detection Utilizing a Mechanically Switched Inductor", *Proceedings of the 8th International Workshop on Advances in Sensors and Interfaces*, Otranto, Italy, 1-5, 2019, doi:10.1109/IWASI.2019.8791307

4. **Gazivoda, M.**, Oletić, D., Bilas, V., "Characterization and Comparison of Envelope Detectors for Wake-up Sensor Interfaces at Audio Frequencies", *Proceedings of the 2020 IEEE International Instrumentation and Measurement Technology Conference (I2MTC)*, Dubrovnik, Croatia, pp. 1–6., 2020, doi:10.1109/I2MTC43012.2020.9128810

Životopis

Marko Gazivoda rođen je 1992. godine u Zagreb, u Hrvatskoj, gdje je pohađao osnovnu školu i XV. gimnaziju. Nakon završetka srednje škole, upisuje Fakultet elektrotehnike i računarstva Sveučilišta u Zagrebu, na kojem 2016. godine stječe titulu magistra inženjera elektrotehnike i informacijske tehnologije s najvećom pohvalom (summa cum laude) te priznanjem i brončanom plaketom Josip Lončar za posebno istaknuti uspjeh na diplomskom studiju.

Od kraja 2017. godine zaposlen je kao asistent na Zavodu za elektroničke sustave i obradu informacija na Fakultetu elektrotehnike i računarstva Sveučilišta u Zagrebu. Sudjelovao je u radu na jednom znanstvenom projektu Hrvatske zaklade za znanost (IP-2016-06-8379, SENSIRRIKA), i jednom znanstvenom projektu U.S. Office of Naval Research Global (ONRG-NICOP-N62909-17-1-2160, AWAKE).

Njegovi istraživački interesi obuhvaćaju senzore i senzorska sučelja niske potrošnje, arhitekture senzorskih sučelja i biomedicinsku elektroniku. Autor je četiri časopisna i tri konferencijska rada te koautor na jednom konferencijskom radu.